REPORT A219 30 NOVEMBER 1963

AFCRL-63-782 VOL II

INVESTIGATION OF MAGNETOHYDRODYNAMIC WAVES

VOLUME II THEORY

FINAL REPORT

COPY NO. 48

SUBMITTED UNDER CONTRACT NO. AF19(628)-239

Prepared for:

AIR FORCE CAMBRIDGE RESEARCH LABORATORIES
OFFICE OF AEROSPACE RESEARCH
UNITED STATES AIR FORCE
BEDFORD, MASSACHUSETTS

PREPARED BY C.D. Joerger
C.D. Joerger

APPROVED BY M. A. Glatt
M.A. Glatt

APPROVED BY Anatole Browde
A. Browde

MCDONNELL AIRCRAFT CORPORATION
LAMBERT - ST. LOUIS MUNICIPAL AIRPORT, BOX 516, ST. LOUIS 66, MO.

FOREWORD

This report, Volume II, is one of a series of three volumes, reporting work accomplished under Contract AF19(268)-239 initiated in December 1961.

The purpose of this program was to investigate by theory and experiment the pertinent factors influencing the creation, propagation and detection of a type of magnetohydrodynamic wave, the Alfvén wave, that could exist in a partially ionized, low density medium.

The theoretical aspects of magnetohydrodynamic waves, as might be generated under ionospheric conditions and excited in a simulated environment, are investigated in this report. Experimental design and subsequent test results of wave propagation in three McDonnell plasma facilities, are reported in Volume III. Volume I of this series provides the reader with a brief summary of Volumes II and III.

This program required the cooperation and assistance of many persons. The chief contributors, in addition to C. D. Joerger, Project Leader were: J. L. Hickerson and E. W. Hobbs for plasma wave theory; T. R. McPherron, E. S. Thompson, G. L. Elder, and J. L. Walker for experimental design and execution; and H. J. Fivel and J. N. Holsen for thermodynamic analyses.

TABLE OF CONTENTS (CONTINUED)

LIST OF FIGURES

LIST OF TABLES

MHD Wave Investigation
II - theory

REPORT NO. A219
30 NOVEMBER 1963

1. SUMMARY

This report is submitted in fulfillment of Contract AF19(268)-239 for the investigation of magnetohydrodynamic waves. Under this contract McDonnell has successfully generated Alfvén waves in an arc discharge tube and further, has evidence that this phenomena was also detected in the ionized flow of a Hypervelocity Impulse Tunnel (HIT). The goal of this program was to determine by means of theory and experiment the pertinent factors influencing the creation, propagation, and detection of the Alfvén wave that can exist in a partially ionized, low density atmosphere. This volume discusses the theoretical studies conducted during this program to describe plasma wave propagation in the ionosphere and in a laboratory generated plasma environment.

The equations that describe the wave motion in a plasma have been treated by a number of authors; however, solutions are available only for a limited number of cases, treating conditions in which coupling between the ion and the neutral gases is either very small or very large for the ionosphere, and whereas for laboratory plasmas the coupling is usually intermediate. The inability to generate a plasma of even modest size has prevented other experimenters from trying to scale laboratory plasmas to ionospheric phenomena. The effect of neutral particle damping, which is a major contributor to Alfvén wave attenuation in the ionosphere has not been previously studied because of the severe attenuation of the wave in the experimental facilities (the mere presence of a large percentage of non-ionized gas rapidly attenuates the wave).

Previous major experimental investigations have treated the thermonuclear and not the ionospheric problem. Important requirements for ionospheric simulation are availability of a facility, large in size, generation of a realistic percentage of gas ionization, and a low ion neutral collision frequency.

It was hypothesized that these parameter requirements could be met in the flow of the Hypervelocity Impulse Tunnel (HIT) under high arc chamber temperatures. This type of facility had previously been used only for aerodynamic testing in non-ionized gas flow.

The first part of this volume discusses the theory of plasma waves based upon a three fluid description (neutral, ion, and electron gases). A general dispersion equation was derived and then specialized, to enumerate the properties of transverse and longitudinal waves propagating along and across magnetic field lines. Additionally, special solutions of the equation were used to describe propagation in a plasma waveguide and to enumerate the existence criteria for Alfvén waves in the ionosphere, HIT, and plasma waveguide.

The complete dispersion relationship for the Alfvén wave was programmed on an IBM 7094 computer. Parametric data was obtained for the attenuation distance and phase velocity of the wave as a function of disturbance frequency, ion concentration and ion percentage, magnetic field strength, temperature, and molecular weight. These solutions were found to agree with the asymptotic solutions obtained by other authors. For a low frequency disturbance the Alfvén wave has long attenuation distances and propagates with a phase velocity determined by the total density of the gas. As the coupling between the ions and neutrals breaks down, the phase velocity increases to a maximum determined by the ion density. The computed attenuation distances did not indicate the increased damping predicted for the intermediate coupling case; instead it indicated that the phase velocity of the wave increased so as to compensate for the shorter time of wave existence. The range of frequencies for which the dispersion equation is valid includes the ion cyclotron frequency.

The second part of this volume relates the characteristics of the ionosphere to the characteristics of the ionized flow existing in the initial

phases of the HIT flow, and describes the properties of two small plasma facilities, an electromagnetic shock tube and an arc discharge tube.

The Hypervelocity Impulse Tunnel can be described as a large nozzle, whose flow is generated by arc heating a precharged volume of gas, nitrogen in this case. Two ionized flow regions are present: (1) the shock excited region created by the initial shock generated by the bursting of a diaphragm during the arc heating of the gas, and (2) the initial phase of blow-down flow which follows the initial shock.

The shock excited flow is generated within a fraction of a millisecond of the initiation of the arc discharge. As the shock travels through the divergent nozzle it loses strength. Three analyses have been performed to predict the magnitude of this shock attenuation and the available test time. While the duration of ionized flow between the shock and the initial gases expanding from the arc chamber theoretically lasts a fraction of a millisecond, experiments have shown that test times up to 2 milliseconds actually exist. The high temperature low density gas behind this shock is highly ionized.

The blow-down period, with about four milliseconds of ionized flow, provided the conditions in which the Alfvén wave experiments were performed. At the 12,000°K arc chamber temperature used, nitrogen is highly dissociated and highly ionized. The ionization at the throat is principally N^+ ions. During the rapid expansion of gas through the nozzle into the test section, the recombination of these ions through three-body interactions is not realized, and thus the N^+ concentration remains intact. On the other hand, the N_2^+ ion rapidly disappears through dissociative recombination and does not exist in the test section in the charged state. Theoretically, ion concentrations of greater than 10^{11} ions/cm^3 should exist in the test section. As the arc chamber temperature drops, the number of N^+ ions created rapidly decreases, and ionization in the test

section ceases. Two analyses were performed to verify this effect, a simplified frozen flow analysis and a non-equilibrium flow analysis using the IBM 7094 computer.

The two smaller plasma sources used for experimentation and instrumentation development were an electromagnetic shock tube and an arc discharge tube. The electromagnetic shock tube creates a moving plasma by discharging a short high current pulse across a coaxial electrode. A piston of fully ionized hot gas is propelled down the tube, compressing and heating the gas in front while itself losing strength. The processes in the discharge and the acceleration of the gases are not well understood; however, the high ionization can be readily measured.

Similar to the electromagnetic shock tube is the second facility employed in these experiments, an arc discharge tube. An arc is struck along the axis of an evacuated tube, and the experiments are performed while the arc is still burning. The resulting plasma is more highly ionized than that in the shock tube.

Although the analysis of arc heated gas effects presented many theoretical difficulties the experiments performed have provided valuable empirical data.

2. WAVES IN PLASMAS

2.1 INTRODUCTION. - Prior to starting any basic experimental program a theoretical analysis is required to provide the proper background for designing the experiment. The most logical starting point from which to launch this analysis is by a thorough literature survey in order to achieve an indication of the existence or non-existence of the desired phenomenon. For this program a realistic theory was sought, capable of predicting and describing general plasma oscillations in a partially ionized gas. A review of pertinent literature revealed the theoretical approach of Lehnert (Reference 2-1) to be the most suitable, since it could be adapted to experiments in practically any facility. In his development Lehnert considered a three-component gas consisting of electrons, ions and neutral particles. By means of the basic force equations (derivable from the Boltzmann equation), the continuity equations, and Maxwell's equations, he obtained a set of linearized equations which he combined, after specialization, to give a wave equation for transverse oscillations of the magnetic flux density. Later papers by other authors, notably Tanenbaum and Mintzer (Reference 2-2), developed a somewhat more general dispersion relationship, describing the various types of wave motions that could exist in partially and fully ionized fluids permeated by constant magnetic fields. The direct use and adaptation of these works furnished a theoretical background for the experimental program.

In the following development a basic dispersion relationship, valid for a variety of plasma disturbances, and a reasonably general wave equation for transverse oscillations are derived using Lehnert's approach. A discussion of interesting specializations of the dispersion equation with emphasis on Alfvén waves in unbounded media and wave guides is carried out in section 2.4. In

section 2.4.4 the dispersion relationship is reformulated for parametric analysis by a digital computer. Sections 2.5, 2.6 and 2.7 are concerned with the application of the theory to two of McDonnell's experimental facilities and the F region of the ionosphere. The propagation velocity and attenuation of Alfvén waves for large ranges of parameter values are derived from the computer plots and then compared with qualitative curves for the limiting cases investigated by Tannenbaum (Reference 2-3). In each case, existence criteria, as determined by theoretical considerations and the computer results, are summarized. Frequency range, phase velocity and attenuation properties of waves capable of existing in the three media are examined. The possibility of wave channeling in the ionosphere is also investigated.

2.2 THREE FLUID DESCRIPTION. - The basic plasma force equations, continuity equations, perfect gas equations of state and Maxwell's equations can be utilized to derive expressions for momentum transfer between the gas constituents and a generalized Ohm's law. From these equations a basic wave equation can be implied, and its corresponding dispersion relationship obtained. Following the derivation of Lehnert (Reference 2-1), a three-component ideal gas of N_e electrons, N_i ions and N_n neutrals per unit volume is considered. From the basic plasma equations, the rate of momentum transfer between the particles and between the fields and particles is expressed by the following set of relations:

$$N_e m_e \hat{D}_e \vec{v_e} = -e N_e (\vec{E} + \vec{v_e} \times \vec{B}) - N_e M_{ei} \nu_{ei} (\vec{v_e} - \vec{v_i}) - N_e M_{en} \nu_{en} (\vec{v_e} - \vec{v_n}) - \nabla P_e - \rho_e \nabla \phi \qquad (2\text{-}1)$$

for the electron gas,

$$N_i m_i \hat{D}_i \vec{v_i} = e N_i (\vec{E} + \vec{v_i} \times \vec{B}) - N_i M_{ie} \nu_{ie} (\vec{v_i} - \vec{v_e}) - N_i M_{in} \nu_{in} (\vec{v_i} - \vec{v_n}) - \nabla P_i - \rho_i \nabla \phi \qquad (2\text{-}2)$$

for the ion gas, and:

$$N_n m_n \hat{D}_n \vec{v_n} = - N_n M_{ni} \nu_{ni} (\vec{v_n} - \vec{v_i}) - N_n M_{ne} \nu_{ne} (\vec{v_n} - \vec{v_e}) - \nabla P_n - \rho_n \nabla \phi \qquad (2\text{-}3)$$

for the neutral gas.

In these equations, N_s is the s-particle concentration where s is either e, i or n, and m_s, its mass. The positive charges are taken to be singly ionized neutral particles with net charge e. The macroscopic average for s-particle velocity is denoted by v_s, and the notation M_{sr} represents the reduced mass for s and r-particle interactions. The corresponding "collision" frequency is υ_{sr}. The scalar pressure and gravitational potential are denoted by P_s and ϕ, while $\vec{E}$ and $\vec{B}$ represent the macroscopic electric field and magnetic flux density due to both the plasma constituents and external sources. The operator D_s is the hydrodynamic derivative for the s-particle gas. Conservation of mass and charge is implied by the use of the continuity equations:

$$\frac{\partial N_s}{\partial t} + \nabla\cdot(N_s \vec{v_s}) = 0;\ s = e,\ i,\ n \tag{2-4}$$

Spatial variations in the pressure will be assumed to occur rapidly enough for the adiabatic condition for ideal gases to apply. Then:

$$\nabla P_s = C_s^2 \nabla \rho_s;\ \ s = e,\ i,\ n \tag{2-5}$$

where:

$$\rho_s = N_s m_s$$

and:

$$C_s^2 = \gamma_s k T_s / m_s$$

with k being the Boltzmann constant, γ_s the ratio fo specific heats and T_s the temperature of the s-particle gas. Under the assumption of electrical neutrality for the whole gas:

$$N_e = N_i = N \tag{2-6}$$

For the manipulation of equations (2-1) through (2-3) it is convenient to define the following relations:

$$\left.\begin{aligned} \rho_n &= N_n m_n \\ \rho &= N_i m_i + N_e m_e = N_m \\ m &= m_i + m_e \\ R &= \frac{\rho}{\rho + \rho_n} \end{aligned}\right\} \tag{2-7}$$

$$\vec{j} = N_e (\vec{v}_i - \vec{v}_e) \tag{2-8}$$

$$\left.\begin{aligned} \vec{v}_i &= \vec{v} + \frac{m_e}{Nem}\,\vec{j} \\ \vec{v}_e &= \vec{v} - \frac{m_i}{Nem}\,\vec{j} \\ \vec{v} &= N(m_i \vec{v}_i + m_e \vec{v}_e)/\rho \end{aligned}\right\} \tag{2-9}$$

$$P = P_i + P_e \tag{2-10}$$

The symbol $\vec{j}$ denotes the current density due to the moving charges, irrespective of the cause of their motion.

The three-component gas can now be reduced to a two-component gas, whose constituents are referred to as the plasma and neutral gas. Substitution of the relations (2-7) through (2-10) into (2-1) and (2-2) yields:

$$N m_e \hat{D}_e\left(\vec{v} + \frac{m_i}{Nem}\,\vec{j}\right) = -N_e\left(\vec{E} + \vec{v}\times\vec{B}\right) + \frac{m_i}{m}\,\vec{j}\times\vec{B} + \frac{1}{e}\left(M_{ei}\nu_{ei} + \frac{m_i}{m}\,M_{en}\nu_{en}\right)\vec{j}$$
$$- N M_{en}\nu_{en}\left(\vec{v} - \vec{v}_n\right) - \nabla P_e - \rho_e \nabla\phi \tag{2-11}$$

and

$$N m_i \hat{D}_i\left(\vec{v} + \frac{m_e}{Nem}\,\vec{j}\right) = N_e\left(\vec{E} + \vec{v}\times\vec{B}\right) + \frac{m_e}{m}\,\vec{j}\times\vec{B} - \frac{1}{e}\left(M_{ie}\nu_{ie} + \frac{m_e}{m}\,M_{in}\nu_{in}\right)\vec{j}$$
$$- N M_{in}\nu_{in}\left(\vec{v} - \vec{v}_n\right) - \nabla P_i - \rho_i \nabla\phi \tag{2-12}$$

Adding (2-11) and (2-12) and expanding $\hat{D}_e$ and $\hat{D}_i$ gives:

$$\rho\hat{D}\vec{v} + \frac{m_e m_i}{e}\left(\vec{j}\cdot\nabla\right)\frac{\vec{j}}{\rho} = \vec{j}\times\vec{B} + \beta\vec{j} - \rho\alpha(\vec{v} - \vec{v}_m) - \nabla P - \rho\nabla\phi \tag{2-13}$$

where the definitions:

$$\hat{D} = \frac{\partial}{\partial t} + (\vec{v}\cdot\nabla) \tag{2-14}$$

$$\alpha = \frac{1}{m}\left(M_{en}\nu_{en} + M_{in}\nu_{in}\right) \tag{2-15}$$

$$\beta = \frac{M_{ie}}{e}(\nu_{ei} - \nu_{ie}) + \frac{m_i}{e}\left[\frac{M_{en}}{m}\nu_{en} - \frac{M_{in}}{m}\left(\frac{m_e}{m_i}\right)\nu_{in}\right] \tag{2-16}$$

have been employed. With similar substitutions, equation (2-3) becomes:

$$\rho_n \hat{D}_n \vec{v}_n = -\bar{\beta}\vec{j} + \rho\bar{a}(\vec{v} - \vec{v}_n) - \nabla P_n - \rho_n \nabla\phi \tag{2-17}$$

where:

$$\bar{a} = \frac{1}{mq}(M_{ne}\nu_{ne} + M_{ni}\nu_{ni}) \tag{2-18}$$

$$\bar{\beta} = \frac{m_i}{eq}\left[\frac{M_{ne}}{m}\nu_{ne} - \frac{M_{ni}}{m}\left(\frac{m_e}{m_i}\right)\nu_{ni}\right] \tag{2-19}$$

with:

$$q = \frac{N}{N_n} \tag{2-20}$$

The action of the operator given by (2-14) on $\vec{v}$ gives the acceleration of a particular macroscopically infinitesimal plasma element, and is defined by the sum of the rate of change of plasma velocity at a fixed point in the gas and the instantaneous rate of change of plasma velocity between points of the gas.

The interpretation given to a is that of a mean, or effective, collision frequency of the plasma with the neutral gas. Since only the plasma and the neutral gas are involved, conservation of momentum implies that the collision frequency of the neutrals with the plasma be equal to a, that is $\bar{a} = a$. Under conditions of thermal equilibrium, use of the formulas (B-37) from Appendix B for collision frequency yields the relations:

$$\left.\begin{aligned} \nu_{in} &= \frac{\nu_{ni}}{q} \\ \nu_{en} &= \frac{\nu_{ne}}{q} \\ \nu_{ei} &= \nu_{ie} \end{aligned}\right\} \tag{2-21}$$

Then noting that:

$$\left.\begin{aligned} M_{in} = M_{ni} &\approx \frac{1}{2}m_i \\ M_{en} = M_{ne} &\approx m_e \\ m &\approx m_i \end{aligned}\right\} \tag{2-22}$$

expressions (2-15) and (2-18) yield:

$$a = \bar{a} \approx \frac{m_e}{m_i} \nu_{en} + \frac{1}{2} \nu_{in} \tag{2-23}$$

This result substantiates the interpretation of a, since in order to maintain a non-equilibrium condition, momentum is not conserved unless the disturbing energy source is included. Only then is $\bar{a} \neq a$.

The quantity β takes on the form of a scalar magnetic field in the center of mass frame of an elementary volume of the gas. With the gas constituents at thermal equilibrium, (2-21) and (2-22) imply that:

$$\beta = \bar{\beta} \approx \frac{m_e}{e} (\nu_{en} - \tfrac{1}{2}\nu_{in}) \tag{2-24}$$

Since (2-11) and (2-12) are the force equations for the charged particles of an elementary volume of the cps, a generalization of Ohm's law can be obtained by multiplying (2-11) by $\frac{m_i}{e\rho}$ and (2-12) by $\frac{m_e}{e\rho}$ and then subtracting the resulting expressions; thus:

$$\frac{m_i m_e}{e^2} \hat{D}\left(\frac{\vec{i}}{\rho}\right) + \frac{m_i m_e}{e^2 \rho} (\vec{j} \cdot \nabla)\vec{v} + \frac{m_i m_e (m_i - m_e)}{e^3 \rho} (\vec{j} \cdot \nabla)\left(\frac{\vec{i}}{\rho}\right) =$$

$$\vec{E} + \vec{v} \times \vec{B} - \frac{m_i - m_e}{e\rho} (\vec{j} \times \vec{B}) - \gamma\left(\frac{\vec{i}}{\rho}\right) + \beta(\vec{v} - \vec{v}_n) + \frac{1}{e\rho} (m_i \nabla P_e - m_e \nabla P_i) \tag{2-25}$$

where:

$$\gamma = \frac{m M_{ie}}{e^2} \left[\left(\frac{m_e}{m}\right) \nu_{ie} + \left(\frac{m_i}{m}\right) \nu_{ei} \right] + \frac{m}{e} \left[\left(\frac{m_e}{m}\right)^2 \left(\frac{M_{in}}{e}\right) \frac{\nu_{in}}{2} + \left(\frac{m_i}{m}\right)^2 \left(\frac{M_{en}}{e}\right) \nu_{en} \right] \tag{2-26}$$

For the condition of thermal equilibrium:

$$\gamma \approx \frac{m_i m_e}{e^2} \left[\nu_{en} + \nu_{ei} + \frac{m_e}{2m_i} \nu_{in} \right] \tag{2-27}$$

In a three constituent gas the usual resistivity term must include the effects of momentum transfer between the plasma and neutral gas, therefore $\frac{\gamma}{\rho}$ is the proper first order expression for the gas resistivity. It can be argued that, for a negligible difference in the accelerations of the ions and electrons and small gradients and rotations of the ion and electron velocities, the terms involving $\hat{D}\left(\frac{\vec{J}}{\rho}\right)$ and the operator $(\vec{J} \cdot \nabla)$ are of no relative consequence in (2-25).

With these terms discarded, equations (2-13) and (2-25) can be written as:

$$\rho \hat{D}\vec{v} = \vec{j} \times \vec{B} + \beta \vec{j} - \rho a (\vec{v} - \vec{v_n}) - \nabla P - \rho \nabla \phi \qquad (2\text{-}28)$$

$$\vec{E} + \vec{v} \times \vec{B} = \frac{m_i - m_e}{e\rho} \vec{j} \times \vec{B} + \frac{\gamma}{\rho} \vec{j} - \beta (\vec{v} - \vec{v_n}) - \frac{m_i}{e\rho} (\nabla P_e - \frac{m_e}{m_i} \nabla P_i) \qquad (2\text{-}29)$$

If the particle masses are included in (2-11), the result is:

$$\frac{\partial \rho_s}{\partial t} + \nabla \cdot \rho_s \vec{v_s} = 0; \quad s = e \text{ or } n \qquad (2\text{-}30)$$

The set of equations (2-17), (2-28), (2-29) and (2-30) are sufficient to describe the evolution of particle velocities and densities in space-time; and hence, account for the net current density. Maxwell's equations then furnish the connection between the time varying currents and the general space-time varying magnetic field produced in the plasma. The required relationships are:

$$\nabla \times \vec{E} = - \frac{\partial B}{\partial t} \qquad (2\text{-}31)$$

and:

$$\nabla \times \vec{B} = \mu_o \vec{j} + \mu_o \epsilon \frac{\partial \vec{E}}{\partial t} \qquad (2\text{-}32)$$

where μ_o is the permeability of the gas, essentially that of free space, and is the permittivity, assumed here to be a scalar quantity. Except for large phase velocities of the disturbances in the plasma, the displacement current in (2-32) makes a negligible contribution to $\nabla \times \vec{B}$.

As is customary in the investigation of complex phenomena, a first order analysis of the above set of equations will now be performed. Each quantity is mathematically decomposed into a constant component, which includes any initial

value, and a perturbation, thus:

$$\left.\begin{aligned}
\vec{B} &= \vec{B}_o + \vec{b}' \\
\vec{E} &= \vec{E}_o + \vec{E}' \\
\vec{i} &= \vec{i}_o + \vec{i}' \\
\vec{v} &= \vec{V}_o + \vec{v}' \\
\vec{v}_n &= \vec{V}_o + \vec{v}_n' \\
\rho_s &= \rho_{so} + \rho_s' ;\ s = e, i, n \\
\rho &= \rho_o + \rho'
\end{aligned}\right\} \qquad (2\text{-}33)$$

where all the zero subscripted quantities are taken to be constant in space and time. Incorporation of (2-33) into the equations expressing momentum transport (2-28) and (2-17), the generalized Ohm's law (2-29), the equations of continuity (2-30), and the field and current relationships from Maxwell's equations (2-31) and (2-32), produces a set of equations, where all second order terms of the type $(j'b'), (\rho'v'), (\rho'\nabla\cdot\vec{v}'), \left(\rho'\frac{\partial\vec{v}'}{\partial t}\right)$ and $\frac{\rho'}{\rho_o}$ are neglected. Thus the linearized equations are:

$$\rho_o \hat{D}_o \vec{v}' = \vec{i}\times\vec{B}_o + \beta\vec{i}' - \rho_o\alpha(\vec{v}-\vec{v}_n) - \left(C_e^2\nabla\rho_e' + C_i^2\nabla\rho_i'\right) \qquad (2\text{-}34)$$

$$\rho_{no}\hat{D}_o\vec{v}_n' = -\beta\vec{i} + \rho_o\bar{\alpha}(\vec{v}'-\vec{v}_n') - C_n^2\nabla\rho_n' \qquad (2\text{-}35)$$

$$\vec{E}+\vec{v}'\times\vec{B}_o = \frac{m_i - m_e}{e\rho_o}\vec{i}\times\vec{B}_o + \frac{\gamma}{\rho_o}\vec{i} - \beta(\vec{v}'-\vec{v}_n') - \frac{m_i}{e\rho_o}\left[C_e^2\nabla\rho_e' - \frac{m_e}{m_i}C_i^2\nabla\rho_i'\right] \qquad (2\text{-}36)$$

$$\frac{\partial\rho_s'}{\partial t} + \rho_{so}\nabla\cdot\vec{v}_s' = 0 \qquad (2\text{-}37)$$

$$\nabla\times\vec{E}' = -\frac{\partial\vec{b}'}{\partial t} \qquad (2\text{-}38)$$

$$\nabla\times\vec{b}' = \mu_o\vec{i} + \mu_o\epsilon\frac{\partial\vec{E}'}{\partial t} \qquad (2\text{-}39)$$

In (2-34) and (2-35) the $\rho_s \nabla\phi$ terms have also been neglected, since in almost any experiment or terrestrial atmospheric disturbance they represent a constant but insignificant part of the total gas energy. The zero subscript on the hydrodynamic derivatives means that the variable velocity is replaced by the constant velocity V_o.

Since all of the quantities expressed in (2-33) are macroscopic averages and the primed quantities are capable of Fourier analysis for any physical case, a normal mode analysis is justified. This procedure requires all the primed variables in (2-33) to vary in proportion to $e^{i(\omega t + \vec{\kappa}\cdot\vec{r})}$, where κ is the wave vector and $\vec{r}$ is the directed distance from the origin of coordinates to a point on the wave front. To be physically applicable, the gas in which such disturbances take place must essentially be homogeneous and infinite in extent. Upon making the above normal mode substitution for the dependent variables, the new linearized set becomes:

$$i\rho_o(\omega + \vec{\kappa}\cdot\vec{V}_o)\vec{v}' = \vec{j}\times\vec{B}_o + \beta\vec{j} - \rho_o\alpha(\vec{v}' - \vec{v}_n') - i(C_e^2\rho_e' + C_i^2\rho_i')\vec{\kappa} \qquad (2\text{-}40)$$

$$i\rho_{no}(\omega + \vec{\kappa}\cdot\vec{V}_o)\vec{v}_n' = -\beta\vec{j} + \rho_o\alpha(\vec{v}' - \vec{v}_n') - iC_n^2\rho_n'\vec{\kappa} \qquad (2\text{-}41)$$

$$\vec{E} + \vec{v}'\times\vec{B}_o = \frac{m_i - m_e}{e\rho_o}\vec{j}\times\vec{B}_o + \frac{\gamma}{\rho_o}\vec{j} - \beta(\vec{v}' - \vec{v}_n') - i\frac{m_i}{e\rho_o}\left(C_e^2\rho_e' - \frac{m_e}{m_i}C_i^2\rho_i'\right)\vec{\kappa} \qquad (2\text{-}42)$$

$$\frac{\rho_s'}{\rho_{so}} = -\frac{1}{\hat{U}}(\vec{v}_s'\cdot\vec{\iota}_\kappa);\ s = e, i, n \qquad (2\text{-}43)$$

$$\vec{E}' = \hat{U}(\vec{\iota}_\kappa\times\vec{b}') \qquad (2\text{-}44)$$

$$\vec{j} = \frac{i\kappa}{\mu_o}\left[1 - \left(\frac{\hat{U}}{c}\right)^2\right](\vec{\iota}_\kappa\times\vec{b}') \qquad (2\text{-}45)$$

with:

$$\hat{U} = \frac{\omega}{\kappa} \tag{2-46}$$

as the complex phase velocity in the direction of $\vec{\kappa}$, or simply, the phase velocity operator. The permittivity ϵ has been taken to be a scalar whose value is that of the permittivity of free space, ϵ_o. Then in the MKS system the vacuum speed of light becomes:

$$c = \frac{1}{\sqrt{\mu_o \epsilon_o}}$$

In these equations $\vec{\iota}_\kappa$ is the unit vector in the direction of $\vec{\kappa}$; hence:

$$\vec{\iota}_\kappa = \frac{\vec{\kappa}}{|\vec{\kappa}|}$$

Upon introduction of the parameters:

$$F = \frac{\rho_{no}\omega}{\rho_o \overline{a}} \left(1 + \frac{\vec{V}_o \cdot \vec{\iota}_\kappa}{\hat{U}}\right) \tag{2-47}$$

and:

$$G = \frac{\rho_o}{\rho_{no}} \frac{\overline{a}}{a} F \tag{2-48}$$

equation (2-41) may be solved for $\vec{v}_n'$ and this result used in (2-40) to relate $\vec{v}'$ to $\vec{j}$ and the ρ_s'. Thus:

$$i\rho_o a \left(G + \frac{F}{1+iF}\right)\vec{v}' = -\vec{B}_o \times \vec{j} + \left(\beta - \frac{a/\overline{a}}{1+iF}\,\overline{\beta}\right)\vec{j} - i\kappa\left(C_e^2 \rho_e' + C_i^2 \rho_i' + \frac{a/\overline{a}}{1+iF}\, C_n^2 \rho_n'\right)\vec{\iota}_\kappa \tag{2-49}$$

In the same manner equation (2-42) becomes:

$$\vec{B}_o \times \vec{v}' - \frac{iF\beta\vec{v}'}{1+iF} = \frac{m_i - m_e}{e\rho_o}\vec{B}_o \times \vec{j} + \left(\frac{\beta/\overline{a}}{\rho_o(1+iF)}\overline{\beta} - \frac{\gamma}{\rho_o}\right)\vec{j} + \vec{E} + i\kappa\left[\frac{\beta}{a\rho_o}\frac{1}{1+iF}\, C_n^2 \rho_n' + \frac{m_i}{e\rho_o}\left(C_e^2 \rho_e' - \frac{m_e}{m_i} C_i^2 \rho_i'\right)\right]\vec{\iota}_\kappa \tag{2-50}$$

The parameter $\frac{1}{F}$ is interpreted as a coupling factor between the plasma and neutral gases, since $\frac{\rho_o}{\rho_{no}} a$ is the expected number of plasma-neutral collisions per unit time, and $\frac{1}{\omega}$ is the period over which a disturbance takes place. It

follows that for $\frac{1}{F} \gg 1$, the neutrals readily participate in the motion of the ions; while for $\frac{1}{F} \ll 1$, the plasma and neutral gas retain their individuality. This interpretation of $\frac{1}{F}$ is reasonable for nearly stationary gases, where $|\vec{V}_o| \ll |\hat{U}|$; but its meaning for the general case is somewhat obscure since the real part of $\hat{U}$ is not, in general, the phase velocity of the disturbance.

Using the definitions:

$$\left.\begin{aligned} \rho_* &= \rho_o\left(1 + \frac{F/G}{1+iF}\right) \\ \beta_* &= \beta - \frac{a/\bar{a}}{1+iF}\,\bar{\beta} \\ \lambda_* &= \frac{1}{\mu_o \rho_o}\left(\gamma - \frac{\beta/\bar{a}}{1+iF}\,\bar{\beta}\right) \\ a_* &= \frac{a/\bar{a}}{1+iF} \end{aligned}\right\} \qquad (2\text{-}51)$$

equation (2-49) and (2-50) can be written as:

$$i\rho_*\left(1 + \frac{\vec{V}_o}{\hat{U}}\cdot\vec{\iota}_\kappa\right)\vec{v}' = \beta_*\vec{i} - \vec{B}_o \times \vec{i} - i\kappa\left(C_e^2\rho_e' + C_i^2\rho_i' + a_* C_n^2 \rho_n'\right)\vec{\iota}_\kappa \qquad (2\text{-}52)$$

and:

$$\vec{B}_o \times \vec{v}' - \beta_* \vec{v}' = \frac{m_i - m_e}{e\rho_o}\vec{B}_o \times \vec{i} - \mu_o \lambda_* \vec{i} + \vec{E} \qquad (2\text{-}53)$$

$$+ i\kappa\left[\frac{m_i}{e\rho_o}\left(C_e^2\rho_e' - \frac{m_e}{m_i}C_i^2\rho_i'\right) + \frac{\beta a_*}{\bar{a}\rho_o}C_n^2\rho_n'\right]\vec{\iota}_\kappa$$

The density perturbations are related to the current density and plasma velocity by means of equation (2-43), with the substitutions for $\vec{v}_e'$ and $\vec{v}_i'$ from (2-9), and for $\vec{v}_n'$ from (2-41). The resulting expression for ρ_n' is:

$$\rho_n' = \frac{\rho_{no}}{\hat{U}(1+iF)\left(1 + \frac{i\kappa C_n^2 \rho_{no}}{\hat{U}(1+iF)\bar{a}\rho_o}\right)}\left[\vec{v}' - \frac{\beta}{\rho_o \bar{a}}\vec{i}\right]\cdot\vec{\iota}_\kappa \qquad (2\text{-}54)$$

The starred quantities of (2-52) have definite physical interpretations for nearly stationary plasmas at thermal equilibrium. For strong plasma-neutral

coupling, $F \ll 1$, ρ_* becomes the total unified gas density, and β_*, the effective scalar magnetic field, assumes the form:

$$\beta_* = iF\beta \tag{2-55}$$

which is smaller than β by just F, thus indicating the reduction in forces that are perpendicular to $\vec{j} \times \vec{B}_o$ on the gas elements. Accordingly, the resistivity of the gas, $\mu_o \lambda_*$, is reduced in the direction of the elementary currents as exhibited by:

$$\mu_o \lambda_* \approx \frac{\gamma}{\rho_o} - \frac{\beta^2}{a\rho_o} \tag{2-56}$$

For small percentages of ionization:

$$\nu_{in}, \nu_{ei} \ll \nu_{en} \tag{2-57}$$

and therefore:

$$\mu_o \lambda_* \approx \frac{m_e \nu_{en}}{N_e e^2} \left[1 - \frac{1}{1 + \left(\frac{m_i}{m_e}\right)\left(\frac{\nu_{in}}{\nu_{en}}\right)} \right] \tag{2-58}$$

which is essentially:

$$\mu_o \lambda_* \approx \frac{m_e \nu_{en}}{N_e e^2} \tag{2-59}$$

At the other extreme, that of weak coupling, $F \gg 1$ implies that ρ_* is essentially ρ_o, the plasma density, and β_* is just β. The resistivity term is the usual scalar resistivity for the predominant electron contribution, ν/ρ_o, provided $F \gg \left(\frac{m_e}{m_i}\right)\left(\frac{\nu_{en}}{a}\right)$, which is generally of the order of unity. In this case, σ, the scalar conductivity, it is properly expressed as:

$$\sigma = \frac{N_e e^2}{m_e \nu_{ei}} \tag{2-60}$$

The neutral gas acoustic coupling is determined by:

$$a_* = \frac{1}{1 + iF}$$

and hence, for weak coupling, a_* tends to zero. This implies that for weak coupling, acoustic distrubances of the plasma do not involve the neutrals, except perhaps, as a dissipation mechanism. The role of β_* in the theory is

quite important since the magnetostrictive pressure, which is responsible for transverse plasma oscillations, is effective when $|\vec{B}_o|$ is significantly larger than $|\beta_*|$. This discussion further illustrates the meaning of F, in that for $F \ll 1$ the gas motion is unified, while for $F \gg 1$, the component gases act nearly independent of one another.

To facilitate manipulation of the combination of equations (2-33), (2-44), (2-45), (2-52), (2-53) and (2-54) the dyadic formalism is employed, and the nonian form of the operators $\vec{\iota}_\kappa\vec{\iota}_\kappa$ and $\vec{\iota}_{B_o}\times$ is utilized, where:

$$\vec{\iota}_{B_o} = \frac{\vec{B}_o}{|\vec{B}_o|} ,$$

After using (2-44) and (2-45) to reduce E in (2-53), the momentum equation (2-52) and the generalized Ohm's law (2-53), can be written as:

$$(a_1\vec{I} + a_2\vec{\iota}_\kappa\vec{\iota}_\kappa)\cdot\vec{v}' + (a_3\vec{I} + a_4\vec{\iota}_\kappa\vec{\iota}_\kappa + a_5\vec{\iota}_{B_o}\times)\cdot\vec{i} = (a_6\vec{I} + a_7\vec{\iota}_{B_o}\times)\cdot\vec{i}_o \qquad (2\text{-}61)$$

and:

$$(c_1\vec{I} + c_2\vec{\iota}_\kappa\vec{\iota}_\kappa + c_3\vec{\iota}_{B_o}\times)\cdot\vec{v}' + (c_4\vec{I} + c_5\vec{\iota}_\kappa\vec{\iota}_\kappa + c_6\vec{\iota}_{B_o}\times)\cdot\vec{i}'$$
$$= (c_7\vec{I} + c_8\vec{\iota}_\kappa\vec{\iota}_\kappa + c_4\vec{\iota}_{B_o}\times)\cdot\vec{i}_o + \vec{E}_o \qquad (2\text{-}62)$$

where $\vec{I}$ is the unit dyadic. The coefficients a_j and c_k are as follows:

$$\begin{aligned}
a_1 &= \omega\rho_* \left(1 + \frac{\vec{V}_o\cdot\vec{\iota}_\kappa}{\hat{U}}\right) \\
a_2 &= \frac{i\kappa}{\hat{U}}\left(C_e^2\rho_{eo} + C_i^2\rho_{io} + \eta C_n^2\rho_{no}\right) \\
a_3 &= -\beta_* \\
a_4 &= \frac{-i\kappa}{\hat{U}}\left[\frac{m_i}{\bullet\rho_o}\left(C_e^2\rho_{eo} - \frac{m_e}{m_i}C_i^2\rho_{io}\right) + \frac{\beta}{a\rho_o}\eta C_n^2\rho_{no}\right] \\
a_5 &= B_o \\
a_6 &= \beta_* + i\frac{\kappa}{\hat{U}}\frac{\beta}{\bar{a}\rho_o}\eta C_n^2\rho_{no} \\
a_7 &= a_5
\end{aligned} \qquad (2\text{-}63)$$

$$c_1 = a_3$$

$$c_2 = a_4$$

$$c_3 = a_5$$

$$c_4 = \mu_o \left[\lambda_* + i \frac{\hat{U}}{\kappa \left(1 - \frac{\hat{U}^2}{c^2} \right)} \right]$$

$$c_5 = \frac{i\kappa}{\hat{U}} \left[\left(\frac{m_i}{e \rho_o} \right)^2 \left(C_e^2 \rho_{eo} + \frac{m_e^2}{m_i^2} C_i^2 \rho_{io} \right) + \frac{\beta^2}{a \bar{a} \rho_o^2} \eta C_n^2 \rho_{no} \right] \qquad (2\text{-}64)$$

$$c_6 = - \frac{m_i - m_e}{e \rho_o} B_o$$

$$c_7 = - c_4$$

$$c_8 = - \frac{\beta^2}{a \bar{a} \rho_o^2} \eta C_n^2 \rho_{no}$$

$$c_9 = - c_6$$

where:

$$\eta = \frac{a_*}{(1 + iF) \left(1 + i \frac{\kappa C_n^2 \rho_{no}}{\bar{a} \rho_o \hat{U} (1 + iF)} \right)}$$

Equations (2-61) and (2-62) can be more compactly expressed by the matric equation

$$\begin{bmatrix} \vec{A}_{11} & \vec{A}_{12} \\ \vec{A}_{21} & \vec{A}_{22} \end{bmatrix} \begin{bmatrix} \vec{v}' \\ \vec{i}' \end{bmatrix} = \begin{bmatrix} \vec{R}_1 \\ \vec{R}_2 \end{bmatrix} \qquad (2\text{-}65)$$

with the $\vec{A}_{jk}$ as the dyadic coefficients and $\vec{R}_1$ and $\vec{R}_2$ as the constant vectors on the right side of (2-61) and and (2-62), respectively. It can be shown that the inverse of the square matrix exists, and therefore, (2-65) may be solved for $\vec{v}'$ and $\vec{j}'$.

2.3 THE BASIC DISPERSION RELATIONSHIP. - From the homogenous form of equation (2-65), that is,

$$\vec{R}_1 = \vec{R}_2 = \vec{0} \tag{2-66}$$

a general dispersion relationship can be found. Equation (2-66) implies that no constant electric field or current is maintained in the fluid by external energy sources; hence:

$$\vec{E}_o = \vec{i}_o = \vec{0} \tag{2-67}$$

With this restriction, and the definition of $\vec{v}$ (equations 2-33 with 2-9), (2-65) can be written as:

$$\begin{bmatrix} \vec{A}_{11} & \vec{A}_{12} \\ \vec{A}_{21} & \vec{A}_{22} \end{bmatrix} \begin{bmatrix} \vec{v}'_e \\ \vec{0} \end{bmatrix} + \begin{bmatrix} \vec{A}_{11} & \vec{A}_{12} \\ \vec{A}_{21} & \vec{A}_{22} \end{bmatrix} \begin{bmatrix} \vec{v}'_i \\ \vec{i}' \end{bmatrix} = \begin{bmatrix} \vec{0} \\ \vec{0} \end{bmatrix} \tag{2-68}$$

Since the column matrices are independent, the left hand terms of (2-68) must vanish separately, in order for the matric equation to be valid. Tanenbaum and Mintzer (Reference 2-1) have analyzed only the first term. However, from the standpoint of developing a dispersion equation, either term may be used. If (2-65) is expanded and solved for $\vec{v}'$, the following result is obtained, when the inverse of $\vec{\vec{A}}_{22}$ exists:

$$(\vec{\vec{A}}_{11} - \vec{\vec{A}}_{12} \cdot \vec{\vec{A}}_{22}^{-1} \cdot \vec{\vec{A}}_{21}) \cdot \vec{v}' = \vec{0} \tag{2-69}$$

Once a base-system of vectors is chosen (e.g. the unit vectors of a rectangular Cartesian coordinate system), equation (2-69) is found to be satisfied only if certain relationships exist between the a_j and c_k of (2-63) and (2-64). These relationships, taken together, specify a dispersion equation for wave propagation in an infinite gas of any degree of ionization. This equation will involve ω and κ, either or both of which may be complex.

The dispersion equation may be regarded as a polynominal in either ω or κ, whichever is appropriate to the physical situation. If a spatial disturbance of wavelength:

$$\lambda = \frac{2\pi}{\kappa} \tag{2-70}$$

is maintained throughout the measuring of propagation characteristics such as attenuation and propagation velocity, κ is real and specified, and therefore, the polynomial should be solved for complex ω. The roots will give the eigen-frequencies and associated attenuation time, defined as the time for the wave amplitude to reach 1/e of its initial value. Since the time dependent variables are taken as proportional to $e^{i\omega t}$, the attenuation of time τ becomes

$$\tau = \frac{1}{|\mathrm{Im}(\omega)|} \tag{2-71}$$

If instead of wavelength the angular frequency is specified, the dispersion polynomial should be solved for complex κ. The roots will then yield the proper wavelength for a given ω; and since the space variables go as $e^{i\vec{\kappa}\cdot\vec{r}}$, the attenuation distance can be obtained from:

$$d = \frac{1}{|\mathrm{Im}(\kappa)|} \tag{2-72}$$

Should the wave be excited by an energy pulse localized in space, either ω or k may be specified as complex quantities and the dispersion relationship solved for the other. Attenuation in both time and space will occur.

The propagation velocity will be the phase velocity for the first two cases just discussed. It is always expressed as:

$$U_{ph} = \frac{R_e(\omega)}{R_e(\kappa)} \tag{2-73}$$

For small spatial damping, that is $\mathrm{Im}(\kappa) \ll \mathrm{Re}(\kappa)$:

$$U_{ph} = R_e(\hat{U}) \tag{2-74}$$

In the situation where a localized pulse initiates the disturbance, the propagation velocity of the signal is the group velocity U_{gr} defined by:

$$U_{gr} = \frac{\partial R_e(\omega)}{\partial R_e(\kappa)} \tag{2-75}$$

Each frequency component or wavelength will have its own phase velocity, as given by (2-73).

2.4 SPECIALIZATION OF BASIC DISPERSION EQUATION. - It is obvious that the dispersion equation will contain more information than necessary to construct a reasonably complete picture of the types of waves and their propagation characteristics. It is also apparent that such an expression would be intractable even for a qualitative description of the phenomena. Therefore, it is desirable to examine specific cases which, when taken as a whole, yield a good qualitative description of permissible disturbances. The approach taken by various investigators is to discuss longitudinal and transverse wave propagation, under thermal equilibrium of a stationary gas, perpendicular to and parallel to a permeating constant magnetic field, whose flux density is $\vec{B}_o$. Such was the approach selected in the investigations. The conditions for which the remaining discussions of section 2 are valid are enumerated in the following statements:

Thermal Equilibrium: $T_e = T_i = T_n$; $a = \overline{a}$, $\beta = \overline{\beta}$

Stationary Gas: $\vec{V}_o = \vec{0}$; $\frac{F}{\overline{a}} = \frac{\rho_{no}\omega}{\rho_o a}$, $G = \frac{\omega}{a}$

A rectangular coordinate system is used, and the $\vec{i}_z$ axis is taken parallel to $\vec{B}_o$.

With the above substitutions the factors in (2-63) and (2-64) become:

$$\left.\begin{aligned} a_1 &= i\omega\rho_* \\ a_2 &= \frac{i\kappa}{\hat{U}}\left(2C^2\rho_o + \eta C_n^2 \rho_{no}\right) \\ a_3 &= -\beta_* \\ a_4 &= \frac{-i\kappa}{\hat{U}}\left[\frac{1}{Q}C^2\rho_o + \frac{\beta}{a\rho_o}\,\eta C_n^2 \rho_{no}\right] \\ a_5 &= B_o \end{aligned}\right\} \qquad (2\text{-}76)$$

and:

$$\left.\begin{aligned} c_1 &= a_3 \\ c_2 &= a_4 \\ c_3 &= a_5 \\ c_4 &= \mu_o \left[\lambda_* + i \frac{\hat{U}}{\kappa\left(1 - \frac{\hat{U}^2}{c^2}\right)}\right] \\ c_5 &= \frac{i\kappa}{\hat{U}}\left[\frac{1}{Q^2} C^2 \rho_o + \left(\frac{\beta}{a\rho_o}\right)^2 \eta C_n^2 \rho_{no}\right] \\ c_6 &= \frac{B_o}{Q} \end{aligned}\right\} \qquad (2\text{-}77)$$

where:

$$\left.\begin{aligned} \eta &= \frac{1}{(1+iF)\left[1+iF\left(1+\frac{C_n^2}{\hat{U}^2}\right)\right]} \\ C^2 &= \frac{\gamma k T}{m} \\ Q &= N_e \simeq \frac{e\rho_o}{m_i} \end{aligned}\right\} \qquad (2\text{-}78)$$

These expressions will now be used to find the explicit dispersion relationships for the four cases mentioned above.

2.4.1 Wave Propagation Perpendicular to Magnetic Field. - The relation between the propagation vector and magnetic field vector in this case is such that $\vec{k}$ is perpendicular to $\vec{b}_o$. For convenience $\vec{k}$ will be taken parallel to the x-axis. Equation (2-69) now reduces to:

$$\left.\begin{bmatrix} w_{11} & w_{12} & 0 \\ w_{21} & w_{22} & 0 \\ 0 & 0 & w_{33} \end{bmatrix} \begin{bmatrix} v_x' \\ v_y' \\ v_z' \end{bmatrix} = \begin{bmatrix} 0 \\ 0 \\ 0 \end{bmatrix}\right\} \qquad (2\text{-}79)$$

where:

$$w_{11} = (a_1 + a_2) + \frac{1}{c_o^2}\{c_3(c_3c_4 - 2c_1c_6) - [2c_2(c_3c_6) + (c_1 + c_2)^2 c_4 + c_3^2 c_5]\}$$

A

$$w_{12} = -\frac{1}{c_o^2}\{(c_1 + c_2)(c_3c_4 + c_1c_6) + c_3[c_3c_6 - c_1(c_4 + c_5)]\}$$

$$w_{21} = -\frac{1}{c_o^2}\{(c_1 + c_2)(c_3c_4 - c_1c_6) + c_3[c_3c_6 + c_1(c_4 + c_5)]\} \qquad (2\text{-}80)$$

$$w_{22} = a_1 + \frac{1}{c_o^2}\{c_3(c_3c_4 - c_1c_6) - c_1[c_3c_6 + c_1(c_4 + c_5)]\}$$

$$w_{33} = a_1 - \frac{c_1^2}{c_4}$$

and:

$$c_o^2 = c_4(c_4 + c_5) + c_6^2$$

Equation (2-79) implies the existence of a transverse wave, linearly polarized in the direction of the magnetic field. Hence:

$$w_{33} = 0 \qquad (2\text{-}81)$$

is required, since v_z' may have any value that is consistent with the linearization used in deriving (2-65). For moderately strong plasma-neutral coupling (2-81) can be expressed as follows, when the appropriate substitutions are made:

$$\frac{\omega^2}{\kappa^2 c^2} = 1 - \frac{\Omega^2}{\kappa^2 c^2\left(1 + i\frac{\nu}{\omega}\right)} \qquad (2\text{-}82)$$

where:

$$\nu = \frac{\rho}{\rho_n}\left(1 + \frac{\rho}{\rho_n}\right)\left(\frac{a\gamma}{\beta^2} - 1\right)a$$

and

$$\Omega^2 = \frac{\rho}{\rho_n}\left(1+\frac{\rho}{\rho_n}\right)\left(\frac{c}{U_o}\right)^2\left(\frac{B_o}{\beta}\right)^2\alpha^2$$

A This is essentially, a result obtained in magneto-ionic theory for electromagnetic waves which are altered by the charged particle response to the radiation fields. Such disturbances can propagate without attenuation when $\nu = 0$ and $\omega > \Omega$; but the attenuation is a fairly complicated function of ω if ν is allowed arbitrary values. For ν tending to infinity, the phase velocity operator (ω/κ) is real, and the wave propagation is non-dispersive and unattenuated. The phase velocity is therefore equal to the speed of light in a vacuum.

The system of equations in the v_x' and v_y' components of (2-79) imply a coupling of longitudinal and transverse disturbances. Physically, this is due to the charged particles which are moving in the direction of propagation being subjected to a Lorentz force from the presence of $\vec{B}_o$. The dispersion equation is:

$$w_{11}w_{22} - w_{21}w_{12} = 0 \qquad (2\text{-}83)$$

When expanded, this expression is a complicated fourth order equation in k. It has been amply discussed in Reference 2-1 for very high and very low wave frequencies, showing that at low frequencies coupled acoustic and magneto-hydrodynamic waves involving the entire gas occur. As the frequency is increased, several critical regions are passed, with the oscillations eventually going from plasma acoustic waves to ion acoustic waves. A qualitative description of the complicated wave behavior for propagation across the magnetic field is presented in Figure 2-1, which is reproduced from that article.

2.4.2 Longitudinal Wave Propagation Parallel to Magnetic Field. - In this instance (2-69) can be expanded to:

$$\begin{bmatrix} w_{11} & w_{12} & 0 \\ -w_{12} & w_{11} & 0 \\ 0 & 0 & w_{33} \end{bmatrix}\begin{bmatrix} v_x' \\ v_y' \\ v_z' \end{bmatrix} = \begin{bmatrix} 0 \\ 0 \\ 0 \end{bmatrix} \qquad (2\text{-}84)$$

MHD Wave Investigation

II - theory

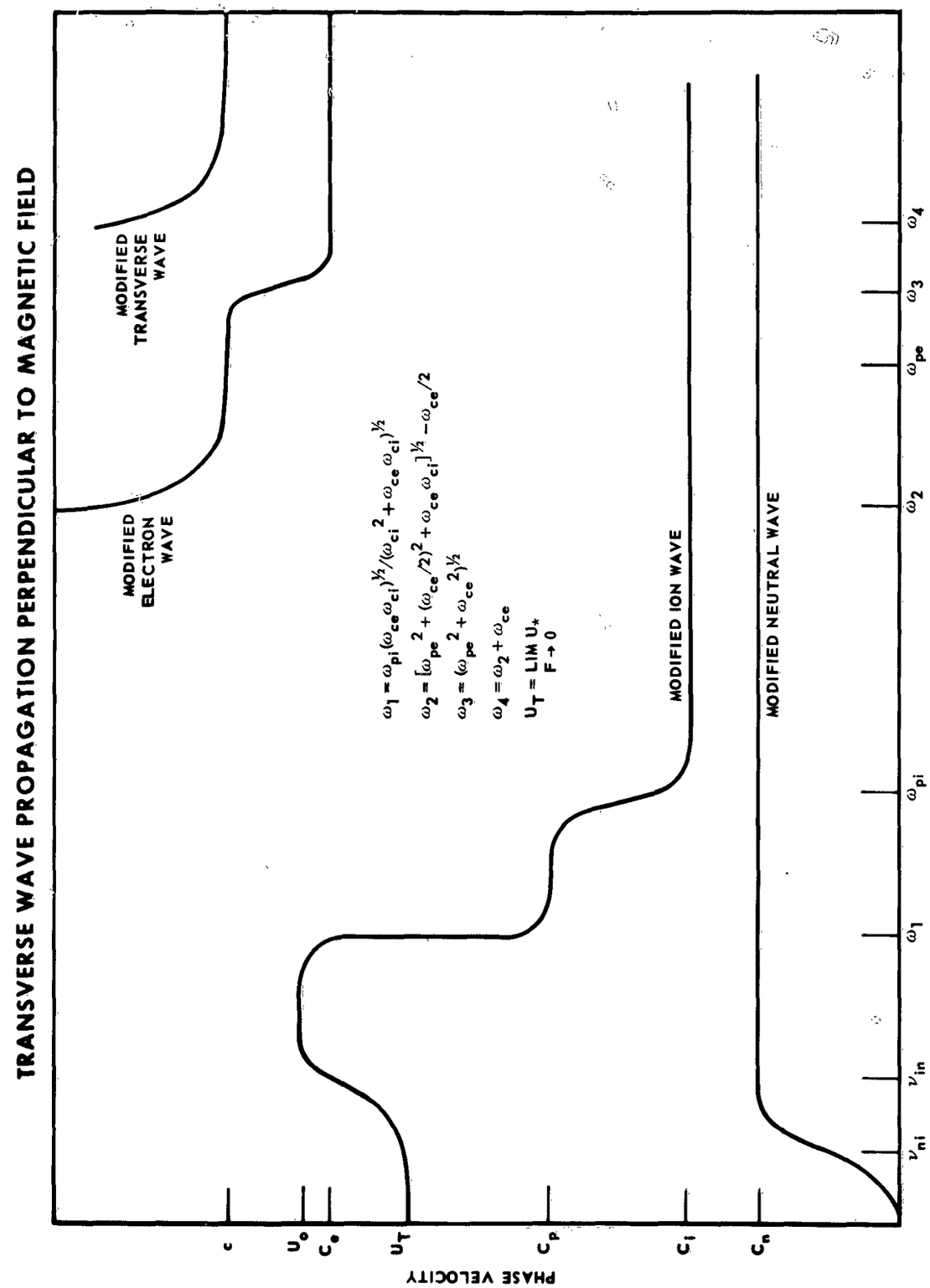

FIGURE 2-1

with:

$$w_{11} = a_1 - \frac{1}{c_o^2}\left[c_1(c_1c_4 + c_3c_6) - c_3(c_3c_4 - c_1c_6)\right]$$

$$w_{12} = \frac{1}{c_o^2}\left[c_3(c_1c_4 + c_3c_6) + c_1(c_3c_4 - c_1c_6)\right] \qquad (2\text{-}85)$$

$$w_{33} = a_1 + a_2 - \frac{(c_1 + c_2)^2}{c_4 + c_5}$$

and:

$$c_o^2 = c_4^2 + c_6^2$$

Again, an appropriate solution exists if:

$$w_{33}\,(w_{11}^2 + w_{12}^2) = 0 \qquad (2\text{-}86)$$

Since the ν_z component for a longitudinal wave cannot be identically zero, the requirement for wave propagation becomes:

$$w_{33} = 0 \qquad (2\text{-}87)$$

As pointed out by Reference 2-1, examination of the dispersion equation (2-87) reveals that at low frequencies the constituent gases unify, and an acoustic wave with velocity characteristic of the entire gas is propagated. When $\omega > \text{Max}\,[\nu_{in}, \nu_{ni}]$ the coupling factor $(1/F)$ becomes quite small for low degrees of ionization. Hence, two acoustic waves, one associated with the plasma and another with the neutral gas, are disseminated. As ω becomes even larger, such that $\omega \sim \omega_{ci}$, the plasma breaks up. At this point an ion acoustic wave and an electron acoustic wave propagate with their separate phase velocities going to the appropriate acoustic velocities. In the range $\omega_{ci} < \omega < \omega_{ce}$, the wave velocity mathematically may exceed c by a considerable amount. This may be interpreted as a "stiffening" of the electron gas, or a velocity resonance condition. When the phase velocity of the electron disturbance is greater than c or the wavelengths become so short that the continuum assumptions in the basic equations are invalid, the wave cannot be regarded as a physical entity.

Such conditions exist in part of the range $\omega_{ci} < \omega < \omega_{ce}$.

2.4.3 Transverse Wave Propagation Parallel to Magnetic Field. - For the over-all objectives of the program this case is the most relevant. As will be shown in the ensuing discussions, a singularily important type of wave, called an Alfvén wave, emerges. This wave usually prevails for a wide range of disturbance frequencies. At the higher frequencies $\omega > \omega_{ci}$, the transverse waves of the magneto-ionic theory come into existance.

The proper dispersion equation is again derived from equation (2-69). Now, however, v_z' must be identically zero, while v_x' and v_y' cannot both vanish. Thus, from (2-69):

$$\begin{bmatrix} w_{11} & w_{12} \\ -w_{12} & w_{11} \end{bmatrix} \begin{bmatrix} v_x' \\ v_y' \end{bmatrix} = \begin{bmatrix} 0 \\ 0 \end{bmatrix} \tag{2-88}$$

Therefore:

$$w_{11}^2 + w_{12}^2 = 0 \tag{2-89}$$

is required. This implies that:

$$w_{11} = \pm i w_{12} \tag{2-90}$$

If this result is then used in (2-88) it is found that:

$$v_x' = \pm i v_z' \tag{2-91}$$

or that the transverse waves are circularly polarized. When viewed along the normal to the plane of rotation, the plus sign is seen to properly represent a left circularly polarized wave (LCP), and the minus sign, a right circularly polarized wave (RCP). Expanding (2-90) yields:

$$a_1 (c_4^2 + c_6^2) - [(c_1 c_4 + c_3 c_6) \pm i (c_3 c_4 - c_1 c_6)](c_1 \pm i c_3) = 0 \tag{2-92}$$

After substituting the values from (2-76) and (2-77) and manipulating the resulting expression, while neglecting $(\hat{U}/c)^2$ as compared to unity, the

dispersion relationship becomes:

$$(\hat{U}^2 \pm \frac{\omega}{\omega_o} U_o^2) - U_*^2 \left(1 \pm i \frac{\beta_*}{B_o}\right)^2 - i\omega \lambda_* = 0 \qquad (2\text{-}93)$$

A If the gas is not stationary but moving with velocity $\vec{V}_o$ along $\vec{\imath}_z$, equation (2-93) is modified to

$$\left(\hat{U}^2 \pm \frac{\omega}{\omega_o} U_o^2\right)\left(1 + \frac{V_o}{\hat{U}}\right) + U_*^2 \left(1 \pm i \frac{\beta_*}{B_o}\right)^2 + i\omega\lambda_* \left(1 + \frac{V_o}{\hat{U}}\right) = 0 \qquad (2\text{-}94)$$

In these equations:

$$\omega_o = \frac{e B_o}{m_i - m_e}$$

$$U_o^2 = \frac{B_o^2}{\mu_o \rho_o} \qquad (2\text{-}95)$$

$$U_*^2 = \frac{B_o^2}{\mu_o \rho_*}$$

These quantities are the modified cyclotron frequency, the Alfvén velocity for a fully ionized gas and the Alfvén velocity operator for a partially ionized gas. It is the reciprocal of ω_o , as it appears in (2-93), that has physical meaning thus:

$$\frac{1}{\omega_o} = \frac{m_i - m_e}{e B_o} = \frac{1}{\omega_{ci}} - \frac{1}{\omega_{ce}}$$

which is the difference in the time required for an ion and an electron to subtend one radian of arc about the $\vec{B}_o$ field "lines". In a fully ionized medium $\frac{U_o}{\omega_o}$ is just the distance a constant phase point of the Alfvén wave moves in the time $\frac{1}{\omega_o}$.

At low frequencies $\omega \ll \frac{\rho_o a}{\rho_{no}}$, and therefore, $1/F \gg 1$, indicating strong coupling. At these frequencies ρ_* is essentially the total gas density $(\rho_o + \rho_{no})$. Thus, the Alfvén velocity operator is real and becomes the Alfvén velocity for the whole gas, that is:

$$U_* = \frac{B_o}{\sqrt{\mu_o (\rho_o + \rho_{no})}} \qquad (2\text{-}96)$$

When $\omega \gtrsim \frac{\rho_o a}{\rho_{no}}$, the coupling is weak and U_* is complex, then U_o is the Alfvén

velocity of the plasma, and the role of the neutral gas is to dissipate the wave energy through the plasma-neutral collisions. It can be shown (Reference 2-2) that for

$$\omega \gg \text{Min}\left[\omega_{ci}, \frac{\omega_{ci}\,\omega_{ce}}{\nu_{ei}+\nu_{en}}\right] \qquad (2\text{-}97)$$

the dispersion equation (2-93) becomes that of magneto-ionic theory for wave propagation along a magnetic field (Reference 2-4).

Equation (2-93) is the dispersion relationship which determines the existence or non-existence of an Alfvén type plane wave under the conditions of total gas neutrality, negligible gravitational gradients and turbulence, scalar gas pressure and small transverse perturbations of a stationary gas. The positive and negative signs imply that there are different dispersion equations for left and right circularly polarized plane waves.

2.4.3.1 The Wave Equation for Alfvén Waves in a Partially Ionized Gas. - An examination of the wave equation to which (2-93) applies is useful for several reasons. A better understanding can be obtained of what combination of basic parameters (collision frequencies, cyclotron frequencies, densities, etc.) are effective in defining the spatial characteristics of a wave. The use of the classical form of a wave equation allows a somewhat easier analysis in situations involving boundary conditions. In addition Alfvén wave existence criteria may be readily formulated from the wave equation. To derive this equation in such a way that it explicitly displays the perturbed component of the magnetic flux density, a directly measurable variable, equation (2-68) is solved for $\vec{j}'$ and (2-45) is used to get an equation similar to (2-68) but in terms of $\vec{b}'$. Combining the restrictions in Section 2.4, which were used for the specialized dispersion relationship, with the form of (2-88) to eliminate the pressure terms, equations (2-52) and (2-53) with (2-44) and (2-45) can be combined to give:

$$\vec{b}' + \frac{U_*^2}{\omega^2}\nabla\times\left\{\left[(\nabla\times\vec{b}')\times\vec{i}_z\right]\times\vec{i}_z\right\} + \left[\frac{\beta_*^2 U_*^2}{\omega^2 B_o^2} - i\frac{\lambda_*}{\omega}\right]\left[\nabla\times\nabla\times\vec{b}'\right] + \frac{2\beta_* U_*^2}{\omega^2 B_o} - i\frac{U_o^2}{\omega\omega_o}\left\{\nabla\times\left[(\nabla\times\vec{b}')\times\vec{i}_z\right]\right\} = 0 \qquad (2\text{-}98)$$

where terms in $(U/c)^2$ and (V_o/U) have been neglected. The complex operator $i\vec{\kappa}$ has been replaced by the differential operator ∇ in this expression. If (2-98) is multiplied by $(-\omega^2)$ and the operator substitution $i\omega = \partial/\partial t$ is used, equation (2-98) is found to be the desired general Alfvén wave equation. For plane waves in an unbounded medium, equation (2-93) is the corresponding dispersion relationship. If an experiment is performed in a cylindrical chamber, where the geometry is such that the radial dimension is sufficiently less than the length, and the constant magnetic field B_o is along the cylinder axis, the apparatus is referred to as a hydromagnetic (HM) wave guide (Reference 2-5). Under such circumstances, cylindrical coordinates are used in (2-98), and a dispersion relationship which exhibits discrete frequency modes is acquired from the usual conditions on a solution to the differential equation. Since nearly fully ionized stationary gases can be produced in an HM wave guide, the assumption of a complete plasma medium is warranted. In the next section, a discussion of the wave equation for a fully ionized gas and a development of the wave equation for wave guides are presented.

2.4.3.2 The Wave Equation for Alfvén Waves in a Fully Ionized Gas. - Appendix A is a derivation of the wave equation for a fully ionized gas using the original approach of Alfvén; however, it is instructive to examine equation (2-98) in this case and compare the result with that found in the Appendix. By dividing (2-98) by the coefficient of its second term and defining:

$$\left.\begin{aligned} \xi &= \frac{\omega^2}{U_*^2} \\ \zeta &= \frac{\beta_*^2}{B_o^2} - i\,\frac{\lambda_*\omega}{U_*^2} \\ \psi &= 2\frac{\beta_*}{B_o} - i\,\frac{U_o^2\omega}{U_*^2\omega_o} \end{aligned}\right\} \qquad (2\text{-}99)$$

equation (2-98) can be written as:

$$\xi\vec{b}' + \nabla\times\{\vec{\imath}_z\times[\vec{\imath}_z\times\nabla\times\vec{b}']\} + \zeta[\nabla\times(\nabla\times\vec{b}')] - \psi\nabla\times[\vec{\imath}_z\times(\nabla\times\vec{b}')] = 0 \qquad (2\text{-}100)$$

After repeated use of certain vector identities and rearranging terms, equation (2-100) further reduces to:

$$\nabla^2(\zeta\vec{b}' - b_z'\vec{\imath}_z) - \psi(\nabla\times\frac{\partial b'}{\partial z}) + \vec{\imath}_z\times(\nabla\times\frac{\partial\vec{b}'}{\partial z}) - \xi\vec{b}' = 0 \qquad (2\text{-}101)$$

For complete ionization of a stationary gas, the following conditions exist:

The neutral density ρ_n is zero, and consequently.

$$\alpha = \beta = 0$$

and:

$$\gamma \approx \frac{m_i m_e \nu_{ei}}{e^2} \qquad (2\text{-}102)$$

Since F remains finite:

$$\left.\begin{aligned} \beta_* &= 0 \\ \lambda_* &= \frac{\gamma}{\mu_o\rho_o} \\ U_* &= U_o \end{aligned}\right\} \qquad (2\text{-}103)$$

Therefore:

$$\left.\begin{aligned} \xi &= \frac{\omega^2}{U_o^2} \\ \zeta &= -i\,\frac{\nu_{ei}\,\omega}{\omega_{ce}\omega_{ci}} \\ \psi &= -i\,\frac{\omega}{\omega_{ci}} \end{aligned}\right\} \qquad (2\text{-}104)$$

where the approximation $m \approx m_i$ has been used. After substituting (2-104), equation (2-101) becomes:

$$\frac{i\omega\nu_{ei}}{\omega_{ce}\omega_{ci}}\nabla^2\vec{b}'+\nabla^2 b_z'\vec{\imath}_z-\vec{\imath}_z\times\left(\nabla\times\frac{\partial\vec{b}'}{\partial z}\right)-i\frac{\omega}{\omega_{ci}}\nabla\times\frac{\partial\vec{b}'}{\partial z}+\frac{\omega^2}{U_o^2}\vec{b}'=0 \qquad (2\text{-}105)$$

Alfvén's result, equation (A-29), can be written in the form:

$$\frac{i\omega}{U_o^2\mu_o\sigma}\nabla^2\vec{b}'+\frac{\partial^2\vec{b}'}{\partial z^2}+\frac{\omega^2}{U_o^2}\vec{b}'=0 \qquad (2\text{-}106)$$

The assumption that $\omega \ll \omega_{ci}$ is at least reasonable, if not necessary, when discussing Alfvén waves; hence, the fourth term in (2-105) may be neglected. Upon substituting for U_o and recalling from (2-60) the expression for the conductivity, the coefficient of $\nabla^2\vec{b}'$ in (2-106) is seen to be just that of the corresponding term in (2-105). By expanding the third term in (2-105) it is found that:

$$\vec{\imath}_z\times\left(\nabla\times\frac{\partial\vec{b}'}{\partial z}\right)=\frac{\partial^2\vec{b}'}{\partial z^2}-\nabla\frac{\partial b_z'}{\partial z} \qquad (2\text{-}107)$$

Hence the terms $\nabla^2 b_z'\vec{\imath}_z$ and $\nabla\frac{\partial b_z'}{\partial z}$ that are present in (2-105), are missing from (2-106). For transverse wave disturbances, however, these two terms vanish, and either equation is valid. Expressing ∇^2 in cylindrical coordinates with j_z along the wave guide axis, equation (2-106) in matric form becomes

$$\begin{bmatrix}\hat{\Omega}-\frac{1}{r^2} & -\frac{2\partial}{r^2\partial\theta} & 0\\ \frac{2\partial}{r^2\partial\theta} & \hat{\Omega}-\frac{1}{r^2} & 0\\ 0 & 0 & \hat{\Omega}\end{bmatrix}\begin{bmatrix}b_r'\\ b_\theta'\\ b_z'\end{bmatrix}=\begin{bmatrix}0\\0\\0\end{bmatrix} \qquad (2\text{-}108)$$

where the operator $\hat{\Omega}$ is given by:

$$\hat{\Omega}=\frac{i\omega}{U_o^2\mu_o\sigma}\nabla^2_{r,\theta,z}+\frac{\partial^2}{\partial z^2}+\frac{\omega^2}{U_o^2} \qquad (2\text{-}109)$$

The electric field E can be expressed by (2-32) with $\vec{j} = \sigma \vec{E}$. For the longitudinal components, Gould (Reference 2-6) writes:

$$b'_z = \sum_{s,n} C_{sn} J_n(\Gamma_{sn} r) e^{i(\omega t - K_{sn} z - n\theta)} \tag{2-110}$$

and

$$E'_z = \sum_{s,n} D_{sn} J_n(\Lambda_{sn} r) e^{i(\omega t - K_{sn} z - n\theta)} \tag{2-111}$$

where J_n is the n-th order Bessel function, K_{sn} is the longitudinal wave number and Γ_{sn} is related to Λ_{sn} by:

$$\Lambda_{sn}^2 = \Gamma_{sn}^2 \left[\frac{(U_o/c)^2 - 1/\zeta}{(U_o/c)^2 + 1/(1-\zeta)} \right] \tag{2-112}$$

with:

$$\Gamma_{sn}^2 = \frac{\omega^2}{c^2} + \frac{1}{U_o^2(1-\zeta)} - K_{sn}^2 \tag{2-113}$$

These are determined by the boundary condition imposed on either b'_z or E'_z. The coefficients C_{sn} and D_{sn} are calculated by utilizing the orthogonality property of the Bessel functions and the physical specifications of the wave exciter. The transverse $\vec{b}'$ and $\vec{E}'$ components, which cause the torsional mode, may be found by first substituting (2-110) and (2-111) into (2-108), and making use of (2-112). Rather than using this method, the equations for b'_z and E'_z are used for the discussion of transverse modes for n = 0, which is of primary importance to investigations in the EM wave guide. For Alfvén waves the displacement current is negligible compared to the conduction current. Using (2-113) in (2-112) and discarding the terms U_o^2/c^2 and the terms ω^2/c^2, which are absent in (2-98), the dispersion equation applicable to the propagation of Alfvén waves in a wave guide is found to be:

$$\Lambda_{so}^2 + (1 - 1/\zeta) K_{so}^2 = 0 \tag{2-114}$$

for the circularly symmetric modes (n = 0).

The solutions of transverse wave dispersion equations for an unbounded

medium and a hydromagnetic wave guide were considered very important to the achievement of the over-all program objectives. It was, therefore, desirable to investigate these equations for a wide variety of plasma conditions in order to obtain qualitative and quantitative information as to the existence and propagation characteristics of Alfvén waves in both the laboratory apparatus and the ionosphere.

2.4.4 Parametric Analysis of Transverse Wave Dispersion Equations. - A parametric study is valuable in analysis when the situation under investigation is very complicated, or when the number and range of parameter values to be considered is great. Both situations were found to exist when physical interpretations of the dispersion relationships were attempted for the many possible experimental and ionospheric conditions. For these reasons most investigators were forced to consider only limiting cases which, while important from a theoretical standpoint, were not always applicable to experimental conditions. To fill in the missing knowledge for non-limiting cases, and to compile quantitative information on transverse wave propagation characteristics for a large range of parameters and variable values, a program for a high speed digital computer was written. A summary of the capabilities of this program is presented in Table 2-1. The computed curves, which influenced the choice of wave exciters and detectors used in the experimental program, are discussed in section 2.5 for the HIT experiments and section 2.7 for an ionospheric model. The remainder of this section is devoted to the reformulation of equation (2-94) that was found suitable for the computer investigations.

Since the dispersion relations may be considered as polynomials in either ω or κ, they must be formulated in two different ways for computation.

Case 1

If the value of κ is specified, the solutions of the resulting polynomial in ω represent a set of characteristics frequencies which will propagate with the

TABLE 2-1

COMPUTER PROGRAM SUMMARY

INPUT (IN ORDER OF USE)	DESCRIPTION	OUTPUT	EQUATION NO.	VALIDITY
m_i/m_e	MASS RATIO	m_i/m_e	—	———
SIGN	SIGN OF WAVE POLARIZATION	S = 1: LCP WAVE DATA	2–93	$K_S = 0$
		S = −1: RCP WAVE DATA	2–93	$K_S = 0$
K_S	LONGITUDINAL WAVE NUMBER (REAL)	$K_S = 0$: FOUR COMPLEX ω_S ROOTS	2–112 (2–120)	INFINITE PLANE OR TORSIONAL WAVES IN A STATIONARY GAS ($V_o = 0$) FOR WHICH $\beta_* \ll B_o$ AND $\omega_s \ll \omega_o$.
		$K_S = 0$: ω ROOTS	2–115	INFINITE PLANE WAVES, TEST = 0
		$K_S = 0$: κ ROOTS	2–125	INFINITE PLANE WAVES: TEST = 0
V_o	GAS FLOW VELOCITY	V_o	—	INFINITE PLANE WAVES, ($K_S = 0$)
B_o	AXIAL MAGNETIC FLUX DENSITY	B_o	—	
ρ_n	NEUTRAL GAS DENSITY	ρ_n	2–7	———
ρ	PLASMA DENSITY	ρ	2–7	———
ν_{ei}	ELECTRON-ION COLLISION FREQUENCY	ν_{ei}	B–37	———
ν_{en}	ELECTRON-NEUTRAL COLLISION FREQUENCY	ν_{en}	B–37	———
ν_{in}	ION-NEUTRAL COLLISION FREQUENCY	ν_{in}	B–37	———
		(ν_{in}/ν_{en})	—	———
		ω_o	2–95	———
		a	2–15	———
		β	2–24	———
		γ	2–27	———
		R	2–7	———
		U_o	2–95	———
OPTIONS:				
ν_{in}/ν_{en}	———	———	—	———
ν_{ei}/ρ	———	———	—	———
ν_{en}/ρ_n	———	———	—	———
R	IONIZATION RATIO			
ω	WAVE ANGULAR FREQUENCY (REAL)	TWO COMPLEX κ ROOTS	2–125	INFINITE PLANE WAVES ($K_S = 0$), IN A STATIONARY GAS ($V_o = 0$)
κ	WAVE NUMBER (REAL)	FOUR COMPLEX ω ROOTS	2–115	INFINITE PLANE WAVES ($K_s = 0$)
TEST	DISPERSION EQUATION FORMULATION	TEST = 0: ω ROOTS	2–115	———
		TEST = 0: κ ROOTS	2–125	———

specified wave number. In general the characteristic frequencies are complex, the real part giving the real frequency in radians per second and the imaginary part giving the rate of decay of the wave in nepers per second.

For plane waves the general expression given in equation (2-94) may be used. This takes the following form, after substituting (2-95), (2-51) and (2-46), as restricted in section 2.4, and taking ρ_n and ρ to have essentially their undisturbed values ρ_{no} and ρ_o :

$$(A_1 + iA_2)\,x^4 + (A_3 + iA_4)\,x^3 + (A_5 + iA_6)\,x^2 + (A_7 + iA_8)\,x + (A_9 + iA_{10}) = 0 \qquad (2\text{-}115)$$

where:

$$x = i\omega$$

$$A_1 = \mu_o \omega_o r^2 \rho$$

$$A_2 = 0$$

$$A_3 = \omega_o r\,[\mu_o \alpha \rho (2 + r) + r \kappa^2 \gamma]$$

$$A_4 = r^2 (3\mu_o \omega_o \rho \kappa V_o - s \kappa^2 B_o^2$$

$$A_5 = \omega_o [(1 + r)(\mu_o \alpha^2 \rho - r \kappa^2 \beta^2) + (2 + r)(r \kappa^2 \alpha \gamma) - \kappa^2 r^2 (3\mu_o \rho V_o^2 - B_o^2)] + 3s B_o^2 \kappa^3 r^2 V_o$$

$$A_6 = r [(2 + r)\,\alpha\,(2\mu_o \omega_o \rho V_o \kappa - s\kappa^2 B_o^2) + \omega_o \kappa^2 r (2s \beta B_o + 3k V_o \gamma)] \qquad (2\text{-}116)$$

$$A_7 = \kappa^2 \{\omega_o [(1 + r)\,\alpha\,(\alpha\gamma - \beta^2) - (2 + r)\mu_o r \alpha \rho V_o^2 + 2B_o^2 r\alpha - r^2 V_o (4s \kappa \beta B_o + 3\kappa^2 V_o \gamma)] + 2s B_o^2 r\kappa\alpha V_o (2 + r)\}$$

$$A_8 = (1 + r)(\mu_o \rho \alpha^2 \kappa V_o \omega_o - 2\omega_o r \beta^2 V_o \kappa^3 - s\alpha^2 \kappa^2 B_o^2) + 2(2 + r)\,\omega_o \alpha \kappa^3 r V_o \gamma + r\kappa^2 (2r \kappa V_o \omega_o B_o^2 + 3s r \kappa^2 V_o^2 B_o^2 - \mu_o \omega_o \rho r \kappa V_o^3 + 2s \omega_o \beta B_o \alpha)$$

$$A_9 = \kappa^2 \omega_o [(1 + r) r \kappa^2 \beta^2 V_o^2 - (2 + r)\kappa^2 V_o^2 \alpha\gamma r + B_o^2 (\alpha^2 - r^2 V_o^2 \kappa^2) - 2sr\kappa V_o \beta B_o \alpha] + (1 + r)\,\alpha^2 \kappa s B_o^2 V_o - s r^2 \kappa^3 V_o^3 B_o^2\}$$

$$A_{10} = \kappa^2 V_o \{\omega_o [(1+r)\kappa a(a\gamma - \beta^2) - 2s\beta B_o r^2 \kappa^2 V_o$$
$$- \gamma r^2 \kappa^3 V_o^2 + 2a r \kappa B_o^2 + (2+r) s a r \kappa^2 B_o^2 V_o\} \qquad (2\text{-}116)$$
continued

$r = \rho_o/\rho$

$s = \pm 1$

for a stationary medium ($V_o = 0$) the coefficients (2-116) reduce to:

$$A_1 = \mu_o \omega_o r^2 \rho$$
$$A_2 = 0$$
$$A_3 = \omega_o r [\mu_o a\rho(2+r) + r\kappa^2 \gamma]$$
$$A_4 = -sr\kappa^2 B_o^2$$
$$A_5 = \omega_o [(1+r)(\mu_o a^2 \rho - r\kappa^2 \beta^2) + (2+r)(r\kappa^2 a\gamma) + \kappa^2 r^2 B_o^2] \qquad (2\text{-}117)$$
$$A_6 = sr\kappa^2 B_o [2\omega_o \beta r - a(2+r) B_o]$$
$$A_7 = a\kappa^2 \omega_o [(1+r)(a\gamma - \beta^2) + 2r B_o^2]$$
$$A_8 = s a \kappa^2 B_o [2\omega_o r\beta - a(1+r) B_o]$$
$$A_9 = a^2 \kappa^2 \omega_o B_o^2$$
$$A_{10} = 0$$

while for frequencies well below the cyclotron frequency ω_o, the coefficients become:

$$A_1 = \mu_o r^2 \rho$$
$$A_2 = 0$$
$$A_3 = r[\mu_o a\rho(2+r) + r\kappa^2 \gamma]$$
$$A_4 = 3\mu_o \rho r^2 \kappa V_o$$
$$A_5 = (1+r)(\mu_o a^2 \rho - r\kappa^2 \beta^2) + (2+r) r\kappa^2 a\gamma$$
$$- \kappa^2 r^2 (3\mu_o \rho V_o^2 - B_o^2)$$
$$A_6 = r[2\mu_o \rho a V_o \kappa (2+r) + \kappa^2 r (2s\beta B_o + 3\kappa V_o \gamma)] \qquad (2\text{-}118)$$
$$A_7 = \kappa^2 [(1+r) a(a\gamma - \beta^2) - \mu_o \rho r (2+r) a V_o^2 + 2B_o^2 r a$$
$$- r^2 V_o (4s\kappa\beta B_o + 3\kappa^2 V_o \gamma)]$$
$$A_8 = \kappa V_o (1+r)(\mu_o \rho a^2 - 2r\beta^2\kappa^2) + 2ar(2+r)\kappa^3 V_o \gamma$$
$$+ r\kappa^2 (2r\kappa V_o B_o^2 - \mu_o \rho r\kappa V_o^3 + 2s\beta B_o a)$$

$$A_9 = \kappa^2 [r(1+r)\kappa^2 \beta^2 V_o^2 - r(2+r)\kappa^2 V_o^2 \alpha\gamma$$
$$+ B_o^2(\alpha^2 - r^2 V_o^2 \kappa^2) - 2sr\kappa V_o \beta B_o \alpha]$$
$$A_{10} = \kappa^2 V_o [\kappa(1+r)\alpha(\alpha\gamma - \beta^2) - 2s\beta B_o r^2 \kappa^2 V_o$$
$$- \gamma r^2 \kappa^3 V_o^2 + 2\alpha r\kappa B_o^2] \qquad \text{(2-118) continued}$$

If both conditions are satisfied, that is, $V_o = 0$ and $\omega \ll \omega_o$, the coefficients are further simplified to:

$$A_1 = \mu_o r^2 \rho$$
$$A_2 = 0$$
$$A_3 = r[\mu_o \alpha\rho(2+r) + r\kappa^2\gamma]$$
$$A_4 = 0$$
$$A_5 = (1+r)(\mu_o \alpha^2 \rho - r\kappa^2\beta^2) + r(2+r)\kappa^2\alpha\gamma + \kappa^2 r^2 B_o^2 \qquad \text{(2-119)}$$
$$A_6 = 2sr^2\kappa^2\beta B_o$$
$$A_7 = \alpha\kappa^2[(1+r)(\alpha\gamma - \beta^2) + 2rB_o^2]$$
$$A_8 = 2s\alpha\kappa^2 r\beta B_o$$
$$A_9 = \alpha^2\kappa^2 B_o^2$$
$$A_{10} = 0$$

For torsional plane waves in a stationary gas, equation (2-112), with the definitions (2-104), (2-95) and (2-60), yields a polynomial in ω of the form:

$$\omega^4 - 2i\mu_o\sigma c^2\omega^3 - c^2(\mu_o^2\sigma^2 c^2 + \Lambda_s^2 + K_s^2)\omega^2$$
$$+ i\mu_o\sigma c^4(\Lambda_s^2 + K_s^2)\omega + \mu_o^2\sigma^2 c^4 U_o^2 K_s^2 = 0 \qquad \text{(2-120)}$$

where the subscript zero has been dropped and U_o^2/c^2 neglected.

By a change of variable from ω to $x = i\omega$, this equation may be put into the more convenient form:

$$x^4 + 2\mu_o\sigma c^2 x^3 + c^2(\mu_o^2\sigma^2 c^2 + \Lambda_s^2 + K_s^2)x^2$$
$$+ \mu_o\sigma c^4(\Lambda_s^2 + K_s^2)x + \mu_o^2\sigma^2 c^4 U_o^2 K_s^2 = 0 \qquad \text{(2-121)}$$

having all real coefficients.

Case 2

A If the value of ω is specified, the resulting polynomials in κ may be solved for a set of characteristic wave numbers. These also are generally complex valued, the real part being the wave number, in radians per meter, and the imaginary part giving the spatial rate of decay in nepers per meter.

Rearranging equation (2-120) into a polynomial in K_{so} yields the form:

$$[c^2(\omega^2 - i\mu_o\sigma c^2\omega) - \mu_o^2\sigma c^4 U_o^2]\, K_s^2 - [\omega^4 - 2i\mu_o\sigma c^2\omega^3 - c^2(\mu_o^2\sigma^2c^2 + \Lambda_s^2)\omega^2 + i\mu_o\sigma c^4\Lambda_s^2\ \omega] = 0 \qquad (2\text{-}122)$$

which is valid for torsional waves, but restricted to the special case of a stationary medium and a frequency ω much less than the cyclotron frequency

For plane waves in an unbounded medium, a rearrangement of equation (2-94) with the appropriate substitutions gives:

$$(A_1 + iA_2)\kappa^5 + (A_3 + iA_4)\kappa^4 + (A_5 + iA_6)\kappa^3 + (A_7 + iA_8)\kappa^2 + (A_9 + iA_{10})\kappa + (A_{11} + iA_{12}) = 0 \qquad (2\text{-}123)$$

where:

$$\begin{aligned}
A_1 &= sr^2 V_o^3 B_o^2 \\
A_2 &= r^2 V_o^3 \omega_o \gamma \\
A_3 &= 3sr^2 V_o^2 \omega B_o^2 - r(1+r) V_o^2 \omega_o \beta^2 + r(2+r) V_o^2 \omega_o \alpha\gamma + r^2 V_o^2 \omega_o B_o^2 \\
A_4 &= 3r^2 V_o^2 \omega_o \omega\gamma + 2sr^2 V_o^2 \omega_o \beta B_o - sr(2+r) V_o^2 \alpha B_o^2 \\
A_5 &= 3sr^2 V_o \omega^2 B_o^2 - 2r(1+r) V_o \omega\omega_o \beta^2 + 2r(2+r) V_o \omega\omega_o \alpha\gamma \\
&\quad + 2r^2 V_o \omega\omega_o B_o^2 - r^2 V_o^3 \omega\omega_o \mu_o\rho + 2sr V_o \omega_o \alpha\beta B_o \\
&\quad - s(1+r) V_o \alpha^2 B_o^2 \\
A_6 &= 3r^2 V_o \omega^2 \omega_o \gamma + 4sr^2 V_o^2 \omega_o \beta B_o - 2sr(2+r) V_o \omega\alpha B_o^2 \\
&\quad - (1+r) V_o \omega_o \alpha(\alpha\gamma - \beta^2) - 2r V_o \omega_o \alpha B_o^2
\end{aligned} \qquad (2\text{-}124)$$

$$A_7 = sr^2\omega^3 B_o^2 - r(1+r)\omega^2\omega_o\beta^2 + r(2+r)\omega^2\omega_o\alpha\gamma$$
$$- 3r^2 V_o^2\omega^2\omega_o\mu_o\rho + r^2\omega^2\omega_o B_o^2 - s(1+r)\omega\alpha^2 B_o^2$$
$$+ 2sr\omega\omega_o\alpha\beta B_o - \omega_o\alpha^2 B_o^2$$

$$A_8 = r^2\omega^3\omega_o\gamma - sr(2+r)\omega^2\alpha B_o^2 + 2sr^2\omega^2\omega_o\beta B_o$$
$$- (1+r)\omega\omega_o\alpha(\alpha\gamma - \beta^2) - 2r\omega\omega_o\alpha B_o^2 \qquad (2\text{-}124)$$
$$+ r(2+r)V_o^2\omega\omega_o\mu_o\rho\alpha \qquad \text{continued}$$

$$A_9 = (1+r)V_o\omega\omega_o\mu_o\rho\alpha^2 - 3r^2 V_o\omega^3\omega_o\mu_o\rho$$

$$A_{10} = 2r(2+r)V_o\omega^2\omega_o\mu_o\rho\alpha$$

$$A_{11} = (1+r)\omega^2\omega_o\mu_o\rho\alpha^2 - r^2\omega^4\omega_o\mu_o\rho$$

$$A_{12} = r(2+r)\omega^3\omega_o\mu_o\rho\alpha$$

Again this may be simplified for the various special cases.

(a) For a stationary medium, A_1, A_2, A_3, A_4, A_5, A_6, A_9 and A_{10} reduce to zero, leaving:

$$(A_7 + iA_8)\kappa^2 + (A_{11} + iA_{12}) = 0 \qquad (2\text{-}125)$$

with:

$$A_7 = sr^2\omega^3 B_o^2 - r(1+r)\omega^2\omega_o\beta^2 + r(2+r)\omega^2\omega_o\alpha\gamma$$
$$+ r^2\omega^2\omega_o B_o^2 - s(1+r)\omega\alpha^2 B_o^2 + 2sr\omega_o\omega\alpha\beta B_o$$
$$- \omega_o\alpha^2 B_o^2$$

$$A_8 = r^2\omega^3\omega_o\gamma - sr(2+r)\omega^2\alpha B_o^2 + 2sr^2\omega^2\omega_o\beta B_o \qquad (2\text{-}126)$$
$$- (1+r)\omega\omega_o\alpha(\alpha\gamma - \beta^2) - 2r\omega\omega_o\alpha B_o^2$$

$$A_{11} = (1+r)\omega^2\omega_o\mu_o\rho\alpha^2 - r^2\omega^4\omega_o\mu_o\rho$$

$$A_{12} = r(2+r)\omega^3\omega_o\mu_o\rho\alpha$$

(b) For $\omega \ll \omega_o$,

$$A_1 = 0$$

$$A_2 = r^2 V_o^3\gamma \qquad (2\text{-}127)$$

$$A_3 = rV_o^2[(2+r)\alpha\gamma - (1+r)\beta^2 + rB_o^2]$$

$$A_4 = r^2 V_o^2(3\omega\gamma + 2s\beta B_o)$$

$$A_5 = r V_o [2(2+r)\,\omega a\gamma - 2(1+r)\,\omega\beta^2 + 2r\omega B_o^2 - r V_o^2\,\omega\mu_o\rho + 2s\,a\beta\,B_o]$$

$$A_6 = V_o [3r^2\omega^2\gamma + 4sr^2 V_o\,\beta B_o - (1+r)\,a\,(a\gamma - \beta^2) - 2r\,a B_o^2]$$

$$A_7 = r(2+r)\,\omega^2 a\gamma - r(1+r)\,\omega^2\beta^2 - 3r^2 V_o^2\,\omega^2\,\mu_o\,\rho + r^2\omega^2\omega_o B_o^2 + 2sr\,\omega a\beta\,B_o - a^2 B_o^2 \qquad \text{(2-127) continued}$$

$$A_8 = \omega[r^2\omega^2\gamma + 2sr^2\,\omega\beta\,B_o - (1+r)\,a\,(a\gamma - \beta^2) - 2r\,a\,B_o^2 + r(2+r)\,V_o^2\,\mu_o\rho a]$$

$$A_9 = (1+r)\,V_o\,\omega\mu_o\rho a^2 - 3r^2 V_o\,\omega^3\,\mu_o\rho$$

$$A_{10} = 2r(2+r)\,V_o\,\omega^2\,\mu_o\rho a$$

$$A_{11} = (1+r)\,\omega^2\,\mu_o\rho a^2 - r^2\omega^4\mu_o\rho$$

$$A_{12} = r(2+r)\,\omega^3\,\mu_o\,\rho a$$

(c) For a stationary medium and $\omega \ll \omega_o$ all coefficients vanish except A_7, A_8, A_{11} and A_{12} leaving:

$$A_7 = r(2+r)\,\omega^2 a\gamma - r(1+r)\,\omega^2\beta^2 + r^2\omega^2 B_o^2 + 2sr\,\omega^2 a\beta\,B_o - a^2 B_o^2$$

$$A_8 = r^2\omega^3\gamma + 2sr^2\,\omega^2\beta\,B_o - (1+r)\,\omega a\,(a\gamma - \beta^2) - 2r\,\omega a\,B_o^2 \qquad \text{(2-128)}$$

$$A_{11} = (1+r)\,\omega^2\,\mu_o\,\rho a^2 - r^2\omega^4\,\mu_o\rho$$

$$A_{12} = r(2+r)\,\omega^3\,\mu_o\rho a$$

Three of the above expanded equations, (2-112), (2-115) and (2-125), were put into one computer program with the selection of the one appropriate equation being made part of the input data. Only the collision frequencies are required to be computed outside of the program.

Up to this point considerable effort has been spent establishing a reasonably firm background in the theory of MHD waves, with the bulk of the analysis concerned with Alfvén waves. The sections that follow apply part of the

theory directly and part of it indirectly through the results of the computer studies. Application is made to the three pertinent physical situations: experiments in McDonnell's hypervelocity impulse tunnel, experiments in McDonnell's arc discharge tube, and disturbances in the F-region of the ionosphere. In each case criteria for the existence of Alfvén waves and their propagation characteristics are discussed.

2.5 ALFVEN WAVES IN THE HYPERVELOCITY IMPULSE TUNNEL. - Section 3.4.2.6 establishes the plasma environment for the experiments. The various means of wave excitation and the actual experiments performed are delineated in Sections 4.1 and 7.1 of Vol. III. To utilize the computer results for an unbounded medium, the experiment instrumentation and tunnel conditions must be such that the density, temperature, ionization ratio and magnetic field are essentially constant over a characteristic distance X_o. This distance is established by the requirement that:

$$X_o > U_{ph}\, t_o \tag{2-129}$$

where:

$$t_o = \frac{Z_o}{U_{ph}} + t_m \tag{2-130}$$

with Z_o being the distance from the point of excitation to the detector and t_m, the time during which measurements are taken. Assuming this to be the experimental situation a set of "most probable" conditions was taken as a reference. Quantitative investigations in the six dimensional space of parameters were made about this set by varying one parameter at a time. These conditions and the associated primary natural frequencies are given in Table 2-2.

2.5.1 Existence of Alfvén Waves in the Tunnel. - Two approaches are taken here; one involves examination of the computer curves for wave existence, and the other utilizes a fairly obvious general criterion suggested by Watanabe (Reference 2-2). For the computer analysis approach only a limited study has been performed using equation (2-115) for ω as a function of κ, since the case

TABLE 2-2
HIT REFERENCE CONDITIONS

PARAMETER	DESCRIPTION	VALUE
m_i/m_e	MASS OF N^+ TO MASS OF ELECTRON	$2.55\ (10^4)$
ρ_n	NEUTRAL PARTICLE DENSITY CORRESPONDING TO 10^{-3} ATMOSPHERES PRESSURE	$1.72\ (10^{-4})\ kg/m^3$
R	IONIZATION RATIO, $R = \frac{\rho}{\rho + \rho_n}$	10^{-3}
T	EQUILIBRIUM TEMPERATURE	10^3 °K
V_o	GAS FLOW VELOCITY	$V_o \ll U_{ph}$
B_o	AXIAL CONSTANT MAGNETIC FLUX DENSITY	10^{-1} WEBER/m^2
ν_{en}	ELECTRON-NEUTRAL COLLISION FREQUENCY (A-37)	$1.14\ (10^7)$/SEC.
ν_{in}	ION-NEUTRAL COLLISION FREQUENCY (A-37)	$4.04(10^5)$/SEC.
ν_{ei}	ELECTRON-ION COLLISION FREQUENCY (A-37)	$1.03\ (10^6)$/SEC.
ω_{ce}	ELECTRON CYCLOTRON FREQUENCY	$1.67\ (10^9)$RAD./SEC.
ω_o	$\omega_o = \frac{e B_o}{m_i - m_e} = \omega_{ci}$, ION CYCLOTRON FREQUENCY	$6.90\ (10^5)$ RAD./SEC.

for which equation (2-125) is valid more accurately represents the conditions which existed during the HIT program. The case of interest is that for which a disturbance frequency is maintained and the spatial progress is to be measured. The computer program for determining the κ roots is not capable of handling moving plasmas, which involve a fifth order polynomial in κ (2-123); therefore, the results portrayed in Figures 2-2 through 2-14 are for stationary plasmas. Examination of these figures indicates that existence is determined by the amount of information necessary to at least ascertain the periodicity of the disturbance. Although a fairly reliable prediction might be obtained by extrapolation of a detected partial cycle, it is intuitively more desirable to detect a full cycle of the disturbance before claiming existence. This somewhat arbitrary criterion can be expressed as:

$$\delta d \geq \lambda \qquad (2\text{-}131)$$

MHD Wave Investigation

II - theory

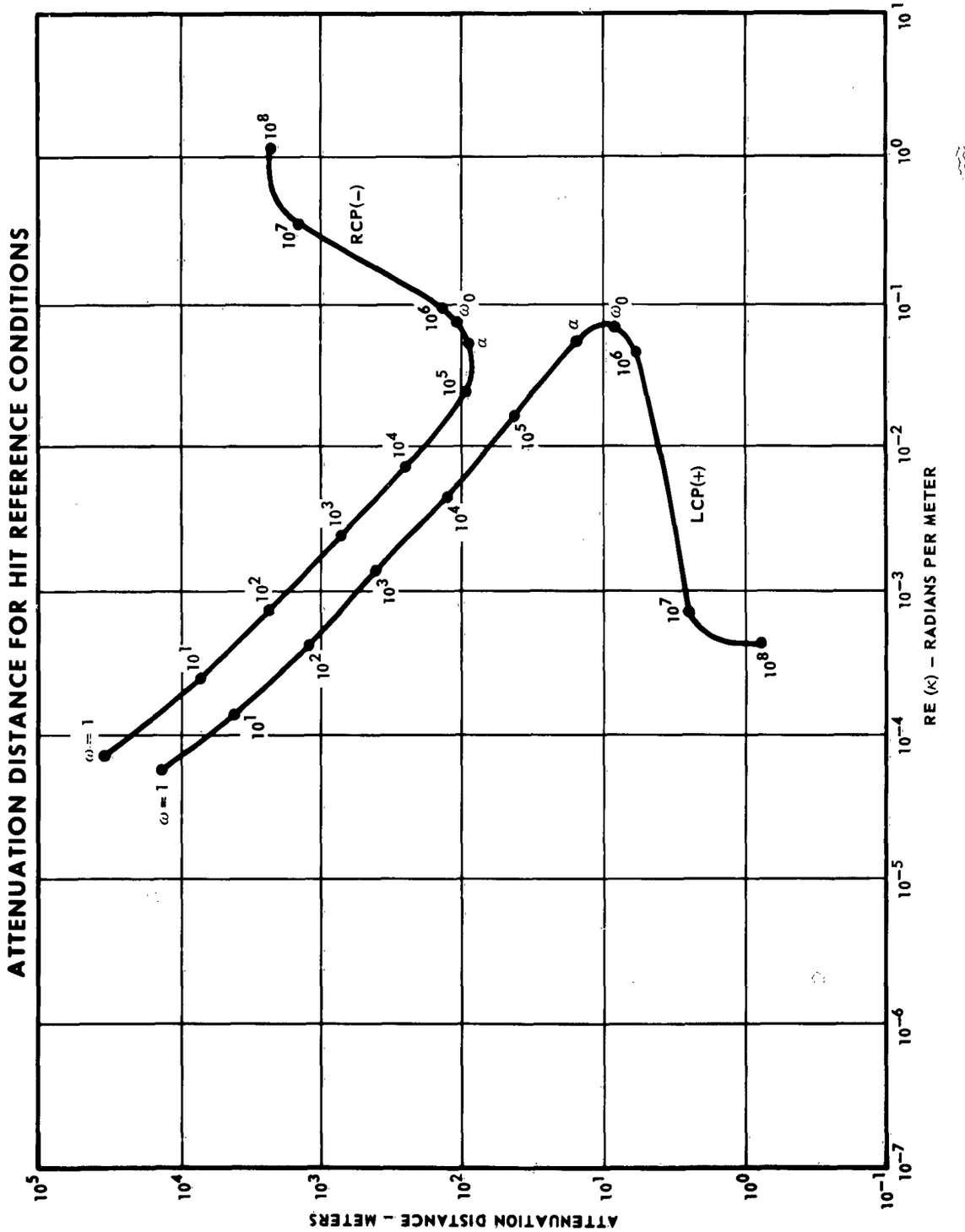

FIGURE 2-2

RATIO OF PHASE VELOCITY TO ALFVEN VELOCITY
FOR H I T CONDITIONS

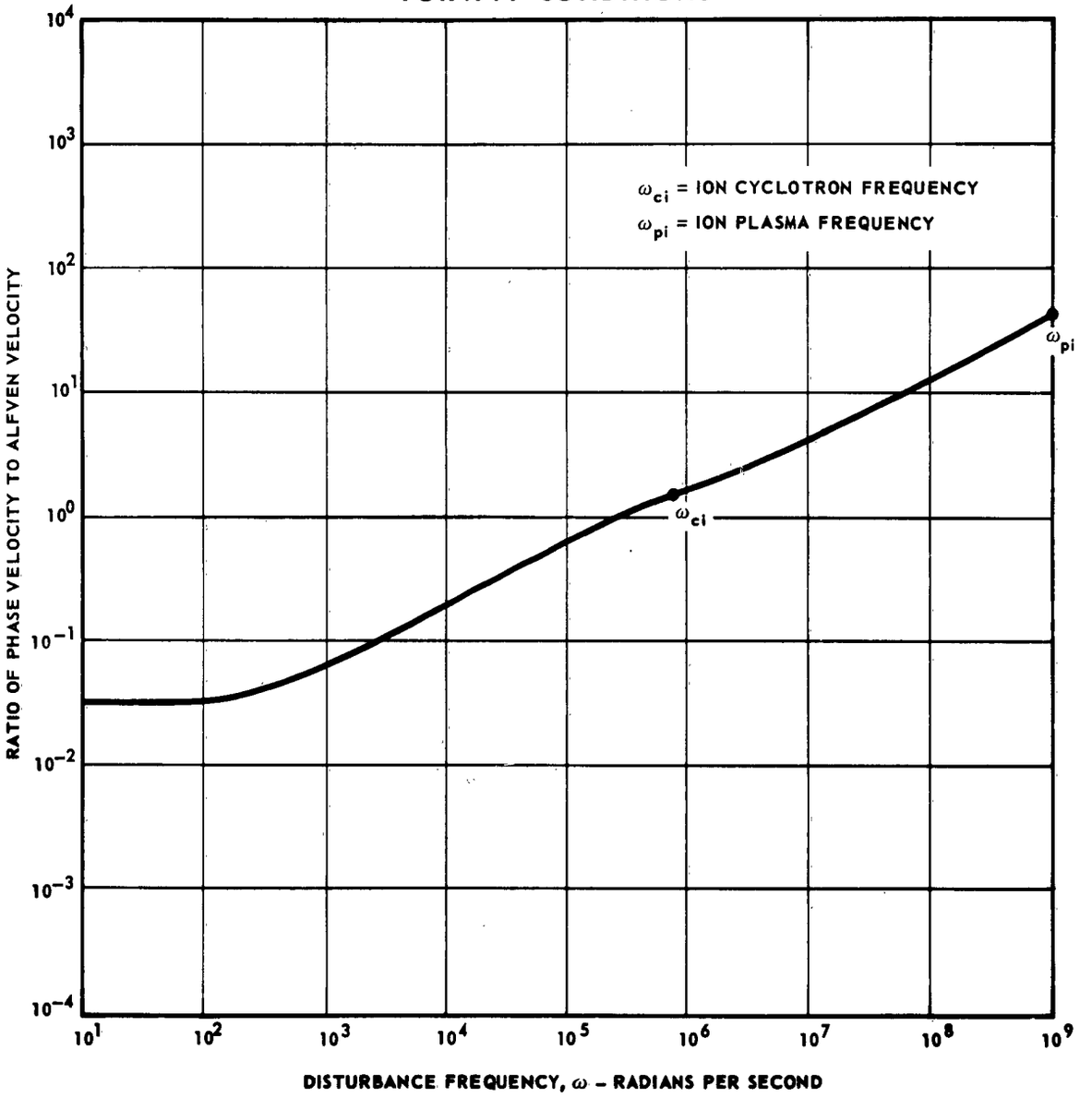

FIGURE 2-3

MHD Wave Investigation
II - theory

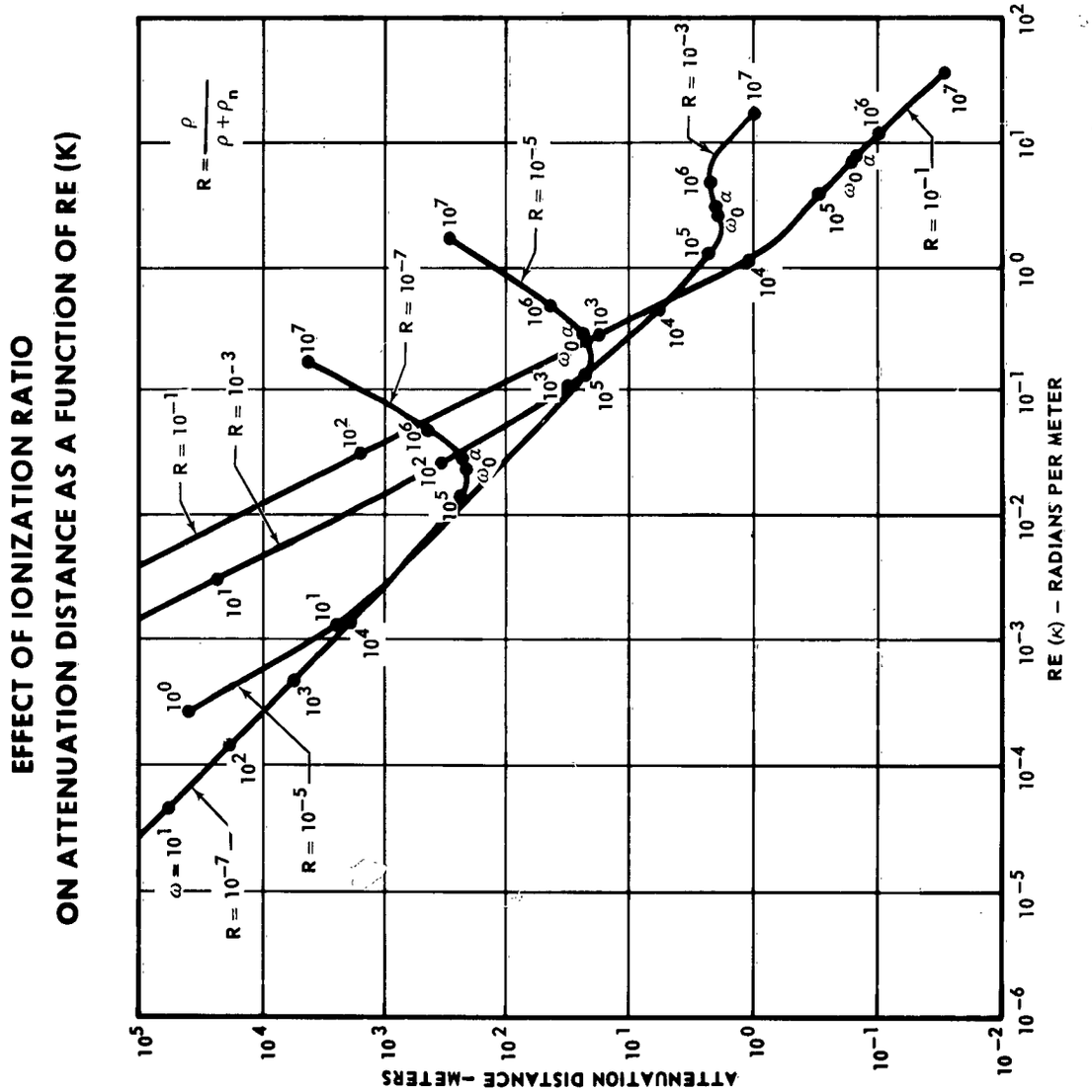

FIGURE 2-4

EFFECT OF IONIZATION RATIO ON ATTENUATION DISTANCE AS A FUNCTION OF ω

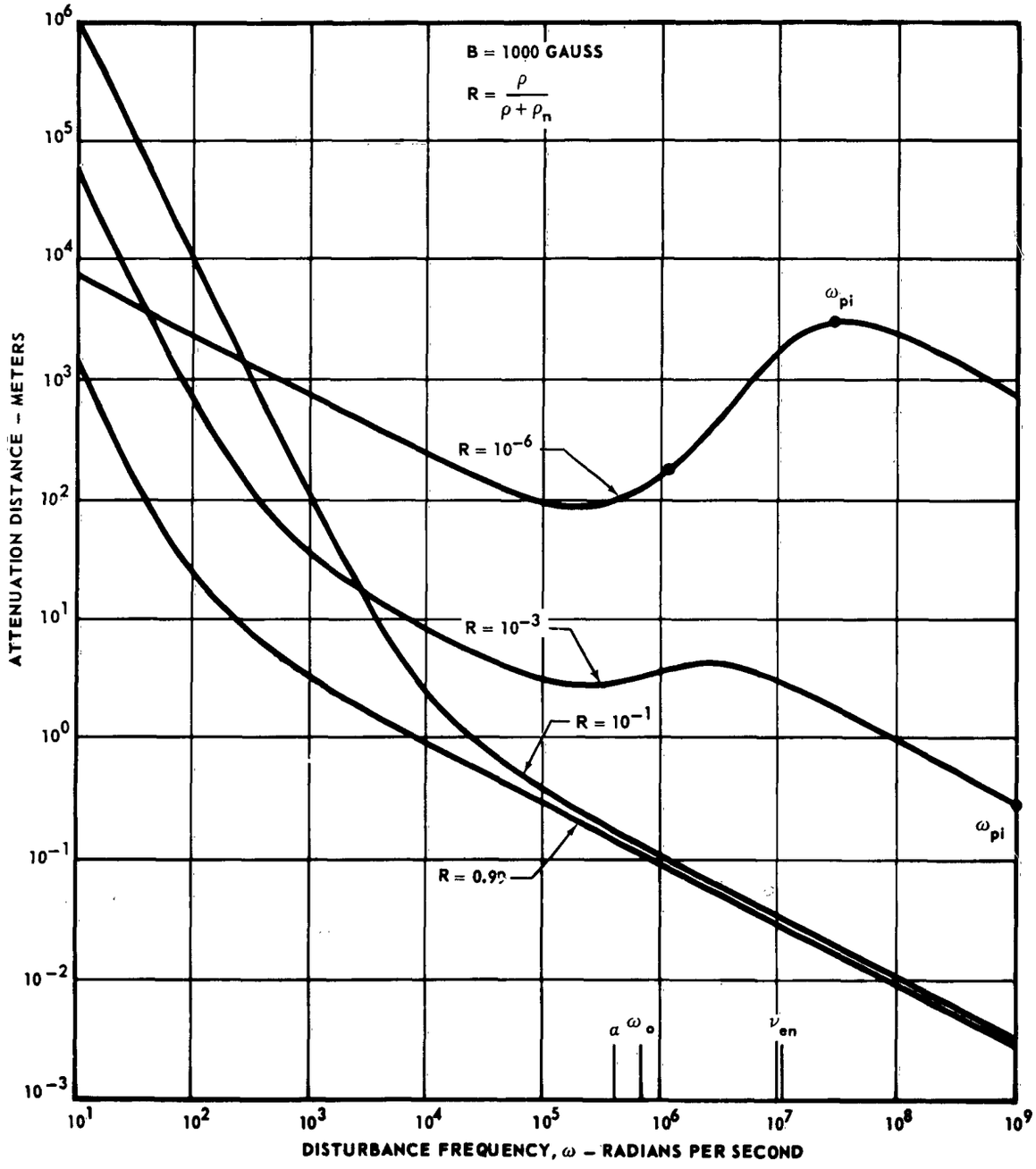

FIGURE 2-5

EFFECT OF NEUTRAL GAS DENSITY ON ATTENUATION DISTANCE

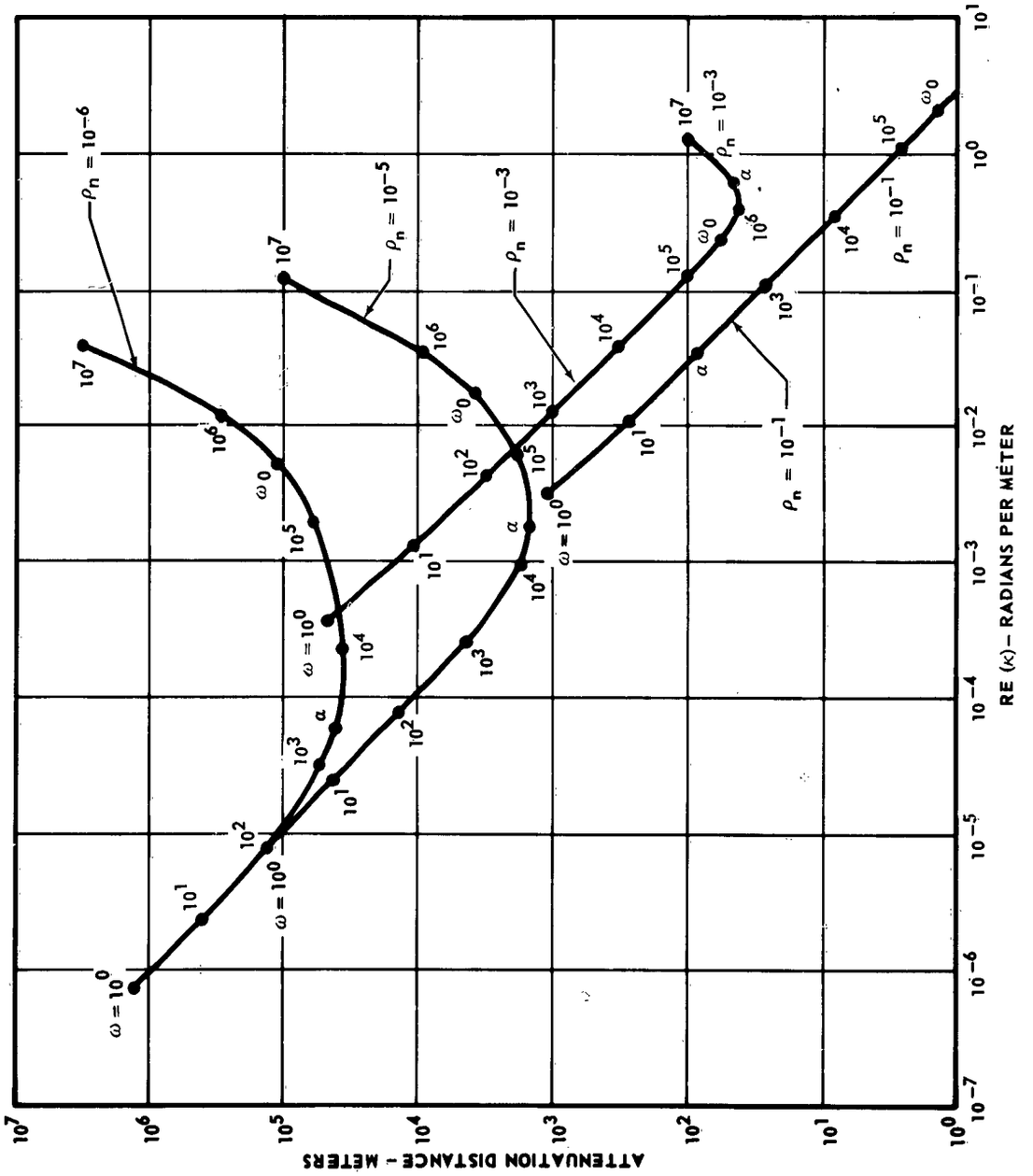

FIGURE 2-6

EFFECT OF MAGNETIC FIELD ON ATTENUATION DISTANCE AS A FUNCTION OF RE(K)

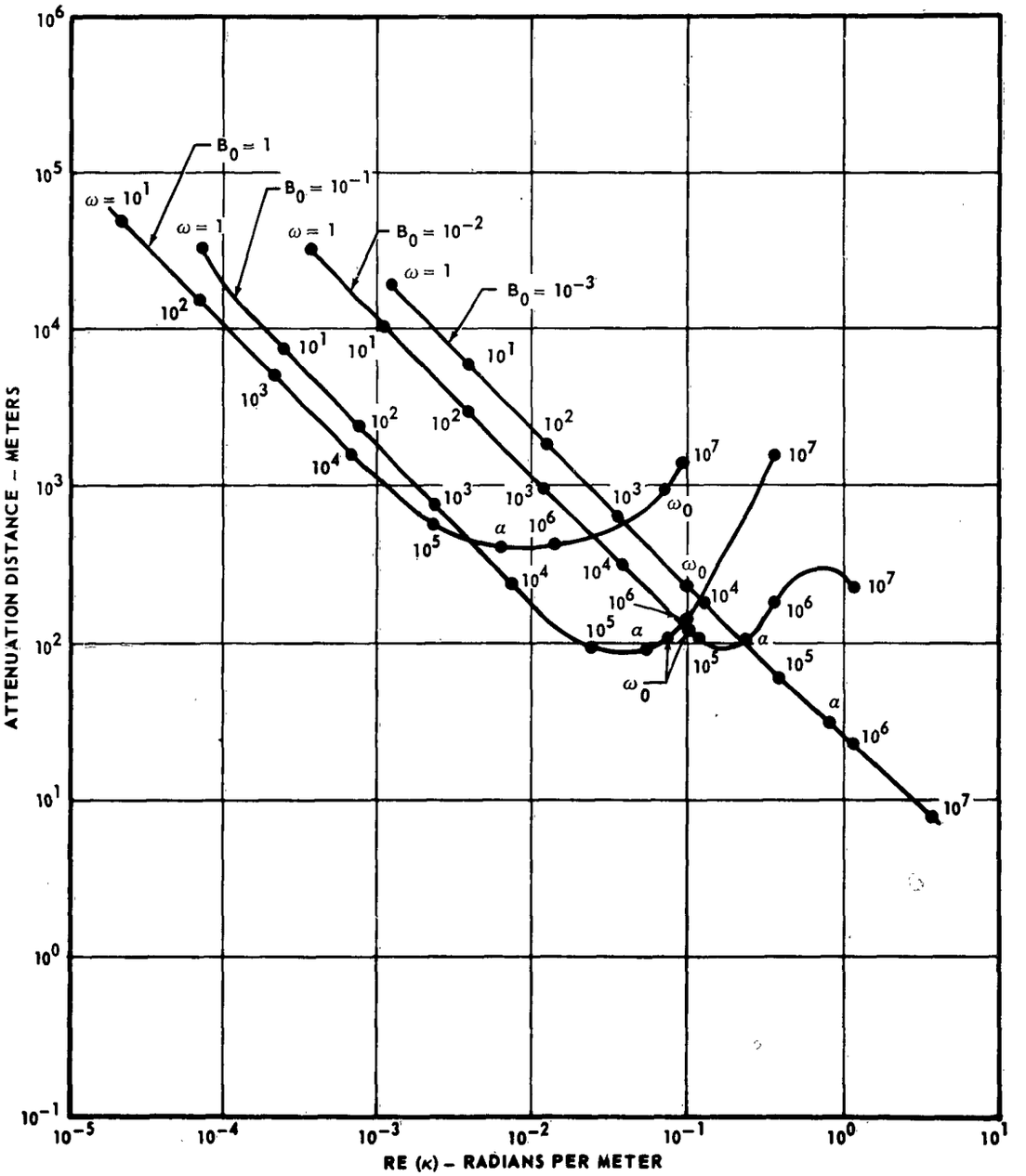

FIGURE 2-7

EFFECT OF MAGNETIC FIELD ON ATTENUATION DISTANCE AS A FUNCTION OF ω

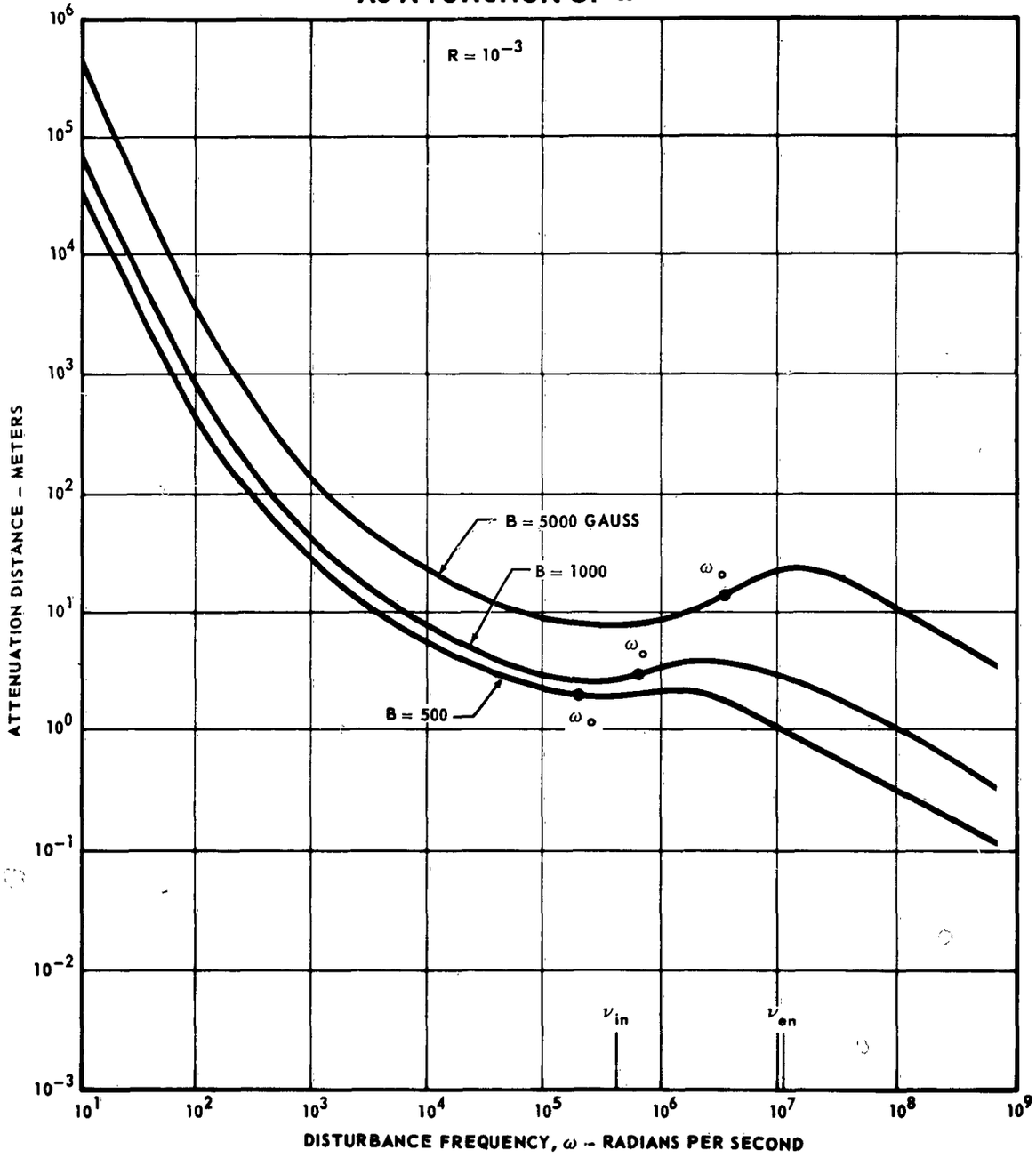

FIGURE 2-8

EFFECT OF GAS TEMPERATURE ON ATTENUATION DISTANCE

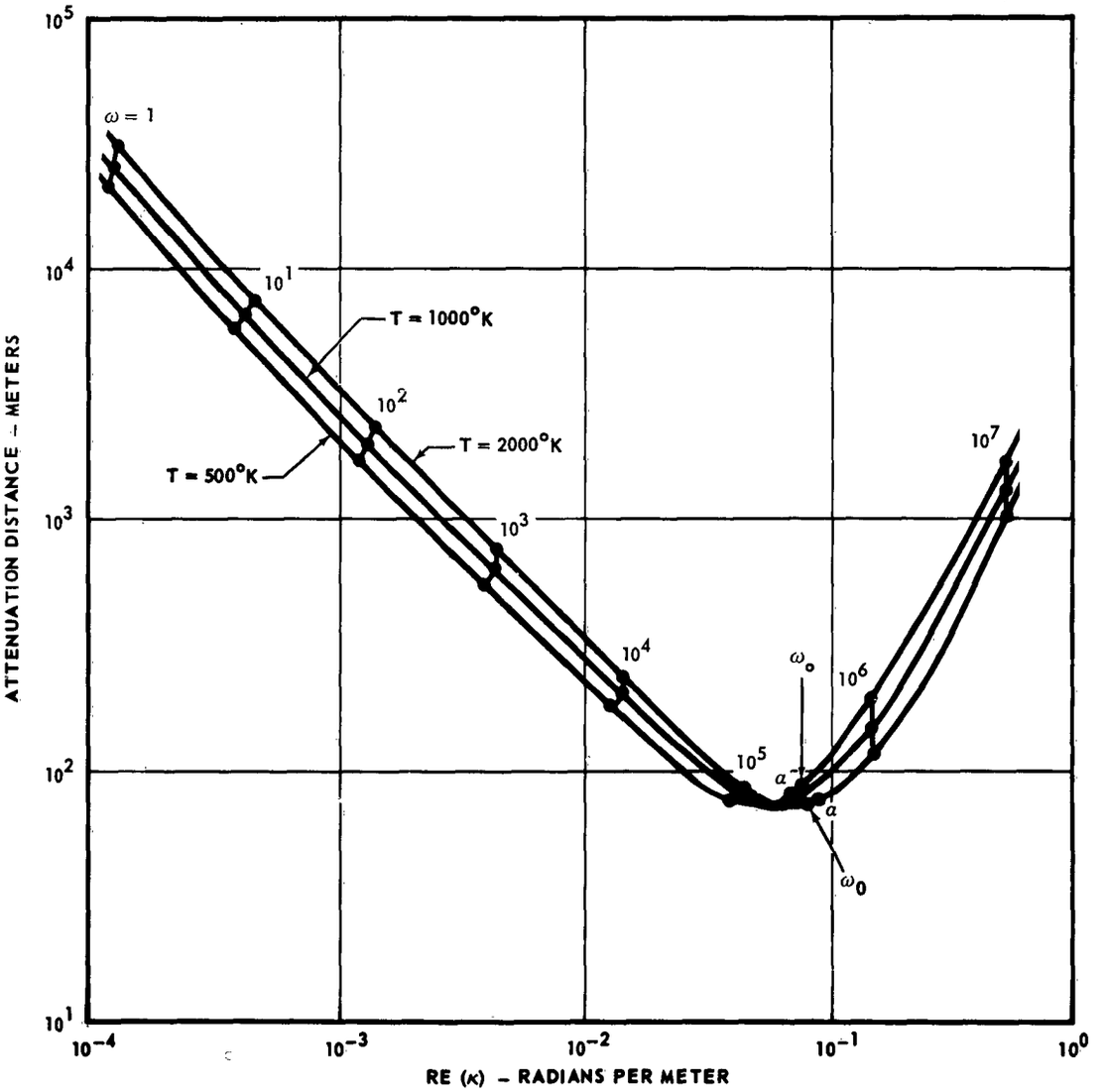

FIGURE 2-9

EFFECT OF MOLECULAR WEIGHT ON ATTENUATION DISTANCE

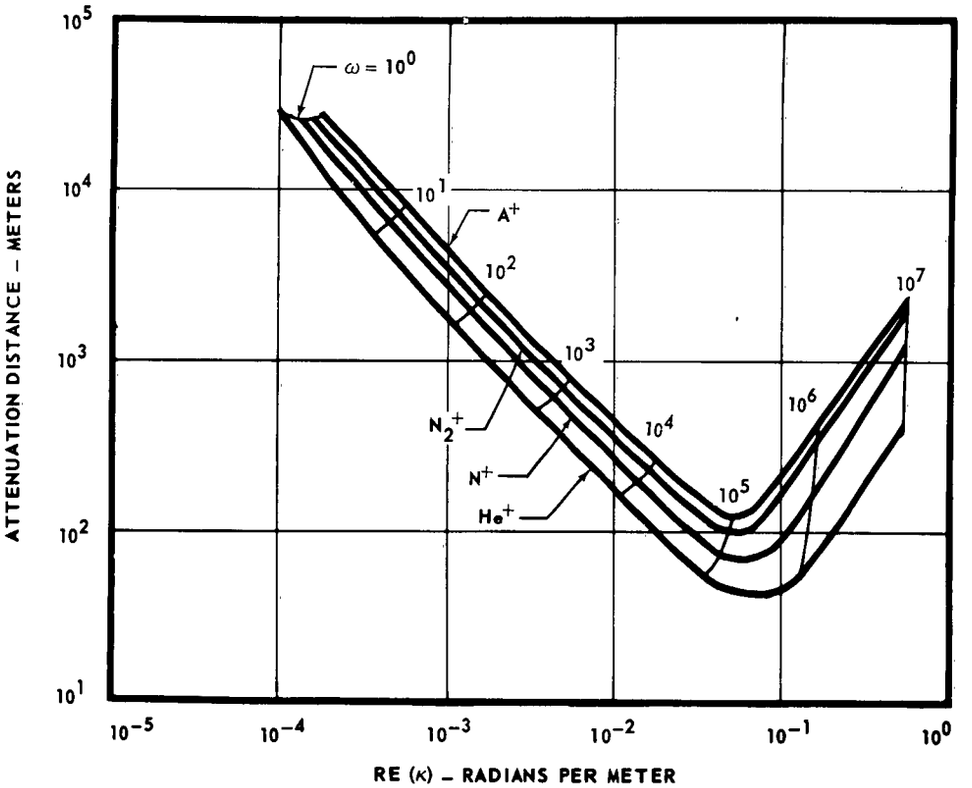

FIGURE 2-10

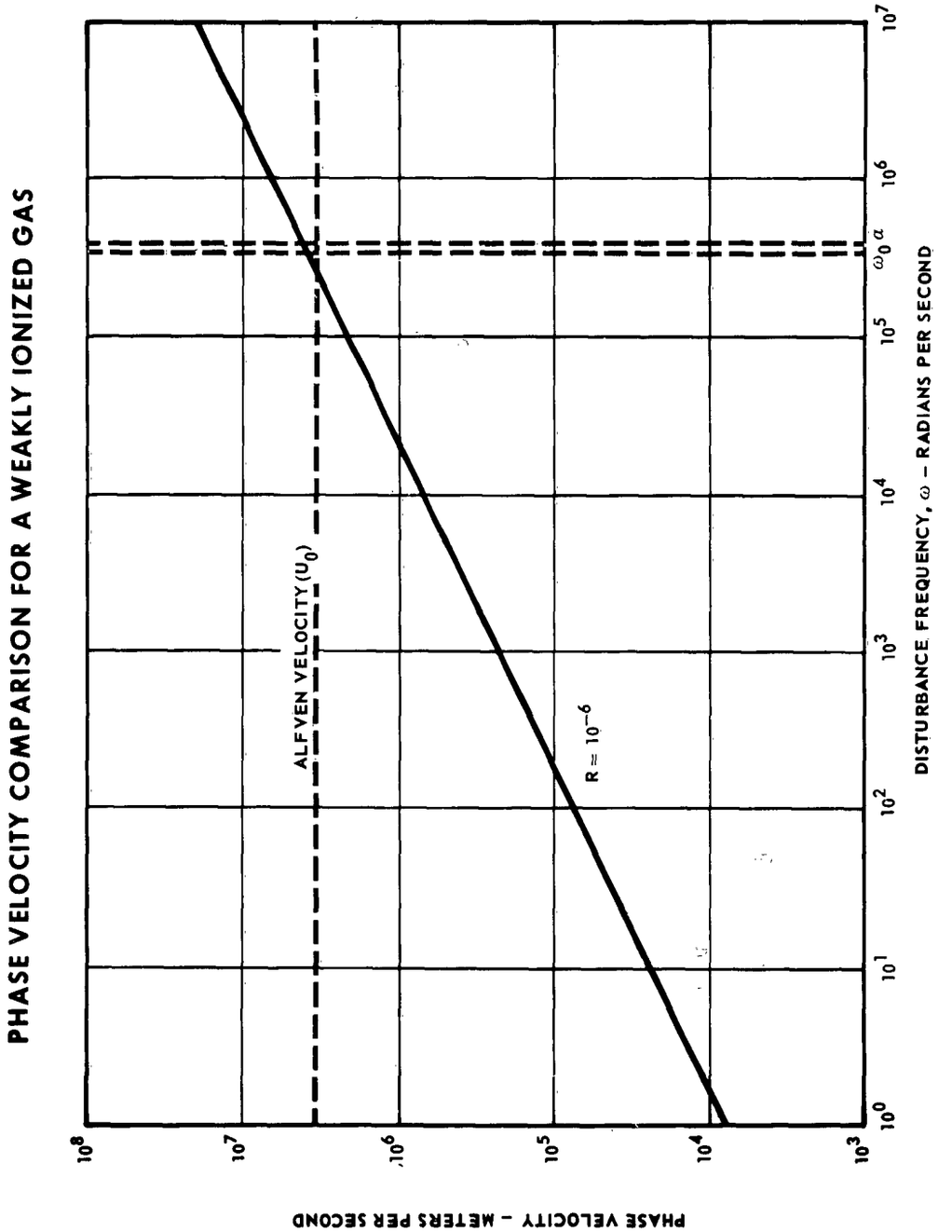
PHASE VELOCITY COMPARISON FOR A WEAKLY IONIZED GAS
ALFVEN VELOCITY (U_0)
$R \approx 10^{-6}$
$\omega_0 a$
DISTURBANCE FREQUENCY, ω - RADIANS PER SECOND
PHASE VELOCITY - METERS PER SECOND
10^0 10^1 10^2 10^3 10^4 10^5 10^6 10^7
10^8 10^7 10^6 10^5 10^4 10^3

FIGURE 2-11

EFFECT OF IONIZATION RATIO ON PHASE VELOCITY

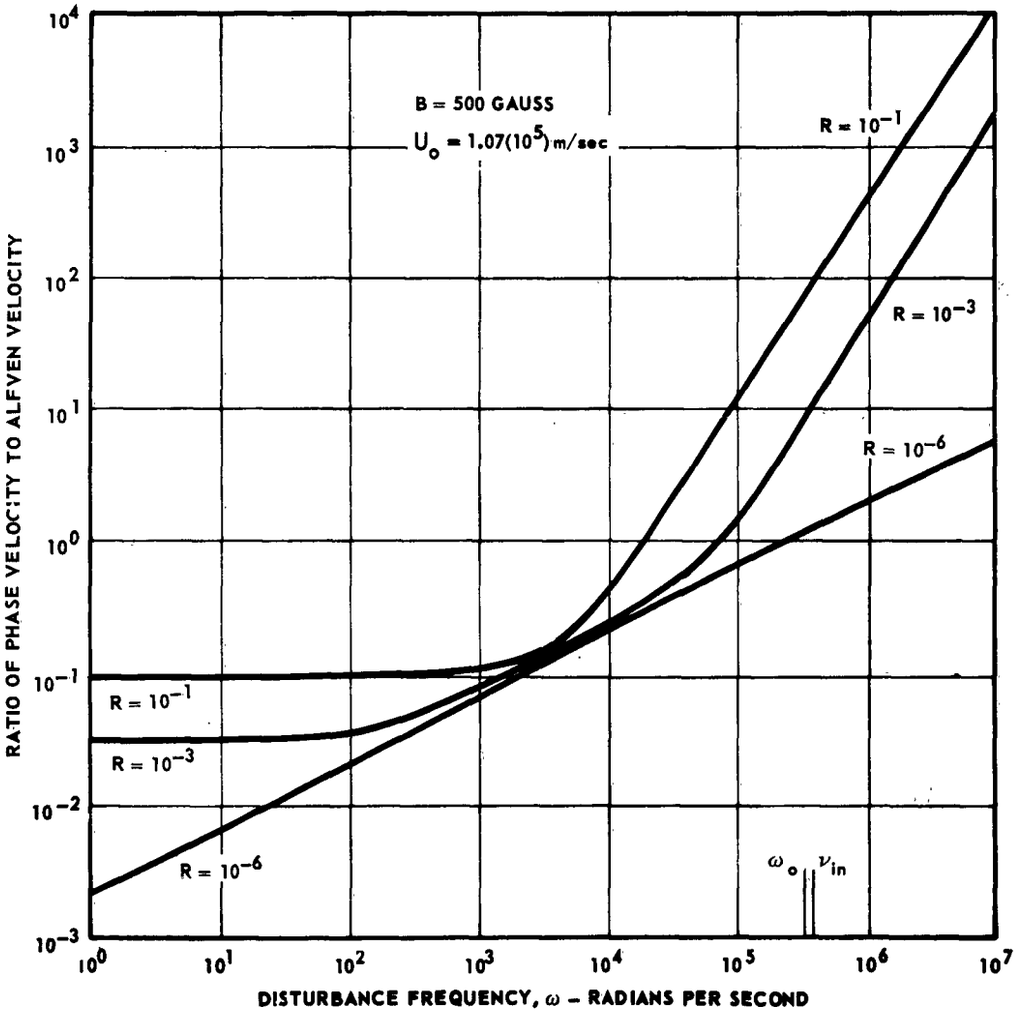

FIGURE 2-12

DAMPING FACTOR FOR ALFVÉN WAVES IN THE HIT

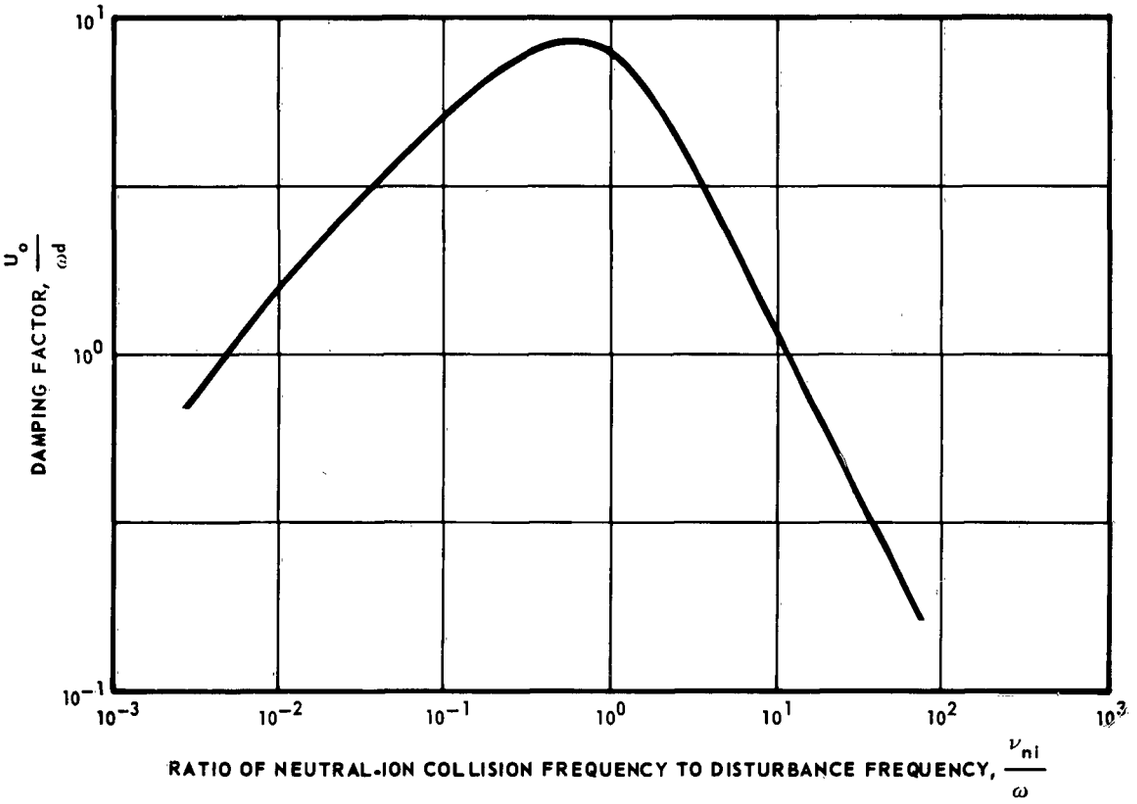

FIGURE 2-13

IONOSPHERIC PLASMA WAVE ATTENUATION vs WAVE NUMBER (300 KM ALTITUDE)

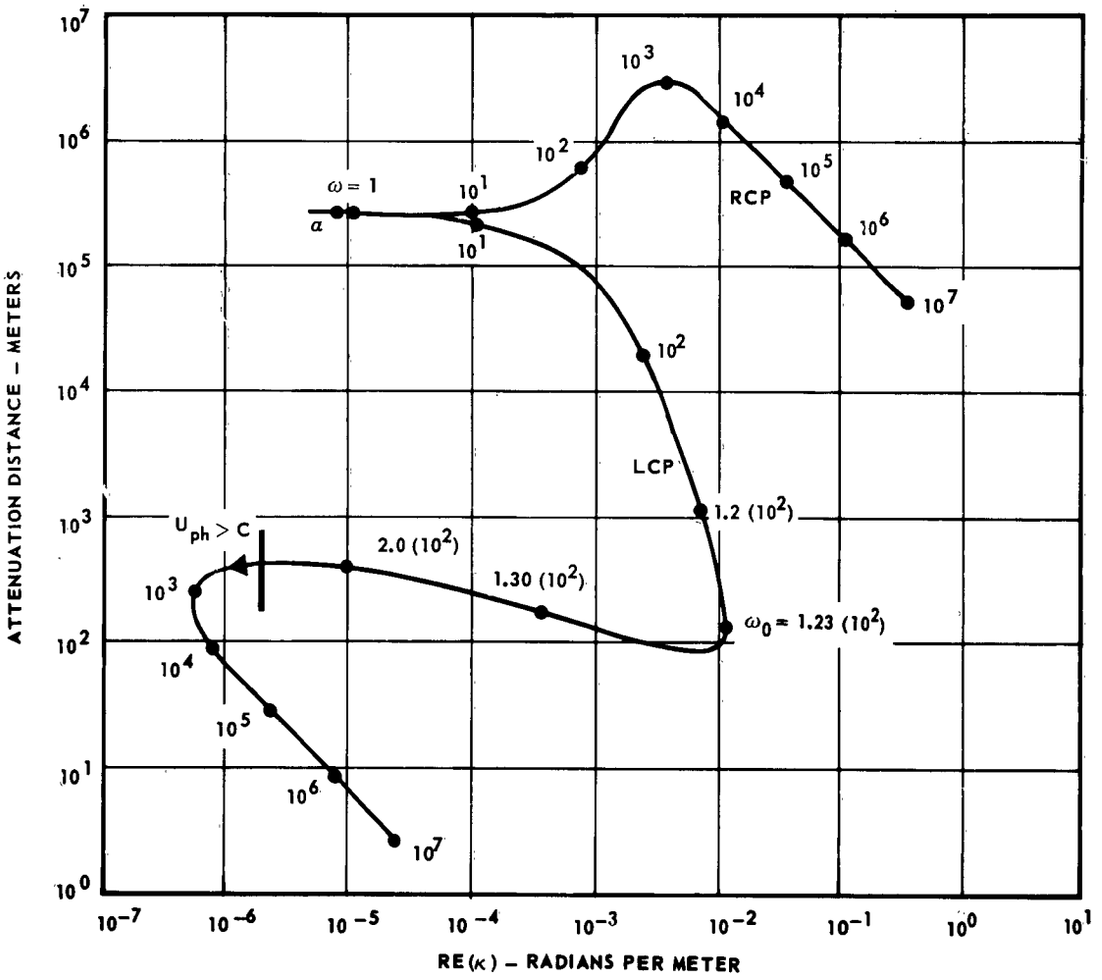

FIGURE 2-14

where δ is an intelligibility, or sensitivity, factor greater than zero. It indicates the minimum signal strength that can be differentiated from noise at the detector system output. For the single frequency disturbances under consideration δ is conveniently obtained from:

$$\delta = \ln \frac{S_o}{S_m} \tag{2-132}$$

with S_o being the initial maximum strength in space and S_m the minimum detectable signal strength. From the relationships (2-70) and (2-72) requirement (2-131) is found to imply that:

$$\left| \frac{\text{Im}(\kappa)}{\text{Re}(\kappa)} \right| \leq \frac{\delta}{2\pi} \tag{2-133}$$

This can be easily met in the frequency range below the relative minimum attenuation distance depicted in the curves. The criterion then becomes

$$\omega \ll \text{Min}[\omega_o, \alpha] \tag{2-134}$$

From Figure 2-2 it is observed that for either curve σ must be greater than unity.

Another method of deriving existence criteria is that used by Watanabe in Reference 2-7. He uses criteria which essentially reduce equation (2-98) to the form of (2-106), without the first term, thereby transforming it to the original equation discovered by Alfvén for totally ionized gases. Weakly ionized gases act the same in most respects as fully ionized gases, if the coupling parameter, 1/F, is small. The criteria so developed are somewhat stringent, since they are a result of requiring the waves to be completely free of frictional damping. However, if these conditions are satisfied, the probability of generating a wave is greatly enhanced. Since in the HIT B_o = 0.1 weber/m^2 and B = 6.3 (10^{-5}) weber/m^2, that is, the vector field is much stronger than the average of the random scalar field, the existence requirements in the weakly ionized gas of the HIT become equivalent to those for a strong field as defined by Watanabe. If in addition the plasma-neutral coupling is small, 1/F is much

less than unity, requiring:

$$\omega >> \frac{\rho}{\rho_n} a \tag{2-135}$$

This restriction is augmented by the fact that in order to appreciably reduce the drag of the neutrals on the plasma:

$$\omega >> a \tag{2-136}$$

As was pointed out at the end of Section 2.4.3.1, equation (2-98) can be shown to agree with (2-106), for plane waves in a fully ionized gas. But in going from (2-98) to (2-105) and then to (2-106) a damping term:

$$\frac{i\omega}{\omega_{ci}} \nabla X \frac{\partial b'}{\partial z}$$

was neglected. This is justified provided:

$$\omega << \omega_{ci} \tag{2-137}$$

The remaining damping term in (2-105) can be reduced to frequency factors by making use of the relations:

$$\sigma = \frac{1}{\mu_o \lambda_*}$$

and:

$$F >> 1$$

Then:

$$\frac{i\omega}{U_o^2 \mu_o \sigma} = \frac{i\omega\nu}{\omega_{ce}\omega_{ci}}$$

where:

$$\nu = \nu_{ei} + \nu_{en} + \frac{m_e}{2m_i} \nu_{in} \tag{2-138}$$

Hence the additional requirement:

$$\omega << \frac{\omega_{ce}\omega_{ci}}{\nu} \tag{2-139}$$

must be imposed. Thus, the result of taking (2-136), (2-137) and (2-139) together implies that Alfvén waves can be generated if ω is restricted as follows:

$$a << \omega << \text{Min}\left[\omega_{ci}, \frac{\omega_{ce}\omega_{ci}}{\nu}\right] \tag{2-140}$$

Inserting the reference conditions for the HIT requires:

$$4.05\,(10^5) \ll \omega \ll 5.90\,(10^5) \text{ radians/sec.} \tag{2-141}$$

The frequency range is seen to occur in the region of relatively small attenuation distances for the curves of Figure 2-2. But the inequality (2-141) cannot be met under these conditions, and therefore the attenuation in this range need not be small.

For strong coupling, $1/F \ll 1$, implying that:

$$\omega \ll \frac{\rho a}{\rho_n} \tag{2-142}$$

Thus, the results (2-55) and (2-56) are valid. Upon multiplying (2-98) by $\frac{\omega^2}{U_*^2}$ the reduction of damping to a negligible amount requires that:

$$\frac{2\beta F}{B_o} - \frac{U_o^2\,\omega}{U_*^2\,\omega_{ci}} \ll 1 \tag{2-143}$$

and:

$$\frac{\omega \lambda_*}{U_*^2} \ll 1 \tag{2-144}$$

where (2-55) has been used for β_*. Since for strong coupling and strong field conditions $\beta \ll B_o$ and $F \ll 1$, relation (2-143) becomes:

$$\frac{U_o^2\,\omega}{U_*^2\,\omega_{ci}} \ll 1 \tag{2-145}$$

By making the substitutions (2-95), this reduces to:

$$\omega \ll \frac{\rho}{\rho_n}\,\omega_{ci} \tag{2-146}$$

Using (2-56) and (2-95), condition (2-144) becomes:

$$\frac{\rho_o\,\omega}{\rho\,B_o^2}\,(\gamma - \beta^2/a) \ll 1 \tag{2-147}$$

From the definitions of a, β and γ it can be shown that:

$$\frac{\beta^2}{a} \ll \gamma$$

and therefore, (2-147) yields the requirement:

$$\omega \ll \frac{\rho}{\rho_n}\,\frac{\omega_{ce}\,\omega_{ci}}{\nu} \tag{2-148}$$

where ν is given by (2-138). Thus the condition for wave existence is:

$$0 < \omega \ll \frac{\rho}{\rho_n}\,\text{Min}\left[a,\ \omega_{ci},\ \frac{\omega_{ce}\,\omega_{ci}}{\nu}\right] \tag{2-149}$$

The HIT reference parameters then give the following range for ω :

$$0 < \omega \ll 0.2 \text{ radian/sec.} \qquad (2\text{-}150)$$

A Since the total test time was only about 5 milliseconds, this criterion could not be used to establish the exciter frequency.

2.5.2 Alfvén Wave Characteristics for Tunnel Conditions. - The characteristics of interest are the frequency range, wave lengths, phase velocities and attenuation distances for Alfvén waves that can be generated in the HIT. Figure 2-2 shows the attenuation distance as a function of the real part of the wave number for the reference gas, illustrating the difference in propagation characteristics of right (plus sign) and right (minus sign) circularly polarized waves. The curve for the right circularly polarized wave (RCP) exhibits a relative minimum attenuation distance at Re $[\kappa] \approx 6.31 \times 10^{-2}$ radians/meter. Both curves change direction at high frequencies, and eventually, each achieves a slope of minus one, this having been verified analytically. The second change always occurs when ω is greater than either a or ω_o , and consequently, the coupling factor is much less than $\frac{\rho}{\rho_n}$, implying that no appreciable coupling exists between the plasma and neutral particles. Furthermore, such frequencies are well above the electron-ion and ion-electron collision frequencies, and the electrons, therefore, tend to move independent of the much more massive ions. Because of the high frequencies involved, this occurs beyond the region where Alfvén waves should exist. The wave lengths for the RCP curve soon become so short, that the curve has no physical realization. On the other hand, the LCP waves, while exhibiting the long wave lengths associated with magneto-ionic disturbances, are so rapidly attenuated that they also loose their physical significance. Figure 2-3 relates phase velocity to Alfvén velocity for the RCP waves. There is an inflection point near ω_o where the wave begins to change its identity. This occurs far below the ion plasma frequency ω_{pi} which is defined

in the usual way:

$$\omega_{pi} = \left(\frac{N_i e^2}{\epsilon_o m_i} \right)^{1/2}$$

For the LCP, U_{ph} exceeds c at a point near $\omega = 2(10^6)$ radians per second.

The result of varying the parameters about the reference conditions is shown in Figures 2-4 through 2-13. They portray the influence of the parameters R (ionization ratio), ρ_n , B_o, T and m_i. Only the curves for the RCP wave are given since the LCP wave reaches a critical point at ω_o , and thereafter, its behavior becomes extremely complex.

Figure 2-4, for a partially ionized gas, may be compared with Figure A-1, for a fully ionized gas. It is observed that the region of increasing attenuation distance, d, does not occur for a fully ionized gas. The relationship between r_o, and R in the figures is:

$$r_o = \frac{10^6 R}{1 - R}$$

Hence $R = 10^{-2}$ corresponds, approximately, to $r_o = 10^4$. The partially ionized and fully ionized propagation characteristics are thus seen to merge quite smoothly. The region of increasing d occurs when the neutral particles predominate. For the conditions considered in Figure 2-4, the neutral gas is by far the major component; it thereby becomes a mechanism for energy exchange with the plasma. A much smaller attenuation distance results for a given ω in the partially ionized case. In the region of increasing attenuation distance less attenuation may be exhibited than for the fully ionized medium since not only is the frictional force reduced in this region, but also the Lorentz force which gives rise to the transverse oscillations. The increase in d beyond the minimum of α or ω_o then represents a transition from Alfvén waves to the waves of magneto-ionic theory. Here the phase velocity is always greater than the Alfvén velocity U_o, while in other portions of the curves, the phase velocity

may have almost any value, depending on the degree of ionization. For large enough ω, U_{ph} will always exceed c.

Figure 2-5 summarizes the effect of ω on attenuation distance for various ionization ratios. In this figure the curve for a given ionization (R) crosses only curves of higher charge concentration. Hence, for all values of ω below an intersection, the wave corresponding to higher ionization has the least attenuation. The tendency for the neutral particles to support and then separate from the gas disturbance is clearly exhibited in the range $\omega \leq a$.

The resulting of holding R constant at 10^{-6} and varying ρ_n is portrayed in Figure 2-6. For the rarefied gases of the upper curves the attenuation distance is nearly constant over several orders of magnitude of ω. The inequality (2-148) is approximately satisfied for the $\rho_n = 10^{-6}$ curve. As ρ_n increases, the neutrals take more and more energy from the plasma motion at low ω, and the flattened regions indicating unified gas motion diminish until at the curve of greatest ρ_n the Alfvén wave is practically non-existent. Figures 2-7 and 2-8 show that the effect of increasing the stationary magnetic field B_o is similar to decreasing ρ_n. Hence, combinations of ρ_n and B_o in an experiment should be able to satisfy most requirements for long and constant attenuation distances over a broad range of wave lengths or frequencies.

The position of the relative attenuation minimum depends on the value of $a = a(T)$. Thus in the curves of Figure 2-9 the minima shift to the right as the temperature is increased. For fixed ω greater than a and fixed wave number, $Re(\kappa)$, there is an attenuation distance associated with each value of T. In this region the phase velocity of the wave is independent of temperature, since multiple particle, and therefore, Alfvén wave field, oscillations occur before collisions with neutrals can introduce particle drag.

In Figure 2-10, showing the effect of molecular weight, curves are shown

for singly ionized helium, monatomic nitrogen, diatomic nitrogen, and argon. A gas pressure of 10^{-3} atmospheres has been chosen, so that the gas density $(\rho_n + \rho)$ is proportional to the molecular weight.

Over the frequency range $0 \leq \omega \leq 10^9$ radian/second, the phase velocity for a fully ionized gas is nearly constant and equal to the Alfvén velocity U_o. Figure 2-11 shows the phase velocity as a function of angular frequency for the standard condition $R = 10^{-6}$ and the fully ionized condition $R = 1$, with $\rho = 1.72 \times (10^{-10}) kg/m^3$. The curve for $R = 10^{-6}$ can be represented by a simple exponential equation.

The ratio of phase velocity to Alfvén velocity for changing ω is presented in Figure 2-12 with R as a parameter. Here it is seen that for intermediate frequencies $\omega < 10^3$ radians/second, the phase velocity for waves in a partially ionized gas is much less than the phase velocity for a fully ionized gas, indicating the effect of the neutral gas inertia. At the attenuation minima displayed in Figure 2-4 the phase velocities approach the velocity computed for a fully ionized gas having the reference neutral density. The phase velocities have a tendency to attain the same value in the frequency range $10^3 < \omega < 10^4$ radians per second. All curves for $R < 10^{-6}$ fall nearly on top of the $R = 10^{-6}$ curve.

Figure 2-13 depicts the relationship of $\frac{U_o}{\omega d}$ to $\frac{\nu_{ni}}{\omega}$ for the HIT reference conditions. The quantity $\frac{U_o}{\omega d}$ is referred to as the "damping factor" by Tanenbaum and Mintzer in Reference 2-2. Since $2\pi \frac{U_o}{\omega}$ is the wave length for an Alfvén wave in a fully ionized gas and d is the attenuation distance in a partially ionized gas, the damping factor provides a conservative lower limit for δ in (2-131). Thus, the detector sensitivity requirement varies appreciably with ω as portrayed in the figure.

2.6 ALFVÉN WAVES IN THE ARC DISCHARGE TUBE. - A description of the conditions prevalent in the arc tube is given in Section 3.4.3.2. This facility

is an example of an HM wave guide and is similar to the one used by Wilcox et al (Reference 2-8). A discussion of the existence and propagation of waves in this device must proceed from the solutions (2-110) and (2-111) of the longitudinal components of the wave equations for $\vec{b}$ and $\vec{E}$. Since the allowed values of wave number K_s are discrete, each mode s (corresponding to the s-th zero of the Bessel function J_o) has its own propagation characteristics. Therefore both existence conditions and propagation features can be determined from a mode analysis.

2.6.1 Existence of Alfvén Waves in the Arc Tube. - Three modes, or types, of propagation can be considered - the transverse magnetic mode (TM), the transverse electric mode (TE), and the transverse electromagnetic mode (TEM). The TM modes are derivable from E_z' and are called E modes, and TE modes are derivable from b_z' and are called B modes. The TEM modes are characterized by both E_z' and b_z' vanishing.

Considering first the TM modes for the axial symmetry of the arc tube (n = 0), putting (2-111) into (2-32) with $\vec{J} = \sigma \vec{E}$ and expanding produces:

$$\left.\begin{aligned} E_z' &= \sum_s D_{so} J_o(\Lambda_{so} r) e^{i(\omega t - K_{so} z)} \\ E_r' &= \sum_s D_{so} \left(1 - \frac{1}{\zeta}\right) \frac{i K_{so}}{\Lambda_{so}} J_1(\Lambda_{so} r) e^{i(\omega t - K_{so} z)} \\ E_\theta' &= 0 \end{aligned}\right\} \qquad (2\text{-}151)$$

$$\left.\begin{aligned} b_\theta' &= \sum_s D_{so} \frac{\mu_o \sigma}{\Lambda_{so}} J_1(\Lambda_{so} r) e^{i(\omega t - K_{so} z)} \\ b_r' &= b_z' = 0 \end{aligned}\right\} \qquad (2\text{-}152)$$

These are the principal modes discussed by Newcomb (Reference 2-5). For the case of infinite conductivity σ, the dispersion relationship (2-114) gives the following expression for the longitudinal wave number:

$$K_{so}^2 = \frac{\omega^2}{U_o^2} \tag{2-153}$$

In the limit of high conductivity, therefore, K_{so} is independent of Λ_{so}. Hence there is no cut-off frequency for this mode.

The TE modes may be examined by substituting (2-110) into (2-31) and expanding. Thus:

$$\left.\begin{aligned} b_z' &= \sum_s C_{so} J_o(\Gamma_{so} r)\, e^{i(\omega t - K_{so} z)} \\ b_r' &= \sum_s \frac{i K_{so}}{\Gamma_{so}} C_{so} J_1(\Gamma_{so} r)\, e^{i(\omega t - K_{so} z)} \\ b_\theta' &= 0 \end{aligned}\right\} \tag{2-154}$$

$$\left.\begin{aligned} E_\theta' &= \sum_s \frac{-i\omega}{\Gamma_{so}} C_{so} J_1(\Gamma_{so} r)\, e^{i(\omega t - K_{so} z)} \\ E_r' &= 0 \end{aligned}\right\} \tag{2-155}$$

In order for K_{so} to be real, implying no axial attenuation, K_{so}^2 must be positive. Therefore:

$$\omega^2 > \Gamma_{so}^2 U_o^2 \tag{2-156}$$

which defines a low frequency cut-off ω_{so}^c. This existence condition may impose serious restrictions on the use of a TE mode exciter in an experiment. Gould (Reference 2-6) discusses an exciter consisting of a current loop coaxial with the tube as one possibility for the TE mode. The cut-off frequency places a restriction on the radial dimension R of the tube. If χ_{so} is the value of the argument for the s-th zero of $J_o(\Gamma_{so} r)$ and λ_{so}^c the wave length corresponding to ω_{so}^c, the requirement on R becomes:

$$R > \frac{\chi_{so}}{2\pi} \lambda_{so}^c \tag{2-157}$$

For waves to exist in the arc tube, boundary conditions such as those used to find (2-157) must be met. Wilcox et al (Reference 2-8) have found, experiment-

ally, that $j_r(R,z) = 0$ for a similar facility. Using equation (2-151), this leads to the boundary condition:

$$J_1(\Lambda_{so}R) = 0 \tag{2-158}$$

On the other hand, Gould (Reference 2-6) puts $E_z'(R,z) = 0$ and finds that the condition:

$$J_o(\Lambda_{so}R) = 0 \tag{2-159}$$

is appropriate. For the TM mode of excitation used in the arc tube, E_r' is given by the expression for a concentric electrode capacitor, namely:

$$E_r' = \begin{cases} \dfrac{V_o}{r \ln \dfrac{R}{R'}} & , R' < r < R \\ 0 & , 0 < r < R' \end{cases} \tag{2-160}$$

where V_o is the initial voltage and R' and R are the radial distances of the inner and outer electrodes from the tube axis. The coefficients D_{so} in equations (2-151) and (2-152) can be determined from the orthogonality property of the J_n and the above relation for E_r'. Substituting (2-160) into (2-151) and integrating over r from the tube axis to outer electrode:

$$\int_o^R \frac{V_o}{r \ln \frac{R}{R'}} J_1(\Lambda_{so}r)\, r\,dr = \sum_s D_{so}\left(1 - \frac{1}{\zeta}\right) \int_o^R \frac{i K_{so}}{\Lambda_{so}} J_1(\Lambda_{so}r)\, J_1(\Lambda_{to}r)\, r\,dr \tag{2-161}$$

Then using (2-158) and the recurrence relation for Bessel Functions:

$$J_2^2(\Lambda_{to}R) = J_o^2(\Lambda_{to}R)$$

the integration yields:

$$\left(1 - \frac{1}{\zeta}\right)\frac{i K_{so}}{\Lambda_{so}} D_{so} = -\frac{2V_o}{R^2 \Lambda_{so} \ln\left(\frac{R}{R'}\right)} \frac{J_o(\Lambda_{so}R) - J_o(\Lambda_{so}R')}{J_o^2(\Lambda_{so}R)} \tag{2-162}$$

Then substituting into (2-152) the value of D_{so} obtained from (2-162) gives the magnetic flux density for the torsional mode which was experimentally investigated in the McDonnell arc tube. The derived result is:

$$b'_\theta = \frac{2V_o \mu_o \sigma}{\left(1 - \frac{1}{\zeta}\right) R^2 \ln\left(\frac{R}{R'}\right)} \sum_s \frac{J_o(\Lambda_{so}R) - J_o(\Lambda_{so}R')}{K_{so}\Lambda_{so}J_o^2(\Lambda_{so}R)} i J_1(\Lambda_{so}r) e^{i(\omega t - K_{so}z)} \quad (2\text{-}163)$$

A

2.6.2 Alfvén Wave Characteristics in the Arc Tube. - For the case of a strong axial magnetic field B_o and infinite conductivity, the field lines are fixed in the plasma, and the Alfvén waves travel along them unattenuated. In the case of TM modes there is, in addition, no dispersion. The magnetic field for the TM modes is tangential, and hence, a torsional wave propagates. For TE modes there exists a radial component of $\vec{b}'$, causing E_θ' to encompass the $\vec{B}_o$ lines. The attenuation distance $\frac{1}{|\mathrm{Im}(K_{so})|}$ is obtained from the roots of dispersion equation (2-114). In the case of small damping of the wave and an Alfvén velocity U_o much less than the velocity of light c, equation (2-114) can be manipulated to give:

$$d_{so} = \frac{2\mu_o \sigma U_o}{\Lambda_{so}^2 + (\mathrm{Re}(K_{so}))^2} \quad (2\text{-}164)$$

The value of E_z' along the tube axis is just the z - component of the gradient of the potential $V(r,\Theta,z,t)$, hence:

$$E_z' = \frac{\partial V}{\partial z}$$

For given r, Θ, and t, this electric field is proportional to the voltage associated with the attenuated wave, therefore:

$$E_z' = \frac{dV}{dz} = -\frac{V}{d_{so}} \quad (2\text{-}165)$$

Utilizing the roots of (2-114), the phase velocity along the tube axis can be found from:

$$U_{ph}^s = \frac{\mathrm{Re}(\omega_s)}{\mathrm{Re}(K_{so})} \quad (2\text{-}166)$$

2.7 ALFVÉN WAVES IN THE IONOSPHERE. - The ionospheric region of interest and its pertinent characteristics are defined in Section 3.2. An altitude of 300 km has been chosen for reference conditions. Two models can be examined,

an unbounded medium and an array of wave channels. A wave channel model seems most reasonable, particularily since there are two wave restraining phenomena, the magnetic pressure and the ionized gas pressure. The existence criteria are the same as those hypothesized in paragraph 2.5.1 for both models, but the propagation characteristics must be considered separately. The conditions for applicability of the infinite medium model are outlined at the beginning of Section 2.5. While a discussion of propagation in an infinite medium is straightforward, the discussion for a wave channel is considerably more complex, and only a cursory examination is presented here.

2.7.1 Existence of Alfvén Waves in the Ionosphere. - Applying the criterion expressed by (2-133) to the curves of Figure 2-15, it is found that δ need not be greater than unity to detect LCP waves in the range ω = 10 to 100 radians per second. For RCP waves the results are even more favorable. It can be demonstrated that for very low frequencies, in the VLF band of $\omega < 10^{-2}$ radians per second, the curves remain together and achieve a slope of minus two as ω tends to zero. This implies that if any portion of the perturbed field can be detected at these frequencies, the wave will be found to exist according to the requirement (2-131).

Since $B_o \approx 2.75\ (10^{-5})$ weber/m^2 and $\beta \approx 1.43\ (10^{-10})$ weber/m^2 at 300 km, the strong field criteria of Watanabe for negligible damping can be used. For $\omega >> 1.45\ (10^{-3})$ radians per second, the plasma-neutral coupling is weak. Therefore, Alfven waves with ω in the range a = 0.85 to $\omega_o = 1.23\ (10^2)$ radians per second can be excited by a suitable technique. Considering the case where the coupling is strong, extremely low frequency (ELF) distrubances occur for any $\omega << 1.45\ (10^{-3})$ radians per second. The computed curves of Figures 2-15 and 2-16 begin in the VLF range. In the ELF range the traces are qualitatively the same

IONOSPHERIC PLASMA WAVE ATTENUATION vs FREQUENCY

(300 KM ALTITUDE)

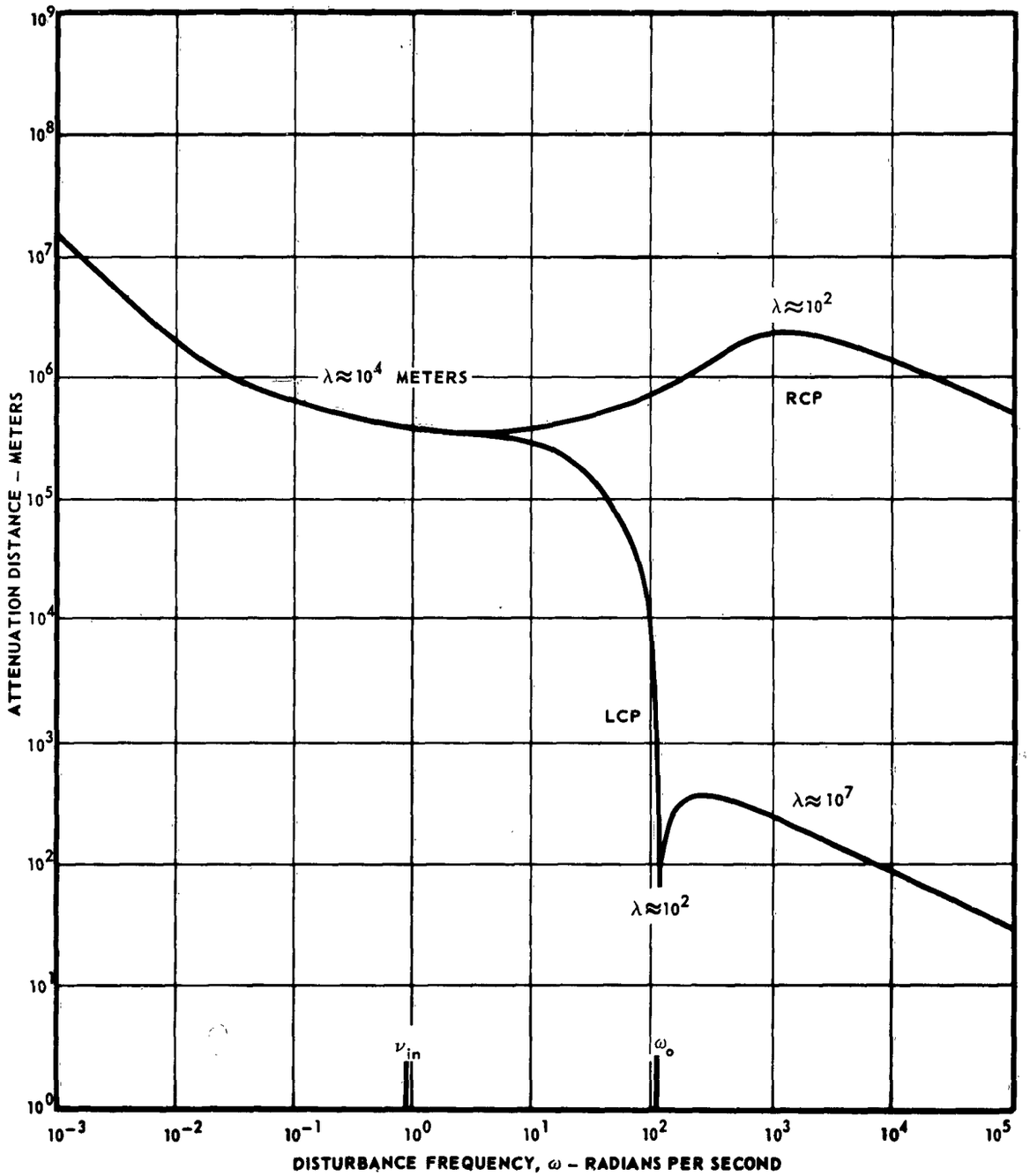

FIGURE 2-15

MHD Wave Investigation

II - theory

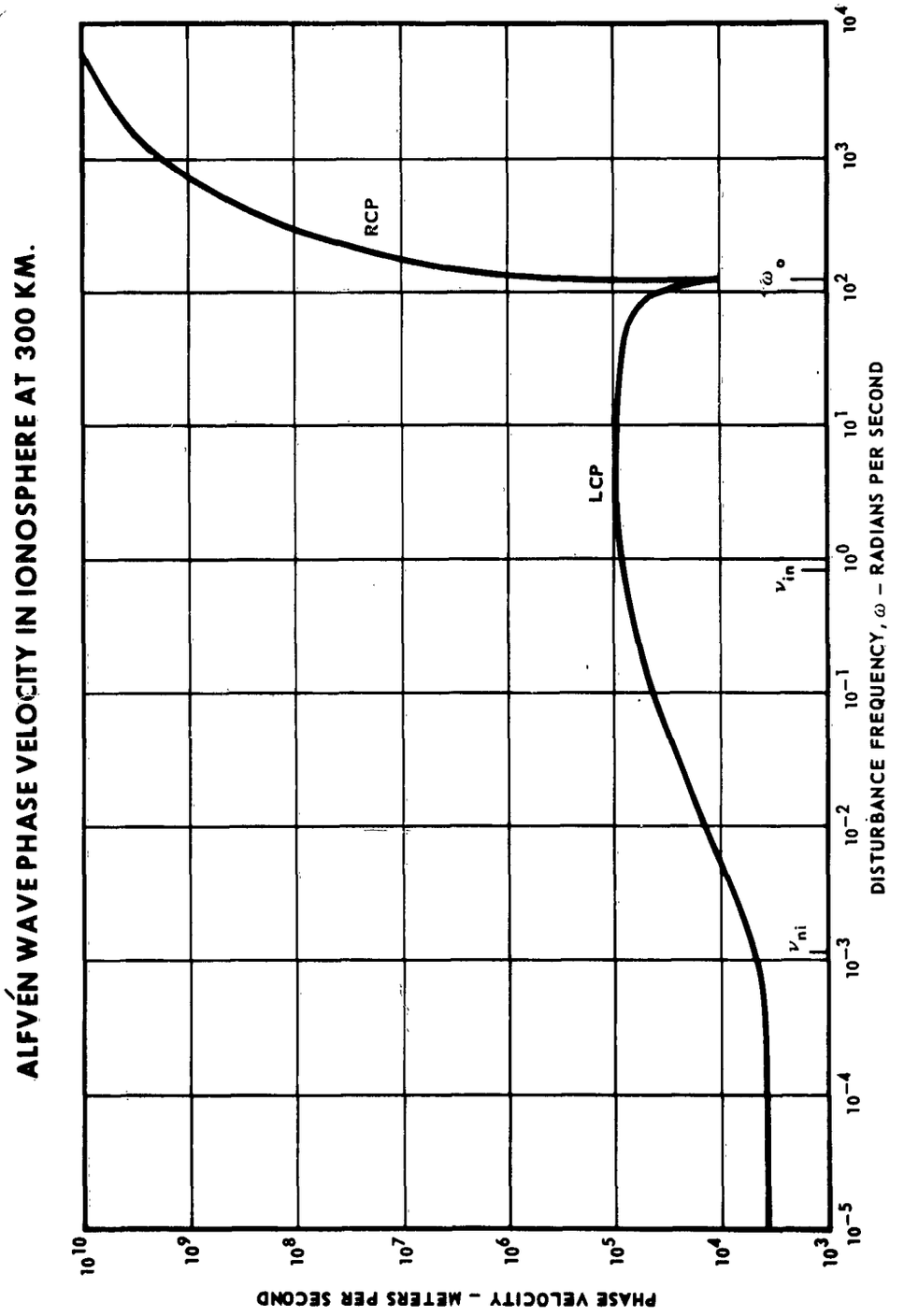

FIGURE 2-16

as those for the HIT reference condition, in the VLF range, Figure 2-2.

2.7.2 Alfvén Wave Characteristics in the Ionosphere. - An infinite gas model has been assumed and the conditions at the reference altitude have been used in equation (2-125) to obtain the curves of Figures 2-15 and 2-16. The attenuation distance d, while reasonably long even for large ω, varies appreciable with wave number as indicated in the figures. The curves begin in a region of constant d, which is the Alfvén wave region for VLF disturbances. This region has ended before $\omega = \omega_o = 123$ radians per second for both curves. When ω approaches ω_o the LCP curve loses its monotonic character. Above $\omega = 10^2$ radians per second, the LCP curve for the ionosphere has the same characteristics as the LCP curve for the HIT reference conditions. Their RCP curves are also similar when the slope reversal for $\omega > 10^7$ is considered. Again, for Alfvén waves, ω_o is near the transition point.

The ionosphere may be represented to some degree by an arrangement of channels, or ducts, whose axes are defined by the relation:

$$\nabla\left(p + \frac{B_o^2}{2\mu_o}\right) = \frac{1}{\mu_o}(\vec{B}_o \cdot \nabla)\vec{B}_o \qquad (2\text{-}167)$$

where p is the partial pressure of the charged particles. Equation (2-167) expresses the requirement that no net force be exerted on a fluid element, that is:

$$\hat{D}\vec{v} = 0 \qquad (2\text{-}168)$$

(c.f. Appendix A, equation (A-22), without the displacement current). If the spatial rate of change of $\vec{B}_o$ along an arbitrary flux line is negligible, (2-167) can be integrated to yield:

$$p + \frac{B_o^2}{2\mu_o} = \text{constant} \qquad (2\text{-}169)$$

The usual concept of the magnetic field being frozen in the fluid is associated with (2-169). The right side of (2-167) can be evaluated by means of a magnetic

field model such as a dipole, or it can be determined semi-empirically by using satellite and rocket probe data to evaluate the coefficients in a spherical harmonic expansion of $\vec{B_o}$. It is found in the ionosphere that:

$$p \ll \frac{B_o^2}{2\mu_o} \qquad (2\text{-}170)$$

hence, using (2-169), the waves will propagate along lines of constant flux density.

If the phase velocity for the ionospheric reference conditions is examined over the ELF to intermediate frequency range, the curve of Figure 2-17 results. Up to $\omega = \nu_{ni}$, corresponding to strong coupling, the phase velocity is essentially constant and is given by U_* in the limit of F = 0. Between ν_{ni} and ν_{in} the plasma-neutral coupling diminishes until, at $\omega \approx \nu_{in}$, $U_{ph} = U_o$ for the plasma. As the transition point or ω_o is approached, the Alfvén wave ceases to exist since it does not propagate or is highly attenuated. For $\omega > \omega_o$, the LCP wave, whose velocity curve essentially matches that of the RCP wave when $\omega < \omega_o$, continues to propagate. However, it soon looses its physical identity in that U_{ph} exceeds c, and the corresponding wavelengths become excessively large. The characteristics of this curve are discussed qualitatively in Reference 2-2.

In the light of certain calculations and satellite observations, the assumption of thermal equilibrium in the ionosphere may not be entirely justified (Reference 2-9). If it is not, the restrictions of paragraph 2.4 would have to be removed. Not only would the development of the wave equation and associated dispersion equation be much more laborious, but an additional relationship to account for the mechanism sustaining the deviation from equilibrium would have to be incorporated. From Reference 2-9, a reasonable estimate of the deviation puts the electron temperature at five times the ion temperature. Since the mean plasma-neutral collision frequency and effective scalar magnetic field are roughly inversely proportional to the square root of temperature, the effect of the non-equilibrium is probably

small. The other quantity affected by this condition is the resistivity $\mu_o \lambda_*$, which is inversely proportional to the three-halves power of the temperature (Reference 2-4). Thus, the resistivity will be somewhat smaller in the direction of $\vec{B}_o$.

FIGURE 2-17

3. THE LABORATORY PLASMA ENVIRONMENT

3.1 INTRODUCTION. - Prior to and concurrent with the theoretical study of waves in plasmas, theoretical and experimental investigations of actual plasma environments were conducted in McDonnell's laboratory facilities. Consideration of the HIT flow field properties originally suggested the possibility of simulating ionospheric conditions and conducting plasma wave experiments. A knowledge of the gas conditions in terms of constituents, total gas density, temperature, ionization and flow velocity and an estimate of the gas turbulence was essential to the selection of the wave theory. Since numerical estimates for the important parameters involved in the wave theory were not available, a considerable amount of preliminary experimentation was necessary. The result of these experiments was the development of both a theoretical model for the HIT and the necessary instrumentation for plasma wave investigations. Parameter values which could not be measured directly were obtained by utilizing the HIT model.

Before Alfvén wave experiments could be sensibly performed in the shock and arc discharge tubes, quantitative results from the HM wave guide theory were required. Again the problems of parameter estimation and appropriate instrumentation arose. Preliminary experimentation was performed in each apparatus, and a literature survey was conducted in order to establish suitable models. Application of the models to determine the parameter values of the theory resulted in certain changes in the two devices.

The remainder of this volume is devoted to the description of the plasma environment in the HIT, the electromagnetic shock tube and the arc discharge tube, with the particular goal of determining the extent of their similarity to the ionospheric environment.

The generation of a plasma environment, the control of that environment, and the accurate measurement of the plasma conditions are active areas of present day study. These investigations have largely neglected the study of plasmas for simulating ionospheric conditions because of the particular difficulty of scaling the size, ionization percentage, and low gas density. As far as Alfvén wave experimentation is concerned, the only published data has been obtained in liquid metals and nearly fully ionized gases, none of which can be easily related to ionospheric conditions. This section therefore details the theoretical considerations which were necessary in designing the plasma environments, and in determining their plasma characteristics.

Section 3.2 outlines the general characteristics of the ionosphere which were to be simulated, including the important gas and magneto-ionic conditions and the method by which each of these parameters was derived. Section 3.3 discusses the importance of various parameters for the experimental study, and Section 3.4 treats the methods by which these parameters may be generated.

The major theoretical activity in the development of a laboratory plasma environment was the study of the ionized flow in the hypervelocity impulse tunnel. Such a tunnel had not previously been used specifically for its ionized flow, thus a major effort was required to predict the ionized flow conditions. The results of this study indicated two highly ionized regions of flow, one region behind the starting shock and a second region in the early portion of the blow-down. However, wide variation had to be allowed in the parameter values, because the complicated physical and chemical processes were not fully explained by theory. The detailed analyses of the conditions in the arc chamber, in the shock excited flow and in the blow-down flow are discussed in Section 3.4.2.5 and 3.4.2.6.

During the course of the program the uncertainties in the tunnel flow conditions and in the experimental results made a redirection of effort necessary.

The economics of operating a large and highly complex HIT facility demanded that only a few, carefully prepared developmental experiments be programmed. To prepare for such shots the electromagnetic shock tube and, later, the arc discharge tube were constructed and employed. Section 3.4.3 discusses the characteristics of these two plasma generators. The arc discharge tube experiments proved to be of most use to the program.

3.2 GENERAL CHARACTERISTICS OF THE IONOSPHERE. - The upper portion of the atmosphere has a number of ionized regions which make up the ionosphere. These regions are created through the interaction of solar radiation and the atmospheric constituents which is called photo-ionization. Due to the nature of the process and the variation in atmospheric density and composition, there exist several regions of relative maximum ionization at any instant, this having been confirmed by sounding experiments. The lack of a complete understanding of the processes involved and a firm knowledge of the spectral distribution of the impinging solar radiation makes it impossible to predict, theoretically, the observed electron density distribution.

A typical distribution of ion densities as obtained from radio measurements indicates three distinct layers of ionization, the E layer beginning at about 100 kilometers, the F1 layer at 200 kilometers, and the F2 layer at 450 kilometers. A fourth layer, the D layer, exists only in the daytime and can be detected by its large absorption of radio waves. Rocket measurements during periods of high absorption have determined the position of the D layer to be in the altitude range from 60 to 80 kilometers. These layers may act as dielectric wave guides in channeling MHD waves, changing however, as a function of season and time of day.

In many parts of the ionosphere additional ionized formations, which are stable for several hours, frequently occur, and extend from ten to hundreds of kilometers. These additional layers, which do not appreciably affect the behavior of the rest of the ionosphere, are called sporadic layers. The most regularly

occurring of these is the E_{spor} layer, located slightly above the E layer. It exists frequently enough, that from 25 to 90 percent of the time, long range propagation in the 15 mcps band is made possible in the mid latitudes. A sporadic E2 layer can also be observed, but less frequently. During solar flare disturbances, radio sounding of the ionosphere is made useless by abnormally high absorption in the D-layer, because of increased electron concentrations in this region. Also magnetic storms greatly affect the conditions in the ionosphere.

The electron concentration profile above the maximum of the F2 region is known only from measurements made by artificial earth satellites. The slope of the curve of electron concentration versus altitude has been found to be smaller above the position of the maximum than below it.

The ionosphere should not be thought of as a quiet medium, but rather a turbulent one. This is particularly evident from the rapid fluctuations of radio returns from the ionosphere. In addition to the turbulence, the ionosphere exhibits a regular drift, the various ionized formations moving between 10 and 1200 meters per second.

The standard ionospheric model chosen for the MHD experiment, Tables 3-1 and 3-2, give an average value of the important parameters required for computing the wave propagation and wave generation characteristics. These important parameters include both non-ionized gas conditions, Table 3-1, which are taken from the ARDC Model Atmosphere (Reference 3-1), and the magneto-ionic condition, Table 3-2, which are computed. The following paragraphs indicate the meaning and give a derivation of each of the pertinent parameters.

Atmosphere Parameters - Altitude, as used in this report, is the geometric altitude measured from sea level. The altitude used in the ARDC calculations of gas conditions is the geopotential altitude, which is related to the potential energy of a unit mass at that altitude. Because of the change in gravity as a function of altitude, this measurement differs from the geometric altitude.

TABLE 3-1
ARDC MODEL ATMOSPHERE

GEOPOTENTIAL ALTITUDE (KILOMETERS)	100	150	200	250	300	350	400	450	500
GEOMETRIC ALTITUDE (KILOMETERS)	102	154	206	260	314	370	428	484	542
ACCEL. OF GRAVITY (METERS/SEC.)	9.499	9.348	9.201	9.051	8.905	8.757	8.608	8.468	8.326
TEMPERATURE (°K)	206.6	1102	1413	1416	1428	1458	1505	1560	1623
MOLECULAR SCALE TEMP. (°K)	207.2	1133	1573	1750	1923	2099	2279	2450	2630
PRESSURE (MICRONS OF Hg.)	1.58×10^{-1}	3.55×10^{-3}	1.08×10^{-3}	3.841×10^{-4}	1.53×10^{4}	6.49×10^{-5}	2.91×10^{-5}	1.439×10^{-5}	7.37×10^{-6}
DENSITY (KILOGRAMS/M^3)	2.596×10^{-7}	1.456×10^{-9}	3.19×10^{-10}	1.02×10^{-10}	3.70×10^{-11}	1.44×10^{-11}	5.93×10^{-12}	2.729×10^{-12}	1.305×10^{-12}
MOLECULAR ωt	28.88	28.19	26.01	23.44	21.51	20.12	19.12	18.44	17.92
NUMBER DENSITY (PART/M^3)	5.413×10^{18}	3.11×10^{16}	$7.38 \times 10^{+15}$	$2.62 \times 10^{+15}$	$1.035 \times 10^{+15}$	$4.3 \times 10^{+14}$	$1.87 \times 10^{+14}$	$8.914 \times 10^{+13}$	$4.387 \times 10^{+13}$
PARTICLE SPEED (M/SEC)	389.2	910	1072	1131	1186	1239	1291	1338	1385
COLLISION FREQ. (SEC.$^{-1}$)	1.247×10^{3}	$1.68 \times 10^{+1}$	4.69	1.75	7.26×10^{-1}	3.15×10^{-1}	1.43×10^{-1}	7.06×10^{-2}	3.60×10^{-2}
MEAN FREE PATH (METERS)	3.12×10^{-1}	$5.43 \times 10^{+1}$	$2.29 \times 10^{+2}$	$6.54 \times 10^{+2}$	$1.63 \times 10^{+3}$	$3.928 \times 10^{+3}$	$9.04 \times 10^{+3}$	$1.895 \times 10^{+4}$	$3.85 \times 10^{+4}$

TABLE 3-2

MAGNETO-IONIC GAS CONDITIONS

GEOMAGNETIC ALTITUDE (KILOMETERS)	100	150	200	250	300
MAGNETIC FIELD (GAUSS)	.300	.293	.287	.281	.275
ION DENSITY (PART/CM^3)	1.3×10^5	2.8×10^5	4×10^5	1.1×10^6	1.8×10^6
PLASMA FREQ. (RAD/SEC.)	2.05×10^7	3×10^7	3.6×10^7	5.9×10^7	7.5×10^7
IONIZED TO NEUTRAL PARTICLE RATIO	2.4×10^{-8}	9×10^{-6}	5.4×10^{-5}	4.2×10^{-4}	1.7×10^{-3}
ELECTRON CYCLOTRON FREQ. (RAD./SEC.)	$5.26 \times 10^{+6}$	$5.15 \times 10^{+6}$	$5.04 \times 10^{+6}$	$4.94 \times 10^{+6}$	$4.84 \times 10^{+6}$
ION CYCLOTRON FREQ. (RAD./SEC.)	$1.79 \times 10^{+2}$	$1.75 \times 10^{+2}$	$1.71 \times 10^{+2}$	$1.68 \times 10^{+2}$	1.64×10^2
AVERAGE ELECTRON SPEED (CM/SEC.)	8.95×10^6	2.07×10^7	2.34×10^7	2.34×10^7	2.35×10^7
AVERAGE ION SPEED (CM/SEC.)	5.23×10^4	1.21×10^5	1.37×10^5	$1.37\ 10^5$	1.38×10^5
ION NEUTRAL MEAN FREE PATH (CM)	3.12×10^1	5.44×10^3	$2.29 \times 10^{+4}$	$6.45 \times 10^{+4}$	$1.63 \times 10^{+5}$
ELECTRON NEUTRAL MEAN FREE PATH (CM)	1.75×10^2	3.06×10^4	1.29×10^5	3.64×10^5	9.1×10^5
ELECTRON-ELECTRON PARTICLE MEAN FREE PATH (CM)	8.17×10^3	1.085×10^5	1.25×10^5	4.5×10^4	2.9×10^4
ION-ELECTRON MEAN FREE PATH (CM)	1.14×10^4	1.51×10^5	$1.75 \times 10^{+5}$	$6.4 \times 10^{+4}$	$4.0 \times 10^{+4}$
ION-ION MEAN FREE PATH (CM)	8.17×10^3	1.085×10^5	1.25×10^5	4.5×10^4	2.9×10^4
COLLISION FREQ. ION NEUTRAL (ENCOUNTERS/SEC.)	1.68×10^3	22.3	6.0	2.1	8.5×10^{-1}
COLLISION FREQ. ELECTRON NEUTRAL (ENCOUNTERS/SEC.)	5.11×10^4	6.77×10^2	1.8×10^2	6.4×10^1	2.6×10^1
COLLISION FREQ. ELECTRON ION (ENCOUNTERS/SEC.)	7.85×10^2	1.37×10^2	1.3×10^2	3.7×10^2	5.9×10^2
COLLISION FREQ. ELECTRON–ELECTRON (ENCOUNTERS/SEC.)	1.1×10^3	1.9×10^2	1.87×10^2	5.20×10^2	8.10×10^2
COLLISION FREQ. ION–ION ENCOUNTERS/SEC.)	6.4	1.1	1.1	3.0	4.8
EFFECTIVE ELECTRON COLLISION FREQ. ENCOUNTERS/SEC.	5.3×10^4	10^3	5.0×10^2	9.6×10^2	1.4×10^3
EFFECTIVE ELECTRON MEAN FREE PATH (CM)	1.69×10^2	2.07×10^4	4.7×10^4	2.4×10^4	1.6×10^4
EFFECTIVE ION COLLISION FREQUENCY (ENCOUNTER/SEC.)	1.68×10^3	23.4	7.1	5.1	5.6
EFFECTIVE ION MEAN FREE PATH	31.1	5.18×10^3	$1.9 \times 10^{+4}$	2.7×10^4	2.5×10^4
DEBYE SHIELDING RADIUS (CM)	2.74×10^{-1}	4.33×10^{-1}	4.1×10^{-1}	2.5×10^{-1}	1.9×10^{-1}

TABLE 3-2
D-IONIC GAS CONDITIONS

100	150	200	250	300	350	400	450	500
.300	.293	.287	.281	.275	.269	.263	.257	.251
1.3×10^{5}	2.8×10^{5}	4×10^{5}	1.1×10^{6}	1.8×10^{6}	1.8×10^{6}	1.2×10^{6}	8.3×10^{5}	6.9×10^{5}
2.05×10^{7}	3×10^{7}	3.6×10^{7}	5.9×10^{7}	7.5×10^{7}	7.5×10^{7}	6.2×10^{7}	5.1×10^{7}	4.7×10^{7}
2.4×10^{-8}	9×10^{-6}	5.4×10^{-5}	4.2×10^{-4}	1.7×10^{-3}	4.2×10^{-3}	6.4×10^{-3}	9.3×10^{-3}	1.6×10^{-2}
$5.26 \times 10^{+6}$	$5.15 \times 10^{+6}$	$5.04 \times 10^{+6}$	$4.94 \times 10^{+6}$	$4.84 \times 10^{+6}$	4.72×10^{6}	4.62×10^{6}	4.51×10^{6}	4.40×10^{6}
$1.79 \times 10^{+2}$	$1.75 \times 10^{+2}$	$1.71 \times 10^{+2}$	$1.68 \times 10^{+2}$	1.64×10^{2}	1.60×10^{2}	1.57×10^{2}	1.53×10^{2}	1.50×10^{2}
8.95×10^{6}	2.07×10^{7}	2.34×10^{7}	2.34×10^{7}	2.35×10^{7}	2.38×10^{7}	2.41×10^{7}	2.46×10^{7}	2.51×10^{7}
5.23×10^{4}	1.21×10^{5}	1.37×10^{5}	$1.37\ 10^{5}$	1.38×10^{5}	1.39×10^{5}	1.41×10^{5}	1.44×10^{5}	1.47×10^{5}
3.12×10^{1}	5.44×10^{3}	$2.29 \times 10^{+4}$	$6.45 \times 10^{+4}$	$1.63 \times 10^{+5}$	$3.93 \times 10^{+5}$	$9.04 \times 10^{+5}$	$1.90 \times 10^{+6}$	$3.85 \times 10^{+6}$
1.75×10^{2}	3.06×10^{4}	1.29×10^{5}	3.64×10^{5}	9.1×10^{5}	2.22×10^{6}	5.1×10^{6}	1.07×10^{7}	2.15×10^{7}
8.17×10^{3}	1.085×10^{5}	1.25×10^{5}	4.5×10^{4}	2.9×10^{4}	3.0×10^{4}	4.8×10^{4}	7.2×10^{4}	10^{5}
1.14×10^{4}	1.51×10^{5}	$1.75 \times 10^{+5}$	$6.4 \times 10^{+4}$	$4.0 \times 10^{+4}$	$4.2 \times 10^{+4}$	$6.6 \times 10^{+4}$	$1.03 \times 10^{+5}$	$1.4 \times 10^{+5}$
8.17×10^{3}	1.085×10^{5}	1.25×10^{5}	4.5×10^{4}	2.9×10^{4}	3.0×10^{4}	4.8×10^{4}	7.2×10^{4}	10^{5}
1.68×10^{3}	22.3	6.0	2.1	8.5×10^{-1}	3.6×10^{-1}	1.6×10^{-1}	7.6×10^{-2}	3.8×10^{-2}
5.11×10^{4}	6.77×10^{2}	1.8×10^{2}	6.4×10^{1}	2.6×10^{1}	1.1×10^{1}	4.7	2.3	1.1
7.85×10^{2}	1.37×10^{2}	1.3×10^{2}	3.7×10^{2}	5.9×10^{2}	5.7×10^{2}	3.6×10^{2}	2.4×10^{2}	1.8×10^{2}
1.1×10^{3}	1.9×10^{2}	1.87×10^{2}	5.20×10^{2}	8.10×10^{2}	7.95×10^{2}	5.02×10^{2}	3.42×10^{2}	2.51×10^{2}
6.4	1.1	1.1	3.0	4.8	4.6	2.9	2.0	1.5
5.3×10^{4}	10^{3}	5.0×10^{2}	9.6×10^{2}	1.4×10^{3}	1.4×10^{3}	8.6×10^{2}	5.8×10^{2}	4.3×10^{2}
1.69×10^{2}	2.07×10^{4}	4.7×10^{4}	2.4×10^{4}	1.6×10^{4}	1.7×10^{4}	2.8×10^{4}	4.2×10^{4}	5.8×10^{4}
1.68×10^{3}	23.4	7.1	5.1	5.6	4.9	3.1	2.0	1.5
31.1	5.18×10^{3}	$1.9 \times 10^{+4}$	2.7×10^{4}	2.5×10^{4}	2.8×10^{4}	4.6×10^{4}	7.2×10^{4}	1.0×10^{5}
2.74×10^{-1}	4.33×10^{-1}	4.1×10^{-1}	2.5×10^{-1}	1.9×10^{-1}	2.0×10^{-1}	2.4×10^{-1}	3.0×10^{-1}	3.3×10^{-1}

The temperatures at altitudes inaccessible to balloons are derived from measured pressures or densities. The ARDC calculations utilize a molecular-scale temperature that is independent of molecular weight. Since the molecular weight is not well known at altitudes above 90 kilometers, the molecular-scale temperature, T_M, gives a more accurate indication of temperature. It is defined by

$$T_M = \left(\frac{T}{M}\right) M_o$$

where

T = temperature in ^oK

M = molecular weight

M_o = sea-level value of molecular weight

Since (T/M) is directly proportional to the square of the particle kinetic energy, a measurement of the energy enables calculation of (T/M) and therefore, T_M.

Molecular weight is a dimensionless quantity in which the naturally occurring mixture of oxygen isotopes has, by definition, a value of 16. The atmosphere defined by this model is assumed dry, with a sea level molecular weight M_o equal to 28.966. The mean molecular weight curve from the 1959 model results from an attempt to make use of the best available experimental data, and is about 10 to 20 percent heavier than that of the 1956 model.

In Table 3-1 the number density is computed from the density and mean molecular weight. The particle speed is the mean of a Maxwellian distribution of speeds for all air particles within a given element any volume, assuming that all air molecules have the mass associated with the mean molecular weight.

The mean free path is the mean value of the distance traveled by each of the molecules between collisions with other molecules. The expression for mean free path, L, is obtained from kinetic gas theory, assuming elastic collisions between

spherical molecules and is given by:

$$L = \frac{1}{\sqrt{2\pi\sigma^2 n}}$$

where:

σ = average effective collision diameter

n = particle density

The mean collision frequency of the molecules is the average velocity of the molecules divided by their mean free path.

Magneto-ionic Parameters - The magneto-ionic properties of the ionosphere, Table 3-2, were not given for the ARDC atmosphere and, therefore, had to be calculated. The magnetic field strength has been extrapolated from calculated field strengths at the magnetic equator assuming a dipole source. Original calculations gave a field strength of 0.3116 gauss at the earth's surface, and a value of 0.2341 gauss at an altitude of 0.1 earth radii. The field gradient was assumed constant between these values.

Ion densities were available from many sources. Those densities used in the model atmosphere of Figure 3-1 were obtained from a composite of rocket and satellite measurements in mid latitudes during the afternoon. The plasma frequency, ω_p, is a direct measure of the electron concentration and is defined by:

$$\omega_p = \left(\frac{4\pi n_e e^2}{m_e}\right)^{1/2}$$

where:

n_e = electron concentration in particles/cm^3

e = the charge on the electron (4.8×10^{-10} e.s.u.)

m_e = the mass of the electron in grams.

The cyclotron frequency of charged particles, ω_c, is the angular oscillation rate of the particles around a magnetic line of force given as:

$$\omega_c = \frac{q B_o}{cm}$$

QUIET AFTERNOON IONOSPHERE IN MID-LATITUDES

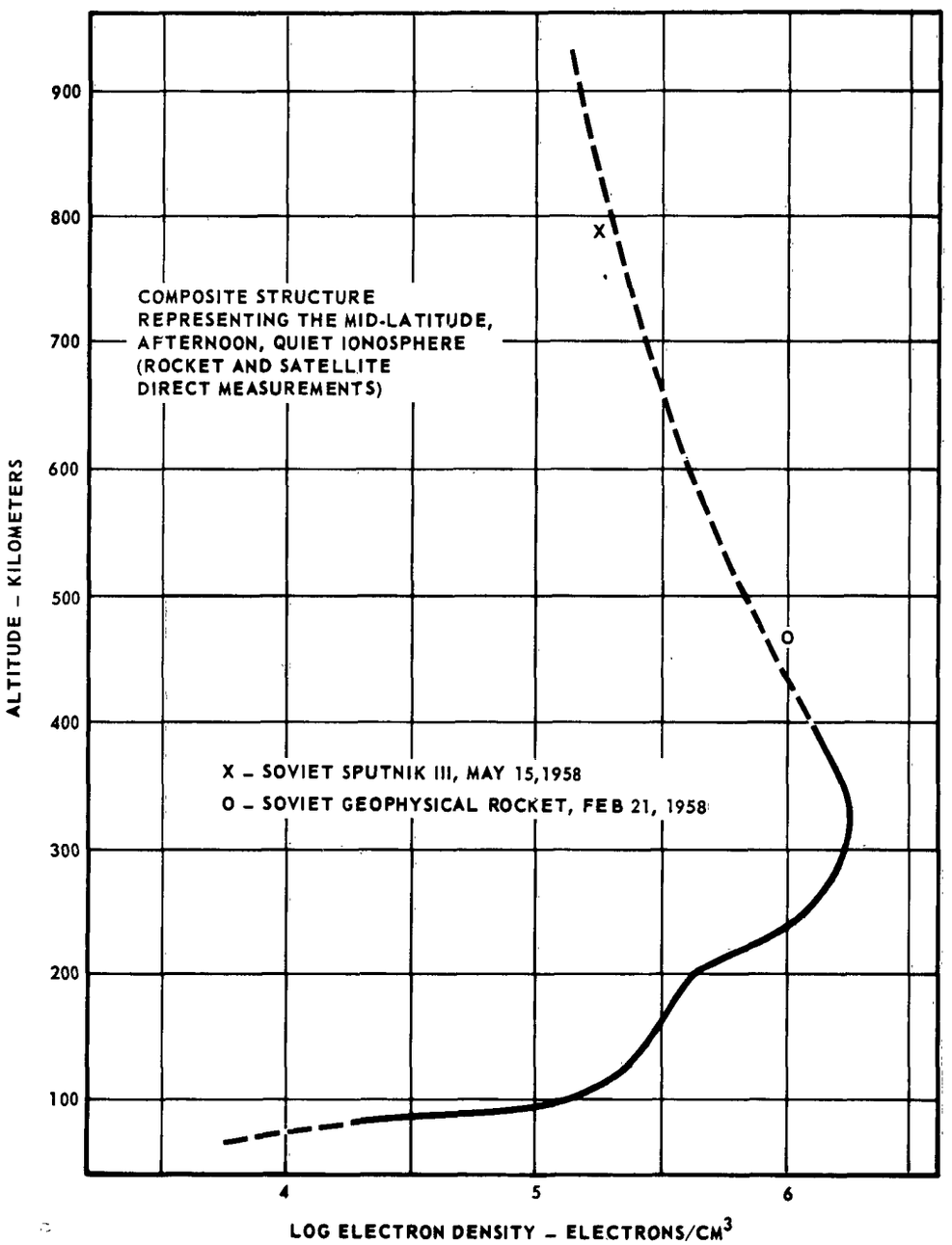

FIGURE 3–1

where:

B = the magnetic field strength in gauss

A q = the charge on the particle

m = the mass of the particle in grams

c = the speed of light in cm/sec (3×10^{10}).

The ion cyclotron frequency has been computed for the atomic oxygen ion which was assumed to be the predominant positive ion.

The ion and electron average speeds are found from the kinetic theory of gases to be equal to:

$$\bar{V} = \frac{2}{\sqrt{\pi}} \left(\frac{2kT}{m}\right)^{1/2}$$

where:

$\bar{V}$ = the average speed in centimeters per second

k = Boltzmann's constant (1.38×10^{-16} ergs/deg K)

T = temperature in ^{o}K

m = mass of the particle.

For molecules of the same size, one molecule will encounter another molecule, if its center is at a distance less than one molecular diameter, d, from the line generated by the motion of the center of the moving particle. Thus, the area for collision will be πd^2, and the volume of collision will be $\bar{V} \pi d^2$. If the average concentration of molecules is n per cubic centimeter, the number of collisions per second will be $n\bar{V} \pi d^2$.

The mean free path, L, is the average distance traveled in one second, divided by the number of collisions per second. For molecules of equal size:

$$L = \frac{\bar{V}}{n\bar{V} \pi d^2} = \frac{1}{n \pi d^2}$$

For the mean free path of two different types of particles having masses m_1 and m_2, radii r_1 and r_2, and mean speeds $\bar{V}_1$ and $\bar{V}_2$, the expression for mean free path of a particle of type 1 colliding with particles of type 2, is:

$$L = \frac{1}{\pi n_2 r_{12}^2 \left[1 + v_2^2/v_1^2\right]^{1/2}}$$

where $r_{12} = r_1 + r_2$ and n_2 is the number of particles of type 2 per cubic centimeter. When $\bar{V}_1$ equals $\bar{V}_2$ this equation reduces to:

$$L = \frac{1}{\sqrt{2} n_2 \pi r_{12}^2}$$

For a collision between two neutral particles or between a neutral particle and a charged particle, the effective diameter is of the order of 10^{-8} centimeters. The ARDC model atmosphere uses an average effective collision diameter of 3.65×10^{-8} centimeters. For these calculations this number is a constant for ions and neutral particles. The assumption of equal effective velocities, while valid for ion and neutral particle encounters, is not true for neutral and electron encounters. If the electron is considered as a point particle moving at a relatively high speed through the gas, the cross-sectional area of the cylinder of interception is just the cross-sectional area of one molecule, which results in a mean free path four times as large as that of the molecules. Assuming the neutral particle velocity to be negligible compared with the electron velocity, the mean free path of electrons with neutrals is found to be:

$$L_e = \frac{1}{n_2 \pi r_2^2} \text{ or } 5.64\, L_n$$

where L_n is the mean free path of neutrals with neutrals. The mean free paths for electron-ion and ion-ion pairs can be calculated by considering the Coulomb interaction. For a collision between an electron and an ion, the effective diameter is of the order of $10^{-5}\ Z_i\ (300/T)$ centimeters, where Z_i is the number of unit charges on the ion. For a collision between two ions, it is about $10^{-5}\ Z_i\ Z_j\ (300/T)$, where Z_i and Z_j are the number of unit charges on the two different ions (Reference 3-2). The collision frequencies for each pair of

particles is simply the ratio of the average particle velocity to the mean free path.

A The effective collision frequency is the total number of collisions with all particles per unit time. The effective mean free path is the average length of path traveled between collisions with all particles, and it is computed from the particle velocity and ratio of collision frequency to mean free path relationship.

The Debye shielding distance, h, is a measure of the distance over which the electron concentration can deviate appreciably from the positive charge concentration, and is defined as:

$$h = \left(\frac{kT}{4\pi n_e e^2}\right) = 6.90\left(\frac{T}{n_e}\right)^{1/2}$$

where T is the temperature in ^{o}K and n_e is the electron concentration in particles per cubic centimeter.

The Alfvén velocity is defined in the cgs system of units by:

$$U_o = B_o\sqrt{\frac{1}{4\pi\rho_i}}$$

where:

ρ_i = density of the ions in gm/cm^3

B_o = magnetic flux density in gauss.

3.3 SIMULATION PARAMETERS. - The experimental environment can only partially simulate and, thus, limits the number of Alfvén wave parameters that may be studied. This is because the low ionization concentrations, the small magnetic fields and the low densities of the ionosphere would normally result in very large characteristic dimensions for these waves. Laboratory experiments are limited to small characteristic dimensions; typical dimensions prior to the initiation of the McDonnell experiments, were a small fraction of a meter. The characteristic dimension of the McDonnell HIT experiments was approximately one meter. The following paragraphs indicate the importance of the major parameters and how each

influences the experimental design.

In the ionosphere two types of Alfvén wave propagation may exist: a plane wave traveling along a magnetic field line, or a guided wave traveling between the dielectric boundaries of various ionospheric layers. In the laboratory only guided waves exist, because of the boundaries of the confined plasma. To obtain plane wave propagation, the attenuation across the magnetic field lines must be great enough and the wave generation must be spatially confined to a region sufficiently far from the walls to eliminate the boundary effects. Therefore, in practice, a plasma of large cross section is required to propagate plane waves. In wave guide propagation, transverse magnetic (TM) and transverse electrical (TE) modes may exist. In general, both of these modes have cutoff frequencies which decrease with increasing experimental cross section; and for a fixed frequency, the attenuation decreases for increasing cross section. The physical size, therefore, determines the type of propagation that may exist, its minimum frequency, and its rate of attenuation.

The ion concentration in the ionosphere is a maximum of about 2×10^6 ions per cubic centimeter in the F2 region. The corresponding neutral particle density is about 10^9 particles per cubic centimeter, or the ionosphere is about 0.1 percent ionized. The ionization concentration determines the velocity of propagation of the wave, that is, the Alfvén velocity. The wave number, as determined by the propagation velocity, is influential in determining attenuation. Wave attenuation is inversely proportional to the conductivity and hence the ionization concentration, and is also affected by ion-neutral particle damping, which in the first approximation, is proportional to the ion-neutral collision frequency and inversely proportional to the Alfvén velocity. The desired condition of small wave damping in a partially ionized gas cannot be met in the laboratory, due to the normally high neutral-ion collision frequency and low conductivity. However, the require-

ment for high conductivity can be relaxed if low disturbance frequencies and large plasma dimensions are used. The only possibility of achieving low damping in a partially ionized gas, is through the generation of a low density plasma or a very cold plasma.

The magnetic field intensity influences the propagation velocity, the wave number, and the wave length, and therefore, the attenuation. The magnetic field determines the ion cyclotron frequency, which sets the upper limit of disturbance frequency. For Alfvén waves to predominate over acoustical disturbances in a plasma, the magnetic pressure $\left(\frac{B_o^2}{4\pi}\right)$ must greatly exceed the hydrostatic pressure. The amplitude of the wave, in theoretical considerations, is usually assumed to be small with respect to the ambient parameters.

In none of the theoretical studies of this program were ionization and recombination processes included. Because of the long recombination times large regions of the ionosphere can not change appreciably within the period of the Alfvén disturbance. Thus, frozen conditions for the characteristic times associated with experiments must be maintained. Other considerations in the choice and design of a plasma environment are:

1. Diagnostic equipment must be available to define plasma and experimental conditions easily and accurately.
2. The plasma generation mechanism should be completely decoupled from the wave excitation mechanism.
3. The propagation and the excitation of the wave should be capable of being studied independently.
4. Control of the simulation should be possible for a wide range of conditions.

3.4 SIMULATION FACILITIES

3.4.1 General. - The generation and propagation of Alfvén waves have been reported in liquid metals by Lundquist (Reference 3-3) and Lehnert (Reference 3-4) and in gaseous plasmas by Wilcox (References 3-5, 3-6 and 3-7) and Jephcott (References 3-8 and 3-9). The liquid metal experiments certainly cannot be scaled to the ionospheric conditions. The gaseous plasma experiments are very pertinent and provide some of the best MHD experiments conducted to date. These experiments have measured for high frequency Alfvén waves (500,000 cps), the phase velocity, attenuation, energy distribution and reflection characteristics. The waves generated were torsional waves, produced by a high current coaxial discharge. The gas used for most of the experiments was hydrogen, at a pressure of 100 microns of Hg. When waves were observed, the gas was nearly fully ionized and the magnetic field strength was above 7000 gauss. The attenuation effect of high ion-neutral collision frequency, which prohibits the study of the waves in a small volume, partially ionized gas, can be reduced in a facility such as a Hypervelocity Impulse Tunnel (HIT) since it is adaptable to the generation of large plasma environments.

The Hypervelocity Impulse Tunnel (Figure 3-2) is a facility having a test section 50 inches in diameter, at a distance of twenty feet from the throat of the expansion chamber. The HIT achieves its particular local flow by expanding the arc chamber high pressure and high temperature gases through a nozzle, resulting in a reduction of the local temperature, and thereby lowering the speed of sound, and an increase in the local flow Mach number, without affecting the stagnation temperature. For the McDonnell facility, Mach numbers up to 27 can be generated for periods up to 100 milliseconds. The end of useful flow occurs when dissociation and ionization of the gas

MCDONNELL AIRCRAFT
HYPERVELOCITY IMPULSE TUNNEL

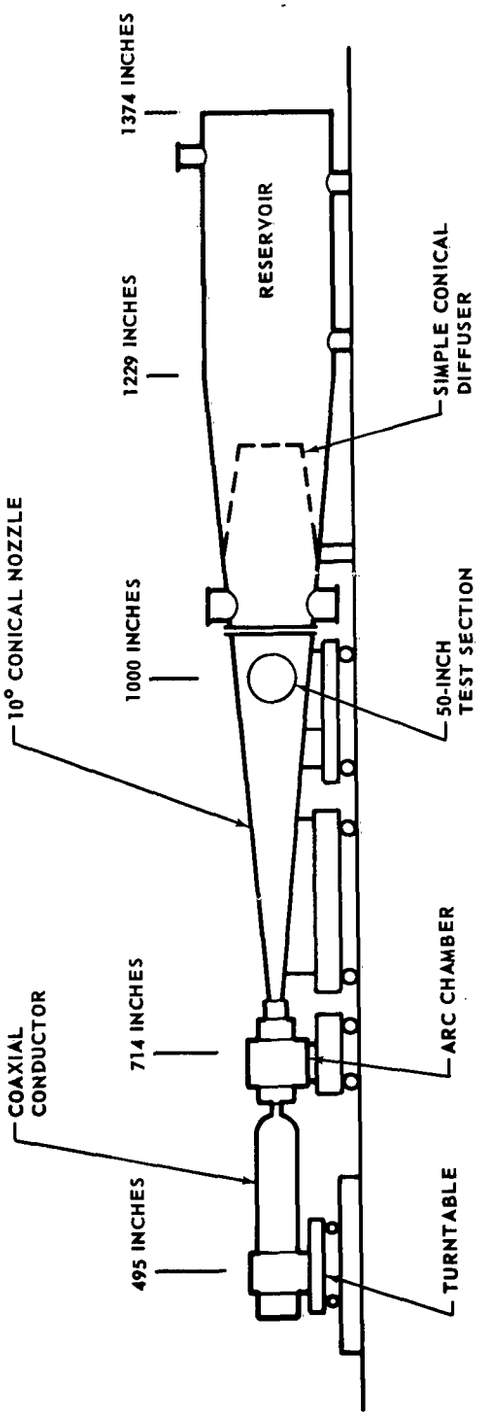

FIGURE 3-2

commences. The purpose of this program was to extend the normal operating range of the HIT into that required for ionospheric simulation, that is, by operating when the flow was partially ionized. Since this facility had not been operated under such conditions prior to the start of this experimental program, a detailed study of the facility was made in order to optimize the flow for the generation of Alfvén waves, their propagation and measurement.

During the course of the program two additional plasma generators served as useful tools augmenting the tunnel experiments. These facilities were capable of inexpensive tests for developing instrumentation and consisted of an electromagnetic shock tube and an arc discharge tube. The theory of operation of both of these facilities is given in Sections 3.4.3.1 and 3.4.3.2.

3.4.2 Plasma Flow in the Hypervelocity Impulse Tunnel

3.4.2.1 Introduction. - While many sources describe flow conditions existing in a hypersonic nozzle or discuss the flow phenomena, few present a comprehensive discussion covering all phases of nozzle or tunnel operation at conditions suitable for plasma experimentation. This section will describe the operation and flow phenomena of the arc chamber and hypervelocity nozzle, of the McDonnell Hypervelocity Impulse Tunnel, and will present the thermodynamic conditions for various phases of operation, comparing several analytical techniques used in describing the flow.

3.4.2.2 Tunnel Construction. - The McDonnell Aircraft Corporation Hypervelocity Impulse Tunnel facility consists of an arc chamber in which a high pressure, high temperature gas is created by an electrical discharge from a capacitor bank, a divergent conical nozzle leading to a constant area test section, and a reservoir which contains a conical diffuser to eliminate shock reflections through the test section. Initially, the arc chamber is

separated from the test section by a diaphragm near the nozzle throat which ruptures during pressure build-up following initiation of the electrical discharge. A schematic drawing of the McDonnell tunnel is shown in Figure 3-2.

The arc chamber consists of an outer case, designed to withstand 100,000 psia, into which a cartridge assembly is inserted prior to each firing. The components of the cartridge assembly are an internal liner, the throat and diaphragm assembly, the electrode assembly, the dump port assembly, and fittings for transducers and gas filling ports. The electrical discharge is initiated by exploding a trigger wire which runs from a trigger assembly within the center electrode to the outer electrode. The exploding wire ionizes the gas in the gap between electrodes, increasing the electrical conductivity in this region and creating a current path for initiating the capacitor bank discharge.

Temperatures and pressures achieved in the arc chamber are determined by the quantity of energy available from the arc discharge and by the volume of gas into which the energy is absorbed. The volume of the internal liner can be varied from 100 to 1200 cubic inches. The maximum storage capacity of the capacitor bank is 7,000,000 joules at 12,000 volts; maximum discharge current is 3,600,000 amperes. The energy level of the discharge is varied by controlling either the voltage or the number of capacitors in the bank.

The diaphragm, which is commonly of Mylar, is placed slightly forward of the nozzle throat. The nozzle throat diameter is adjustable and may be varied from less than 0.1 inch to greater than 1.5 inches, although the larger sizes would not normally be used for aerodynamic testing. Nozzle throat sections are commonly machined from copper or tungsten.

A conical nozzle with a total included angle of 10 degrees leads from the throat to a 50-inch diameter test section. The distance from the nozzle

throat to this test section is approximately 23 feet, with ports for ionization gages or other probes provided at intervals along the nozzle wall. The test section has a 37.5 inch diameter viewing window, which permits high speed photographs of the flow and microwave interferometer measurements of electron concentration.

The test section is followed by a fixed conical diffuser with an area ratio (diffuser throat area to 50-inch diameter test section area) of 0.5. From the diffuser the flow passes into the reservoir. A vacuum system, consisting of both mechanical and oil diffusion pumps, is connected to the reservoir and is capable of evacuating the total volume of the tunnel to 1 micron Hg in 15 minutes.

3.4.2.3 Operating Regimes. - The analysis of the HIT flow is divided into the characteristic regimes of the arc chamber, the starting shock, the blow-down flow, and the flow breakdown.

The arc chamber is first charged with the desired gas. As the capacitor bank is discharged through the electrodes, the gas is heated and the pressure increases rupturing the diaphragm near the nozzle throat and initiating a shock wave which moves downstream into the nozzle. The arc chamber pressure then continues to rise until the discharge is complete. The analysis of the arc chamber, discussed in paragraph 3.4.2.4, will be concerned with the equilibrium concentrations of electrons and ionized species at arc chamber conditions, and with the changes which occur as the arc chamber gas discharges through the throat.

Rupture of the nozzle diaphragm initiates a shock wave which travels downstream into the low pressure gas in the tunnel. During this "starting cycle" the tunnel resembles a shock tube with a divergent nozzle. The initial shock is followed by the contact surface and then by a second shock or rare-

faction wave, depending upon conditions existing in the tunnel. The region between the initial shock and the contact surface, referred to as the "shock-excited" region, is brought to high temperature and pressure by the shock. This region is discussed in detail in paragraph 3.4.2.5 because it was deemed useful for the plasma experiments.

After the shock system, created when the diaphragm bursts, has decayed, the arc chamber discharges into the tunnel in a quasi-steady flow referred to as the blow-down flow. This flow reaches the test section at a relatively high velocity, but low temperature. Because of the rapid expansion, the nozzle flow may occur under nonequilibrium conditions, where chemical and electron recombination reactions are "frozen" at some point in the nozzle. If freezing occurs, the electron concentration may remain at a relatively high level despite the rapid cooling of the gas. Flow conditions in the blow-down region are examined in detail in paragraph 3.4.2.6.

The final stages of discharge from the arc chamber are characterized by a region of unsteady flow referred to as flow breakdown and the flow direction may reverse as the result of an increase in pressure within the reservoir.

3.4.2.4 Arc Chamber Performance. - The performance characteristics of the arc chamber influence the nature of the flow during the starting cycle and blow-down periods. In the initial phase, during discharge of the capacitor bank, thermodynamic changes occur as a result of the finite time required for arc discharge, and in later phases these changes occur as a result of mass loss accompanying expansion of the gases into the tunnel.

In order to obtain the high ion and electron concentrations required for the propagation of Alfvén waves, it was necessary to work with unusually high temperatures in the arc chamber. As a consequence, the initial charge pressures in the arc chamber, being of the order of 25 psig, were much less

then those normally used for aerodynamic testing. For these tests, the arc voltage was lower than usual, and the damping time was correspondingly longer. In Figure 3-3 is presented a typical capacitor bank voltage record for one of the higher temperature tests. For this test the arc voltage during the first half cycle is estimated to be 2.5 KV, and the maximum current, determined graphically, is 2.24×10^6 amperes. The energy input during the first quarter cycle is found to be approximately 2.5×10^6 joules. The stored energy in the condenser is 4.63×10^6 joules. It is evident that over half of the available energy is added within the first half millisecond. The energy stored in the capacitor bank is equal to $1/2\ CE^2$, but the energy delivered to the gas is less, and is determined by the peak arc chamber pressure and the initial gas density.

The temperature rise achieved in the arc chamber as a result of the electrical discharge is determined from the measured arc chamber pressure. A typical pressure trace from an oscillograph record is shown in Figure 3-4. Although the Norwood strain gage transducers have a rapid response time, an appreciable response lag is introduced by a length of small tubing containing several orifices inserted between the transducer and the chamber to protect the transducer from the hot gases. This lag, of the order of 15 milliseconds, is clearly evident in the figure. After peak pressure is reached, the pressure decays at a steady rate due to discharge of gas through the nozzle. An overshoot at the peak value is often observed. Assuming that the pressure decay rate during the first 10 to 15 milliseconds is equal to that measured during the latter phase of the gas discharge, the peak arc chamber pressure is estimated by extrapolating the measured decay rate to its value at 1 millisecond after initiation of arc discharge. The extrapolation is illustrated in Figure 3-4. The temperature rise in the arc chamber is then obtained from

CAPACITOR BANK VOLTAGE RECORD DURING
ARC DISCARGE

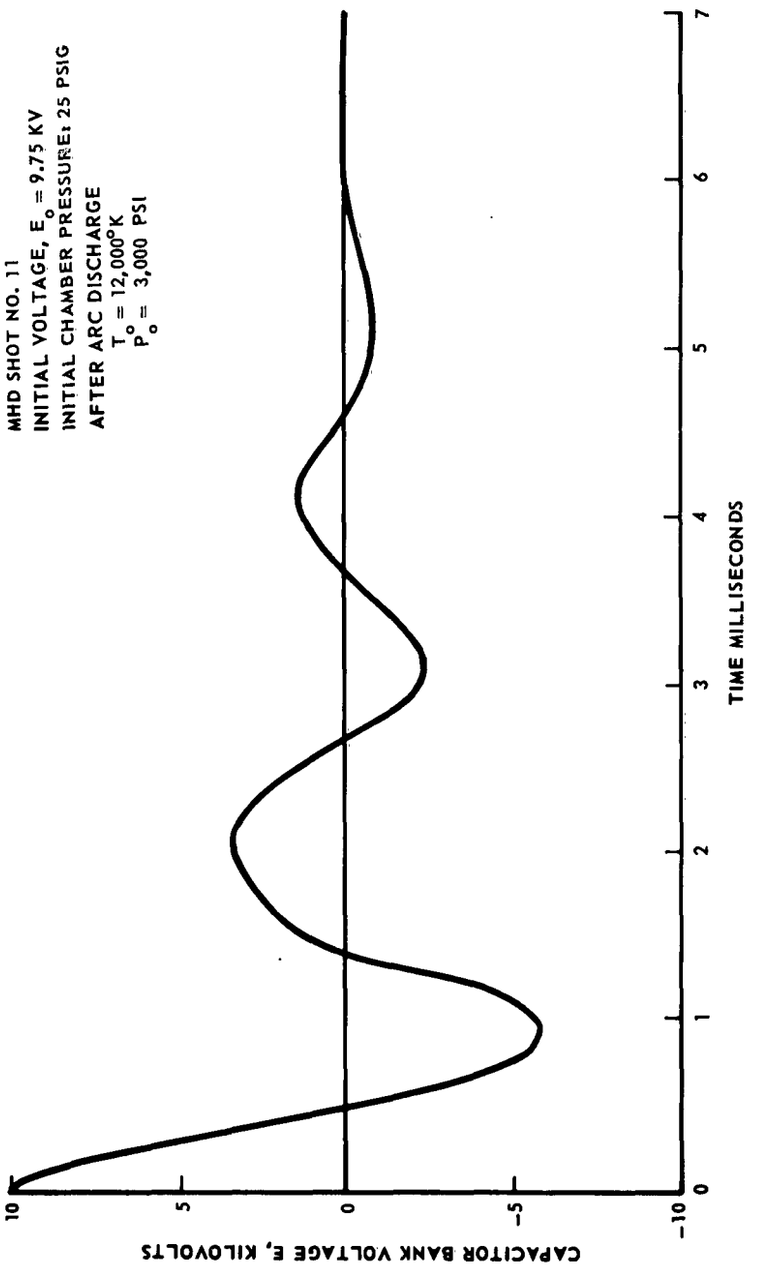

FIGURE 3-3

ARC CHAMBER PRESSURE TRACE

RUN NO. 486
0.4 INCH THROAT DIAMETER
LINEAR VOLUME 675 CU.IN.
CHARGE PRESSURE: 56 PSIG
8.55 KV

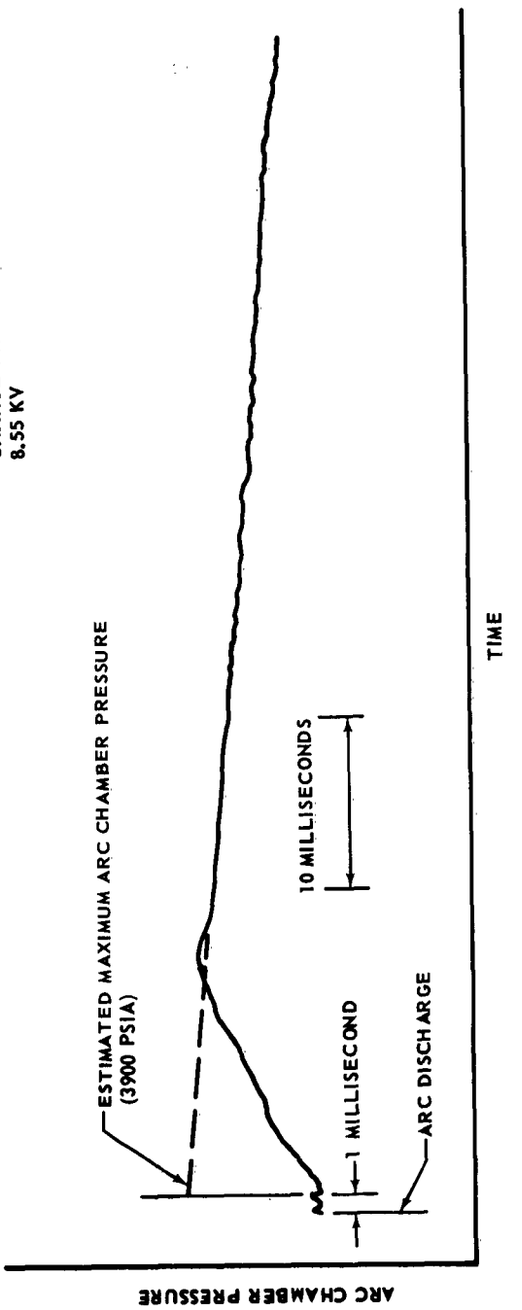

FIGURE 3-4

tables of high temperature gas properties, with the further assumption that energy addition takes place along a constant density path. The pressure decay is the result of a mass loss through the nozzle, as well as a temperature drop.

The degree of ionization represented by the electron concentration is an important thermodynamic parameter for plasma studies. Equilibrium electron concentrations in helium, nitrogen, and air are presented in Figure 3-5 as functions of arc chamber temperature and pressure. The assumption of equilibrium conditions in the arc chamber appears to be justified when the relatively long holding time for the gas in the arc chamber is compared with the ionization and relaxation times. Petcheck and Byron, Reference 3-10, for instance, report that at 10,000°K and 5 cm of Hg pressure the time to reach equilibrium ionization behind a shock wave in argon is of the order of 100 microseconds. At the higher densities of interest, the time required for ionization should be proportionately shorter.

The electron concentration at the nozzle throat may be significantly less than that computed for equilibrium conditions in the arc chamber, as a result of the lowered temperature and density at the throat.

The extent of this reduction for the case of nitrogen flow can be estimated from Figures 3-6, 3-7, and 3-8 where temperature, pressure and density ratios at the throat are compared with the arc chamber conditions. For these figures the usual isentropic compressible flow relations have been used. Equilibrium concentrations at the throat can be found from Figure 3-5 by substituting throat properties for the corresponding arc chamber values.

3.4.2.5 Shock - Excited Flow

General Description. - If a duct is divided by a partition into two sections in which a pressure differential exists, a combination of wave phenomena will follow a sudden removal of this partition. A shock wave propagates into the low

EQUILIBRIUM REAL GAS ELECTRON CONCENTRATION

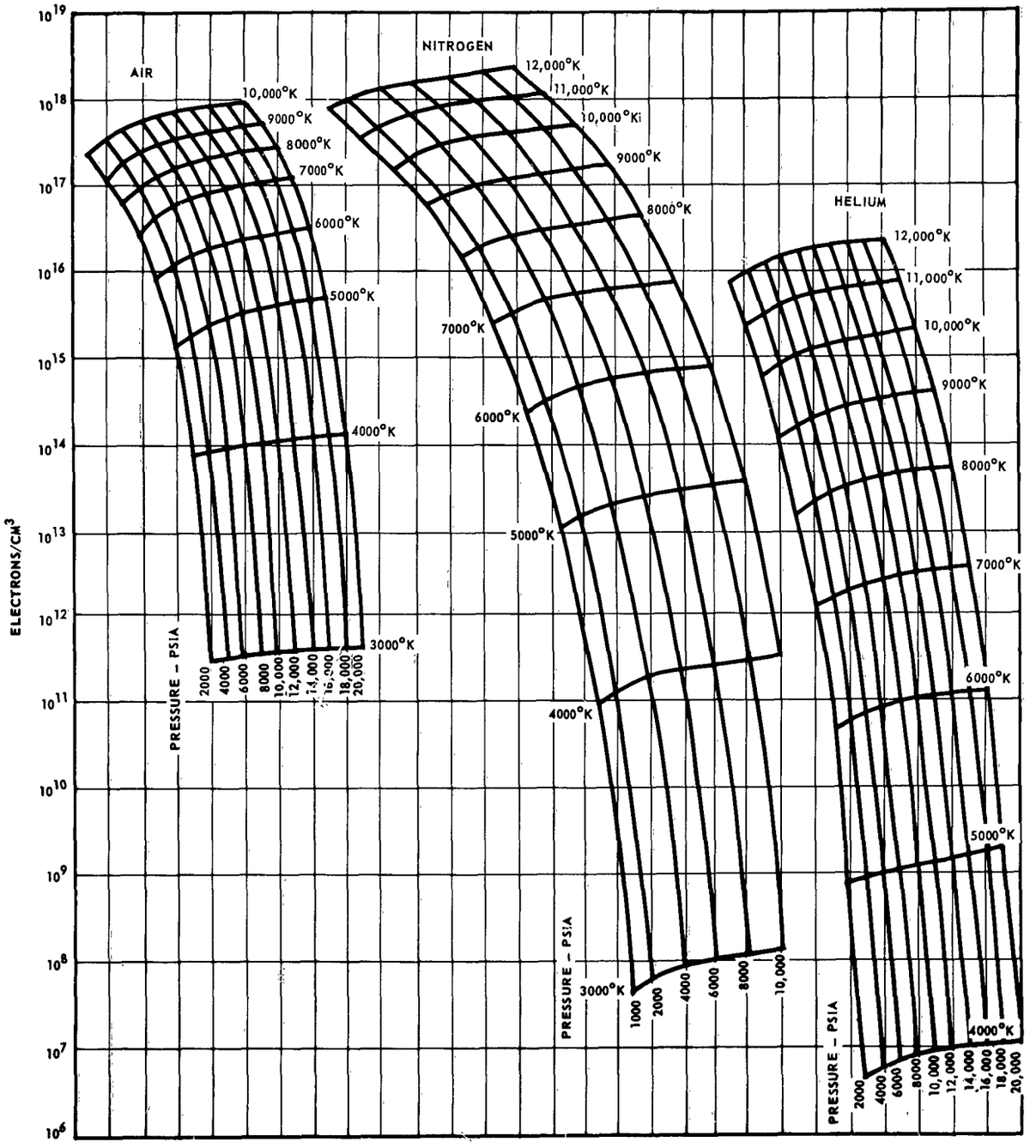

FIGURE 3-5

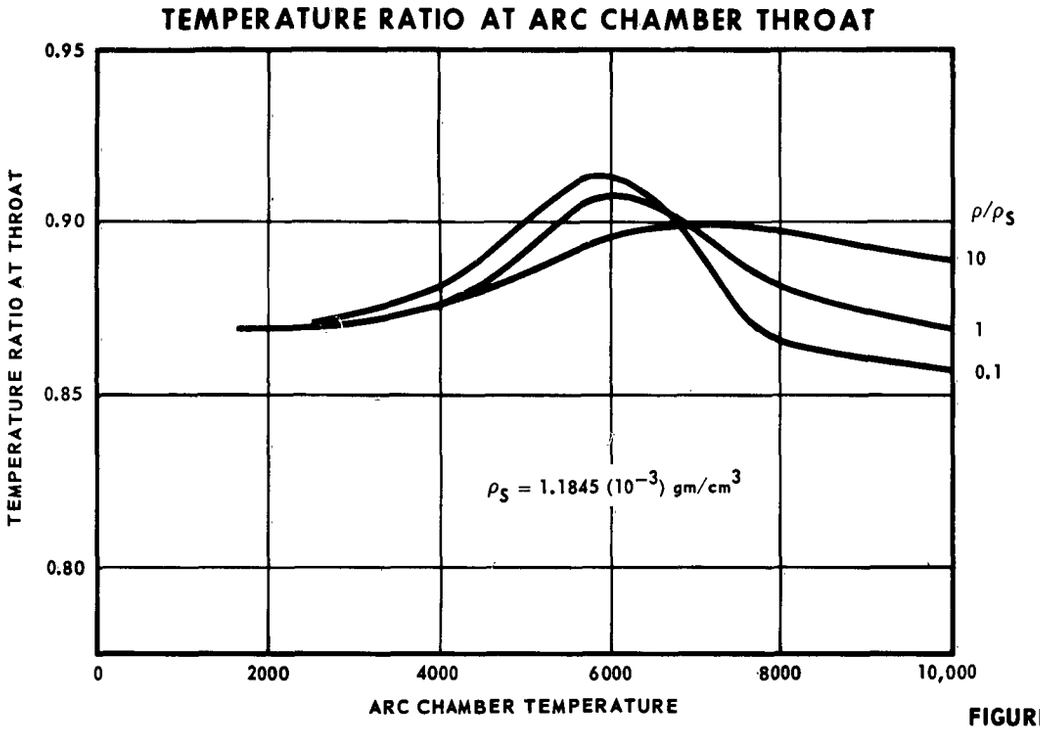

FIGURE 3-6

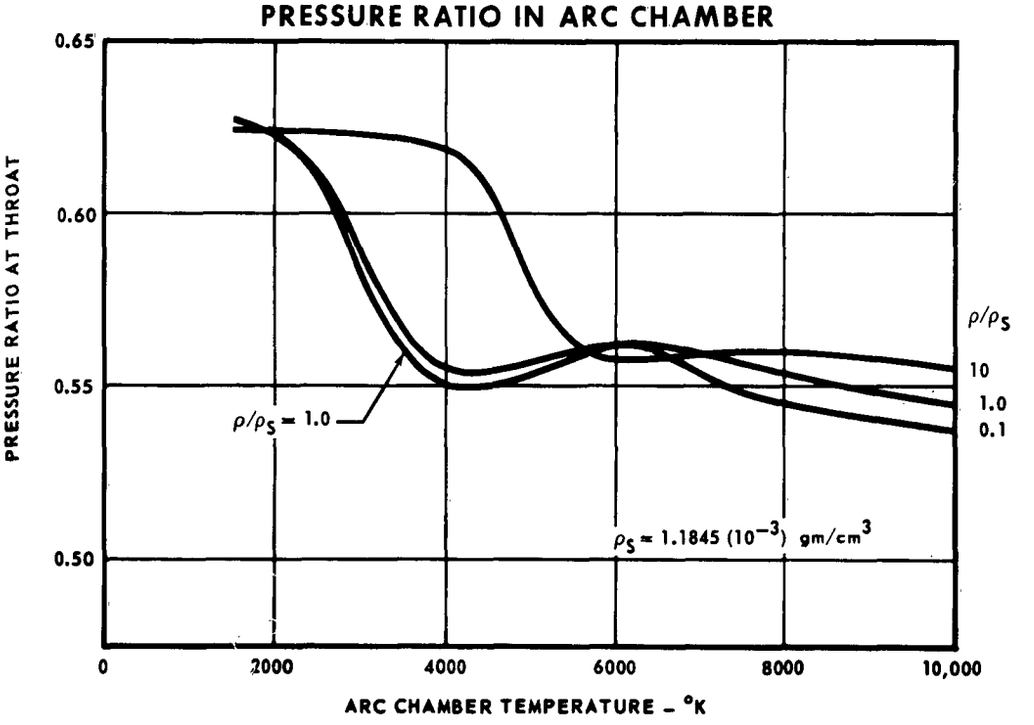

FIGURE 3-7

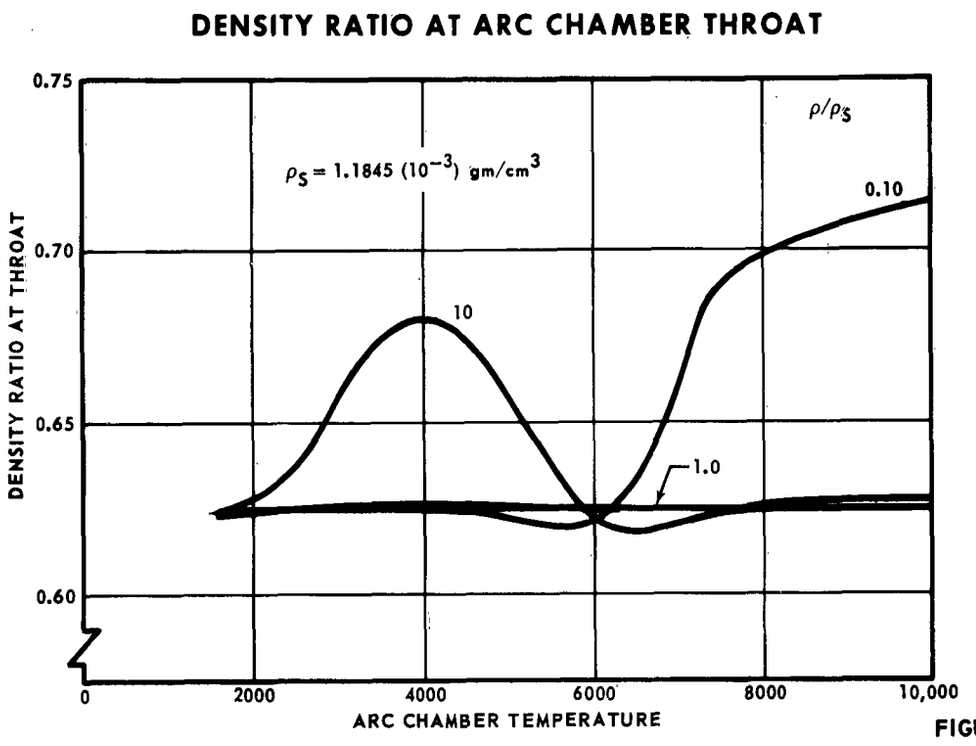

FIGURE 3-8

pressure region and a rarefaction fan propagates into the high pressure gas. The gas particles that were initially in contact with the partition form a contact surface, a temperature discontinuity separating the two adjacent gases. The resultant wave diagram is shown in Figure 3-9. The gas that is swept out by the shock wave is compressed and appears as region 2 in the wave diagram.

If the duct is of constant area, as in the simple shock tube, the downstream propagating shock wave theoretically does not attenuate as it moves down the tube. On the other hand, if the duct has a divergent cross-section, the downstream propagating shock wave decreases in strength, and a secondary wave appears, which propagates in the upstream direction. One possible wave system for the divergent duct considers that the rarefaction fan, which propagates upstream, separating regions 3 and 4, coalesces into the secondary wave of the divergent channel. Depending upon the area ratio, pressure ratio, and initial shock strength, the secondary wave may be either an upstream propa-

MHD Wave Investigation
II - theory

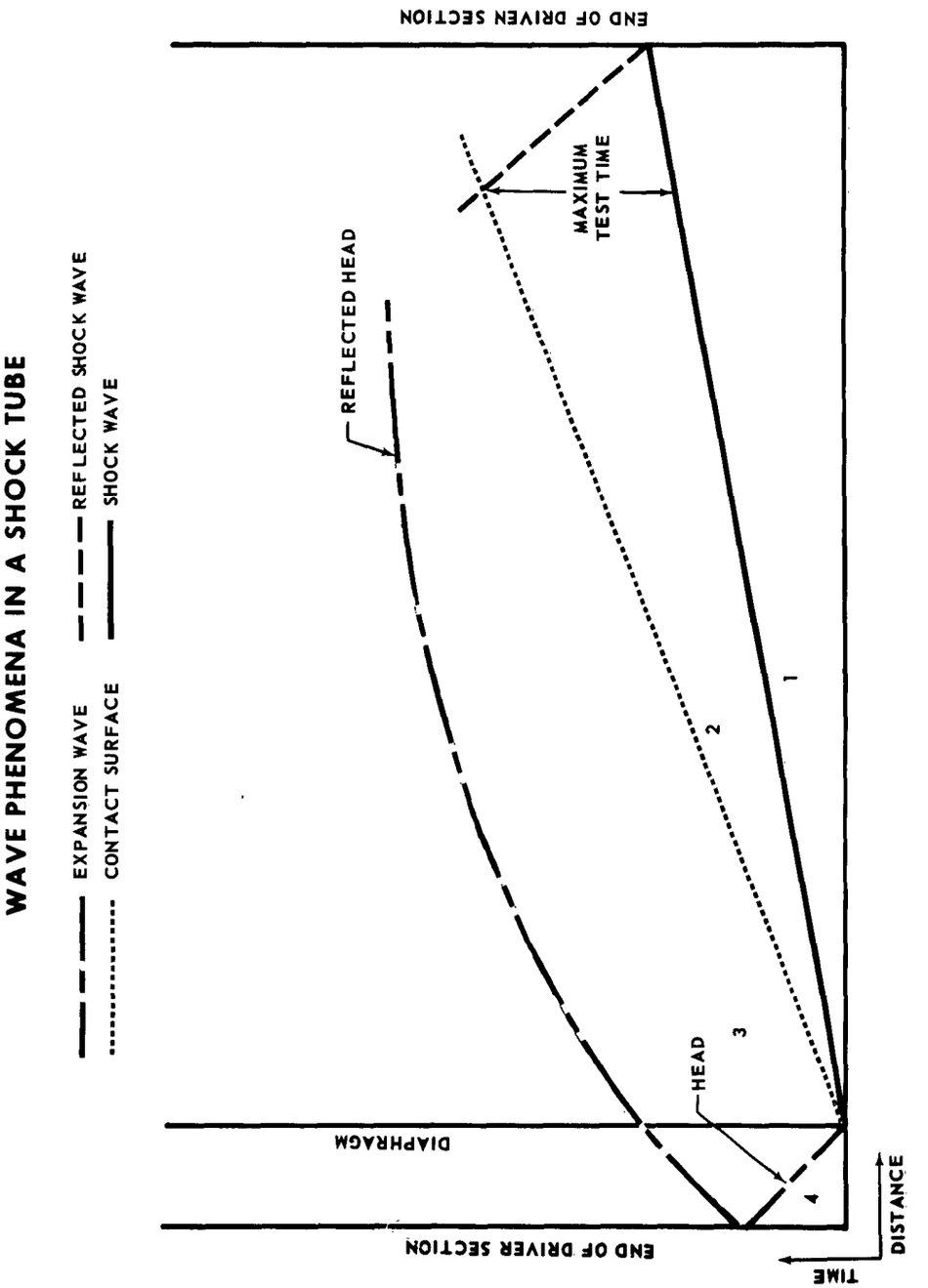

FIGURE 3-9

gating expansion wave or an upstream propagating shock wave. Although the wave propagates upstream in either case, it travels downstream relative to the tube and increases in strength as it does so. This is the wave system assumed for this study.

The basic equations, describing the wave phenomena used in analyzing the shock excited flow in both the constant area shock tube and the diverging hypersonic nozzle, are the same. The analysis presented for the shock excited region is based mainly on ideal gas relationships, although some real gas effects have been taken into account in the discussion of the "integral" approach to the expanding nozzle. Upon diaphragm rupture, three disturbances are created. First, a shock wave forms and travels downstream. Secondly, a contact surface, which separates the high pressure driver gas from the low pressure driven gas, propagates downstream behind the shock wave. Finally, an expansion wave is formed, the head of which propagates upstream into the driver section and is reflected downstream from the end of the driver chamber (arc chamber). The tail of the expansion wave attempts to travel upstream into the driver section, but can be swept downstream by the gas flowing from the driver chamber. Testing normally takes place in the shock processed gas between the shock wave and the contact surface. The test time is, therefore, the duration of time between passage of the shock wave and passage of the contact surface past a given test section. In a closed tube the primary shock is reflected and different properties are found in the region behind it. Test time in the main shock processed gas is limited by either the shock wave reflecting off the downstream end of the tube and interacting with the contact surface, or by the expansion wave, reflected downstream from the back of the driver chamber interacting with the contact surface. Because the length of the driven section (nozzle-reservoir) is long compared to that of the driver

section in most shock tubes, the expansion wave-contact surface interaction does not occur.

The theoretical speed of the shock generated at diaphragm rupture may be determined from the stagnant conditions existing on both sides of the diaphragm before rupture. The pressures and velocities in regions 2 and 3 are equal. The velocities of regions 1 and 4 are equal to zero. The resulting expression for shock strength in the shock tube is:

$$\frac{p_4}{p_1} = \left(\frac{\gamma_1 - 1}{\gamma_1 + 1}\right)\left(\frac{2\gamma_1 M_s^2}{\gamma_1 - 1} - 1\right)\left[1 - \left(\frac{\gamma_4 - 1}{\gamma_1 + 1}\right)\frac{\left(M_s - \frac{1}{M_s}\right)}{a_4/a_1}\right]^{\frac{-2\gamma_4}{\gamma_4 - 1}}$$

where:

p = pressure

γ = ratio of specific heats (c_p/c_v)

M_s = shock Mach number

a = speed of sound

The shock Mach number is a function only of stagnant conditions existing before diaphragm rupture. With increasing diaphragm pressure ratio (p_4/p_1) shock strength increases asymptotically to an upper limit, determined primarily by the speed of sound ratio (a_4/a_1). A low value of γ_4, as well as a high value for a_4/a_1, is desirable to obtain maximum shock strengths. If the initial temperature is the same on both sides of the diaphragm, as is usually the case in simple shock tubes, the maximum attainable shock strengths are given in Table 3-3. However, by going to a driver gas with a much higher temperature than the gas in the low-pressure side, stronger shock waves can be generated, which is an advantage of the arc driven shock tube. The shock Mach numbers are of course only theoretical values, which are not met in practice, but only for Mach numbers of 20 or greater can a high degree of ionization be obtained.

The initial operation in a divergent channel with the diaphragm downstream

TABLE 3-3

MAXIMUM SHOCK STRENGTHS OBTAINABLE IN A SHOCK TUBE

Gas Combination	a_4/a_1	(p_2/p_1) max	$M_{s_{max}}$
Air-air	1.00	44	6.16
Helium-air	2.93	132	10.64
Hydrogen-nitrogen	3.73	574	22.42
Hydrogen-air	3.85	590	22.5

of the throat, as in the McDonnell HIT, is similar to the operation of a shock tube of constant area, except that the gas velocity in region 4, Figure 3-9, is no longer zero, but equal to the local speed of sound. With this one change, equation 3-2 now becomes:

$$\frac{p_4}{p_1} = \left(\frac{\gamma_1 - 1}{\gamma_1 + 1}\right)\left(\frac{2\gamma_1 M_s^2}{\gamma_1 - 1} - 1\right)\left[1 - \left(\frac{\gamma_4 - 1}{\gamma_1 + 1}\right)\frac{\left(M_s - \frac{1}{M_s} - \frac{\gamma_4 + 1}{2a_1} U_4\right)}{a_4/a_1}\right]^{-\frac{2\gamma_4}{\gamma_4 - 1}}$$

where U_4 is the gas velocity in region 4. If the diaphragm is located exactly at the throat, or upstream of the throat, the expansion wave propagates into essentially a stagnant region and initial operation is identical to that of the shock tube.

At diaphragm rupture, a high velocity normal shock wave travels downstream into the undisturbed low pressure driven gas. Sketches of the pressure distribution through the shock excited region, as it progresses down the nozzle, are shown in Figure 3-10. The downstream propagating shock is followed by a region of shock processed gas flow which is terminated by the contact surface. Behind the contact surface is a region of steady flow which is bounded by an upstream propagating disturbance. Behind this disturbance is the quasi-steady blow-down flow. The upstream propagating disturbance starts out at the throat as an unsteady expansion wave, propagating at sonic velocity, but is swept downstream

PRESSURE DISTRIBUTION ALONG NOZZLE

STARTING PROCESS

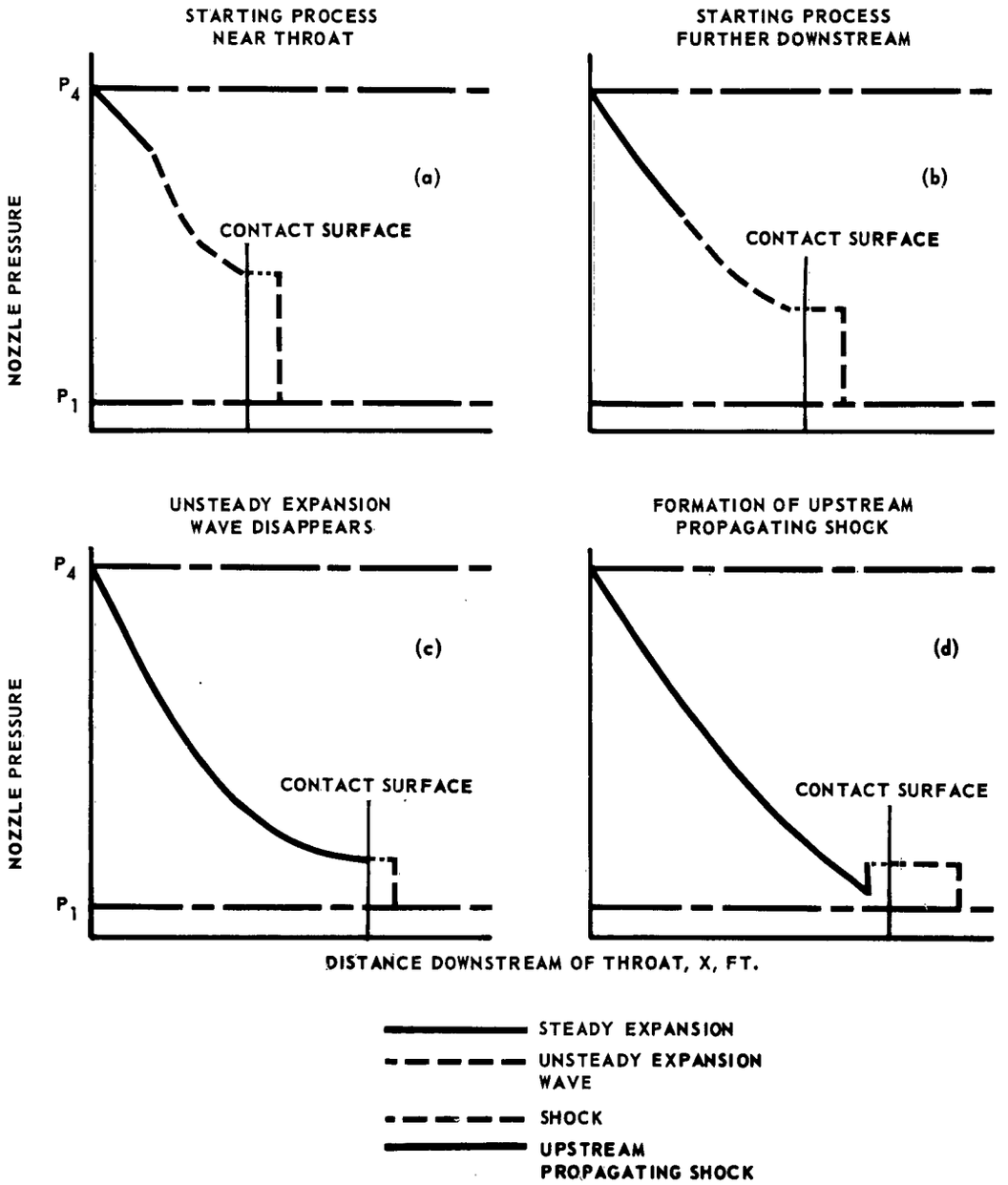

FIGURE 3-10

into the nozzle. It decays in strength as it progresses down the nozzle, Figure 3-10a and 10b. At some nozzle station the expansion wave vanishes (Figure 3-10c), and a weak normal shock wave forms, propagating upstream (Figure 3-10d). This shock increases in strength as it proceeds downstream.

When the unsteady expansion wave vanishes, the pressure of the quasi-steady blow down flow equals the pressure of the initially shock processed gas. As the entire process travels further down the nozzle, the pressure at the head of the quasi-steady blow-down flow decreases. Since the pressure generated by the initial, or downstream, propagating shock is greater than the blow-down pressure, an upstream propagating shock wave is necessary to provide a pressure adjustment. This shock wave adjusts the flow conditions between the HIT starting process and its quasi-steady blow-down flow out of the driver section.

The initial shock strengths at diaphragm rupture in the divergent channel, discussed above, have been calculated and are shown in Figure 3-11 (a-c). The shock Mach number in a divergent channel is greater than the shock Mach number of a simple shock tube for the same conditions, due to the addition of the velocity term, U_4. Figure 3-12 shows this comparison.

The normal shock decreases in strength as it travels down the divergent tube. In this program three different analyses have been used to predict the shock decay, because none seem to be clearly superior to the other two. One method is based on an approximate analysis presented in References 3-11, 3-12 and 3-13. A second approach uses the method of characteristics as defined in References 3-14 and 3-15. The third method is an "integral" approach, utilizing the simultaneous solution of the basic equations describing the wave and flow phenomena existing at discrete intervals along the axis of a divergent channel. Several typical sets of conditions for a helium-air system will be compared in the following paragraphs, utilizing the three approaches to

INITIAL SHOCK IN HYPERSONIC NOZZLE

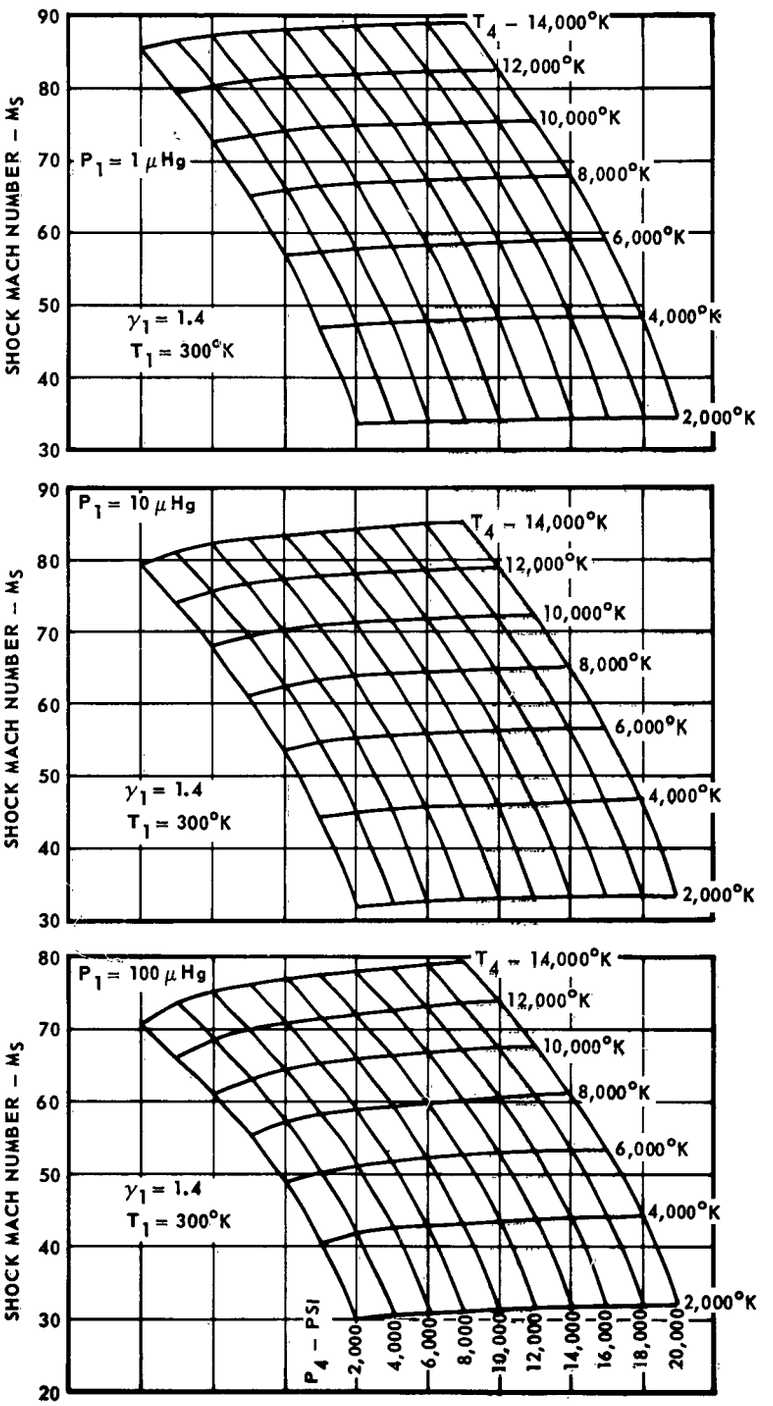

FIGURE 3–11

MHD Wave Investigation
II - theory

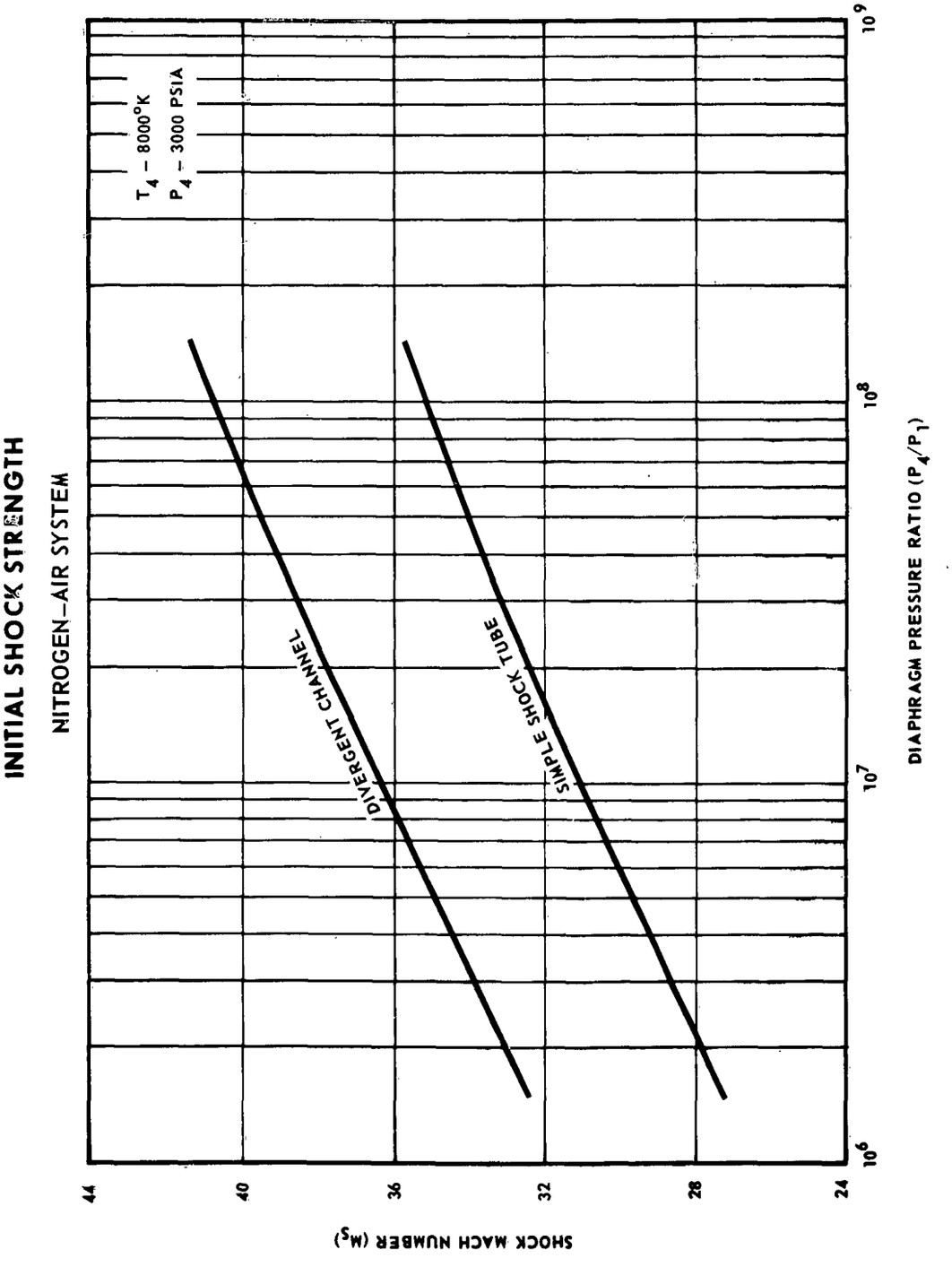

FIGURE 3–12

describe the shock and the shock excited region.

Analytical Approximation - Chisnell has developed an approximate expression for the primary shock wave, as it passes through a diverging duct. The equation is:

$$\frac{M_{s1}}{M_{s2}} = \left(\frac{A_1}{A_2}\right)^{-\frac{K_\infty}{2}}$$

The exponent K_∞ is a function of the specific heat ratio, γ, and is given by the expression:

$$K_\infty = 2\left[\left(1+\sqrt{\frac{2}{\gamma(\gamma-1)}}\right)\left(1+\sqrt{\frac{2(\gamma-1)}{\gamma}}\right)\right]^{-1}$$

Shock wave attenuation curves for three typical values of γ are presented in Figure 3-13. A value for γ of approximately 1.22 is representative of conditions in shock heated air.

Method of Characteristics - The method of characteristics, for the solution of the differential equations describing simple one-dimensional, unsteady duct flow, has been programmed on an IBM 7090 digital computer to arithmetically generate the system of characteristic lines for ideal gas flow. By plotting the generated points and drawing in the network lines, variations in properties throughout the field may also be determined.

Figure 3-14 presents the shock attenuation for several helium-air systems. The related test times are given in Table 3-4. A portion of the characteristics network at approximately 23 feet from the diaphragm for the HIT (10 degree conical nozzle with a 1.5 inch diameter throat) is presented in Figure 3-15, for a 8100°K and 6200 psia helium driver into room temperature air at 5 microns of Hg. A cross plot of the conditions at the test station, presented in Figure 3-16, gives the variation of gas temperature with test time in the shock excited region. The ordinate length between the shock and

MHD Wave Investigation
II - theory

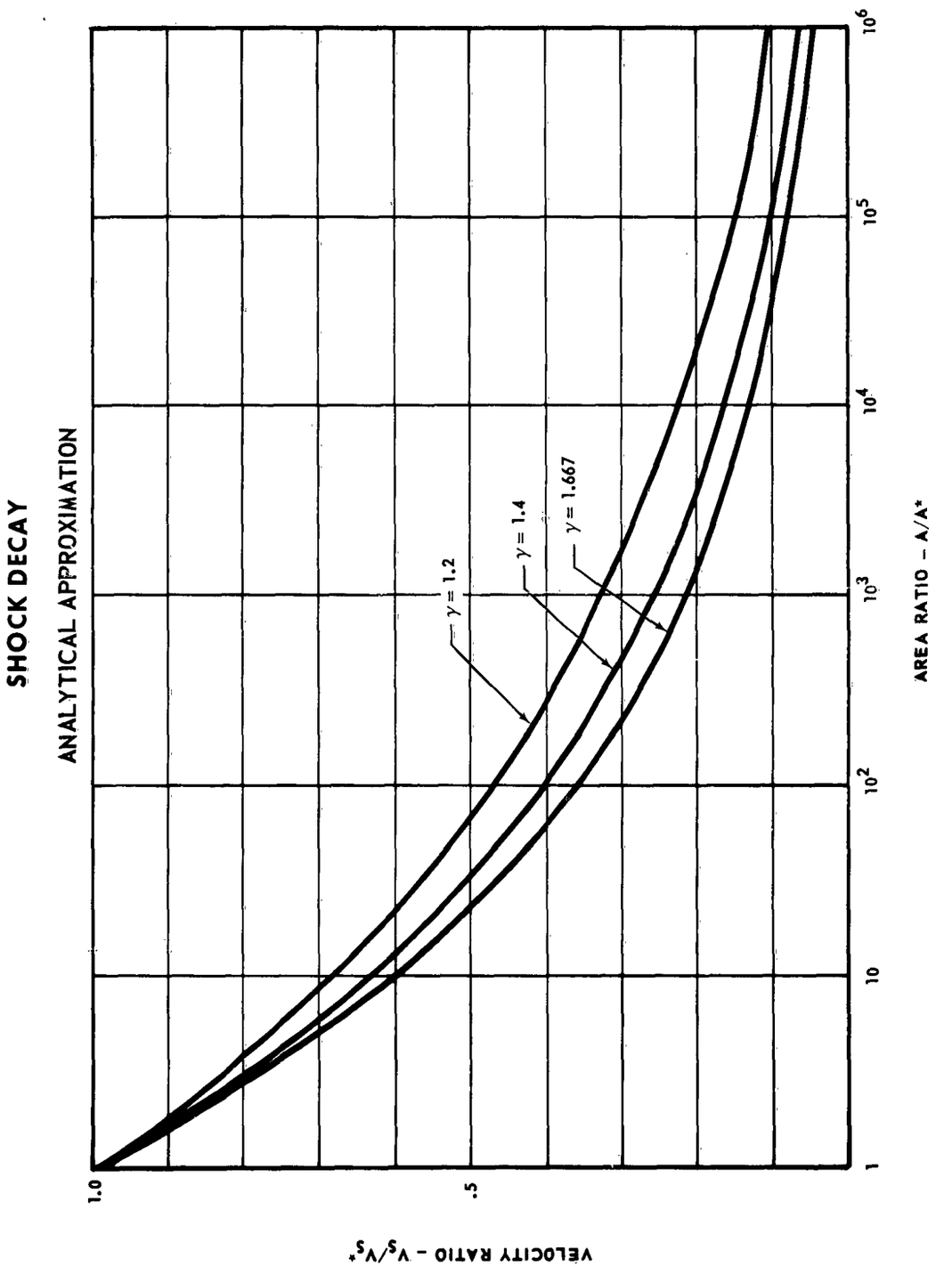

FIGURE 3–13

MHD Wave Investigation
II - theory

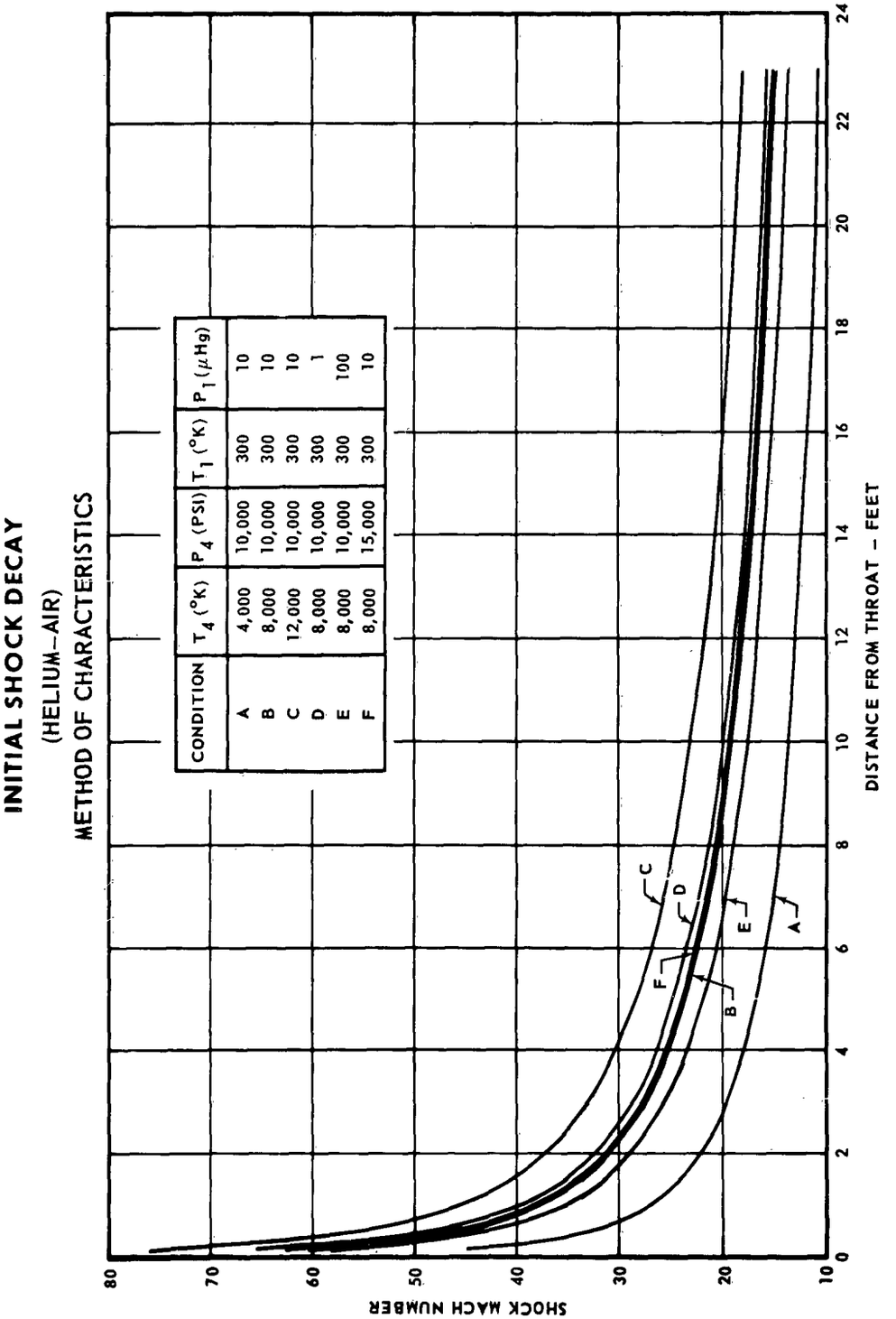

FIGURE 3-14

MHD Wave Investigation
II - theory

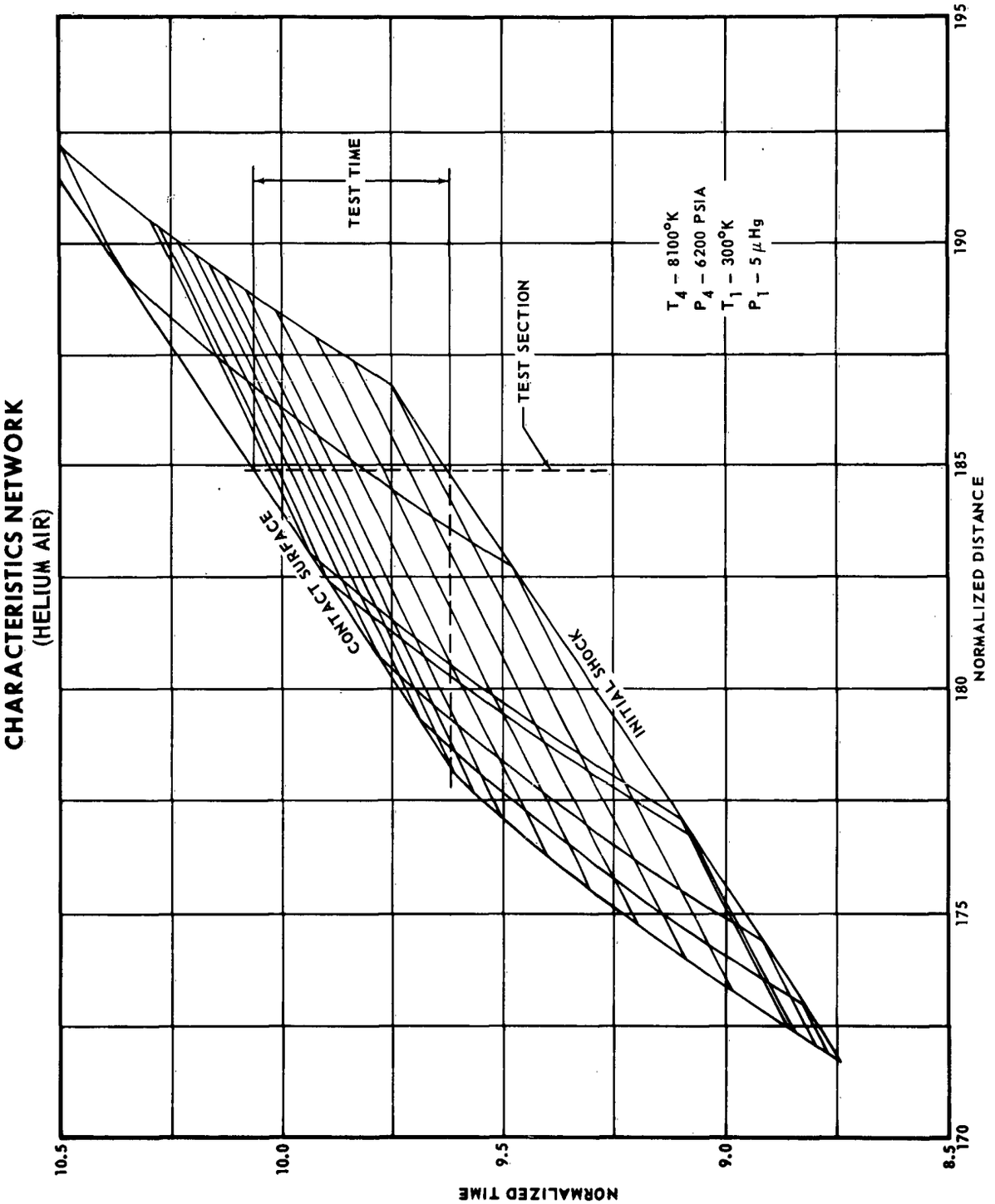

FIGURE 3–15

MHD Wave Investigation
II - theory

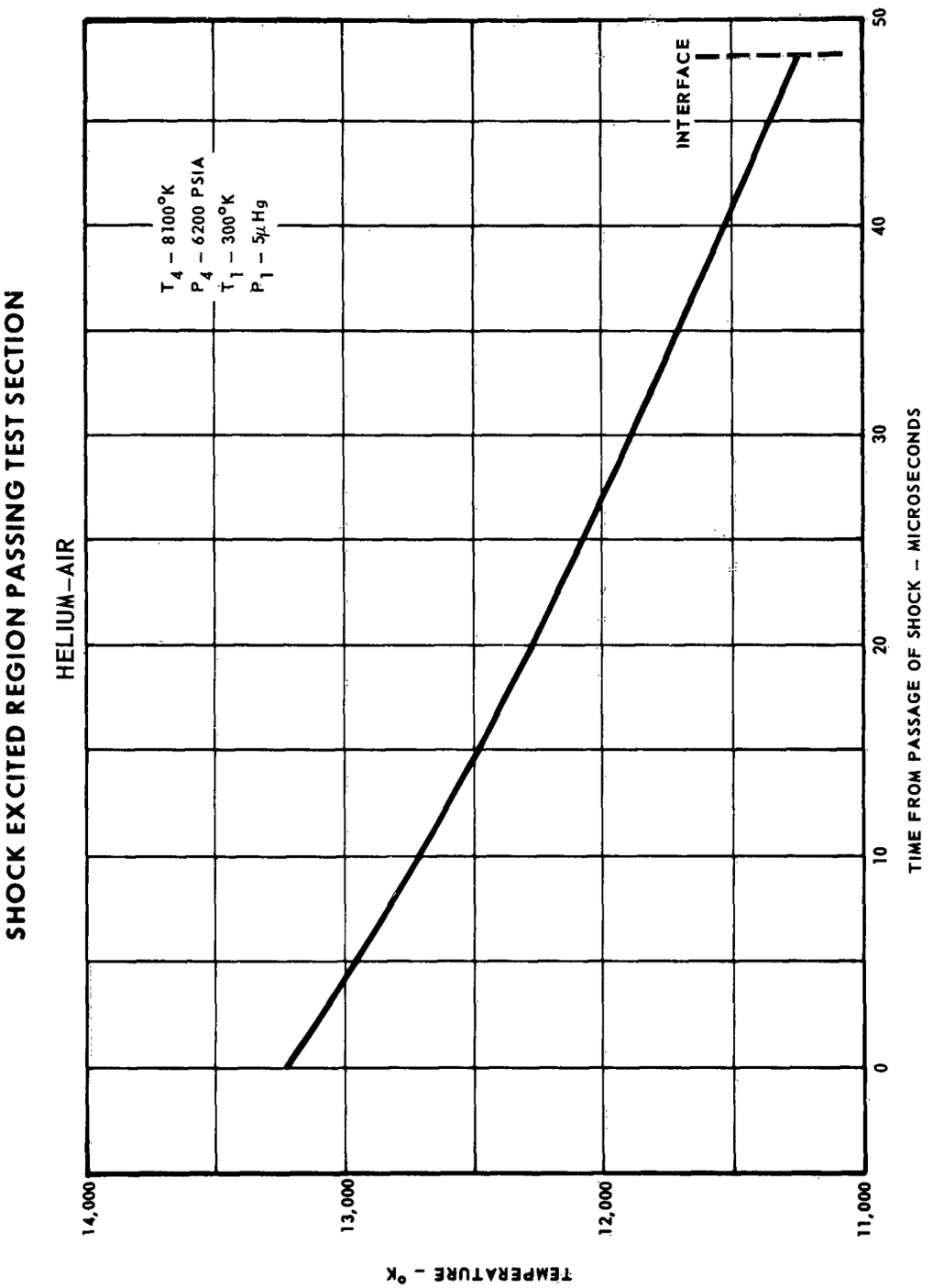

FIGURE 3–16

TABLE 3-4

TEST TIMES

HELIUM–AIR		TEST SECTION AT 23.1 FEET			METHOD OF CALCULATION	INTEGRAL	
CASE	T_4 (°K)	P_4 (PSIA)	T_1 (°()	P_1 (μ Hg.)	CHARACTERISTICS (μ SEC)	IDEAL GAS (μ SEC)	REAL GAS (μ SEC)
A	4000	10,000	300	10	48	177	66
B	8000	10,000	300	10	48	128	38
C	12000	10,000	300	10	48	106	33
D	8000	10,000	300	1	48	119	35
E	8000	10,000	300	100	48	147	43
F	8000	15,000	300	10	48	126	40

the contact surface on the characteristics plot represents the available time for testing in the shock excited region. Figure 3-17 gives the spatial position of the shock and contact surface at one initial condition, and presents the temperature distribution through the shock excited region.

Integral Approach - Rather than use the differential equations themselves to determine the flow properties of the shock excited region, as was done in the previous section for the characteristics solution, the integral equations describing the various wave and flow phenomena are used here. Briefly, at selected points along the divergent duct, properties of the blow-down flow region are determined from the isentropic flow relationships. The blow-down region represents the region into which either the expansion wave or secondary shock wave propagates. The remaining equations describing the relationships across shocks or expansion waves are solved by adjusting the value of the initial shock strength. Here too, the solution has been obtained from a digital computer program, utilizing the ideal gas relationships. Unlike the characteristics solution, each region is considered to have constant properties, and the test times must be determined by first numerically inte-

MHD Wave Investigation

II - theory

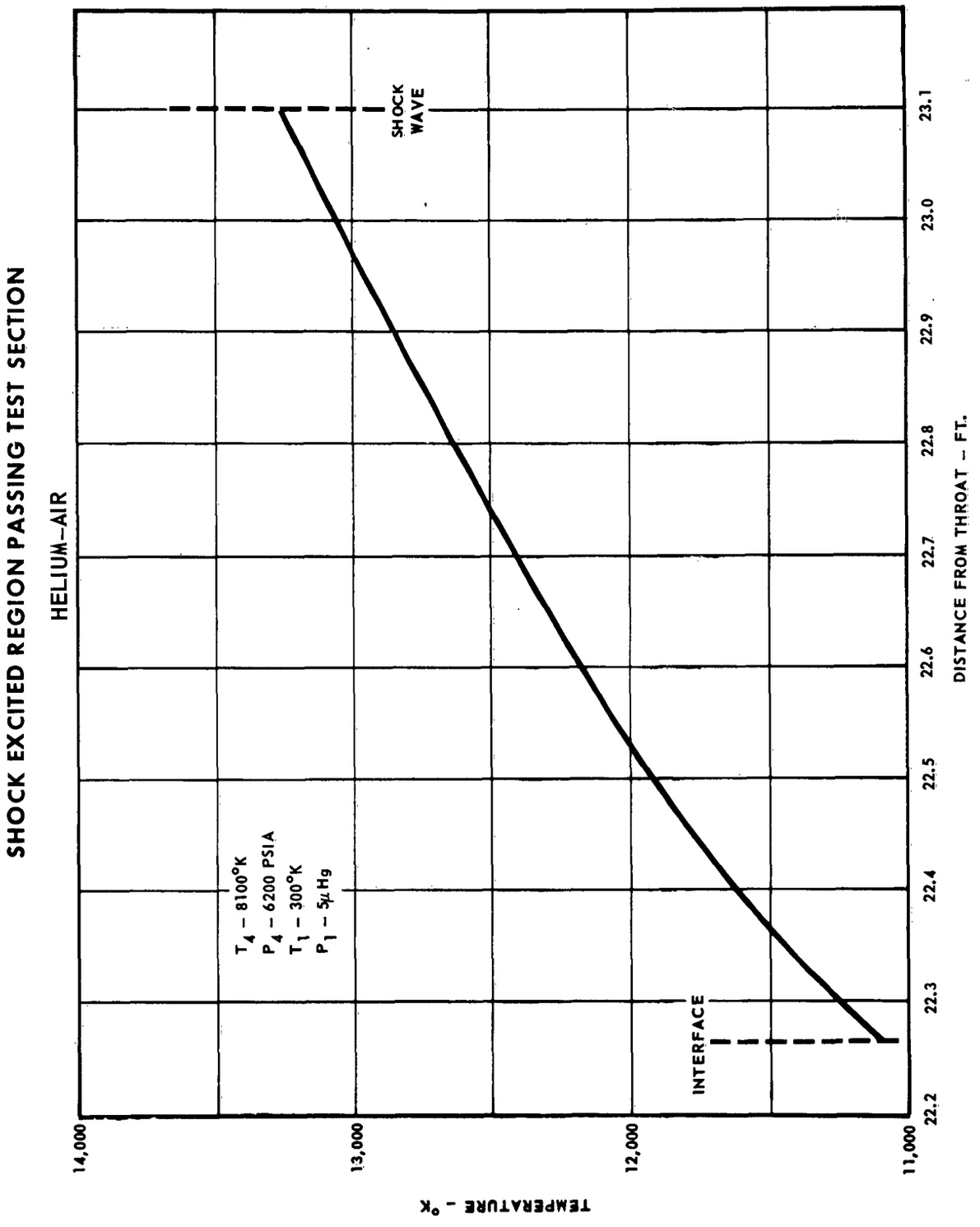

FIGURE 3–17

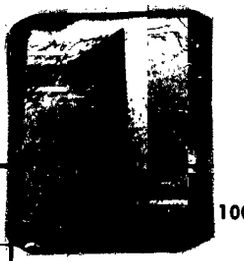

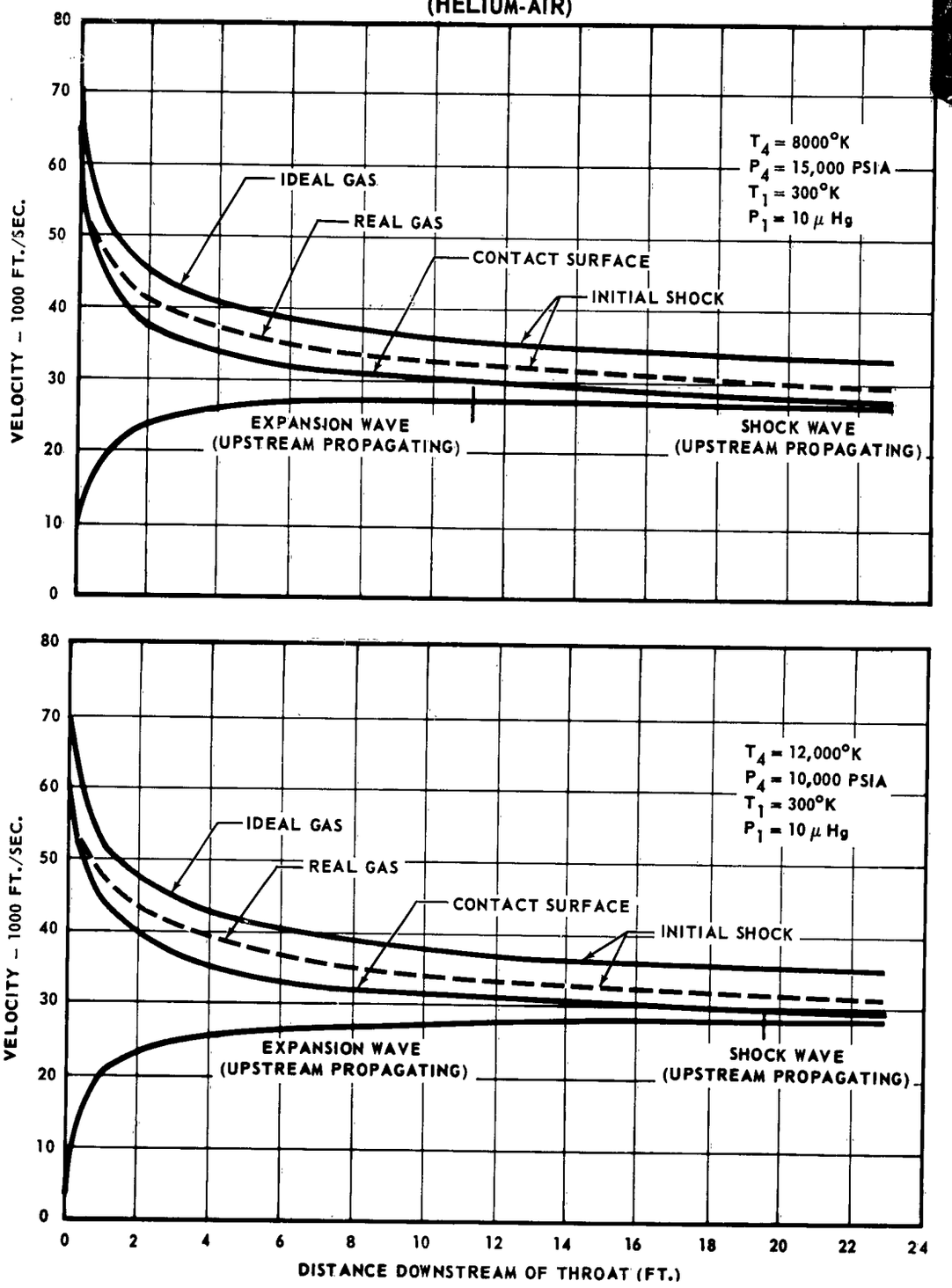
SHOCK EXCITED REGION
EXPANDING NOZZLE
(HELIUM-AIR)
VELOCITY – 1000 FT./SEC.
T_4 = 8000°K
P_4 = 15,000 PSIA
T_1 = 300°K
P_1 = 10 μ Hg
IDEAL GAS
REAL GAS
CONTACT SURFACE
INITIAL SHOCK
EXPANSION WAVE
(UPSTREAM PROPAGATING)
SHOCK WAVE
(UPSTREAM PROPAGATING)
T_4 = 12,000°K
P_4 = 10,000 PSIA
T_1 = 300°K
P_1 = 10 μ Hg
DISTANCE DOWNSTREAM OF THROAT (FT.)

FIGURE 3–18

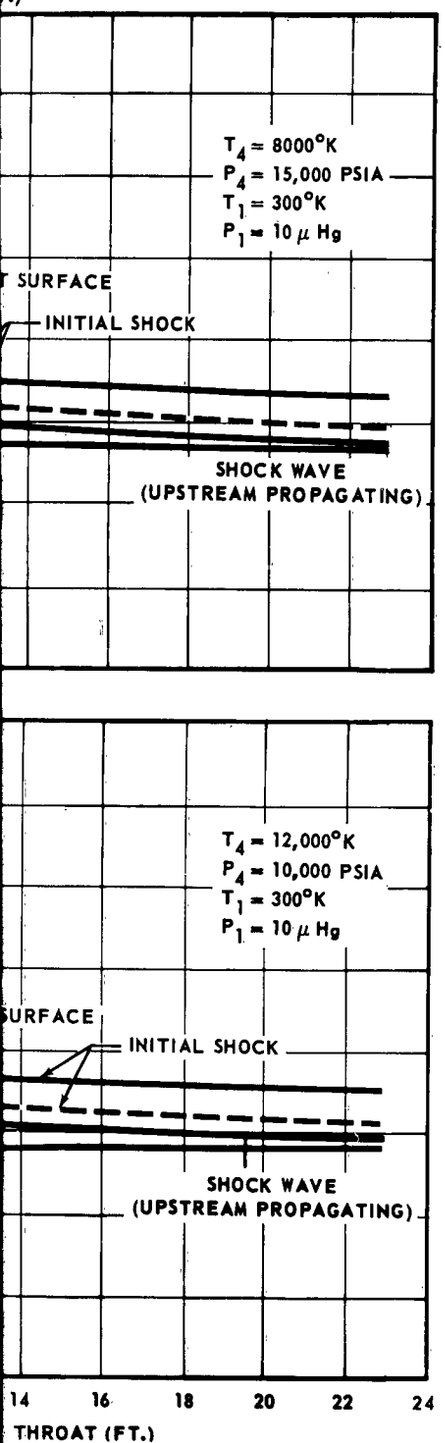
T_4 = 8000°K
P_4 = 15,000 PSIA
T_1 = 300°K
P_1 = 10 μ Hg
T SURFACE
INITIAL SHOCK
SHOCK WAVE
(UPSTREAM PROPAGATING)
T_4 = 12,000°K
P_4 = 10,000 PSIA
T_1 = 300°K
P_1 = 10 μ Hg
URFACE
INITIAL SHOCK
SHOCK WAVE
(UPSTREAM PROPAGATING)
14 16 18 20 22 24
THROAT (FT.)

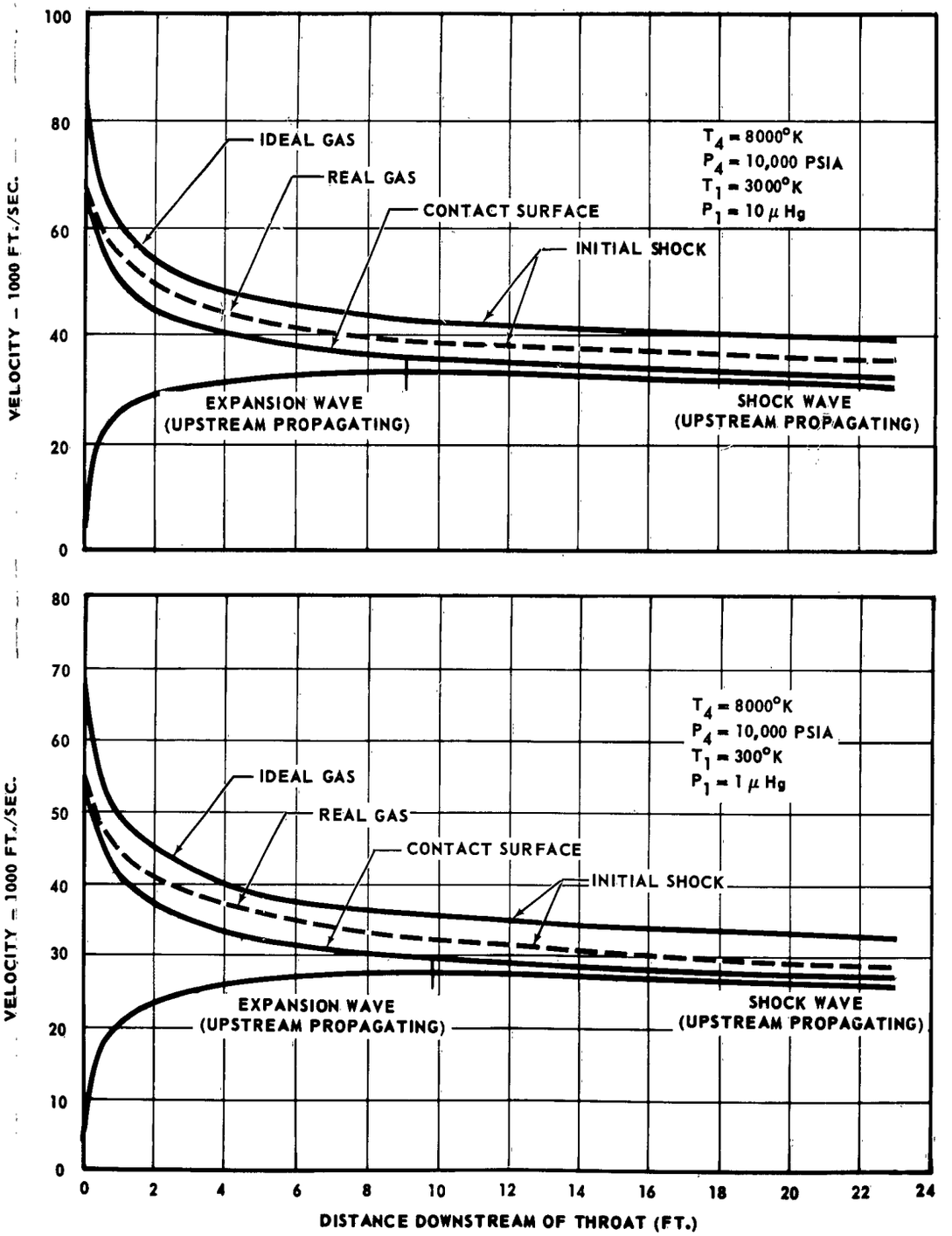
VELOCITY = 1000 FT./SEC.
100
80
60
40
20
0
IDEAL GAS
REAL GAS
CONTACT SURFACE
INITIAL SHOCK
T_4 = 8000°K
P_4 = 10,000 PSIA
T_1 = 3000°K
P_1 = 10 μ Hg
EXPANSION WAVE
(UPSTREAM PROPAGATING)
SHOCK WAVE
(UPSTREAM PROPAGATING)
VELOCITY = 1000 FT./SEC.
80
70
60
50
40
30
20
10
0
IDEAL GAS
REAL GAS
CONTACT SURFACE
INITIAL SHOCK
T_4 = 8000°K
P_4 = 10,000 PSIA
T_1 = 300°K
P_1 = 1 μ Hg
EXPANSION WAVE
(UPSTREAM PROPAGATING)
SHOCK WAVE
(UPSTREAM PROPAGATING)
0 2 4 6 8 10 12 14 16 18 20 22 24
DISTANCE DOWNSTREAM OF THROAT (FT.)

FIGURE 3-18

grating the relationship between velocity and distance according to the expression:

$$t = \int_0^x \frac{dx}{U}$$

to obtain the time for a particular wave or the contact surface to travel down the tunnel to a specified station. Subtracting the propagation time of the initial shock from the time it takes the contact surface to travel down the tunnel, results in the available test time. Curves of the initial shock velocity, interface velocity, and upstream propagating wave velocity are presented in Figure 3-18 (a-d). In addition, a hand computation was performed on the helium-air system cases, using real gas properties for the shock phenomenon occurring in the air, using ideal gas properties for helium. These results are included on Figure 3-18 (a-d). It is seen that the solution using real gas properties predicts lower velocities, than does the ideal gas solution. This is to be expected, since the ideal gas pressure ratio across a shock is greater than the real gas pressure ratio, for the same Mach number and initial conditions. In the integral approach the pressures are balanced. Thus, assuming the same conditions exist in the blow-down region for each case, the pressure ratio across the initial shock must be the same, regardless of ideal or real gas assumptions. For the same pressure ratio then, the real gas assumption predicts a lower shock velocity, and hence a shorter test time. Where exact knowledge of the test time is not required, the assumption of ideal gas properties is satisfactory for determining shock decay. Test times between the passing of the initial shock and the contact surface are compared in Table 3-4 with those computed by other methods.

Electrical Properties Behind a Moving Shock - The electrical properties existing in the shock excited region behind the initial shock can be pre-

dicted from use of hypersonic gas dynamic charts for air, such as are presented by Feldman (Reference 3-16) and by Ziemer (Reference 3-17). Equilibrium densities and temperatures behind a moving normal shock are presented in these references, and are included here in Figure 3-19 as functions of the shock velocity and the density ratio in the evacuated section before the shock is initiated. The equilibrium properties of electron concentration behind the shock and the electron collision frequency are presented in Figures 3-20 and 3-21, and have been determined from the general curves of equilibrium properties at the specific conditions behind the shock, which are shown in Figure 3-19.

3.4.2.6 Blow-Down Flow

General Description. - In an arc driven Hypervelocity Impulse Tunnel, after decay of the initial shock structure, there follows a quasi-steady flow from the arc chamber, which is referred to as the blow-down flow. The blow-down flow at the test station is characterized by a high velocity and a relatively low temperature, pressure and density. Test periods in this flow regime are relatively long, being of the order of 100 milliseconds. The blow-down flow is normally used for aerodynamic testing. During the period of blow-down flow, pressure and temperature at the test station varies slowly, in response to the decrease in pressure and temperature within the arc chamber. In the following discussion flow properties characteristic of the blow-down regime are examined, with particular attention given to the prediction of electron concentration and other plasma properties at the test station.

After the electrical discharge, the gas supply in the arc chamber consists of a complex mixture of molecules, atoms, ions, and electrons which are assumed to be in chemical equilibrium at the arc chamber temperature and pressure. As the gas discharges from the arc chamber and expands through

MHD Wave Investigation
II - theory

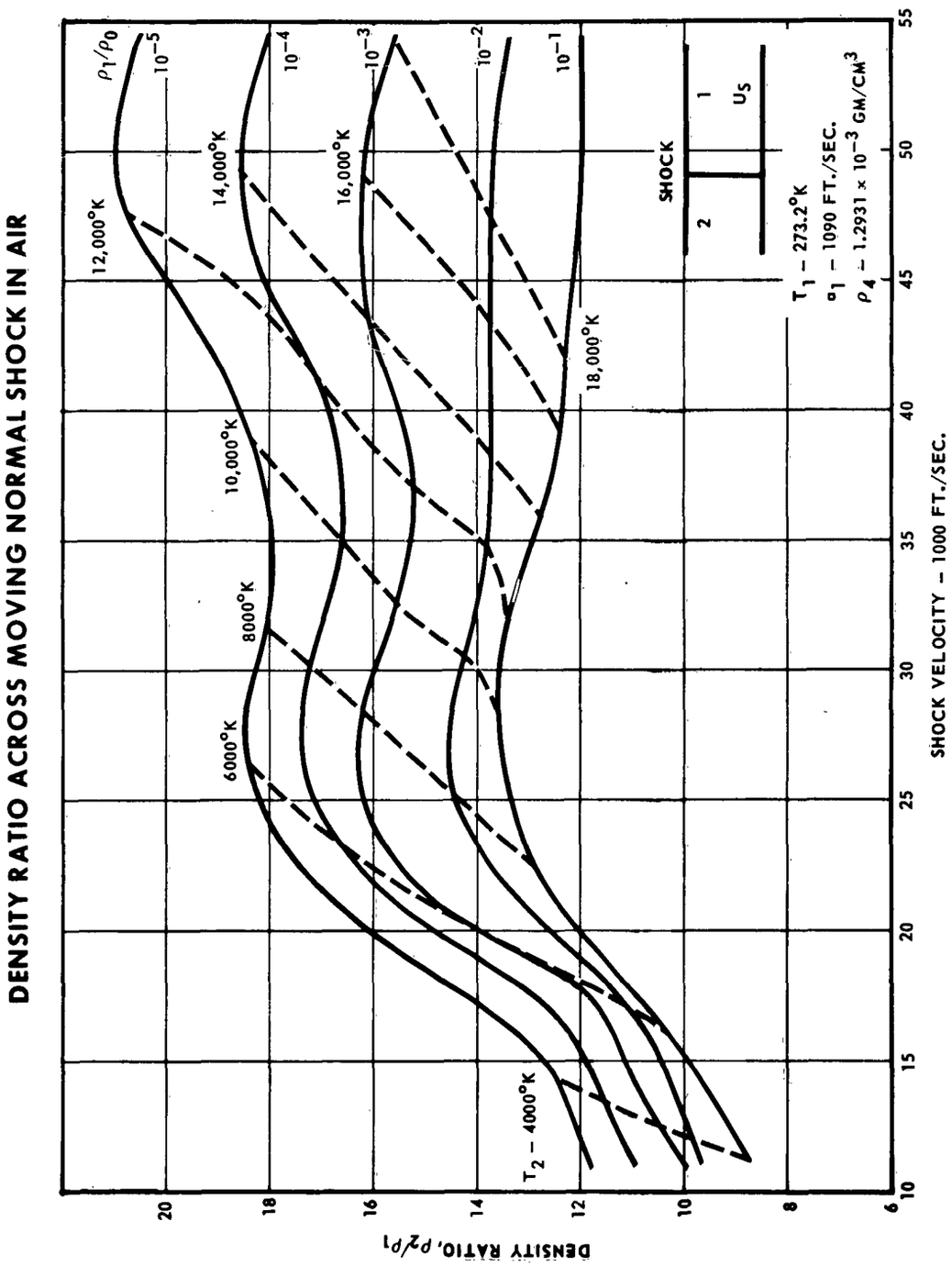

FIGURE 3-19

ELECTRON CONCENTRATION
BEHIND MOVING NORMAL SHOCK IN AIR

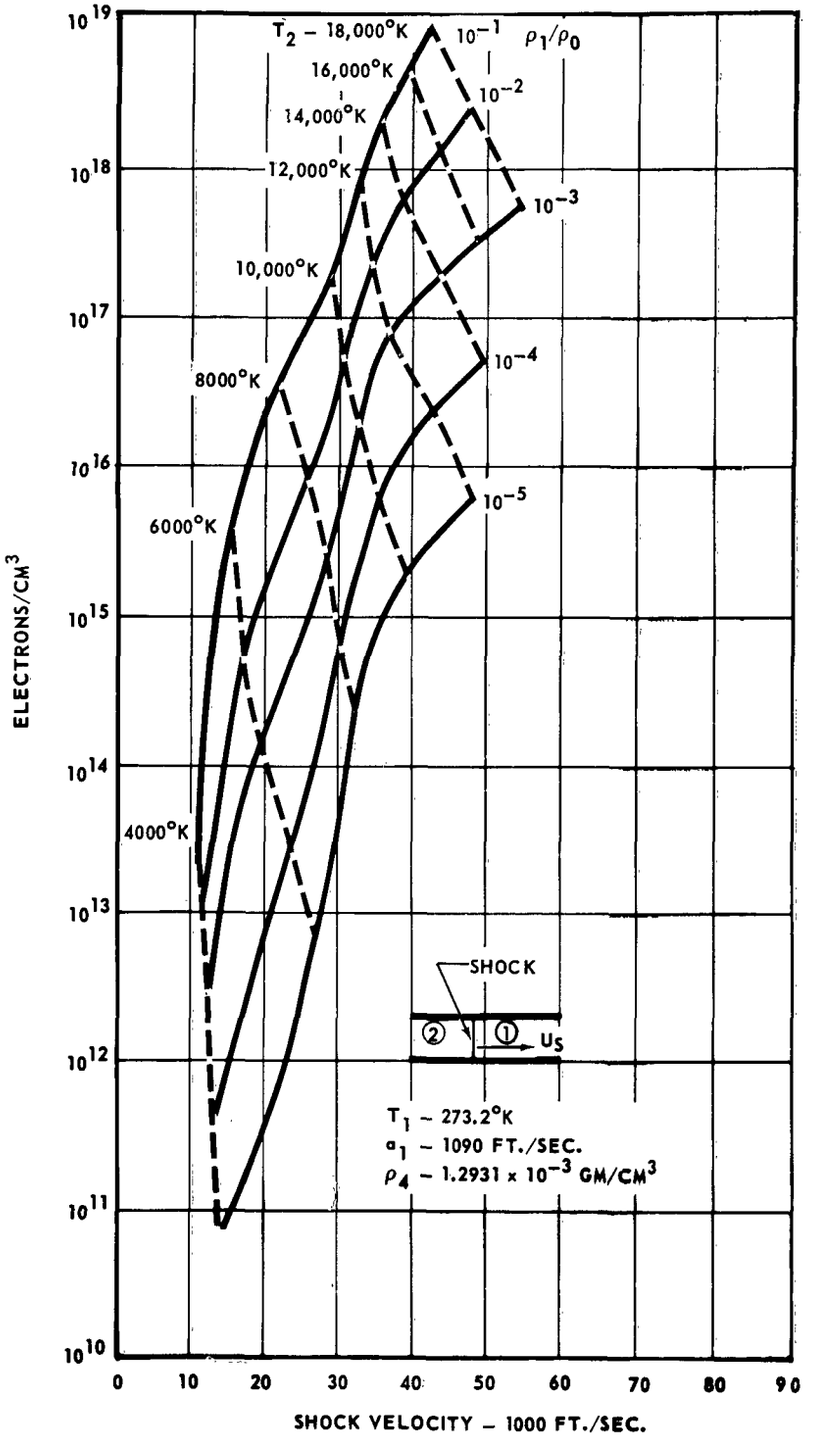

FIGURE 3-20

COLLISION FREQUENCY BEHIND MOVING NORMAL SHOCK IN AIR

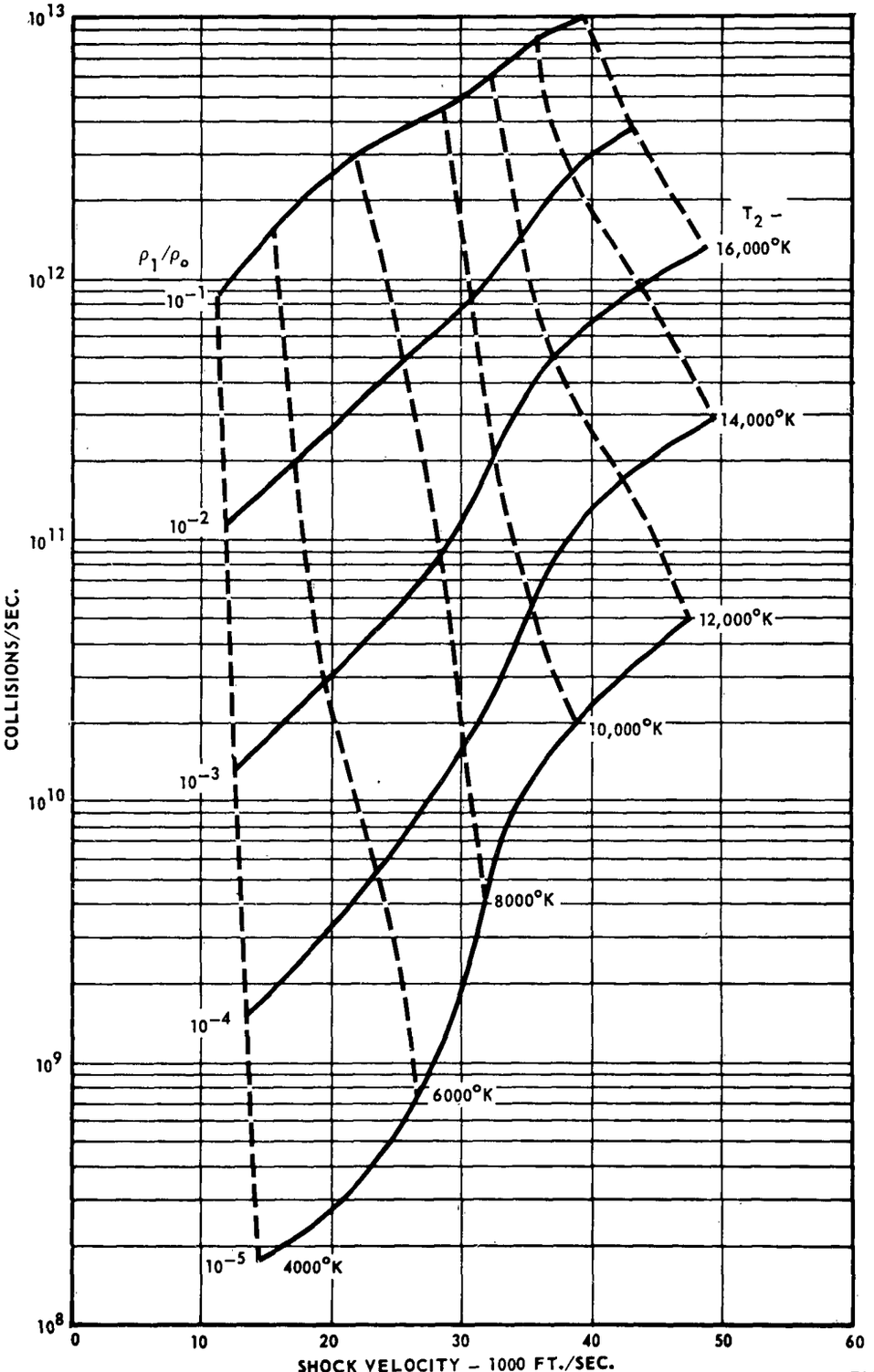

FIGURE 3-21

the divergent nozzle, the thermodynamic state of the gas is altered in accordance with the laws of compressible flow and chemical kinetics. When a gas of constant specific heat and chemical composition flows through a divergent nozzle, the response of the thermodynamic properties to the changing area ratio is rapid with respect to the rate of flow of the gas. For this case, on a microscopic scale, the rate of approach to an equilibrium temperature and pressure is governed by the rate at which a steady state Maxwellian velocity distribution can be achieved. For gases consisting of species of nearly equal mass, the Maxwellian velocity distribution is reached at a time on the order of the time between molecular collisions, or the reciprocal of the collision frequency. When electrons are present, the masses of the particles are no longer nearly equal, and, because electrons normally undergo elastic collisions with particles of greater mass, only a small fraction of the kinetic energy of the electron is transferred to the heavier particle upon colliding. It is possible, therefore, for electrons to maintain a kinetic energy, or electron temperature, which is not in equilibrium with that of the bulk of the gas for a significant period. If chemical reactions and variable specific heats are allowed, the rate of approach to chemical equilibrium is governed by the specific reaction rate constants of the participating chemical reactions, and by the relaxation times for rearrangement of internal molecular degrees of freedom.

Exact calculations for the hypersonic nozzle flow of complex gas mixtures requires the simultaneous solution of a number of rate equations, one for each process, several of which may be highly coupled in a real case. The exact solution is further complicated by a lack of knowledge of the rate constants for many high temperature processes. For engineering purposes it is common, therefore, to define two limiting cases: (1) frozen flow, and (2) equilibrium

flow, corresponding, respectively, to the assumptions of constant chemical composition (infinitely slow rate constants) and equilibrium composition (infinitely fast rate constants). A comparison between the frozen flow calculations and the more appropriate non-equilibrium flow analysis is presented in the following paragraphs.

Frozen Flow Analysis. - Previous theoretical studies of the nature of hypersonic nozzle flow provide the following description: As the gases expand from the nozzle throat into the divergent channel there is an initial period in which the gases are in chemical equilibrium. The dissociation and recombination reactions between atomic and diatomic species requires the presence of a third, inert particle; thus, these reactions are density dependent. As the gases expand and the density decreases, there is a short transition period, which is followed by a third region characterized by constant composition, i.e., frozen flow. Once frozen, the flow is not observed to return to an equilibrium composition at a more distant section of the nozzle, although this possibility exists by the nature of the chemical rate equations. Freezing normally occurs a short distance from the nozzle throat. As an approximation, for engineering calculations, freezing may be assumed to occur at the nozzle throat or in the upstream reservoir, i.e., in the arc chamber, where the equilibrium composition is readily obtained. For the calculations presented here, freezing is assumed to occur at the equilibrium arc chamber composition.

Although the composition may be frozen, it is still necessary to specify the specific heats and the specific heat ratio, γ , at every point in the nozzle. Specific heats are functions of temperature and may also be considered to be either (1) frozen, (2) in equilibrium, or (3) in a non-equilibrium state, characterized by a relaxation time for the rearrangement of the internal molecular degrees of freedom. Such relaxation times are known to be longer at

high temperatures, where they approach in magnitude the times characteristic of the chemical reactions. The assumption of equilibrium specific heats, or
A frozen vibrational energy, has been made for the calculations presented in this section. It can be shown that the predicted density, and, therefore, the electron concentration, will not be appreciably affected by this assumption.

Heims (Reference 3-18) and Inger (Reference 3-19), among others, have discussed the calculations for expanding gases in frozen, dissociated flow. Following Heims, the local isentropic exponent for adiabatic flow of a perfect gas may be obtained as follows for an adiabatic expansion:

$$p = \rho^{\gamma}$$

where, for a perfect gas,

$$\gamma = \frac{C_p}{C_v} = \frac{dh}{de}$$

If the density ρ is expressed on a mass basis, then h and e represent enthalpy and internal energy per unit mass, respectively. One degree of freedom is assigned to each of the three components of translation for both diatomic and atomic species, and two degrees of freedom to rotation of diatomic species. If X is the mass fraction dissociated, then, for a gas consisting of atoms and molecules, the isentropic exponent can be expressed by:

$$\gamma = \frac{dh}{de} = \frac{(7 + 3X) + (2 + 3T)\frac{dX}{dT} + 2\frac{de_v}{dT}}{(5 + X) + (2 + T)\frac{dX}{dT} + 2\frac{de_v}{dT}}$$

where e_v is the internal vibrational energy per unit mass. If the vibrational energy and fraction dissociated is assumed constant, then:

$$\gamma = \frac{7 + 3X}{5 + X}$$

The above equations describe the frozen expansion of a dissociated gas, the

contributions from ionic species and electrons being negligible.

In Figures 3-22 and 3-23 are presented charts of temperature and electron concentration at a 36 inch diameter test section in the McDonnell HIT. These figures describe test station properties for the assumed frozen flow of nitrogen, initially at equilibrium in the arc chamber. The charts apply to an area ratio of 8100, corresponding to a 0.4 inch diameter nozzle throat. In the Alfvén wave experiments a solenoid for the magnetic field B_o, inserted into the diverging nozzle, had an internal diameter of 36 inches, which then became the geometric area available for flow. If the charts are to be used as labeled, it is implicitly assumed that the composition at which freezing occurs does not differ appreciably from arc chamber conditions. It may be more appropriate to assume that the flow to the throat is in chemical equilibrium; for this case chemical composition, temperature and pressure at the throat may be estimated from the previous data of section 3.4.2.4, and these values may be substituted for the corresponding arc chamber values on the figures.

The effect of a divergent nozzle on test station properties for nitrogen flow is illustrated in Figures 3-24 and 3-25, where temperature and electron concentrations are shown as functions of area ratio for specific values of temperature and pressure in the arc chamber.

Equilibrium molar compositions at arc chamber conditions have been computed from data on equilibrium constants, supplemented with the published results for nitrogen of Treanor and Logan (Reference 3-20) and the recent high temperature calculations of Drellishak (Reference 3-21).

Non-Equilibrium Flow Analysis. - A more nearly correct computation for the flow conditions in a hypersonic nozzle may be obtained from a simultaneous solution of the flow equations, together with the rate equations for the chemical reactions and material balances for the several species. Bray (Reference

FROZEN EXPANSION OF NITROGEN

TEMPERATURE

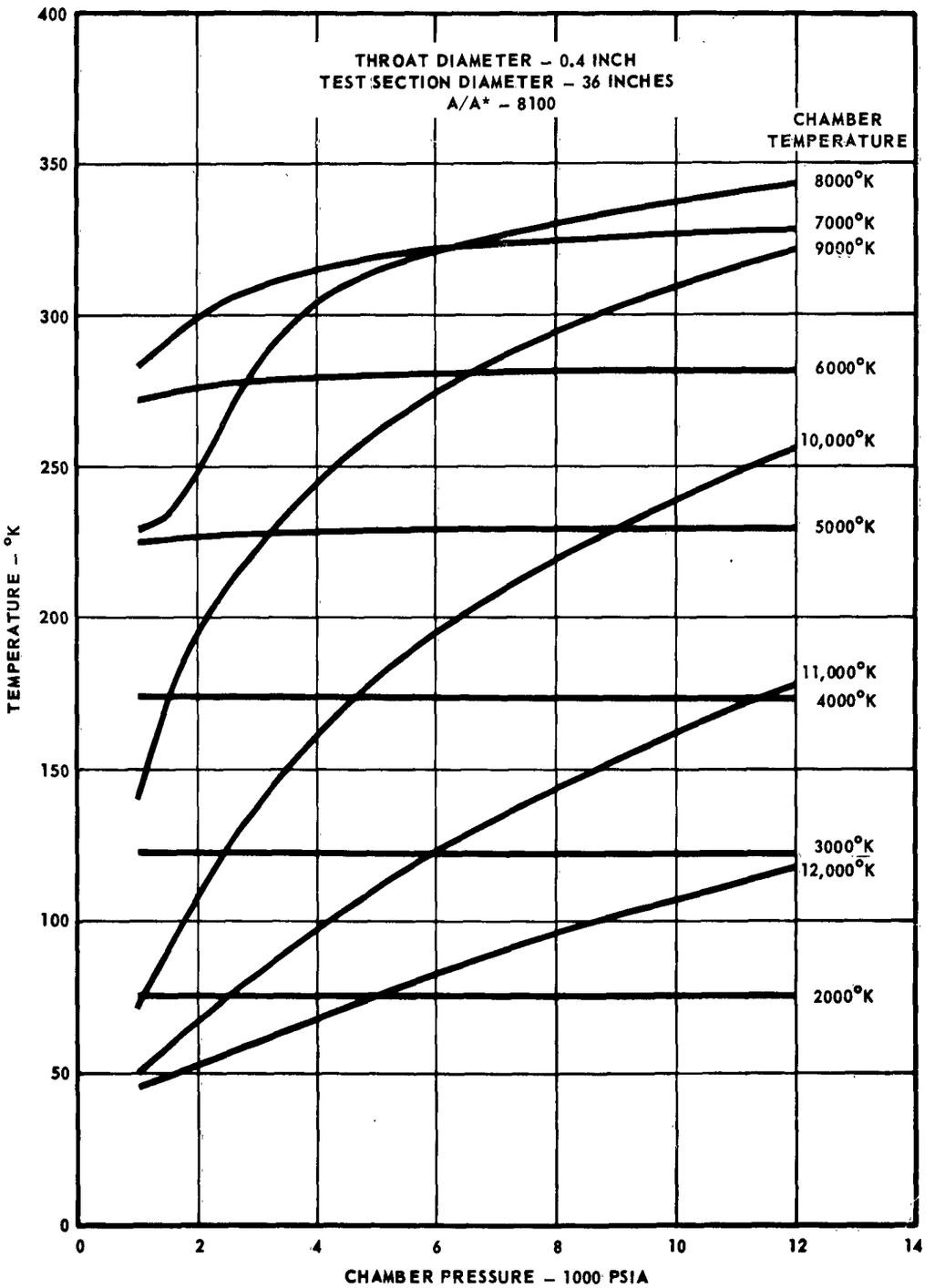

FIGURE 3-22

FROZEN EXPANSION OF NITROGEN
ELECTRON CONCENTRATION

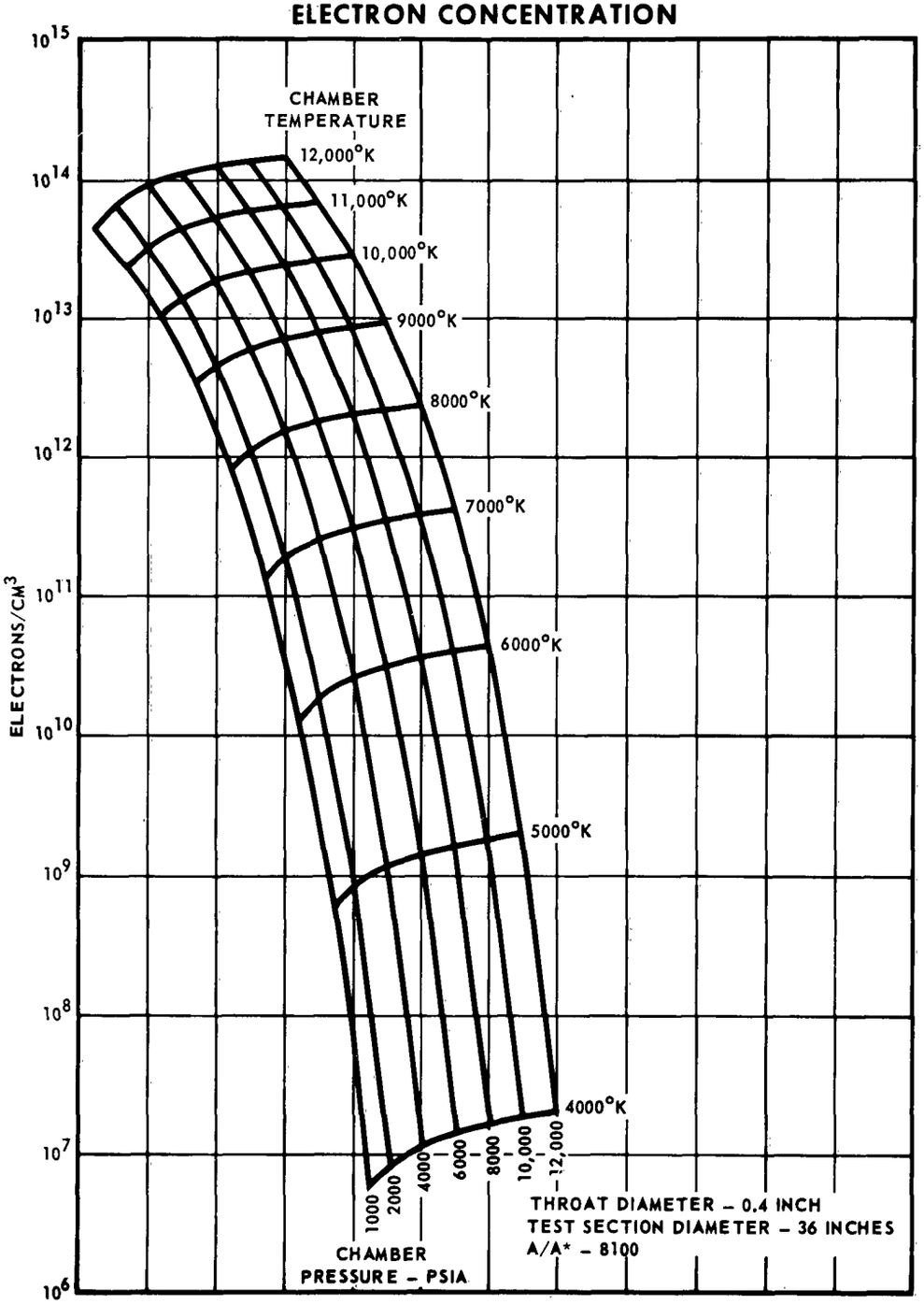

FIGURE 3-23

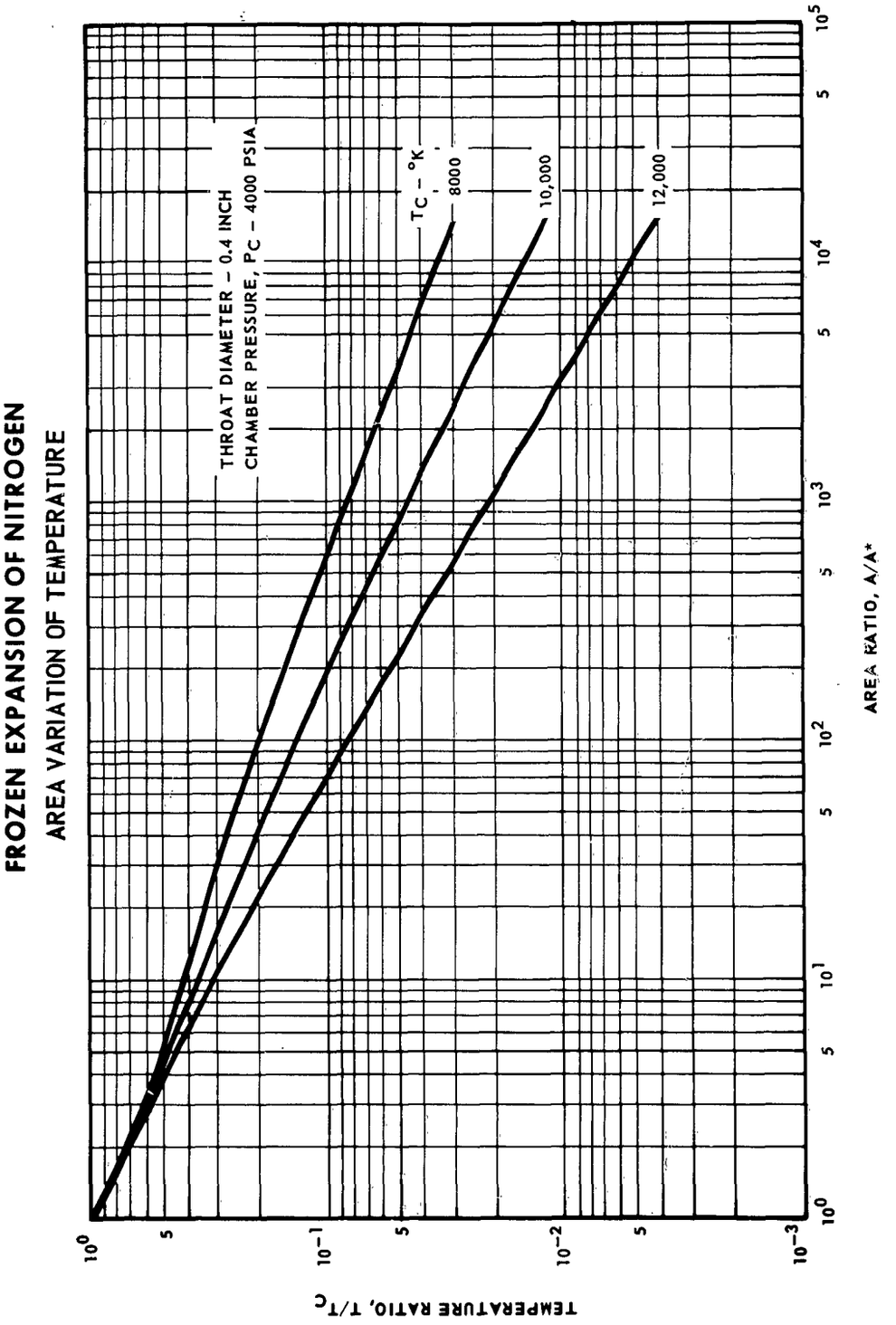
FROZEN EXPANSION OF NITROGEN
AREA VARIATION OF TEMPERATURE
THROAT DIAMETER – 0.4 INCH
CHAMBER PRESSURE, P_C – 4000 PSIA
T_C – °K
8000
10,000
12,000
AREA RATIO, A/A*
TEMPERATURE RATIO, T/T_C
10^0
5
10^{-1}
5
10^{-2}
5
10^{-3}
10^0
10^1
10^2
10^3
10^4
10^5

FIGURE 3-24

FROZEN EXPANSION OF NITROGEN

AREA VARIATION OF ELECTRON CONCENTRATION

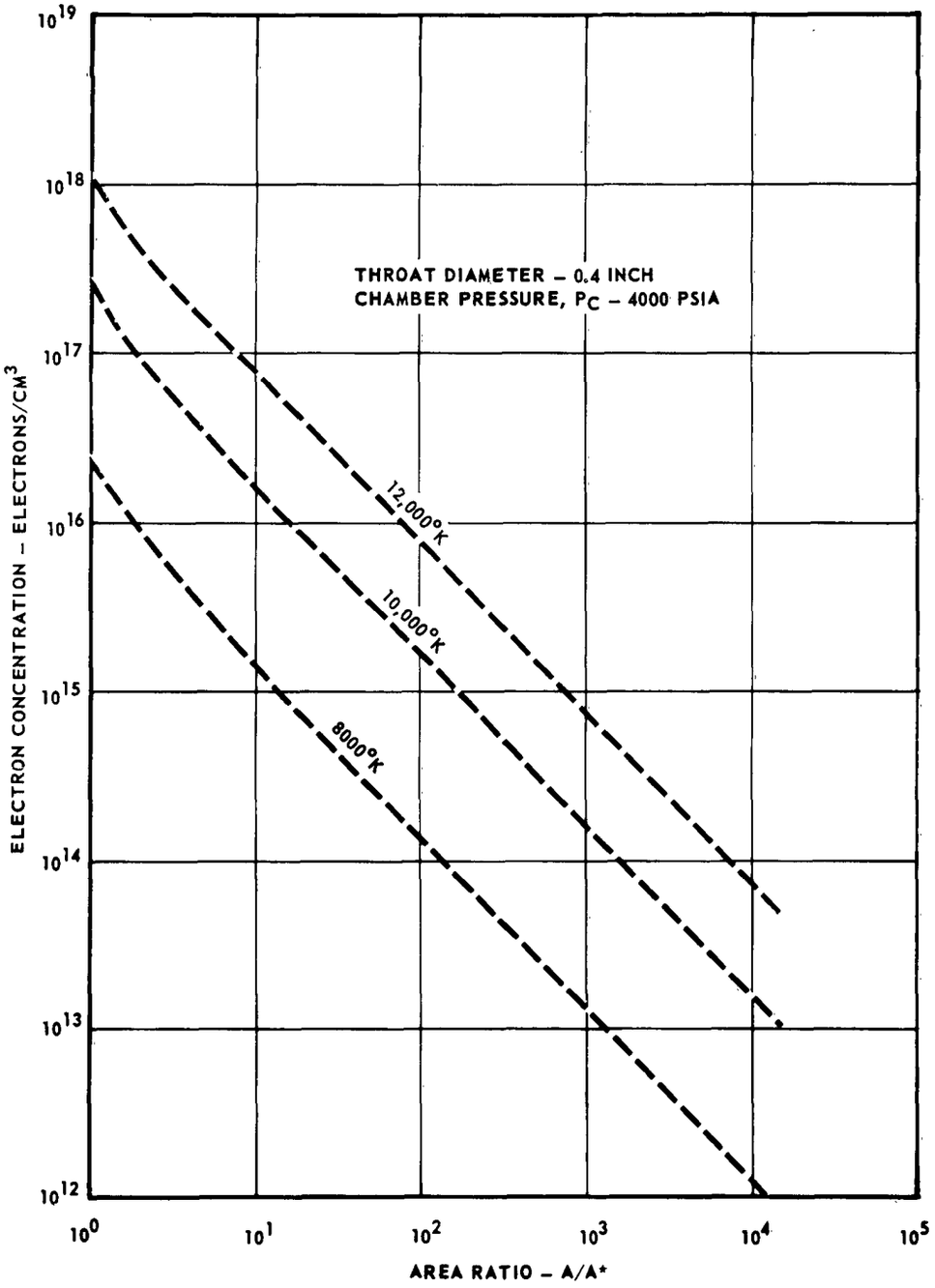

FIGURE 3-25

3-22), Emanuel and Vincenti (Reference 3-23), Westenberg and Favin (Reference 3-24), and Eschenroeder (References 3-25 and 3-26) have described, in general, the approach to non-equilibrium flow calculations. The analysis presented here follows more closely the study of Westenberg and Favin. It is assumed that the internal molecular degrees of freedom are in equilibrium at the local temperature, and that the electron temperature is everywhere equal to the local flow temperature. Almost no information is available concerning the effect of electron temperature on the kinetics of the recombination reactions. A stepwise iterative calculation is required. Let A be the cross-sectional area of the nozzle at any point z along the nozzle axis, and let A* be the cross-sectional area at the nozzle throat. Then the area ratio, $\eta = A/A^*$, is a function of z. The flow through the divergent nozzle is described by the following equations:

(1) Equation of continuity:

$$m = \rho v \eta A^*$$

(2) Equation of motion:

$$\rho v \frac{dv}{dz} + \frac{dp}{dz} = 0$$

(3) Equation of energy balance:

$$\frac{dh}{dz} + \frac{v}{J} \frac{dv}{dz} = 0$$

(4) Equation of state:

$$p = \rho RTJ \left(\sum_i F_i\right)$$

where the subscript i refers to the ith species and the other symbols are defined as follows:

m = mass flow rate (gm/sec)

ρ = gas density

v = velocity of an elementary volume

h = enthalpy (cal/gm)

J = mechanical equivalent of heat (erg/cal)

R = Universal gas constant

T = gas temperature (^{o}K)

F = component concentration (gmols./gm)

If H denotes the enthalpy per mole, then:

$$h_i = H_i F_i$$

For a perfect gas, enthalpy is a function of temperature only, hence:

$$\frac{dH_i}{dz} = \frac{dH_i}{dT} \frac{dT}{dz} = C_{p_i} \frac{dT}{dz}$$

The above set of equations may be solved to yield the derivatives of temperature and density with respect to axial distance, z:

$$\frac{dT}{dz} = \frac{JY\Sigma\left(H_i \frac{dF_i}{dz}\right) + TX}{1 - JY\Sigma (F_i C_{p_i})}$$

$$\frac{d\rho}{dz} = \frac{\frac{\rho^3 A^{2*} \eta^2}{m^2} \left[\frac{dT}{dz} - TX\right]}{Y} - \frac{\rho}{\eta} \frac{d\eta}{dz}$$

where:

$$X = \left[\frac{1}{\eta} \frac{d\eta}{dz} - \frac{1}{(\Sigma F_i)} \frac{d(\Sigma F_i)}{dz}\right]$$

and:

$$Y = \left[\frac{1}{RJ(\Sigma F_i)} - \frac{T \rho^2 A^{2*} \eta^2}{m^2}\right]$$

The chemical composition at each point z is obtained from the appropriate forms of the chemical rate equations and component material balances. In general, for the j-th reaction:

$$\sum_R A_{R,i} = \sum_P A_{P,i}$$

where the summations are taken over the components of the reactants and products, respectively. The rate of reaction may be expressed by:

$$r_i = k_j \{ \prod_R (\rho F_{R,i}) - \frac{1}{K_j} \prod_P (\rho F_{P,i}) \}$$

The indicated products are to be taken over all components which appear as reactants of products in a given reaction. Here k_j is the reaction rate constant and K_j is the equilibrium constant. The component material balances are of the form:

$$\sum n_{e,i} F_i = \text{constant}$$

where $n_{e,i}$ denotes the number of atoms of element e in component i. For the nitrogen flow calculations the elemental constituents can be considered to be the singly charged nitrogen atom and the electron. In this case reactions may be selected, such that the above set of equations can be solved directly by a finite difference technique. In other cases simultaneous solutions may be required. For each component described uniquely by one of the chemical reactions:

$$\frac{dF_i}{dz} = \frac{\eta A^*}{m} r_i$$

and:

$$(F_i)_{z+\Delta z} = (F_i)_z + \left(\frac{dF_i}{dz}\right) \Delta z$$

For the remaining components, compositions at the end of an interval, $(F_i)_{z+\Delta z}$ are determined from the material balances. Average densities and temperatures over the interval, obtained by iteration, are used to calculate the reaction rates.

Calculations for the hypersonic flow of ionized nitrogen in a divergent

nozzle will be now described. The species present in the arc chamber are: N_2, N_2^+, N^+, N and electrons, e^-. An associate species, N_4^+, may become significant at high pressures, but will not be important here. Because of the variety of possible recombination mechanisms, a large number of reactions between the five species may be described.

The recombination reactions are exothermic and cannot occur unless some means is provided for the removal of the excess energy of the reaction products. For the recombination of ions and electrons energy may be removed (a) by radiation, (b) by excitation of at least two electrons, (c) by energy of molecular dissociation, or (d) as kinetic energy imparted to a third body. The corresponding recombination reactions, illustrated for the species of ionized nitrogen, are:

(a) Radiative recombination:

$$N^+ + e^- = N + h\nu$$

$$N_2^+ + e^- = N_2 + h\nu$$

where $h\nu$ represents the energy quantum.

(b) Dielectronic recombination:

$$N^+ + e^- = N^{**}$$

where N** represents a doubly excited atom.

(c) Dissociative recombination:

$$N_2^+ + e^- = N + N$$

(d) Three body recombination:

$$N^+ + e^- + M = N + M$$

$$N_2^+ + e^- + M = N_2 + M$$

where M represents any third species. In many systems electron loss may also occur through electron attachment to neutral species, but this does not happen with nitrogen and the rare gases. Recombination mechanisms have been discussed

by a number of authors, of which the work of Brown (Reference 3-27) and Massey (Reference 3-28) will be cited, and by Bialecke and Dougal (Reference 3-29), with particular reference to the nitrogen system.

It is conventional to define an ionic recombination coefficient, α_r, regardless of the mechanism, by:

$$-\frac{dn_e}{dt} = \alpha_r n_e n_i$$

where n_e and n_i denote number densities of electrons and ions, respectively. Probable maximum values of the recombination coefficients for radiative and dielectronic recombination are of the order of 10^{-11} and 10^{-12} $cm^3/sec.$, respectively. Dielectronic recombination can usually be expected to be negligible in relation to the other mechanisms, and will not be considered further here.

For a monatomic ion such as N^+, only radiative and three body collision processes need be considered. The relative importance of the two mechanisms will depend upon the pressure and, to a lesser extent, upon the nature of the third body; third body recombination will be dominant at the higher pressures. For a molecular ion such as N_2^+, dissociative recombination can be expected to be dominant, although three body recombination may be a significant factor at the higher pressures.

Massey (Reference 3-28) has discussed the theoretical derivation by J.J. Thomson for the three body recombination coefficient between positive and negative ions. If appropriate simplifications are made for electron-ion recombination, the recombination coefficient for a three-body process is given by:

$$\alpha_r = \left(\frac{8kT}{\pi m}\right)^{1/2} \frac{8}{3} \frac{\pi r_o^3 m}{M_i L}$$

where

$r_o = 2\ e^2/3\ k\ T$

e = the charge of an electron

A m = mass of an electron, gms

M_i = mass of an ion, gms

L = mean free path of elastic electron-neutral collisions

The mean free path L is given by

$$L = \frac{1}{\pi n r_2^2}$$

where r_2 = molecular radius of the neutral species

n_2 = particle concentration of a neutral species

For the three body recombination of molecular nitrogen ions at typical arc chamber conditions (P = 2000 psi, T = 10,000 K), it is estimated from equation for α_r that α_r is approximately 5×10^{-12} cm^3/sec. Measured recombination coefficients for N_2^+ electron recombination are found to be several orders of magnitude larger, so that for this reaction the dissociative mechanism will predominate. For the recombination of N^+ ions the situation is less clear; for this case the magnitudes of the recombination coefficients for the radiative and three body mechanisms are more nearly equal. Massey (Reference 3-28) tabulates radiative recombination coefficients for atomic oxygen ions. For recombination with high energy electrons, the recombination coefficient is of the order of 0.3×10^{-12} cm^3/sec. The three body recombination coefficient will not differ greatly from the value computed above for N_2^+. On this basis the three body recombination mechanism will predominate, since it is well-known that the recombination of nitrogen atoms to molecular nitrogen takes place through a three-body mechanism.

On the basis of the preceding discussion the following reactions have been selected to describe the reacting mixture.

$$N + N + M = N_2 + M$$

$$N_2^+ + e^- = N + N$$

$$N^+ + e^- + M = N + M$$

A number of authors have studied the rate of dissociation of molecular nitrogen. Wray (Reference 3-30) recommends the data of Byron, which is used here. For the rate of the reverse of the first reaction:

$$k_1' = (4.2 \times 10^{12})\, T^{1/2}\, (D/RT)\, \exp\,(-D/RT)$$

where D = 224,900 cal/gmol is the dissociation energy, and the prime refers to the reverse reaction above. This rate expression applies to reactions in which molecular nitrogen is the third body.

Kuhns (Reference 3-31) has studied the dissociative recombination of N_2^+ ions and reports a value of $\alpha_r = 1.9 \times 10^{-6}$ cm^3/ sec at room temperature and 10 mm Hg. Bialecke and Dougal (Reference 3-29) report $\alpha_r \approx 1.6 \times 10^{-6}$ cm^3/sec at 300°K and at a particle density of 8×10^{16} cm^{-3}. They have also found that the recombination coefficient decreases with increasing temperature and increases with increasing density, but they do not present data for the temperatures and pressures of interest here. The pressure dependence in the observed data is thought to arise from the presence of three-body recombination. Bates (Reference 3-32) has presented a theoretical discussion of the dissociative recombination coefficient and has concluded that it will be temperature dependent by a factor varying from $T^{-1/2}$ to $T^{-3/2}$, depending upon the electron energy as described by initial and final wave functions, which are in general unknown. In view of these uncertainties, a constant value of $\alpha_r = 1.5 \times 10^{-6}$ cm^3/sec has been selected for these preliminary calculations.

For the three body recombination of N^+ ions the equation of J.J. Thomson, referred to earlier, has been used to compute the recombination coefficient. This equation is subject to a high pressure limit, but it can be shown that

this limit is not exceeded at arc chamber pressures.

Reaction rate constants in the form suitable for equation 3.4-3 have been computed from the recombination coefficients cited above. Equilibrium constants for the previously selected reactions have been obtained by rearrangement of the tabulated data of Treanor and Logan (Reference 3-20). Enthalpies and heat capacities have been computed from partition functions, also tabulated by Treanor and Logan. Together with the above data, the equations described in this section have been programmed for solution on an IBM 7090 digital computer.

The results of some preliminary non-equilibrium flow calculations for ionized nitrogen in the divergent section of a hypersonic nozzle are presented in Figure 3-26. These calculations were initiated at the nozzle throat with an equilibrium gas composition corresponding to a temperature of 8000°K, and a density of 1.1845×10^{-2} gms/cm^3, approximately 10 times the atmospheric density. Initial equilibrium mole fractions of each component are tabulated below:

Component	Mole Fraction
N_2	8.437×10^{-1}
N_2^+	5.966×10^{-5}
N^+	3.134×10^{-5}
N	1.561×10^{-1}
e^-	9.099×10^{-5}

Because of the extremely rapid reaction rates, an unusually small step size, initially of the order of 10^{-8} cm., was required for the iterations. A nozzle with a 10 degree total divergent angle has been assumed for these calculations, corresponding to the construction of the McDonnell HTT. The total

MHD Wave Investigation

II - theory

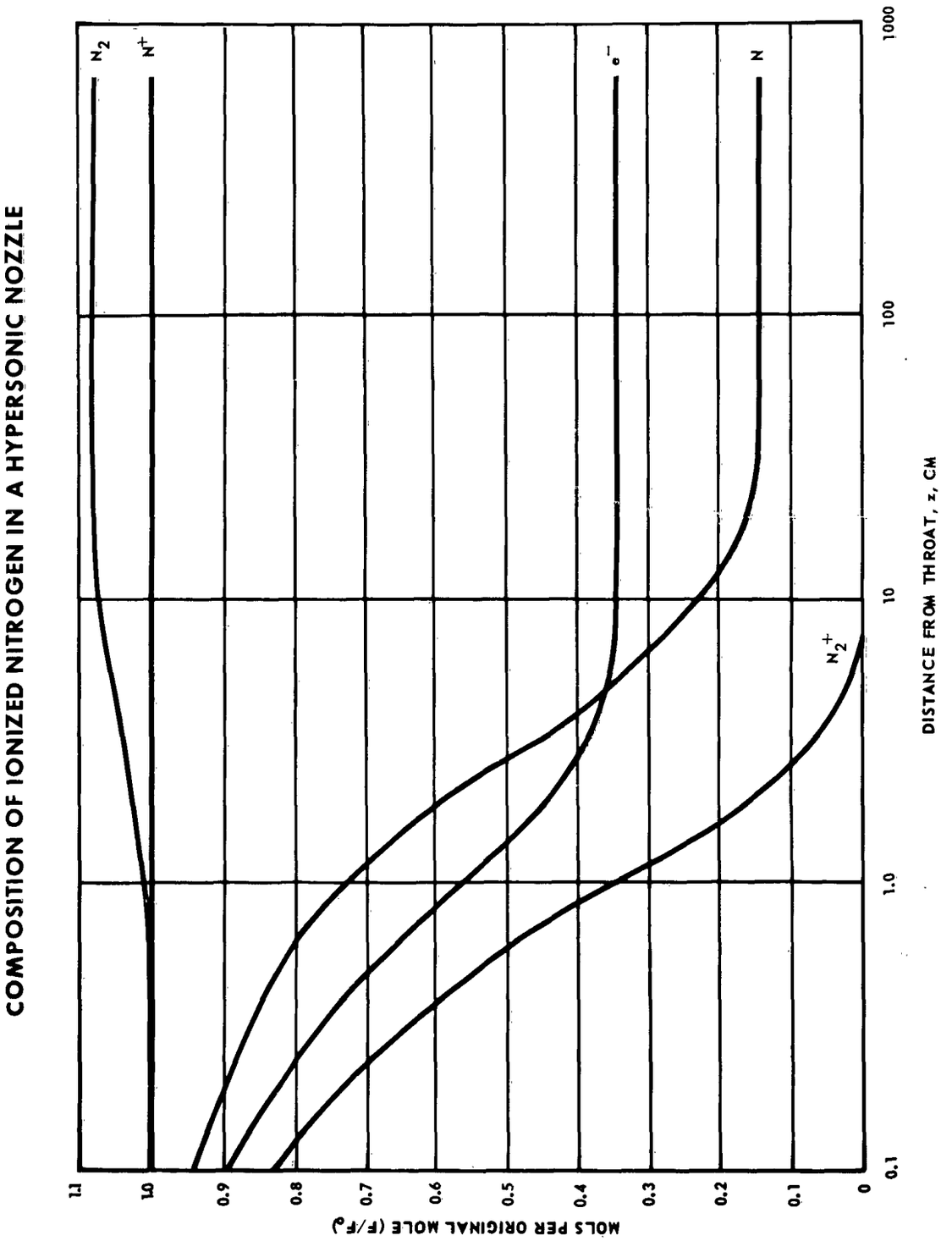

FIGURE 3-26

nozzle length to the 50 inch diameter test station is approximately 720 cm. The preliminary calculations presented here, however, do not take into account the reduction in effective area, which results from the boundary layer in the nozzle. It is reasonable, therefore, to compare these non-equilibrium calculations with the previously presented frozen flow calculations, at equivalent effective area ratios. With the magnetic coil in place, the area ratio was estimated previously to be 8100; this corresponds to a distance of approximately 360 cm. in the present calculations.

From Figure 3-26 it is seen that the rate of recombination of N_2^+ ions is very rapid, and that this species is essentially removed from the gas stream within a distance of 6.4 cm. from the throat. On the other hand, the loss by recombination of N^+ ions is negligible, amounting to less than 0.8 percent of the original N^+ ions present. This reaction is essentially frozen beyond the first 6 cm. The number of electrons remaining in the flow is equal to the number of N^+ ions, and also remains constant beyond the first 6 cm. The reaction leading to the recombination of N atoms to molecular nitrogen N_2, becomes frozen at approximately 20 cm. from the throat; approximately 85 percent of the original N atoms have been lost by recombination at this point. The reactions leading to the recombination of both N^+ ions and N atoms are three body reactions, and the mass rates of these reactions vary with the square of the density. Because of the rapid decrease in density in the nozzle, these reactions become "frozen" and do not again become significant. The recombination of N_2^+ ions, on the other hand, has been assumed to take place through the dissociative mechanism. The mass rate of this reaction is relatively rapid and varies directly with the density. It is not surprising, therefore, that the recombination of N_2^+ ions proceeds to completion.

For comparison, calculations for the same initial conditions have been

carried out with the frozen flow assumption, i.e., all reaction rates have been set equal to zero. In these calculations, specific heats have been computed from the program, and are at an equilibrium value at the local temperature. Because the energy in vibration is small compared to the energy in dissociation and ionization, differences arising from this assumption are expected to be small. A comparison of the frozen flow and non-equilibrium calculations for the same initial conditions is presented in Figure 3-27. It is seen that density and velocity at the test station do not differ significantly for the two cases. There is a significant difference in the temperature, however, which is higher for the non-equilibrium calculations.

The purpose of the non-equilibrium flow calculations is twofold: first, to provide a basis for comparison with the frozen flow calculations, and second, to provide an insight into the dynamic behavior of the component species within the nozzle. Using the density and composition obtained from the non-equilibrium flow calculations at the area ratio of 8100, the electron number density is estimated to be 6×10^{11} cm^{-3}. For ionized nitrogen in equilibrium at 8000°K and a density ratio of 10 relative to standard density, the pressure is approximately 4400 psi. From Figure 3-23 the electron number density predicted from the frozen flow calculations is found to be approximately 1.5×10^{12} cm^{-3}, which is in good agreement with the non-equilibrium calculations, if allowance is made for the fraction of electrons lost by recombination with N_2^+ ions. At typical arc chamber conditions of 12,000°K and 2000 psi for the experimental runs, the number of atomic nitrogen ions exceeds the number of molecular nitrogen ions at equilibrium; hence, proportionately fewer electrons would be lost by recombination with N_2^+, thus, the electron concentration at the test station is expected to differ by less than a factor of two from that obtained by the frozen flow calculations of

COMPARISON OF NON-EQUILIBRIUM CALCULATIONS WITH EQUIVALENT FROZEN FLOW CALCULATIONS

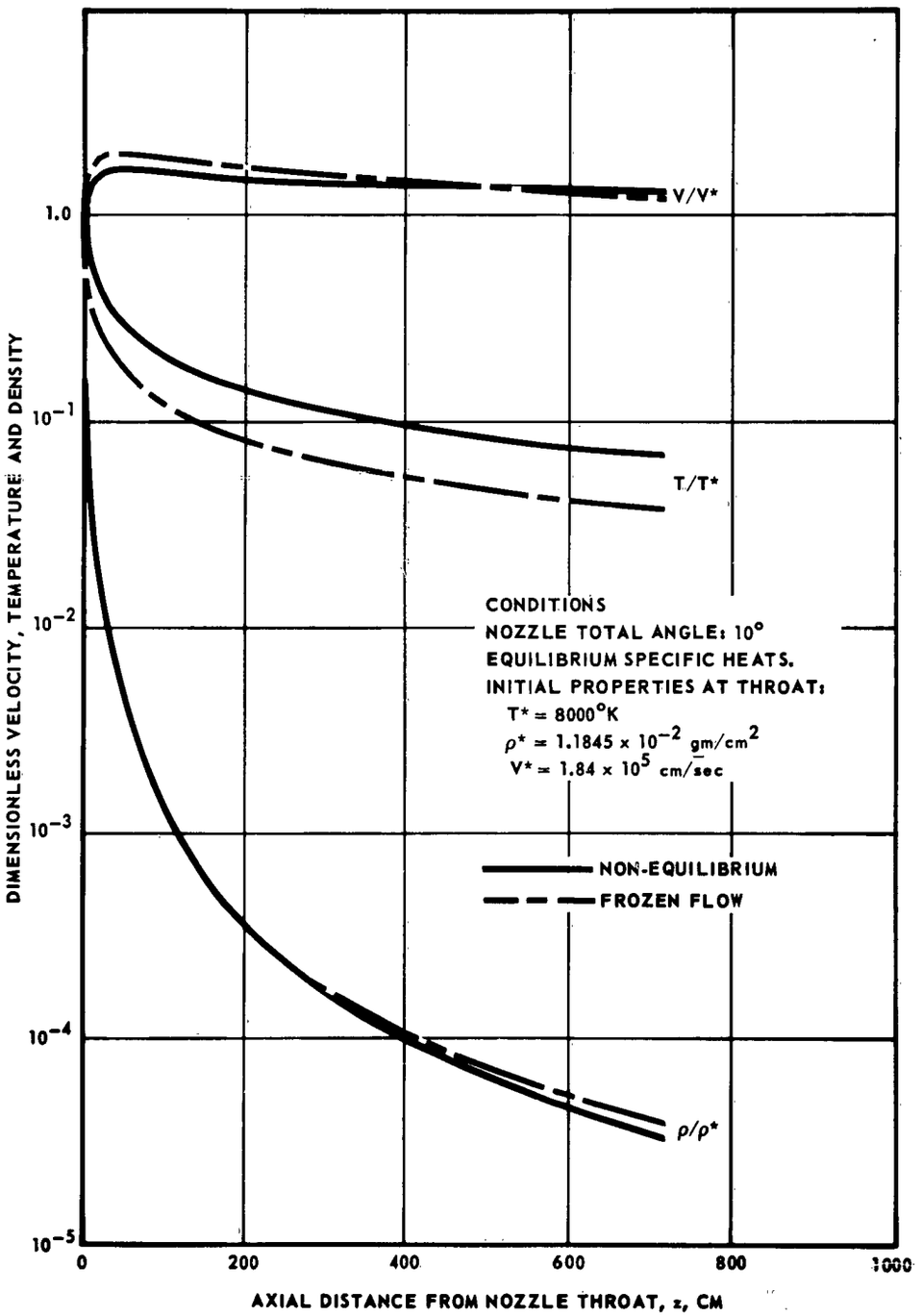

FIGURE 3-27

section 3.4.2.6. For the MHD experiments with which this report is concerned, a loss of electrons of this magnitude is not important. Furthermore, the elimination of the molecular nitrogen ion, N_2^+, results in a significant reduction in the complexity of the plasma wave equations and simplifies the experimental analysis of the observed wave patterns.

The non-equilibrium flow calculations presented here must be considered to be only approximate, because of a lack of knowledge of the true values of recombination rates at the temperatures and pressures of importance to this study. Calculations have been carried out for an initial temperature of 8000°K, rather than 12,000°K, because of the lack of complete published thermodynamic data at the higher temperature. This data is expected to be available soon. A more nearly exact calculation would take into account non-equilibrium specific heats, as well as the calculation of electron temperature, and the effect of electron temperature on recombination rates. Nevertheless, it is believed that these calculations present a reasonably close approximation to the true behavior of ionized nitrogen in a hypersonic nozzle.

Notes on Blow Down Flow Analysis. - The basic analysis presented for the blow down flow has been performed for the geometric area ratio existing between the test section and the nozzle throat ($A/A^* = 8100$). A few additional figures have been presented to indicate how certain conditions vary with area ratio. Although, it is well known, that a boundary layer does indeed exist inside the tunnel, effectively reducing the core size, a lack of data on core size made mandatory certain assumptions in predicting the test section conditions. Certainly, the assumption of effective area ratio equal to the geometric area ratio predicts lower temperatures and electron concentrations than might be expected, thus providing a lower limit on the determination of these values. On the other hand, a minimum of data also means approximate methods must be

devised to provide answers.

As will be pointed out in the sections on instrumentation and on data reduction, (Section 3.2.3 Vol. III) only two types of measurements were available upon which to base any type of flow field analysis. During the electrical exciter experiments, a smear photograph captured luminous particle traces, yielding a gas velocity. During subsequent runs, a pitot-static pressure pickup measured the stagnation pressure behind the normal shock in the test section. The photographically determined velocity was used to determine an area ratio from which a density and a temperature were computed. This computation was based upon the frozen flow analysis computer analysis.

The usual expressions to interpret the pressure measurements are no longer valid when the free stream is dissociated and ionized, as is the case of the blow down flow. The simplest solution has been to ignore this pitfall, and to assume an effective ratio of specific heats, γ , for use in the normal expressions. This effective γ has no bearing on the effective γ used previously in the discussion of the expansion process and frozen flow, since the nozzle expansion normally is based on state conditions initially at the throat, rather than the free stream conditions existing at the test section. Referring again to the computer results for different area ratios, a Mach number and pressure was determined at a given value of area ratio. Assuming an effective γ of 1.3, a calculated stagnation pressure behind the shock was determined and compared with the measured value. A new value of area ratio was then assumed and the process repeated until the calculated and measured pressure agreed. The final area ratio was considered the effective area ratio at which the other conditions could be determined. Para. 3.2-3, Vol. III, has been prepared in this manner. Unavoidably, the effective area ratio upon which this table is based seems much too great in that the predicted tempera-

ture appears unreasonably low. Although it was attempted, a different value for the effective γ might have predicted a more reasonable temperature. At best then, this computation might replace the assumption of $A/A^* = 8100$ as the lower limit on test section conditions. Nevertheless, these computations are based on an essentially sound theory for frozen flow, with additional confirmation coming from the measured electron concentrations at the test section.

3.4.3 Plasma Generation by an Electromagnetic Shock Tube and an Arc Discharge Tube. - Two small plasma facilities acquired during this program complemented the HIT. The addition of these facilities with much greater recycle times became desirable, as the number of necessary development and exploratory experiments increased. Then too, the HIT could not attain the high ionization percentages, which more easily would support Alfvén wave propagation. The electromagnetic shock tube generates a moving plug of plasma by striking an arc coaxially, at one end of a pyrex glass tube. The basic processes involved in producing the plasma are largely unknown, however, the resulting characteristics of high temperature and high ionization percentage can be easily measured. The second facility, an arc discharge tube, produces ionization by striking an arc along the length of a pyrex tube. While the arc is still burning, the experiments are performed. As in the electromagnetic shock tube, the basic processes are not understood, nevertheless, the characteristics of the resulting plasma can be measured.

3.4.3.1 Electromagnetic Shock Tubes. - The electromagnetic (EM) shock tube was originally developed to surmount the limits of attainable shock strength, available from conventional diaphragm type tubes. Basically, the operation of the EM shock tube involves rapidly discharging a capacitor through gas in a chamber, heating and ionizing the gas, and accelerating it

out of the chamber into a region of cold gas. The acceleration takes place, at least in part, because of the interaction between currents in the discharge plasma and the magnetic field of the return currents, through the external circuits supplying the discharge.

If the "plug" of plasma were regarded as a moving piston compressing the cold gas ahead of it, the existence of a shock moving ahead of the driver gas would be predicted. Something resembling a shock has indeed been observed by several investigators under certain conditions of initial gas pressure. Conditions behind the shock would depend on the state of the gas ahead of it and could be calculated from the conservation laws, in combination with the equations of state of the gas. The equations would also have to take into account the fact that gas ahead of the shock may be excited by ultraviolet or x-radiation from the discharge. Theories exist which predict fairly accurately the velocity of the plasma as it leaves the discharge region.

The region of shock heated gas may not endure for long, even in those cases where a well defined shock is seen to exist. If a sample of hot plasma which exists for a fairly long time is desired, a number of intermixing processes must be examined. The initial shock attenuates as it moves down the tube, allowing the hot driver gas to catch up; in the meantime energy is lost by conduction and radiation, and some of the electrons recombine with ions. The driver gas also mixes with the shocked gas by turbulence and diffusion. Most of these effects are rather intractable theoretically, so most of the knowledge of the actual conditions in the tube must be obtained by direct measurement, using probe, microwave, and time resolved spectroscopic techniques. However, it is possible to construct crude models of the interaction of the plug of hot gas with the cool gas in the tube. Theory and experimental measurements both suggest that the gas will leave the discharge with a velocity of

the order of 10^7 cm/sec. The kinetic energy of one gram of this gas is:

$$\tfrac{1}{2} mv^2 = 5 \times 10^{13} \text{ ergs/gm} \sim 10^6 \text{ Cal/gm}$$

For comparison, the chart below gives the internal energy of air at densities corresponding to the pressure range over which tubes of this type are operated (Reference 3-35).

T	$\rho/\rho_o = 10^{-6}$	$\rho/\rho_o = 10^{-4}$	$\rho/\rho_o = 10^{-2}$
3000°K	E = 1.5×10^3 Cal/g	1.4×10^3	1.0×10^3
5000	8.5×10^3	3×10^3	1.5×10^3
8000	1.5×10^4	1.0×10^4	$.8 \times 10^4$
12000	3.5×10^4	2.8×10^4	1.5×10^4
18000	5.2×10^4	3×10^4	2×10^4
24000	9.2×10^4	6×10^4	3×10^4

The quantity ρ_o is the density of air at standard conditions, 1.29×10^{-3} g/cm^3. For air at 50 microns pressure and 0° C, $\rho/\rho_o \simeq 5 \times 10^{-4}$.

It can be seen that the kinetic energy of a given quantity of gas is considerably higher than its internal energy over the temperature range shown on the chart. This gives some justification for a model which ignores detailed thermodynamic or gas dynamic considerations and treats the moving plug of gas as a moving piston. The rate of change of momentum of the plug of gas is equal to the rate at which momentum is added to the cold gas:

$$M \frac{du}{dt} = - mu^2.$$

where:

M = mass of driver gas plug,

m = mass/unit length of shock tube gas,

u = velocity of the plug of hot gas.

Upon integrating:

$$u = \frac{M}{m\,(t + K')}$$

where K' is the constant of integration. With the initial condition $u = u_o$ when $t = 0$ then:

$$u_o = \frac{M}{mK'}$$

and

$$K = \frac{1}{K'} = \frac{mu_o}{M}$$

thus:

$$u = \frac{M}{m\left(t + \frac{M}{mu_o}\right)} = \frac{u_o}{(1 + Kt)}$$

This can be integrated immediately to give distance x traveled by the plug of gas from the exit of the discharge region as a function of time, hence:

$$u = \frac{dx}{dt} = \frac{u_o}{1 + Kt}$$

or:

$$x = u_o \frac{\ln (1 + Kt)}{K}$$

Streak photos made by other investigators of actual shocks show the following features, which seem to support this picture. The velocity of advancement of the luminous front decreases with distance from the discharge region, and the rate of decrease is less for lower pressures. At low enough pressure the luminous gas fills the whole of the tube. The distance of the luminous front can be fitted reasonably well with the above equation, with the proper choice of the parameter K as shown in the table below:

p(mm Hg)	u_o ($\frac{cm}{\mu sec}$)	K	M/m
3	2	.4	5
.3	5	.4	12
.03	5	.05	100

These values of M/m seem reasonable, if it is assumed that at lower pressures most of the gas in the hot plug comes from evaporation of insulation and electrode materials in the discharge region.

It appears that there is sufficient energy available to heat all the gas in the tube to fairly high temperature and a correspondingly high degree of ionization; and that there exists a mechanism for distributing the energy, namely the transformation of ordered velocity into thermal velocity by collisions at the front of the plug. The rate at which thermal energy is added to the cold gas can be determined from the velocity equation above, since the rate at which both kinetic and internal energy is added to the cold gas is equal to the rate at which kinetic energy is lost by the driver gas. Detailed calculations of the temperature history along the tube require further assumptions about the details of the interaction at the front and the energy losses by radiation, diffusion, wall effects and so on.

Another model, which is probably more appropriate for making estimates of conditions behind the shock, is that proposed by Thornton and Cambel (Reference 3-36) in which the one dimensional blast wave theory of Harris (Reference 3-37) is modified to take radiation losses into account. The conclusion is reached that radiation losses are relatively unimportant in shock attenuation except near the discharge region. This gives some justification to the calculation of the conditions behind the shock by classical type shock relations. The results of such calculations are reproduced below, where the calculated temperature and concentrations of various species are shown as a function of total distance traveled by the shock. The model used assumes that the energy of the gas behind the shock is uniformly distributed, but it is doubtful whether completely uniform conditions really prevail. (See Figure 3-28)

The above results are in general agreement with experimental measurements.

TEMPERATURE AND EQUILIBRIUM COMPOSITION OF THE AIR BEHIND THE SHOCK WAVE FOR SHOCK TUBE CONDITIONS

(VOLTAGE = 17,200 V, PRESSURE = 30 μ Hg.)

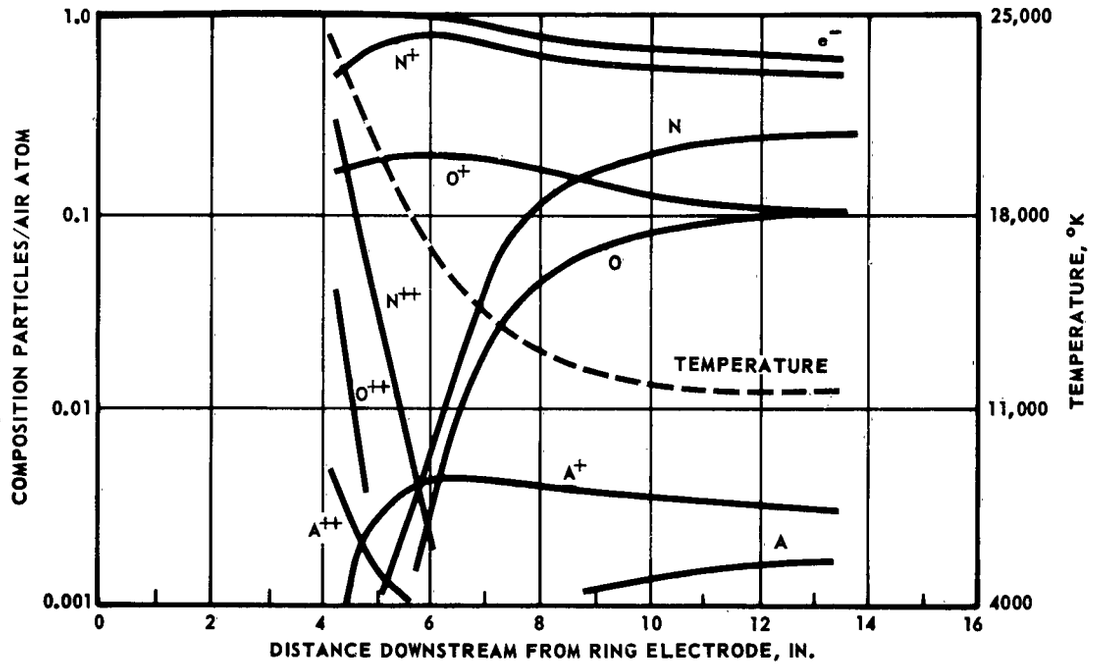

FIGURE 3-28

Thus, it can concluded that the electromagnetic shock tube is capable of generating highly ionized gases near the discharge region. In addition it is a facility that is easily constructed and inexpensive to operate.

3.4.3.2 Arc Discharge Tube. - The arc discharge tube is a 30 inch long, 5 inch diameter pyrex tube, provided with concentric electrodes at each end. For its operation, the tube is evacuated to a desired pressure, and an electric arc is struck across the tube between the center electrodes. The arc ionizes the gas and maintains this ionization as long as the current continues. This facility at McDonnell was utilized in the same manner as that of Wilcox et al (Reference 3-6), who showed its advantages for the study of Alfvén waves in hydrogen and deuterium. Furthermore, it provided an environment in which instrumentation techniques could be economically investigated. The following

paragraphs discuss the characteristics of the ionizing process. As in the case of the electromagnetic shock tube, the basic processes remain, for the most part, undefined.

Electrical discharges in gases are divided into two major classes, namely, self-sustained discharges and non self-sustained discharges. A self-sustained discharge is one which maintains itself without external aid, while the non self-sustained discharge depends upon on an external source, (e.g., a heated cathode) that produces a sufficient number of electrons and ions to maintain the discharge. Electrical discharges can be further subdivided by the magnitude of the applied voltage for the discharge and the amount of current that is observed. Figure 3-29, taken from Reference 3-27, shows roughly the aforementioned subdivisions.

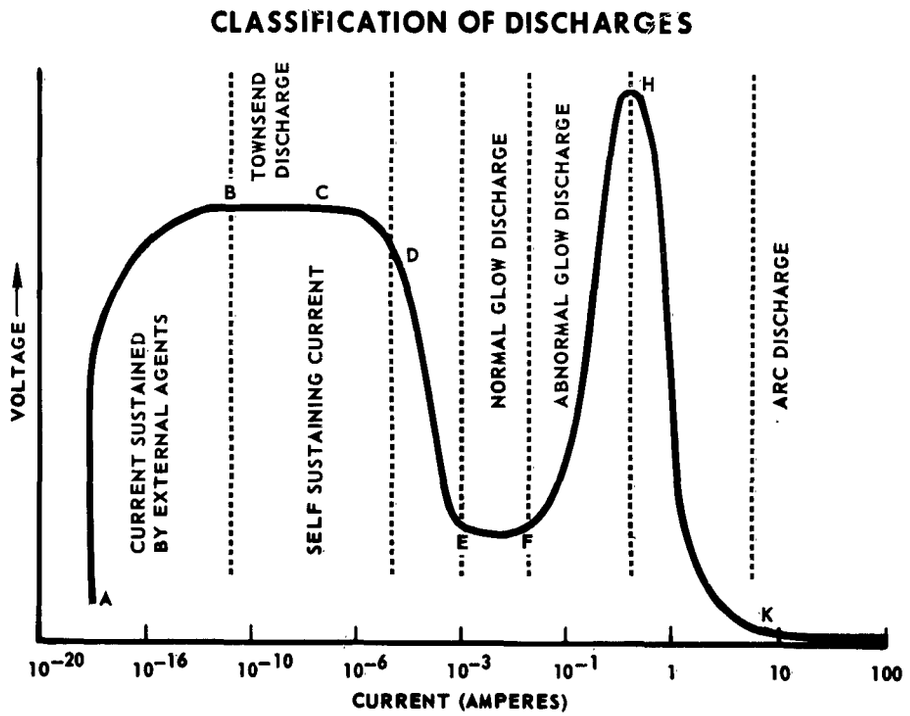

FIGURE 3-29

The operating characteristics of the arc discharge tube determine the nature of the discharge process. The ionization exists for about 10^{-4} sec., with an estimated maximum current of 41,000 amps. Before breakdown occurs the gas in the tube functions as an insulator; however, once the ionization process has been initiated, it becomes a good conductor and the impedance of the external circuit will greatly exceed that of the discharge tube. Thus the majority of the energy is dissipated in the external circuitry. This is characteristic of an arc discharge in that it will support large currents with a relatively small applied potential.

Arc discharges are also subdivided (Reference 3-27) according to the emission process taking place at the cathode and the pressure due to the discharge. High and low pressure discharges can be distinguished on the basis of the temperature of the positive column (References 3-27 and 3-38). In the high pressure arc, the positive column temperature is on the order of thousands of degrees Kelvin, with the gas components in approximate thermal equilibrium. On the other hand, in a low pressure arc, the electron temperature is much larger than the ion or gas temperature, on the order of tens of thousands of degrees Kelvin. The gas pressure for the McDonnell experiments was in the range of 40 to 1000 microns of Hg, thus satisfying the conditions for a low pressure arc.

The four types of arcs that are given in the following list must be examined to determine, if possible, which predominates. The thermionic arc with the neutral cathode is easily dismissed, since the cathode was not externally heated in experiments. Whether the arc is caused by thermionic emission or field emission depends upon the electrode material, as observed by W. Ramberg (Reference 3-39) and noted by Cobine and Brown. For example, C, C_a, M_g, and W are thermionic emitters; while Cu, Hg, Ag, and Au are field

emitters. A third group exists that exhibits both types of emission processes; these are Pt, Sn, Fe, and Cd. Metal arcs are distinguishable by observations of the cathode spot, the cathode temperature, the arc response to a magnetic field, and the cathode impurity effects. Loeb (Reference 3-40) and Thomson (Reference 3-41) hold that all arcs are due to thermionic emission. Without a very detailed examination the type of arc is difficult to determine.

1. Thermionic Arc
   a. A non self-sustained discharge with the cathode being heated to maintain the discharge.
   b. A self-sustained discharge, i.e., the cathode is heated by the discharge only.
2. Field Emission Arc — The electron current at the cathode is produced by very strong electric fields present at the cathode surface.
3. Metal Arcs — This classifies metal arcs on the basis of their response to a magnetic field, temperature of the cathode, and the influence of impurities on the cathode surface, whether or not the cathode spot moves on the cathode surface.

The burning voltage of the low pressure arc discharge is made up of three parts:

1. The cathode drop region, where there is a voltage drop on the order of the ionization potential across a thin sheet of the gas.
2. The positive column, where the voltage drop is a function of the gap length, the arc current, and the gas pressure.
3. The anode drop region, which closely resembles the cathode voltage profile.

The current density at the cathode is much greater than that in the glow. The positive arc column is characterized by approximate electrical neutrality, a current principally carried by electrons, and a voltage gradient large enough

to produce an equal amount of ionizing collisions to balance ions lost to the walls of the tube.

The analysis of the low pressure arc has been carried out for a number of different cases by Tonks and Langmuir (Reference 3-42) and Cobine (Reference 3-43). Following the analysis of Cobine, there are four independent variables for the case of a cylindrical tube, namely, the tube radius r, gas pressure P_g, arc current i_a, and the wall temperature T_w, which must be related to the five independent variables, i.e., the axial electric field E_z, electron concentration at the axis n_{eo}, electron temperature T_e, positive ion current density at the wall j_i, and the number of electrons generated per electron per second λ. At a sufficiently low pressure, such that the mean free path of the gas particles is comparable to the tube radius, T_w can be replaced with the gas temperature T_g.

The ions of plasma are being continuously lost to the walls of the tube, and it is assumed that the ions move under a radial potential with a maximum at the tube axis; however, since the reference point is arbitrary in measuring potential, the zero of potential may be taken to be at the tube axis and, thus, negative everywhere else. The origin of coordinates is taken at the tube axis, i.e., r = 0. The ions generated at some point z, intermediate between the axis and the wall, will have attained a velocity v_z at a distance r from the axis. Then if N_z is the ion production rate per unit volume at the point z, the ion concentration at r is:

$$\frac{N_z\, z\, dz}{r\, v_z}$$

To account for all ions produced at distances less than r the above equation is integrated from zero to r:

$$n_i = \frac{1}{r} \int_0^r \frac{N_z\, z\, dz}{v_z}$$

Boltzmann's relation gives the expression for the number of electrons/cm^3 at

some intermediate point at a potential V in terms of the number of electrons/cm^3 at the axis:

$$n_e = n_{eo}\, e^{eV/rT_e}$$

To get the form of the radial potential distribution, Poisson's equation must be solved. Therefore:

$$\nabla^2 V = -4\pi e\, \rho_{net} = -4\pi e\,(n_i - n_e)$$

or:

$$\nabla^2 V + \frac{4\pi e}{r} \int_o^r \frac{N_z z\, dz}{v_z} - 4\pi e n_{eo} e^{eV/kT_e} = 0$$

This is referred to as the "complete plasma-sheath equation", for it is the general equation for the radial potential distribution including the wall sheath. If the mean free path is long and if N_z is proportional to n_e, Tonks and Langmuir show that the electron density at the axis is given, within an order of magnitude by:

$$n_{eo} = 4.21 \times 10^{13} \left(\frac{m_i}{m_e}\right)^{1/2} j_i^{\;1/2}\, T_e$$

To perform this calculation J_i, the ion current density at the wall, must be measured.

The arc discharge tube is useful in Alfvén wave experiments since, despite the difficulties encountered in determining the processes occurring, the necessary plasma conditions can be measured. Wilcox et al indicate that the ionization is between 80 and 100 percent at pressures of 100 microns of Hg. They have studied the electron concentration as a function of time and found, by observing the first order Stark broadening of Hydrogen Balmer lines, that the electron concentration is down a factor of 2 in 150 microseconds. They estimate the electron temperature, from Alfvén wave dampening, to be greater than 10^4 °K.

4. REFERENCES

2-1 Lehnert, B., Del Nuovo Cimento (Supplement), 13, Ser. 10, 59 (1959)

2-2 Tanenbaum, B.S., Mintzer, D., Phys. Fluids, 5, 1226 (1962)

2-3 Tanenbaum, B.S., "Dispersion Relations in a Stationary Plasma", Physics of Fluids, 4, #10, 1262, October 1961

2-4 Budden, K.G., "Radio Waves in the Ionosphere", Great Britain, Cambridge University Press, 1961

2-5 Landshoff, R.K.M. (Ed.), "Magnetogydrodynamics", California, Stanford University, p. 109, Press, 1957

2-6 Gould, R.W., "Excitation of Alfvén Waves", STL/TR-60-0000-09143, May 1960

2-7 Watanabe, T., Can. J. Phys. 39, 1197, 1961

2-8 Jephcott, D.F., Nature 183, 1652, 1959

2-9 Chopra, K.P., "Reviews of Modern Physics", 33, #2, 153, 1961

2-10 Alfvén, H., Cosmical Electrodynamics, Oxford University Press, 1950

2-11 Chang, H.H.C., Magnetohydrodynamic Waves in the Ionosphere, California, Hughes Research Laboratories, 1961 (USAF CRL-64)

2-12 Fejer, J.A., J. Atmosph. Terr. Phys., 18, 135 (1960)

2-13 Spitzer, L., Physics of Fully Ionized Gases, New York, Interscience Publishers, Inc., 1956

2-14 Landau, L.D., Lifshitz, E.M., Electrodynamics of Continuous Media, Great Britain, Pergamon Press, 1960

2-15 Present, R.D., Kinetic Theory of Gases, New York, McGraw-Hill Book Co., Inc. 1958

2-16 Churchill, R.V., Modern Operational Mathematics in Engineering, New York, McGraw-Hill Book Co., Inc., 1944

2-17 Wills, A.P., Vector Analysis with an Introduction to Tensor Analysis, Dover, Inc., New York, 1958

3-1 Air Force Cambridge Research Center Report TR-59-267, "The ARDC Model Atmosphere," August 1959

3-2 Menzel, D.H., Fundamental Formulas for Physics , 1960 Dower Publications, New York

3-3 Lundquist, S., Ark. for Fys. (Uppsala), 5, 297, 1952

3-4 Lehnert, B., Del Nuovo Cimento (Supplement), 13, Ser. 10, 59, 1959

3-5 Allen, T.K., Baker, W.R., Pyle, R.V., and Wilcox, J.M., Phys. Rev. Letters 2, #9, 383, May 1959

3-6 Wilcox, J.M., Boley, F.I., DeSilva, A.W., Phys. Fluids 3, #1, January-February 1960

3-7 Wilcox, J.M., DeSilva, A.W. Cooper, W.S. III, Phys. Fluids 4, #12, 1506, December 1961

3-8 Jephcott, D.F., Nature 183, 1652, 1959

3-9 Hardcastle, R.A., and Jephott, D.F., Proc. 4th Intern. Conference on Ionization Phenomena in Gases, Uppsala, Vol. II, 786, August 1959

3-10 Petcheck, H., and Byron, S., "Approach to Equilibrium Ionization behind Strong Shock Waves in Argon," Ann. of Phys., 1, 270, 1957

3-11 Whithorn, G.B., "On the Propagation of Shock Waves through Regions of Non-Uniform Area of Flow," Journal of Fluid Mechanics 4, 337-360, August 1958

3-12 Poyne, R.B., "A Numerical Method for a Converging Cylindrical Shock," Journal of Fluid Mechanics 2, Part 2, 185-200, March 1957

3-13 Chisnell, R.F., "The Motion of a Shock Wave in a Channel, With Application to Cylindrical and Spherical Shock Waves," Jour. of Fluid Mechanics 2, Pt. 3, 286-298, May 1957

3-14 Rudinger, G., Wave Diagrams for Non-Steady Flow in Ducts, 1955, D. Von Nostrand Co., New York

3-15 Ascher, H., Shapiro, The Dynamics and Thermodynamics of Compressible Fluid Flow, Volume II , 1954, The Ronald Press Company, New York

3-16 AVCO Research Report No. 40, "Hypersonic Gas Dynamic Charts for Equilibrium Air," January 1957

3-17 Space Technology Laboratory Report TR-60-0000-09093, "Extended Hypervelocity Gas Dynamic Charts for Equilibrium Air," April 1960

3-18 NASA Report TN D-87, "Effects of Chemical Dissociation and Molecular Vibrations on Steady One-Dimensional Flow," August 1959

3-19 Douglas Aircraft Company Missile and Space Systems Engineering Report SM-38523, "One Dimensional Flow of Dissociated Diatomic Gases," 2 May 1961

3-20 Cornell Aeronautical Laboratory Report BE-1007-A-5, "Thermodynamic Properties of Nitrogen from 2000°K to 8000°K," January 1957

3-21 Northwestern University Gas Dynamics Laboratory, Personal Communication, K.S. Drellishak

3-22 Bray, K.N.C., "Atomic Recombination in a Hypersonic Wind Tunnel Nozzle," Journal of Fluid Mechanics, 6 1, July 1959

3-23 AEDC Report AEDC-TDR-62-131, "Method for Calculation of the One-Dimensional Non-equilibrium Flow of a General Gas Mixture through a Hypersonic Nozzle," June 1962

3-24 Applied Physics Laboratory, The Johns Hopkins University, Report CM-1013, "Nozzle Flow with Complex Chemical Reaction," March 1962

3-25 Eschenroeder, A.Q., "Ionization Non-Equilibrium in Expanding Flows," ARS Journal, 32, 196, February 1962

3-26 Cornell Aeronautical Laboratory Report AF-1413-A-2, "Inviscid Hypersonic Airflows with Coupled Non-equilibrium Processes", May 1962

3-27 Brown, S.C., Basic Data of Plasma Physics, 1959, John Wiley and Sons, Inc., New York

3-28 Massey, H.S.W., Recombination of Gaseous Ions, Advances in Physics, 1, 395, October 1952

3-29 Bialecke, E.P., and Dougal, A.A., "Pressure and Temperature Variation of the Electron Ion Recombination Coefficient in Nitrogen," Journal of Geophysical Research, 63, 539, September 1958

3-30 Wray, K.L., "Chemical Kinetics of High Temperature Air," ARS Preprint No. 1975-61, August 1961

3-31 NASA TN D-1191, "Microwave Interferometer Measurements of Electron-Ion Recombination in Nitrogen, Air, and Argon," February 1962

3-32 Bates, D.R., Phys. Rev., 78, 492, 1950

3-33 WADD Report TR 60-341, "Similarity for Dissociating Gases in Hypersonic Low Density Flow," 1960

3-35 The RAND Corporation Report No. RM-1543, Equilibrium Composition and Thermodynamic Properties of Air to 24,000°K," 24 August 1955

3-36 Thronton, J.A., and Cambel, A.B., J. Quant, Spectrosc. Radiat. Transfer., 2, 249, 1962

3-37 U.S. Naval Research Laboratory Report 5858, "Exact and Approximate Treatments of the One-Dimensional Blast Wave." 1956

3-38 Cobine, J.D., Gaseous Conductors, 1958 Dover Publications 290-ff

3-39 Romberg, W., Ann. d. Physik, 12, 319, 1932

3-40 Loeb, L.B., Fundamental Processes of Electrical Discharges in Gases, 1939, John Wiley & Sons, p-631, New York

3-41 Thompson, J.J., and Thomson, G.P., Conduction of Electricity through Gases, 3d ed., Vol. 2, 596, Cambridge University Press, London, 1933

3-42 Tonks, L., and Langmuir, I., Phys. Rev., 34, 876, 1929

3-43 Ibid p-319

APPENDIX A

ALFVÉN WAVES IN A FULLY IONIZED GAS

The following derivation, while classical in the sense that Alfvén first took this approach, has an advantage in that it is the simplest way to analyze transverse disturbances in a fully ionized gas. This approach facilitates incorporation of wave excitation mechanisms, total plasma motion and primary field gradients into the theory.

Working in the MKS system of units, the Maxwell equation which relates the current density to the spatial variation of the magnetic field it induces within the plasma and vice versa, is:

$$\nabla \times \vec{H} = \vec{j} + \frac{\partial \vec{D}}{\partial t}. \qquad \text{(A-1)}$$

As usual, $\vec{j}$ is the current density due to the field $\vec{E} + \vec{V} \times \vec{B}$, where $\vec{E}$ is due both to the plasma constituents and existing externally caused electric fields and:

$$\vec{B} \equiv \vec{B}_o + \vec{b}, \qquad \text{(A-2)}$$

where $\vec{B}_o$ is due to a constant magnetic field, with $\vec{b}$ being induced by moving charges in the plasma. $\vec{V}$ is the total macroscopic plasma velocity, which for an initially moving plasma of velocity $\vec{V}_o$ and an induced plasma velocity $\vec{v}$, is given by $\vec{V} = \vec{V}_o + \vec{v}$. To be sufficiently general, it is necessary to introduce the effects of B on the plasma conductivity. Since $\vec{b}$ is generally found to be oscillatory, the average of $\vec{B}$ over many cycles of $\vec{b}$ is just $\vec{B}_o$, neglecting harmonics. A common but more restrictive condition is to consider only the case where $\vec{b} << \vec{B}_o$. In either event the cyclotron frequencies are due to $\vec{B}_o$, and $\vec{j}$ is related to the induced field through the conductivity tensor as:

$$\vec{i} = \underline{\sigma} \cdot (\vec{E} + \vec{V} \times \vec{B}), \qquad \text{(A-3)}$$

where, in general:

$$\underline{\sigma} = \begin{bmatrix} \sigma_{11} & \sigma_{12} & \sigma_{13} \\ \sigma_{21} & \sigma_{22} & \sigma_{23} \\ \sigma_{31} & \sigma_{32} & \sigma_{33} \end{bmatrix} \qquad \text{(A-4)}$$

For orthogonal external electric and magnetic fields and low frequency internal fields, the tensor elements of $\underline{\sigma}$ have the familiar forms:

$$\sigma_{11} = \sigma_{22} = \frac{\sigma_e}{1 + \left(\frac{\omega_{ce}}{\nu_{ei}}\right)^2} + \frac{\sigma_i}{1 + \left(\frac{\omega_{ci}}{\nu_{ie}}\right)^2}$$

$$\sigma_{21} = \sigma_{12} = \frac{\sigma_e (\omega_{ce}/\nu_{ei})}{1 + (\omega_{ei}/\nu_{ei})^2} + \frac{\sigma_i (\omega_{ci}/\nu_{ie})}{1 + (\omega_{ci}/\nu_{ie})^2} \qquad \text{(A-5)}$$

$$\sigma_{33} = \sigma_e + \sigma_i$$

$$\sigma_i = \frac{N_i e^2}{m_i \nu_{ie}}$$

$$\sigma_e = \frac{N_e e^2}{m_e \nu_{ei}}$$

with the remaining elements zero. In the above expressions m, e, N are the particle mass, charge, and number density, with the subscripts e and i referring to the electrons and ions, respectively; ω_{ce} and ω_{ci} are the electron and ion cyclotron frequencies, and ν_{sr} is the two-body collision frequency for an s-type particle with the r-type particles. For thermal equilibrium of the gas, $\nu_{ei} = \nu_{ie}$.

In equation (A-1) the convection current density has been neglected, and while the displacement current density can usually be neglected with respect to the conduction current density for low frequency plasma disturbances, it will be temporarily considered in this derivation in order to show a more complete form of the basic differential equation. With the relationship:

$$D = \underline{\epsilon} \cdot E \qquad \text{(A-6)}$$

the displacement current density becomes:

$$\frac{\partial \vec{D}}{\partial t} = \frac{\partial}{\partial t} (\underline{\epsilon} \cdot \vec{E}) \tag{A-7}$$

where the permittivity tensor is represented by

$$\underline{\epsilon} = \begin{bmatrix} \epsilon_{11} & \epsilon_{12} & \epsilon_{13} \\ \epsilon_{21} & \epsilon_{22} & \epsilon_{23} \\ \epsilon_{31} & \epsilon_{32} & \epsilon_{33} \end{bmatrix} \tag{A-8}$$

Corresponding to the situation for which (A-5) is valid:

$$\epsilon_{11} = \epsilon_{22} = 2 - i \left[\frac{\Omega_e}{1 + (\omega_{ce}/\nu_{ei})^2} + \frac{\Omega_i}{1 + (\omega_{ci}/\nu_{ie})^2} \right]$$

$$\epsilon_{21} = -\epsilon_{12} = \frac{i (\omega_{ce}/\nu_{ei}) \Omega_e}{1+(\omega_{ce}/\nu_{ei})^2} + \frac{i (\omega_{ci}/\nu_{ie}) \Omega_i}{1 + (\omega_{ci}/\nu_{ie})^2} \tag{A-9}$$

$$\epsilon_{33} = 2 - i (\Omega_e + \Omega_i)$$

$$\Omega_e = \omega_{pe}^2/\omega\nu_{ei}$$

$$\Omega_i = \omega_{pi}^2/\omega\nu_{ie}$$

where ω is the angular frequency of the disturbance and ω_{pe} and ω_{pi} are the electron and ion plasma frequencies. The condition of electrical neutrality is most conveniently expressed by:

$$\nabla \cdot \vec{D} = 0 \tag{A-10}$$

Equation (A-1) may now be rewritten as:

$$\frac{1}{\mu_o} \nabla \times \vec{B} = \sigma \cdot (\vec{E} + \vec{V} \times \vec{B}) + \frac{\partial}{\partial t} (\epsilon \cdot \vec{E}) \tag{A-11}$$

where the constitutive relationship for the medium:

$$\vec{B} = \mu_o \vec{H} \tag{A-12}$$

has been used.

Taking the curl of (A-11), rearranging terms and using the equation:

$$\nabla \cdot \vec{B} = 0 \tag{A-13}$$

gives:

$$\nabla^2 \vec{B} + \mu_o \nabla \times \sigma \cdot [\vec{E} + \vec{V} \times \vec{B}] + \mu_o \frac{\partial}{\partial t} \nabla \times (\epsilon \cdot \vec{E}) = 0 \qquad \text{(A-14)}$$

A second equation which relates $\vec{V}$ and $\vec{B}$ and their derivatives can be found from the Navier-Stokes equation. If the non-electromagnetic, non-viscous forces are conservative, the net force on a plasma element (Reference A-1) is:

$$\rho \hat{D}\vec{V} = \vec{j} \times \vec{B} - \nabla \cdot \underline{\psi} + \eta (\nabla^2 \vec{V} + \frac{1}{3} \nabla \nabla \cdot \vec{V}) + N_q \cdot \vec{E} \qquad \text{(A-15)}$$

where:

$$\hat{D}\vec{V} = \frac{\partial \vec{V}}{\partial t} + (\vec{V} \cdot \nabla)\vec{V} \qquad \text{(A-16)}$$

The quantity $\underline{\psi}$ is the hydrostatic pressure tensor, in general a funcation of position and time, ϕ is the non-electromagnetic potential function, η is the coefficient of viscosity, N is the total electron and ion concentration, and q is the net charge in an elementary volume of the gas. The last term in (A-15) contributes only about $\left(\frac{V}{c}\right)^2$ of the first terms, c being the vacuum speed of light, and it is hereafter neglected. Solving equation (A-1) for $\vec{j}$, substituting into (A-15) and using the vector identity:

$$\vec{B} \times (\vec{\nabla} \times \vec{B}) = \frac{1}{2} \nabla (\vec{B} \cdot \vec{B}) - (\vec{B} \cdot \nabla) \vec{B} \qquad \text{(A-17)}$$

yields:

$$\frac{\partial \vec{V}}{\partial t} + (\vec{V} \cdot \nabla)\vec{V} - \frac{1}{\mu_o \rho} (\vec{B} \cdot \nabla)\vec{B} - \frac{1}{\rho} \vec{B} \times \frac{\partial}{\partial t} (\underline{\epsilon} \cdot \vec{E})$$
$$+ \frac{1}{\rho} \nabla \cdot \psi + \frac{1}{\rho} \nabla \left(\phi + \frac{B^2}{2\mu_o} - \frac{\rho \eta}{3} \nabla \cdot \vec{V}\right) - \frac{\eta}{\rho} \nabla^2 \vec{V} = 0 \qquad \text{(A-18)}$$

Equation (A-14) and (A-18) yield a system of six scalar differential equations in the six components of $\vec{B}$ and $\vec{V}$. To facilitate reduction of these equations certain relative assumptions must be made. Since for tenuous gases viscosity is practically non-existent ($\eta \approx 0$), the off-diagonal terms in $\underline{\psi}$ are negligible. If the pressure components along the principal axes are nearly equal,

the approximation:

$$\nabla \cdot \underline{\psi} = \nabla p \tag{A-19}$$

where p is the scalar pressure, is valid.

Also, $\nabla \phi$ is negligible for most laboratory situations. Then with the aid of the Maxwell equation:

$$\nabla \times \vec{E} = -\frac{\partial \vec{B}}{\partial t} \tag{A-20}$$

Equations (A-14) and (A-18) become:

$$\nabla^2 \vec{B} + \mu_o \nabla \times (\underline{\sigma} \cdot \vec{E}) + \mu_o \nabla \times [\underline{\sigma} \cdot (\vec{V} \times \vec{B})] = -\mu_o \frac{\partial}{\partial t} \nabla \times (\underline{\epsilon} \cdot \vec{E}) \tag{A-21}$$

and:

$$\frac{1}{\mu_o \rho} (\vec{B} \cdot \nabla) \vec{B} - (\vec{V} \cdot \nabla) \vec{V} - \frac{1}{\rho} \nabla \left(\frac{B^2}{2\mu_o} + p \right) = -\frac{1}{\rho} \vec{B} \times \frac{\partial}{\partial t} (\underline{\epsilon} \cdot \vec{E}) + \frac{\partial \vec{V}}{\partial t} \tag{A-22}$$

Due to the form of the conductivity and permittivity tensors, these equations cannot be significantly reduced, unless additional assumptions about the plasma characteristics, such as incompressibility, irrotational flow, no pressure gradients and so forth, are made. The problem is somewhat simplified, if the particle density variations, N, the magnetic induction, $\vec{B}$, and the plasma velocity, $\vec{V}$, are expressed in a linear form, implying that all terms above the first order are negligible. The pressure term ∇p is then related to the particle density by:

$$\nabla p = \gamma k T \nabla N \tag{A-23}$$

where γ is the ratio of specific heats, k, the Boltzmann constant, T, the equilibrium temperature. The electric field $\vec{E}$ is related to the linearized expression for $\vec{B}$ through equation (A-20). When (A-20), (A-21) and (A-22) are expanded, the result is a system of linear homogeneous equations in $\vec{B}$ and the time and spatial derivatives of $\vec{B}$.

Alfvén specialized equations (A-21) and (A-22), finding that they implied an oscillatory motion of the gas transverse to the direction of propagation of the disturbance. Alfvén's conditions were:

(1) The gas is incompressible: $\nabla \cdot \vec{V} = 0$

(2) The gas is inviscid: $\eta = 0$

(3) ρ, σ, and ϵ are scalar constants.

(4) The displacement current is negligible, that is:

$$\epsilon \frac{\partial \vec{E}}{\partial t} \ll \sigma (\vec{E} + \vec{V} \times \vec{B})$$

or equivalently:

$$\epsilon \frac{\partial^2 \vec{B}}{\partial t^2} \ll \sigma \left[\frac{\partial \vec{B}}{\partial t} + \nabla \times (\vec{V} \times \vec{B}) \right]$$

(5) All externally caused non-electromagnetic forces are negligible.

(6) $\left(p + \frac{B^2}{2\mu_o}\right)$ is not a spatially varying function.

(7) $\vec{B} = \vec{B}_o + \vec{b}$ where $\vec{B}_o$ is constant and $\vec{b} \prec\prec \vec{B}_o$.

With these conditions (A-21) and (A-22)) can be written for a stationary plasma ($\vec{V}_o = 0$) as:

$$\frac{\partial \vec{b}}{\partial t} = \frac{1}{\mu_o \sigma} \nabla^2 \vec{b} + (\vec{b} \cdot \nabla)\vec{V} - (\vec{V} \cdot \nabla)\vec{b} + (\vec{B}_o \cdot \nabla)\vec{V} \qquad \text{(A-24)}$$

and:

$$\frac{\partial \vec{V}}{\partial t} = \frac{1}{\mu_o \rho} (\vec{b} \cdot \nabla)\vec{b} - (\vec{V} \cdot \nabla)V + \frac{1}{\mu_o \rho} (\vec{B}_o \cdot \nabla)\vec{b} \qquad \text{(A-25)}$$

These equations suggest the linear relationship:

$$\vec{V} = a\vec{b} \qquad \text{(A-26)}$$

a being a complex quantity but constant in space and time. Upon substituting (A-26) and differentiating with respect to time, (A-24) becomes:

$$\frac{\partial^2 \vec{b}}{\partial t^2} = \frac{1}{\mu_o \sigma} \nabla^2 \frac{\partial \vec{b}}{\partial t} + a (\vec{B}_o \cdot \nabla) \frac{\partial \vec{b}}{\partial t} \qquad \text{(A-27)}$$

and (A-25) gives:

$$\frac{\partial \vec{b}}{\partial t} = \frac{1}{a\mu_o\rho}(\vec{B}_o \cdot \nabla)\vec{b} + \left(\frac{1}{a\mu_o\rho} - a\right)(\vec{b} \cdot \nabla)\vec{b} \qquad \text{(A-28)}$$

If the last term in (A-28) is neglected, then combining (A-27) and (A-28) yields the Alfvén wave equation:

$$\frac{\partial^2 \vec{b}}{\partial t^2} \approx \frac{1}{\mu_o\sigma}\nabla^2\frac{\partial \vec{b}}{\partial t} + \frac{1}{\mu_o\rho}(\vec{B}_o \cdot \nabla)^2\vec{b} \qquad \text{(A-29)}$$

A relationship between the mean fluid velocity and the perturbed field is obtained by comparing (A-27) with (A-29), and observing that, to a first approximation:

$$a = \pm(\mu_o\rho)^{-1/2} \qquad \text{(A-30)}$$

and therefore:

$$\vec{b} \approx (\mu_o\rho_o)^{1/2}\vec{V} \qquad \text{(A-31)}$$

Working in rectangular Cartesian coordinates with $\vec{B}_o$ along the $\vec{\imath}_z$ axis, the plane wave solution for a medium of infinite extent is:

$$\vec{b} = \vec{b}_o e^{i(\omega t - \kappa z)} \qquad \text{(A-32)}$$

where $\vec{\kappa}$ is the wave number and:

$$\vec{b}_o = b_o\vec{\imath}_x \qquad \text{(A-33)}$$

For a gas with very high electrical conductivity, equation (A-29) reduces to:

$$\frac{\partial^2 \vec{b}}{\partial t^2} = \frac{B_o^2}{\mu_o\rho}(\vec{\imath}_z \cdot \nabla)^2\vec{b} \qquad \text{(A-34)}$$

giving rise to an undamped plane wave of phase velocity:

$$\vec{u}_c = \left(\frac{1}{\mu_o\rho}\right)^{1/2} B_o = a\vec{B}_o \qquad \text{(A-35)}$$

called the Alfvén velocity. In the more general case where the conductivity must be considered, substitution of (A-32) into (A-29) produces the dispersion equation:

$$\kappa = \frac{\pm\omega}{u_o}\left(1 + i\,\frac{\omega}{\mu_o \sigma U_o^2}\right)^{-1/2} \qquad \text{(A-36)}$$

or, in rectangular form:

$$\kappa = \pm \frac{\omega}{U_o\sqrt{2\left(1+\frac{\omega^2}{\mu_o^2\sigma^2U_o^4}\right)}}\left[\sqrt{1+\sqrt{1+\frac{\omega^2}{\mu_o^2\sigma^2U_o^4}}} - i\sqrt{-1+\sqrt{1+\frac{\omega^2}{\mu_o^2\sigma^2U_o^4}}}\right] \qquad \text{(A-37)}$$

A direct measure of the wave attenuation in space is afforded by the distance required for the wave amplitude to fall to 1/e of its initial value b_o. This distance is referred to as the attenuation distance d and is given by the reciprocal of the imaginary part of κ ; thus, in rectangular form:

$$d = \left|\frac{1}{I_m(\kappa)}\right| = \frac{u_o\sqrt{2\left(1+\frac{\omega^2}{\mu_o^2\sigma^2U_o^4}\right)}}{\omega\sqrt{\sqrt{1+\frac{\omega^2}{\mu_o^2\sigma^2U_o^4}}-1}} \qquad \text{(A-38)}$$

from equation (A-37). The phase velocity operator for the damped wave is defined by:

$$\hat{U} \equiv \frac{\omega}{\kappa} = \pm U_o\sqrt{1+i\,\frac{\omega}{\mu_o\sigma U_o^2}} \qquad \text{(A-39)}$$

The correct formula for the phase velocity is now:

$$U_{ph} = \frac{R_e(\omega)}{R_e(\kappa)} \approx U_o \qquad \text{(A-40)}$$

Since the constant a is just the ratio of the phase velocity to the constant component of the field (Equation A-35), it may be inferred that:

$$\vec{b} = \frac{B_o}{U}\vec{V} = \frac{B_o}{U_o}\left(1+i\,\frac{\omega}{\mu_o\sigma U_o^2}\right)^{-1/2}\vec{V} \qquad \text{(A-41)}$$

Since κ is in the form $(\kappa_R + i\,\kappa_I)$, $\vec{b}$ can be written as:

$$\vec{b} = B_o \sqrt{\kappa_R^2 + \kappa_I^2}\; e^{i\phi} \vec{V} \qquad \text{(A-42)}$$

where:

$$\phi = \tan^{-1} \frac{\kappa_I}{\kappa_R} \; ; \; \kappa_I < 0 < \kappa_R \qquad \text{(A-43)}$$

Thus there exists a phase lead of the gas velocity with respect to the wave field.

Figures A-1 and A-2 show, for various angular frequencies and plasma densities, the attenuation distance as a function of the real part of the wave number. The parameter r_o is the ratio of the plasma density to a reference plasma density of 1.72×10^{-10} Kg/m^3.

The result obtained in (A-31) associates the magnetostrictive pressure of the perturbation field with the disturbed component of the gas velocity. In addition, observation of the pinch effect makes the assumption, that the gradient of the quantity in Alfvén condition (6) is zero, not unreasonable. The result of combining condition (6) and equation (A-31) is just the steady state Bernoulli equation relating the mechanical energy density to the magnetic energy density.

If the wave disturbance is maintained by a time varying magnetic field $\vec{\beta}$, perpendicular to the main field $\vec{B_o}$ and fixed at a point in space, equations (A-24) and (A-25) may be used with:

$$\left.\begin{aligned} \vec{B} &= \vec{B}_o + \vec{b} \\ \vec{B}_o &= B_o \vec{\imath}_z \\ \vec{b} &= \beta \vec{\imath}_x + \vec{b}' \\ \vec{V} &= V_o \vec{\imath}_z + \vec{v}' \\ \gamma &= \left(\frac{1}{\mu_o \rho}\right)^{1/2} \\ \zeta &= \left(\frac{1}{\mu_o \sigma}\right)^{1/2} \end{aligned}\right\} \qquad \text{(A-44)}$$

ALFVÉN WAVE ATTENUATION IN A FULLY IONIZED GAS

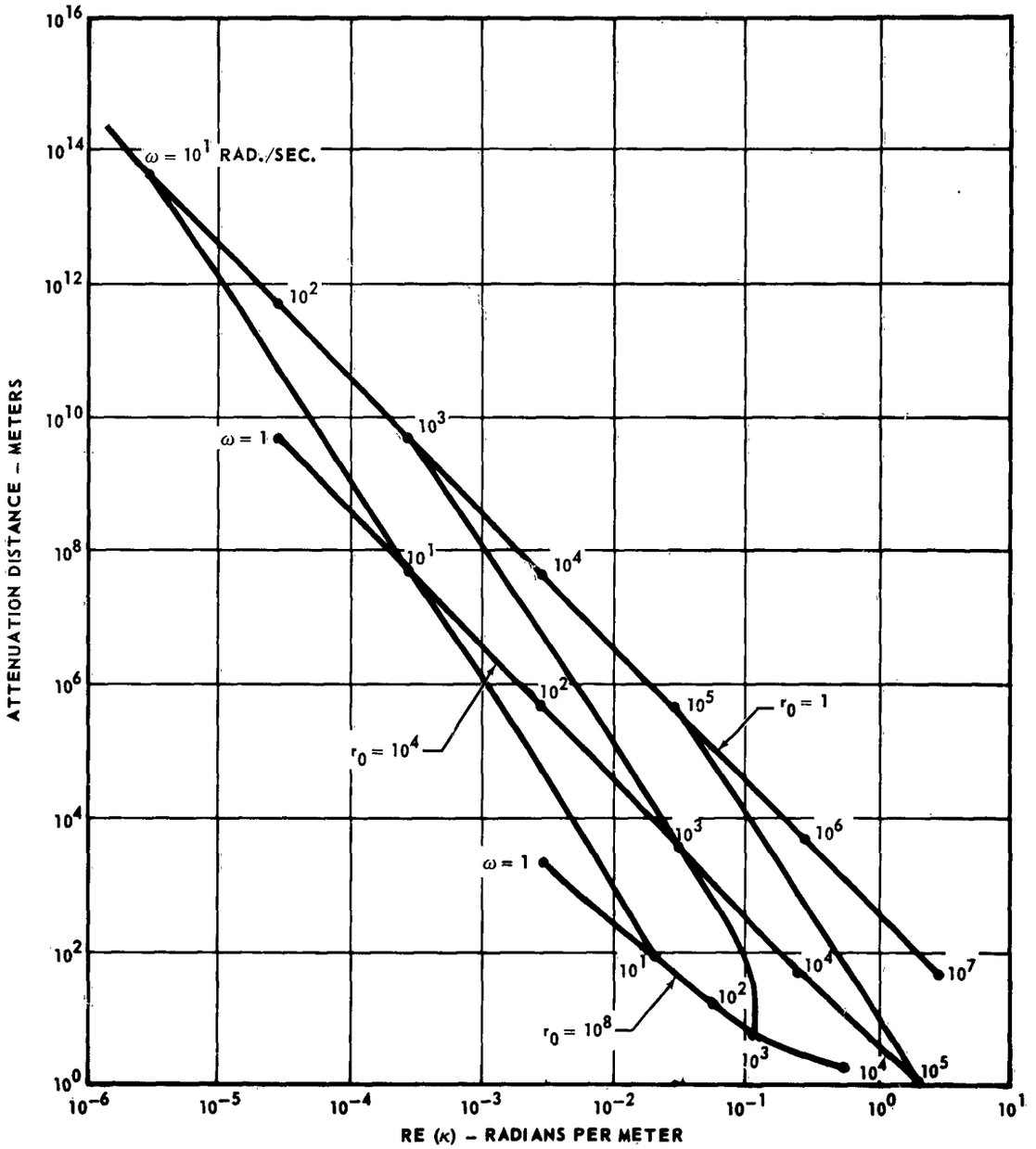

FIGURE A-1

A

ALFVÉN WAVE ATTENUATION IN A FULLY IONIZED GAS FOR EXTENDED FREQUENCY RANGE

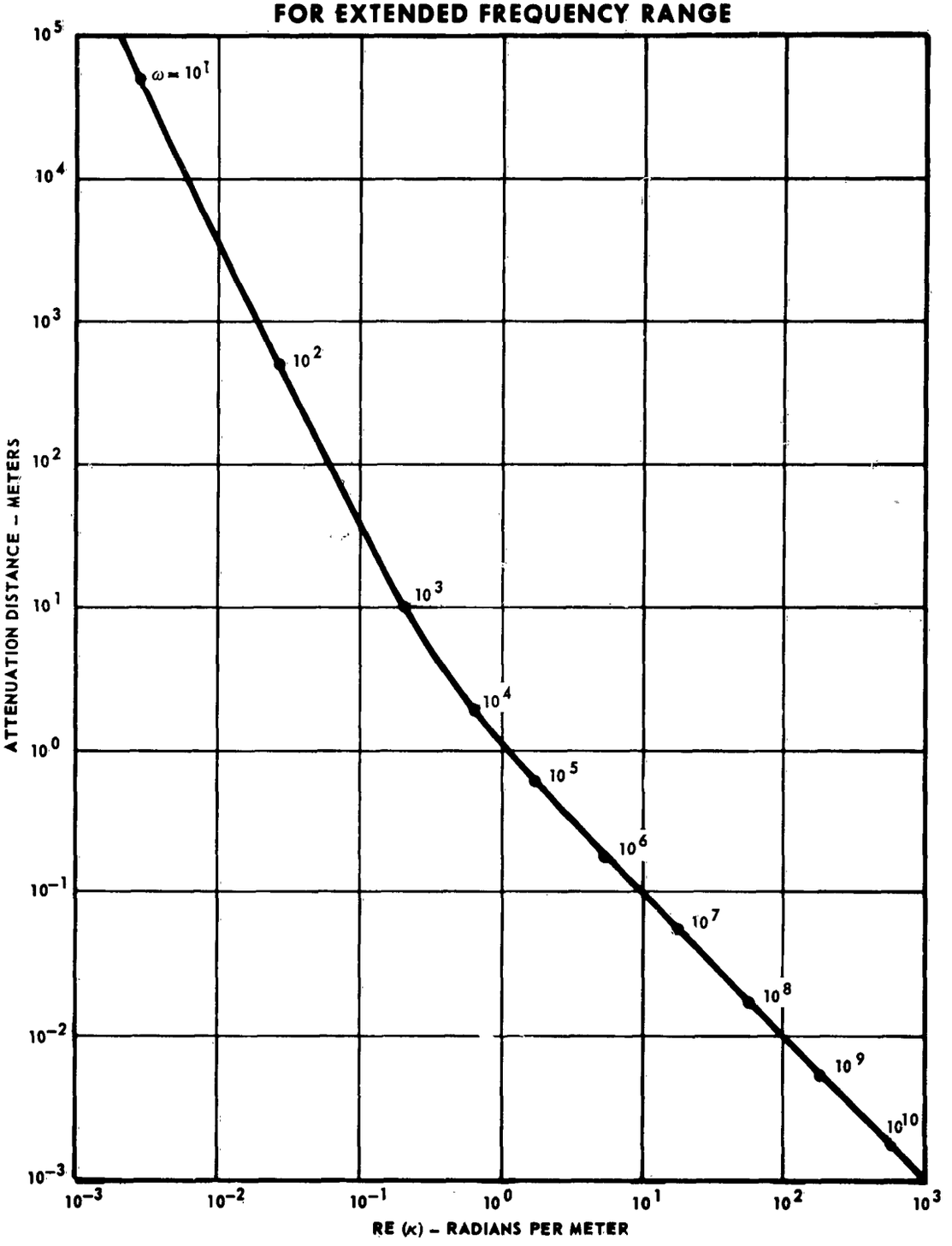

FIGURE A-2

to obtain a more general wave equation.

Thus upon substituting:

$$\frac{\partial \vec{b}'}{\partial t} + \frac{\partial \vec{\beta}}{\partial t} = \zeta^2 \nabla^2 \vec{b}' + (\vec{b}' \cdot \nabla)\vec{v}' + (\vec{\beta} \cdot \nabla)\vec{v}' + (\vec{B}_o \cdot \nabla)\vec{v}' - (\vec{V} \cdot \nabla)\vec{b}' \qquad \text{(A-45)}$$

and:

$$\frac{\partial \vec{v}'}{\partial t} = \gamma^2 (\vec{b}' \cdot \nabla)\vec{b}' + \gamma^2 (\vec{\beta} \cdot \nabla)\vec{b}' - (\vec{V} \cdot \nabla)\vec{V} + \gamma^2 (\vec{B}_o \cdot \nabla)\vec{b}' \qquad \text{(A-46)}$$

Using the linear relation:

$$\vec{v}' = a\vec{b} = a(\vec{\beta} + \vec{b}') \qquad \text{(A-47)}$$

and differentiating both (A-45) and (A-46) with respect to time yields:

$$\frac{\partial^2 \vec{b}'}{\partial t^2} + \frac{\partial^2 \vec{\beta}}{\partial t^2} = \zeta^2 \nabla^2 \frac{\partial \vec{b}'}{\partial t} + [(a\vec{B}_o - \vec{V}_o) \cdot \nabla] \frac{\partial \vec{b}'}{\partial t} \qquad \text{(A-48)}$$

and:

$$\frac{\partial \vec{b}'}{\partial t} + \frac{\partial \vec{\beta}}{\partial t} = \left(\frac{\gamma^2}{a} - a\right)[(\vec{b}' + \vec{\beta}) \cdot \nabla]\vec{b}' + \left[\left(\frac{\nu^2}{a}\vec{B}_o - \vec{V}_o\right) \cdot \nabla\right]\vec{b}' \qquad \text{(A-49)}$$

Using the value of α obtained in (A-30) and the result from (A-35), the relations:

$$a = \gamma \qquad \text{(A-50)}$$

and:

$$U_o = \gamma B_o \qquad \text{(A-51)}$$

are found. Then using (A-50) and (A-51), the final form of the wave equation becomes:

$$\frac{\partial^2 \vec{b}'}{\partial t^2} - \zeta^2 \nabla^2 \frac{\partial \vec{b}'}{\partial t} - [(\vec{u}_o - \vec{v}_o) \cdot \nabla]^2 \vec{b}' = -\frac{\partial^2 \vec{\beta}}{\partial t^2} \qquad \text{(A-52)}$$

as would be expected from equation (A-29). No solution to (A-52) is given here; but by taking the LaPlace transform of the members of (A-52) in the time domain and applying suitable initial conditions, a transformed equation in the spatial coordinates and the transformed variable is acquired. A solution of this equation with appropriate boundary conditions should be possible. Then the inverse transform of this solution would be the desired result. Since the exact form of $\vec{\beta}$ has not been specified, any Fourier analyzable function can be included, and a solution in principle can be obtained.

REFERENCE FOR APPENDIX A

A-1 Chopra, K.P., "Some Problems in Hydromagnetics", AFOSR-TW-59-265, Los Angeles, California, University of Southern California, 1959

APPENDIX B

CALCULATION OF COLLISION FREQUENCIES IN WEAKLY IONIZED GASES

A

Although particle "collisions" within a system in thermal and chemical equilibrium do not affect the state of the system, they are largely responsible for propagating local disturbances and maintaining equilibrium. A useful model for such an ionized gas is the Lorentz gas model. The assumption of a perfect Lorentz electron gas implies that the electrons are considered as being nearly free of fields and existing in a "sea" of much more massive neutrals. The neutrals consist of electrically neutral but polarizable gas molecules. For the case of a weakly ionized Lorentz gas it is proper to consider the "collision" term in the Boltzmann equation as being due to the interaction of moving electrons and stationary neutrals. This "collision" term then couples the Boltzmann equation for the electrons to that of the neutrals. Del Croix, Reference (B-1), designates this term (Jf), where J is called the "collision operator" and f is the phase space distribution function for the electrons as it appears in the Boltzmann equation. (Jf) can always, in principle, be calculated by integrating over the entire ensemble of particle interactions, but the effort required is generally prohibitive due to the complexity of the integrand. With the assumption of a perfect Lorentz gas, however, (Jf) becomes linear in f; and, therefore, f can be expanded in a series of spherical harmonics such as:

$$f_e = a_\infty + \sum_l (a_l^m \cos m\phi + \beta_l^m \sin m\phi)\, w_e^l\, P_l^m(\theta);\ m \le l \qquad \text{(B-1)}$$

where the $P_l^m(\theta)$ are the associated Legendre polynominals of order l, θ and ϕ are the azimuth and colatitude angles. The a_l^m and β_l^m are, in general, functions of time, and w_e, is the magnitude of a possible electron velocity. It is found assuming a centrally directed electron-neutral interaction, that J

commutes with the spatial rotation operators. This commutivity property produces the eigenvalues ($-\nu_l$) corresponding to the eigenfunctions f_l^m of J as exhibited by:

$$J f_l^m = \nu_l f_l^m \tag{B-2}$$

The Boltzmann equation for electrons within a constant magnetic field $\vec{H}_o$ and an electric field $\vec{E}$ is given by:

$$\frac{\partial f_e}{\partial t} + \sum_{i=1}^{3} w_{ei} \frac{\partial f_e}{\partial q_i} + \sum_{i=1}^{3} \left(\frac{e\vec{E}}{m_e} - \vec{w}_e \times \vec{\omega}_{ce} \right)_i \frac{\partial f_e}{\partial w_i} = J_e f_e \tag{B-3}$$

where:

$$\vec{\omega}_{ce} = \frac{e\vec{B}_o}{m_e} \tag{B-4}$$

and:

$$\vec{B}_o = \mu_o \vec{H}_o \tag{B-5}$$

The terms $\frac{\partial fe}{\partial q_j}$ are diffusion terms and may be neglected if the gas inhomogeneities are small at any given instant. The momentum transfer equation, obtained from (B-3) in the usual manner, exhibits a term:

$$\vec{F}_e \equiv \iiint m_e \vec{w}_e [Jf]_e \, d w_{e1} dw_{e2} dw_{e3} \tag{B-6}$$

with:

$$[Jf]_e = \Sigma (J f_l^m) = \Sigma (-\nu_l f_l^m); m \leq l \tag{B-7}$$

Del Croix points out that, due to the orthogonality properties of the spherical harmonics in (B-1), only the anisotropy characterized by $m \leq l = 1$ makes a contribution to the interaction force, which for the electrons is $\vec{F}_e$ It is therefore, possible to calculate ν, by means of classical scattering formulas. The appropriate expression is as follows:

$$\nu_1 = 2\pi N_n V_o \int_o^\infty (1 - \cos \chi) \, pdp \tag{B-8}$$

where p is the impact parameter, χ is the deflection angle and N_n is the

number density of neutral particles. The deflection angle is determined from:

$$\chi(p, V_o) = \pi - 2p \int_d^\infty r^{-2} [1 - (p/r)^2 - \phi(r)/w_o]^{-1/2} dr \qquad \text{(B-9)}$$

A with:

$$w_o = \tfrac{1}{2} \mu V_o^2 \qquad \text{(B-10)}$$

and d the distance of closest approach. In (B-10) w_o is the relative initial energy of the two "colliding" particles, with μ being the reduced mass of the two particle system, and $w_e = V_o$ is their initial relative speed. In general, $\phi(r)$ can be considered as the interaction potential function for any two particles encountered; and, therefore, this analysis is correct even if the "sea" in which the electrons find themselves consists of both neutrals and ions. The three component mixture still employs the Lorentz gas model for the electrons, but a small fraction of the neutrals are now replaced with ions. Under the condition where:

$$N_n \gg N_e = N_i$$

and: $$\qquad \text{(B-11)}$$

$$T_n = T_i = T_e$$

N being the number of particles the type indicated by the subscript per unit volume and, T the temperature for that specie, the interactions that dominate and are of interest in plasma work are the electron-neutral, ion-neutral and electron-ion "collisions". Each interaction is characterized by a different $\phi(r)$. An individual $\phi(r)$ consists of both a classical part and a quantum mechanical part, the latter being significant only for extremely small approach distances, d. Insofar as randomization of particle motion is concerned, the distant encounters, d large, are the most important. For distant encounters then, the potential function takes on the following forms:

Electron-neutral: $\phi_{en} = -\frac{\alpha e^2}{r^4}$ (α = molecular polarization)

Ion-neutral: $\phi_{in} = -\frac{\alpha e^2}{r^4}$

Electron-ion: $\phi_{ei} = -\frac{e}{r}$ (singly ionized gas)

Due to its dependence on the potential function, ν_1 has the exact interpretation of a collision frequency only for impenetrable particles with completely negligible fields ("billiard balls"). Using (B-7) and (B-1), Equation (B-6), written in rectangular coordinates, becomes:

$$\vec{F}_e = m_e \iiint \nu_1 V_o (a_{11} w_x + \beta_{11} w_y + a_{10} w_z)\, d V_{ox}\, dV_{oy}\, dV_{oz} \qquad \text{(B-14)}$$

The macroscopic interaction force on the electrons, $\vec{F}_e$, produces a change in the total macroscopic velocity $\vec{V}_e$ according to the relation:

$$\vec{F}_e = n_e m_e \nu_e \vec{V}_e \qquad \text{(B-15)}$$

where $\underline{\nu}_e$ is the tensor of averaged interaction quantities. The expression for ν_e is:

$$\underline{\nu}_e = \begin{bmatrix} \langle \nu_e \rangle_{xx} & 0 & 0 \\ 0 & \langle \nu_e \rangle_{yy} & 0 \\ 0 & 0 & \langle \nu_e \rangle_{zz} \end{bmatrix} \qquad \text{(B-16)}$$

with:

$$\langle \nu_e \rangle_{xx} = \frac{\int_o^\infty \nu_1 a_{11} V_o^4\, d V_{o_x}}{\int_o^\infty a_{11} V_o^4\, d V_{o_x}} \qquad \text{(B-17)}$$

and analogously for $\langle \nu_e \rangle_{yy}$ and $\langle \nu_e \rangle_{zz}$.

The coefficients a_{10}, a_{11}, and β_{11} are obtained by solving the approximate Boltzmann equation:

$$\frac{\partial f_e}{\partial t} + \sum_{j=x}^{z} \left(\frac{e\vec{E}}{m_e} + \vec{V}_o \times \vec{\omega}_{ce} \right)_j \frac{\partial f_e}{\partial V_{oj}} = J f_e \qquad \text{(B-18)}$$

and retaining only the first order terms in (B-1). These coefficients are, in general, functions of ν_1, $\vec{V}_o$, $\vec{B}$ and $\vec{E}$. Obviously, if ν_1 is independent of $\vec{V}_o$, $\underline{\nu}_e$ becomes the scalar collision frequency ν_e for the electrons.

Equations analogous to (B-14) through (B-18) can be written for the ions, the essential difference being the tendency for the ion-neutral interactions to be

of the "billiard ball" type.

An alternative classical technique for calculating collision frequencies is effected by means of the differential cross section, $\hat{\sigma}$. This quantity is defined by:

$$\hat{\sigma} \equiv \frac{ds}{d\Omega} \tag{B-19}$$

where:

$$s = \pi p^2 \tag{B-20}$$

is the cross section of the incident particle beam, p being the impact parameter, and $d\Omega$ is the element of solid angle into which a number of the particles are scattered. In terms of the deflection angle:

$$d\Omega = 2\pi \sin\chi \, d\chi \tag{B-21}$$

and:

$$\hat{\sigma} = \frac{ds}{dp}\,\frac{dp}{d\Omega} = \frac{p}{\sin\chi}\,\frac{dp}{d\chi} \tag{B-22}$$

For the electron-ion interaction, with ϕ_{ei} from (B-13), $\hat{\sigma}$ has the form:

$$\hat{\sigma}_{ei}(\chi) = \frac{1}{4}\left(\frac{e^2}{\mu V_o^2}\right)^2 \sin^{-4}\left(\frac{1}{2}\chi\right) \tag{B-23}$$

which is Rutherford's scattering formula. The deflection angle is calculated from (B-9), provided d can be determined. The total scattering cross section is given by:

$$\sigma_{ij} = \int_o^{4\pi} \sigma_{ij}\, d\Omega = 2\pi \int_o^{\pi} p_i \left(\frac{dp_i}{d\chi_{ij}}\right) d\chi_{ij} \tag{B-24}$$

Assuming a Maxwellian distribution of initial speeds, V_o, the kinetic theory of gases produces the following expression for the total number of two particle encounters per unit volume and time:

$$N_{ij} = K_{ij}\, n_i\, n_j \left(\frac{\mu}{kT}\right)^{3/2} \left(\frac{2}{\pi}\right)^{1/2} \int_o^{\infty} V_o^3\, e^{-\mu V_o^2/2kT}\, \sigma_{ij}(V_o)\, dV_o \tag{B-25}$$

where:

$$K_{ij} = \begin{cases} 1/2 \text{ for like particles } (i = j) \\ 1 \text{ for unlike particles } (i \neq j) \end{cases} \qquad \text{(B-26)}$$

n_i and n_j are the number densities of particle types i and j, and the other quantities are as previously defined. The collision frequency is directly related to (B-25) by means of:

$$\nu_{ij} = \frac{N_{ij}}{n_i} \qquad \text{(B-27)}$$

The total number of collisions per unit time per type i "test" particle is:

$$\nu_i = \frac{2N_{ii} + N_{ij}}{n_i} \qquad \text{(B-28)}$$

since for a two-particle collision involving the same type of particles, either one is the "test" particle. In (B-25) the proper determination of $\sigma_{ij}(V_o)$ is through quantum mechanical considerations; however, a common technique is to assume an average value for $\sigma_{ij}(V_o)$, commute it with the integral operator and integrate the remaining expression. The result of this procedure is:

$$N_{ij} = \frac{2K_{ij}}{\sqrt{\pi}} \sqrt{\frac{2kT}{\mu}}\, n_i\, n_j\, \bar{\sigma}_{ij} \qquad \text{(B-29)}$$

Then:

$$\nu_{ij} = \frac{2K_{ij}}{\sqrt{\pi}} \sqrt{\frac{2kT}{\mu}}\, n_j\, \bar{\sigma}_{ij} \qquad \text{(B-30)}$$

Since the most probable speed for a Maxwellian distribution of particles of mass μ is:

$$C = \frac{2}{\sqrt{\pi}} \sqrt{\frac{2kT}{\mu}} \qquad \text{(B-31)}$$

and since the classical expression for the mean free path of a particle of mass μ is:

$$L_{ij} = \frac{1}{n_j\, \bar{\sigma}_{ij}} \qquad \text{(B-32)}$$

formula (B-30) is just the usual result:

$$\nu_{ij} = \frac{C}{L_{ij}} \qquad \text{(B-33)}$$

For electron-ion encounters a reasonable expression for $\bar{\sigma}_{ei}$ (Reference B-2) is found to be:

$$\bar{\sigma}_{ei} = \frac{9\pi\,(10^{-6})}{4T^2} \quad (CM^2) \qquad \text{(B-34)}$$

For electron-neutral "collisions" it is common to use the "billiard ball" model. However, because of the small classical radius of the electron, it is essentially a point compared to the neutral particle. Thus, $\bar{\sigma}_{en}$ is just the geometrical cross section of the neutral:

$$\bar{\sigma}_{en} = \bar{\sigma}_{n} \approx \frac{\pi}{4}\,(10^{-16})\ CM^2 \qquad \text{(B-35)}$$

The geometrical ion-neutral cross section is then:

$$\bar{\sigma}_{in} = 4\bar{\sigma}_{n} \approx \pi\,(10^{-16})\ CM^2 \qquad \text{(B-36)}$$

Using (B-34), (B-35) and (B-36) the following first approximations to the three important "collision" frequencies are obtained:

$$\nu_{ei} = \frac{9n_i\,(10^{-6})}{2T^2}\sqrt{\frac{2\pi kT}{m_e}}$$

$$\nu_{en} = \frac{(10^{-16})}{2}\,n_n\sqrt{\frac{2\pi kT}{m_e}} \qquad \text{(B-37)}$$

$$\nu_{in} = 2\sqrt{2}\,(10^{-16})\,n_n\sqrt{\frac{2\pi kT}{m_i}}$$

REFERENCES FOR APPENDIX B

B-1 Del Croix, J.L., "Introduction to the Theory of Ionized Gases", New York, Interscience Publishers, Inc., 1960

B-2 Menzel, D.H., "Fundamental Formulas of Physics", New York, 305, 1960